Using *in vitro* and *in silico* approaches to investigate ibuprofen particulate and formulation dissolution behaviour under different hydrodynamic conditions

by

Marina Navas Bachiller

Being a thesis submitted for the degree of

Doctor of Philosophy in Pharmaceutics

At

Trinity College Dublin, the University of Dublin

Under the supervision and direction of

Deirdre D'Arcy, Assoc. Prof, M. Pharm., Ph.D, M.P.S.I

and

Tim Persoons, Assoc. Prof M. Eng, Ph.D

February 2024

Declaration

I declare that this thesis has not been submitted as an exercise for a degree at this or any other university and it is entirely my own work.

I agree to deposit this thesis in the University's open access institutional repository or allow the Library to do so on my behalf, subject to Irish Copyright Legislation and Trinity College Library conditions of use and acknowledgement.

I consent to the examiner retaining a copy of the thesis beyond the examining period, should they so wish.

Covid-19 impact statement

Due to the Covid-19 pandemic, the work was delayed and spans a 4.5 year timeframe. The restricted access to labs influenced the order of simulation and lab work. During this period of time (March 2020 to September 2020), some literature research work and simulation work was carried out. Shutdown mostly interrupted planned training, as it occurred at the beginning of the project, delaying the start of laboratory data generation for the project. However, the impact of this disruption on results and interpretation was minimised through planning.

Summary

The dissolution of ibuprofen active pharmaceutical ingredient was investigated in the paddle apparatus and the flow-through apparatus in conditions of high and low solubility (pH 6.8 phosphate buffer versus 0.1 M HCl), high and low fluid velocity and three levels of viscosity (0.7 mPa.s, 1.4 mPas and 5.5 mPa.s) with the use of two viscosity enhancing agents (hydroxypropyl methylcellulose (HPMC) and sucrose). In the flow-through apparatus, high average linear fluid velocity was defined as 2.35 mm s^{-1} and low average linear fluid velocity was defined as 0.33 mm s^{-1}. In the paddle apparatus, agitation speeds of 50 rpm and 100 rpm were investigated.

Moderate increases in medium viscosity were investigated based on the findings reported in literature that the human gastric fluid has a viscosity which is slightly higher than that of aqueous buffers. The negative effect of sucrose-containing medium on ibuprofen dissolution in the flow-through apparatus was more evident than that of HPMC-containing media at both velocity conditions studied. The *in vitro* dissolution profiles obtained suggest that the viscosity enhancing agent used impacted dissolution differently, pointing to differing effects on wetting, fluid density and particle motion and highlighting the complexity of isolating the effects of viscosity on *in vitro* dissolution testing.

Moderate increases in viscosity reduced the intrinsic dissolution rate of ibuprofen when either HPMC or sucrose were present in the media. The negative effect of HPMC on the intrinsic dissolution rate of ibuprofen versus the moderate effect of HPMC on ibuprofen particulate dissolution in the flow-through apparatus illustrates the influence of viscosity enhancing agents on particle motion.

An in-house dissolution simulation code, SIMDISSO^{TM}, was used to simulate ibuprofen particulate dissolution in the flow-through apparatus and paddle apparatus. The model estimates the mass transfer coefficient of an individual particle through the Ranz-Marshall correlation and correlates it to solubility and particle surface area to predict the dissolution rate. In the current work three approaches were investigated to ascertain the predictive ability of SIMDISSO^{TM}: inputting a particle size distribution versus a median

particle size, enabling or disabling particle motion and the simulation of a reduced local bulk volume for dissolution. The importance of defining an effective particle size was observed in particular in conditions of low solubility and especially if agglomeration was suspected. The acceptability of using a mean particle size in some cases of fast dissolution for the prediction of dissolution metrics was acknowledged, as it can save computational costs without compromising the accuracy of the simulation. The importance of defining particle motion in high-velocity situations was manifested, as the velocity the particle is exposed to can be very different between a static and moving particle. The effects of changing fluid velocity in a high solubility environment in the flow-through apparatus were predicted with the local volume approach.

The dissolution profiles in conditions of increased viscosity with sucrose were reasonably predicted in SIMDISSO™, whereas the predictions in HPMC-containing medium were less accurate, pointing to factors not included in the simulation affecting *in vitro* drug dissolution in this scenario. A spatial limitation was introduced prior to the realization of these simulations in which particle motion was restricted in the vertical direction by the cell limits, so that enabling or disabling particle motion was not necessary in these simulations. SIMDISSO™ simulations also illustrated the effect of viscosity on particle motion.

The dissolution of ibuprofen from immediate release tablets was investigated in the flow-through apparatus at three levels of viscosity with both viscosity enhancing agents. The observed negative effect of medium viscosity on dissolution was more discernible with sucrose than HPMC, which is in agreement with the results observed for ibuprofen powder. The *in vitro* dissolution profiles of ibuprofen tablets were used as inputs to a GastroPlus® pharmacokinetic model. The results illustrated (a) the potential of the flow-through apparatus to generate dissolution profiles which could be used to predict ibuprofen bioavailability, (b) the consideration of small increases in medium viscosity relevant to the fasted state, as they might affect drug dissolution and the resulting pharmacokinetic profile, and (c) the need to further characterize the effects of viscosity and fluid density on dissolution and absorption with other drugs and formulations.

Table of contents

Acknowledgements

I am extremely thankful for the continuous support of my supervisors Dr. Deirdre D'Arcy and Dr. Tim Persoons through the ups and downs of the PhD journey. Thank you to Dr. Deirdre D'Arcy for her guidance, encouragement and invaluable expertise. Thank you to Dr. Tim Persoons for his patience and for taking the time to share his knowledge.

I would also like to thank Dr. Nikoletta Fotaki for the valuable discussions and expertise provided during the third section of the work. It was an honour to be part of this collaboration.

Thank you to Prof. Anne Marie Healy and Dr. Eduardo Ruiz-Hernandez, members of my thesis committee, for providing an immensely valuable perspective into my work.

I would like to acknowledge Science Foundation Ireland (SFI) and the SFI Research Centre for Pharmaceuticals, the SSPC, for providing the financial support which was essential to complete this project.

Thank you to Dr. Amelia Ultimo for assistance in surface area analysis and to Edana Keavney for assistance with particle size analysis.

To Eva and Tony for your generosity and for making these four years way more enjoyable. To Brunella, for becoming such a good friend so quickly. I'm glad to have you back in Ireland. My thanks extend to every post-grad in the pharmaceutics labs, for creating such a great environment where I have been happy to be for over 4 years.

To my friends outside the PhD. To Evenor, for patiently listening when I tried to explain why you should take a full glass of water with your medicines. To Yaiza and Dani, for that freezing cold January weekend you decided to visit Dublin. To my dear biochemists, Raquel, Santi and Ana, I couldn't have asked for better college friends. And to Simone, for the long and productive library days, and the chats.

To Barry, thank you for your calmness, your patience and your kindness. Your positive outlook on life and your determination to overcome challenges inspires me every day.

And finally, thanks to the support of my parents, my sister and my extended family, even in the distance, for encouraging me to take this opportunity, even if it meant seeing less of each other, and for sharing my excitement whenever I shared good PhD-related news. Thank you for always being there.

Publications associated with this thesis

Publications:

- D'Arcy, D. M., Pham, T. T. V., Navas Bachiller, M., Fotaki, N., Persoons, T. (2020). Using in silico process simulation tools in pharmacy education: Considerations for pivoting to online learning. Pharm Educ, **20** (2), 124-135. https://doi.org/10.46542/pe.2020.202.124135
- Navas-Bachiller, M., Persoons, T., D'Arcy, D.M. (2022). Exploring bulk volume, particle size and particle motion definitions to increase the predictive ability of *in vitro* dissolution simulations. *Eur J Pharm Sci*, **174**, 106185. https://doi.org/10.1016/j.ejps.2022.106185.
- Navas Bachiller, M., Persoons, T., Healy, A., D'Arcy, D. M., (2022). Assessing the effect of moderately increasing medium viscosity on the intrinsic dissolution rate and diffusion coefficient of ibuprofen particles, *Br J Pharm,* **7** (2). https://doi.org/10.5920/bjpharm.1130
- Navas-Bachiller, M., Persoons, T., D'Arcy, D.M. (2023). *In vitro* and *in silico* methods to investigate the effect of moderately increasing medium viscosity and density on ibuprofen dissolution rate. *Eur J Pharm Biopharm,* **193**, 74-88. https://doi.org/10.1016/j.ejpb.2023.10.018
- Chapter 5 of this thesis is currently being prepared for publication in a relevant journal.

Posters:

- Navas-Bachiller, M., Persoons, T., D'Arcy, D.M. Exploring use of a near-particle volume for *in vitro* dissolution simulations as an approach to increase its predictive ability *in the* European Federation for Pharmaceutical Sciences (EUFEPS) Annual Meeting, Virtual meeting, June 7th-9th, 2021.
- Navas-Bachiller, M., Pham, T. T. V., Fotaki, N., Persoons, T., D'Arcy, D. M. Using *in vitro* dissolution simulations to guide a manufacturing design space for repurposed drugs used in Covid-19 trials *in the* American Association of Pharmaceutical Sciences (AAPS) PharmSci 360 meeting, Virtual meeting, October 17th-20th, 2021.

- Navas-Bachiller, M., Persoons, T., Healy, A., D'Arcy, D. M. Assessing the effect of moderately increasing medium viscosity on the intrinsic dissolution rate and diffusion coefficient of ibuprofen particles *in the* Academy of Pharmaceutical Sciences (APS) PharmSci Conference, Belfast, United Kingdom, September 7th-9th, 2022.
- Navas-Bachiller, M., Persoons, T., D'Arcy, D.M. Effect of moderate biorelevant increases in medium viscosity on the dissolution rate of ibuprofen particles *in the* AAPS PharmSci 360 meeting, Boston, USA, October 16th-19th, 2022.

Abbreviations

AAFE	Absolute average fold error
ACAT	Advanced compartmental absorption and transit
ACN	Acetonitrile
ADBL	Aqueous diffusion boundary layer
AFE	Average fold error
AIC	Akaike information criterion
API	Active pharmaceutical ingredient
ASD	Artificial stomach-duodenum
ASF	Absorption scale factor
BCS	Biopharmaceutics classification system
BDDCS	Biopharmaceutics drug disposition classification system
BE	Bioequivalence
BET	Brunauer-Emmett-Teller
BioGIT	Biorelevant gastrointestinal transfer
BioRAM	Biopharmaceutics risk assessment roadmap
BMI	Body mass index
CFD	Computational fluid dynamics
CI	Confidence interval
CMA	Critical material attribute
CMC	Critical micelle concentration
CPP	Critical process parameter
CQA	Critical quality attribute
CR	Controlled release
CRU	Controlled release undissolved
CV	Coefficient of variation
DCM	Dynamic colon model

DCS	Developability classification system
DLM	Diffusion layer model
EMA	European Medicines Agency
ER	Extended release
FaSSCoF	Fasted state simulated colonic fluids
FaSSGF	Fasted state simulated gastric fluid
FaSSIF	Fasted state simulated intestinal fluids
FDA	Food and Drug Administration
FDM	Finite-domain model
FE	Fold error
FeSSCoF	Fed state simulated colonic fluids
FeSSGF	Fed state simulated gastric fluid
FeSSIF	Fed state simulated intestinal fluids
FIP	Fédération Internationale Pharmaceutique
FSM	Fed stomach model
FTA	Flow-through apparatus
GET	Gastric emptying time
GI	Gastrointestinal
GIS	Gastrointestinal simulator
GIT	Gastrointestinal tract
HGF	Human gastric fluid
HPLC	High pressure liquid chromatography
HPMC	Hydroxypropyl methylcellulose
IDAS2	*In vitro* dissolution absorption system
IDR	Intrinsic dissolution rate
IPD	*In vivo* predictive dissolution
IR	Immediate release
IVIVC	*In vitro-in vivo* correlation

LOD	Limit of detection
LOQ	Limit of quantification
MMC	Migrating motor complex
MPS	Median particle size
MR	Modified release
MRI	Magnetic resonance imaging
NMR	Nuclear magnetic resonance
NPV	Near-particle volume
OrBiTo	Oral biopharmaceutics tools project
PB	pH 6.8 phosphate buffer
PBBM	Physiologically based biopharmaceutics modelling
PB-H	pH 6.8 phosphate buffer with HPMC
PBPK	Physiologically based pharmacokinetic modelling
PB-S	pH 6.8 phosphate buffer with sucrose
PE%	Percentage predictive error
Ph Eur	European Pharmacopoeia
PIV	Particle image velocimetry
PK	Pharmacokinetic
PSA	Parameter sensitivity analysis
PSD	Particle size distribution
PTFE	Polytetrafluoroethylene
QbD	Quality by design
QC	Quality control
RMSE	Root mean square error
SC	Schwarz criterion
SD	Standard deviation
SF	Solubility factor
SGF	Simulated gastric fluid

SIF	Simulated intestinal fluid
St-E	Stokes-Einstein equation
t50	Time to 50% dissolution
t85	Time to 85% dissolution
TFA	Trifluoroacetic acid
TIM-1	TNO intestinal model
USP	United States Pharmacopoeia
VBE	Virtual bioequivalence
VEA	Viscosity enhancing agents

Nomenclature

Variable	Name, units	Variable	Name, units
k_a	Absorption rate constant, h^{-1}	m_u	Mass undissolved, kg
ω	Angular velocity, rad s^{-1}	C_{max}	Maximum concentration of drug in plasma, µg ml^{-1}
$\mathrm{m_p}$	Apparent particle mass, kg	Y_{max}	Maximum percentage dissolved *in vitro*, %
AUC	Area under the curve, µg h ml^{-1}	V_l	Near-particle volume, m^3
U_a	Axial velocity, m s^{-1}	k_{NW}	Noyes-Whitney proportionality constant, s^{-1}
k_B	Boltzmann constant, m^2 kg s^{-2} K^{-1}	ρ_p	Particle density, kg m^{-3}
C_b	Bulk concentration, kg m^{-3}	d_p	Particle diameter, m
C_c	Cell concentration, kg m^{-3}	N_p	Particle number
CL	Clearance, L h^{-1}	r_p	Particle radius, m
dC/dt	Concentration transfer rate, kg m^{-3} s^{-1}	U_p	Particle velocity, m s^{-1}
h	Diffusion boundary layer thickness, m	V_p	Particle volume, m^3
D	Diffusion coefficient, m^2 s^{-1}	W_0	Particle weight, kg
r_d	Disk radius, m	U_r	Radial velocity, m s^{-1}
k_{diss}	Dissolution rate constant, s^{-1}	C_r	Reservoir concentration, kg m^{-3}

b	Drag coefficient, N s m^{-1}	V_r	Reservoir volume, m^3
m_o	Initial drug mass, kg	Re	Reynolds number
P_{eff}	Effective permeability, m s^{-1}	Sc	Schmidt number
I	Flow of matter from the disk surface, kg s^{-1}	S^*	Shear Peclet number
s	Flow shear rate, s^{-1}	Sh	Sherwood number
ρ_p	Fluid density, kg m^{-3}	C_s	Solubility, kg m^{-3}
U_f	Fluid velocity, m s^{-1}	A	Surface area of the particle, m^2
μ_f	Fluid viscosity, Pa.s	U_t	Tangential velocity, m s^{-1}
F	Force, N	T	Temperature, K
f_u	Fraction unbound to proteins, %	T_{max}	Time required to reach C_{max}, h
g	Gravitational acceleration, m s^{-2}	t	Time, s
$T_{1/2}$	Half-life, h	K_i	Transfer rate constants, h^{-1}
R	Hydrodynamic radius of the particle, m	C_v	Vessel concentration, kg m^{-3}
ν_f	Kinematic viscosity, m^2 s^{-1}	V_c	Volume of distribution, L
t_{lag}	Lag time, s	$f1$	Weibull fraction factor
C_l	Lumen concentration, kg m^{-3}	max	Weibull maximum amount of drug dissolved, %

m_d	Mass dissolved, kg	$b1$	Weibull shape factor
k	Mass transfer coefficient, m s^{-1}	$a1$	Weibull time scale factor, s
dm/dt	Mass transfer rate, kg s^{-1}	Z	Z-factor, mg ml^{-1} s^{-1}

Origin and scope

This work expands on the work by D'Arcy and Persoons [1, 2] in which a non-commercial in-house dissolution simulation code, SIMDISSO^{TM}, was developed to simulate particulate dissolution in the flow-through apparatus and paddle apparatus based on the fluid dynamics theory. The definition of a limited volume available for a particle to dissolve into was explored in both apparatuses to highlight the importance of dissolution in non-sink conditions and confinement effects. The predictive ability of the model when the reduced, local volume was used was explored under different conditions of particle size definition and particle motion.

The effect of viscosity on the drug diffusion coefficient and on particle suspension was explored by D'Arcy and Persoons [2] using SIMDISSO^{TM}. This work expands this exploration by looking at the effects and interplay of fluid velocity and biorelevant viscosity *in vitro*, in the paddle and flow-through apparatus and *in silico*. Ibuprofen active pharmaceutical ingredient (API) and immediate release (IR) tablets were used. The viscosity values that were investigated were relevant to the fasted state stomach as measured by Pedersen *et al.* [3]. The effect of small yet biorelevant increases in viscosity was also explored in terms of pharmacokinetic modelling with the use of physiologically based pharmacokinetic models (PBPK).

Chapter 1. Introduction

Preface

Due to the length of the project and the Covid-19 extension, this work spans over a 4.5-year timeframe. Some initial literature research was still being conducted during 2020 and, to ensure the topics are explained using current thinking, which in some cases is rapidly evolving, some more recent papers are included in the introduction. In order to distinguish between the research publication dates during the initial literature review, articles published from 2021 onwards are identified as “recent work”.

Some of the sections presented in Chapter 1 were presented in the following papers:

- Navas-Bachiller, M., Persoons, T., D'Arcy, D.M. (2022). Exploring bulk volume, particle size and particle motion definitions to increase the predictive ability of *in vitro* dissolution simulations. *Eur J Pharm Sci*, **174**, 106185. https://doi.org/10.1016/j.ejps.2022.106185.
- Navas-Bachiller, M., Persoons, T., D'Arcy, D.M. (2023). *In vitro* and *in silico* methods to investigate the effect of moderately increasing medium viscosity and density on ibuprofen dissolution rate. *Eur J Pharm Biopharm,* **193**, 74-88. https://doi.org/10.1016/j.ejpb.2023.10.018

1.1. Fundamentals of dissolution

Solid oral dosage forms are the preferred method of drug administration due to safety and convenience. Solid oral dosage forms have to undergo disintegration, dissolution and absorption in the gastrointestinal tract (GIT) before the active pharmaceutical ingredient (API) can be present in the systemic circulation [4]. The dissolution of a solid particle is the transfer of molecules from a solid state into solution [5]. Dissolution occurs in two steps. Firstly, the interactions between the molecules in the solid surface are broken and interactions between solid and solvent molecules are formed, in a process called solvation. Secondly, the solvated molecules are transported from the solid interface to the bulk solution. Generally, the transport step is slower than the solvation step and becomes the rate-limiting step for dissolution.

In vitro dissolution tests can be carried out in seven standardized apparatuses that are included in the United States Pharmacopoeia (USP) [6], four of which are also included in the European Pharmacopoeia (Ph Eur) [7]. The two apparatuses used in this work (2 and 4) as well as intrinsic dissolution measurements are described below.

1.2. Dissolution apparatuses

Apparatus 2 or the paddle apparatus consists of a paddle formed of a blade and a shaft that rotates in a glass cylindrical vessel with a hemispherical base which contains the dissolution medium. A diagram of the paddle apparatus extracted from the Ph Eur [7] can be found in **Figure 1.1**. The vessel is itself contained in a water bath to keep the temperature constant at 37C. The dosage form is placed at the bottom of the cylindrical vessel before rotation is started. Once the apparatus is operating, samples are taken at certain timepoints and generally the volume that is removed from the vessel is replaced with fresh dissolution medium at the same temperature.

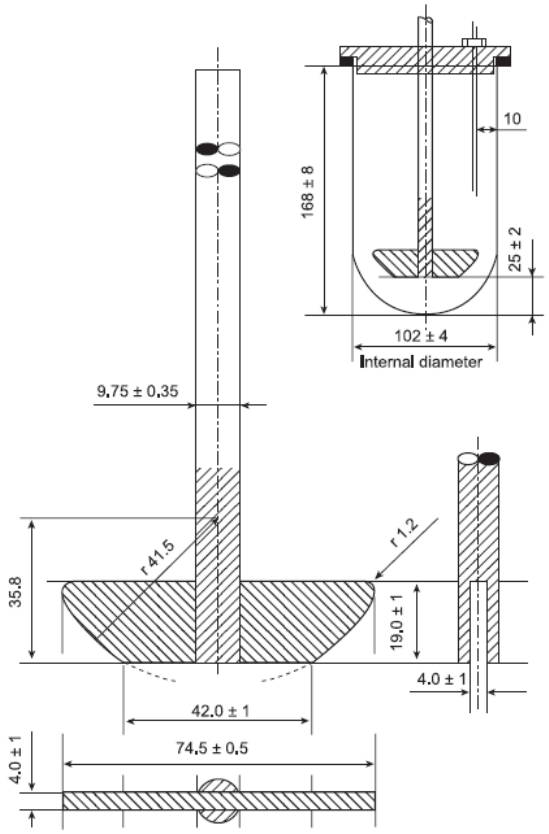

Figure 1.1. Apparatus 2 or paddle apparatus diagram extracted from the Ph Eur **[7]. Dimensions in millimetres.**

Apparatus 4 or the flow-through apparatus (FTA) was recommended as an alternative for *in vitro* drug release testing by the Dissolution Tests working Group of the Fédération Internationale Pharmaceutique (FIP) in 1981 [8] and then incorporated in various pharmacopoeias. A diagram of the apparatus extracted from the Ph Eur [7] can be found in **Figure 1.2**. There is a cell and a reservoir compartment and a pump that introduces the dissolution medium from the reservoir upwards into the cell with a predefined flow rate with or without pulsation. Typical flow rates are 4, 8 and 16 ml min^{-1} (±5% of the nominal flow) and usually, a sinusoidal pulse rate of 120 pulses per minute is used [9]. Medium will flow back from the top of the cell to the same reservoir (closed system) or a different one (open system). The dosage form is placed inside the cell, the dimensions of which can be found in **Figure 1.3**. Two sizes of cells are typically used (with a diameter of 12 mm or 22.6 mm) in which the conical section is filled with 1 mm glass beads and one 5 mm ruby bead to prevent material from entering the inlet tube. A filter is placed on top of the cell to retain undissolved material [9].

The cell is surrounded by a water jacket to keep the temperature constant. Media and flow rate changes can be performed within one run and sink conditions can be maintained in an open system but the use of complex media can be difficult due to filter clogging and flow rate alteration [9, 10].

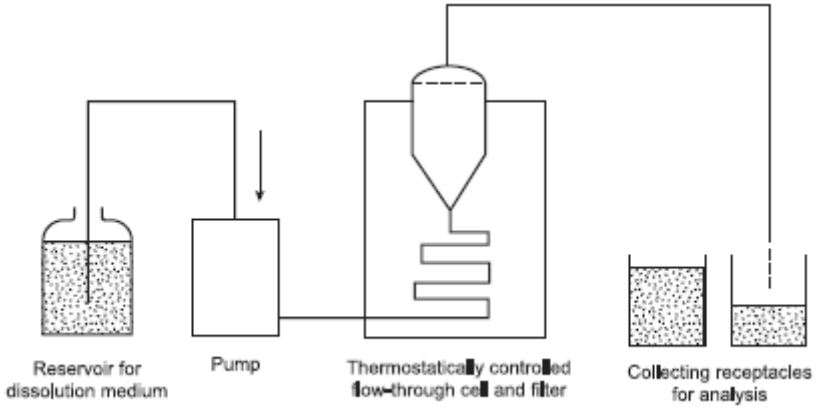

Figure 1.2. USP apparatus 4 or FTA diagram extracted from the Ph Eur **[7].**

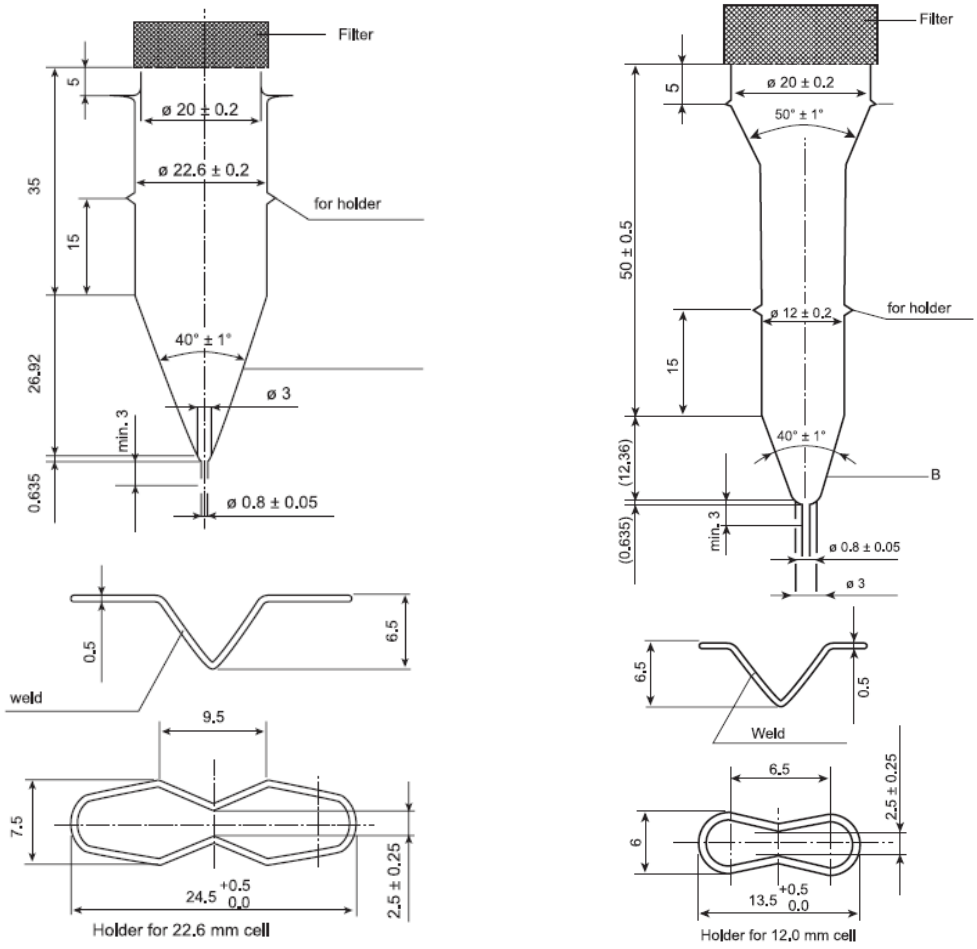

Figure 1.3. FTA 22.6 mm diameter cell (left) and 12 mm diameter cell (right). Diagrams extracted from the Ph Eur **[7]. Dimensions in millimetres.**

Intrinsic dissolution in a rotating disk apparatus measures the dissolution rate from a compact of which only one surface of a specified surface area is exposed to the dissolution medium. As described by the USP [11], first, a non-disintegrating compact is prepared using a compaction device, as presented in **Figure 1.4**. The test material is placed inside the die cavity, which is attached to a polished steel surface plate. This surface plate ensures the generation of a smooth compacted surface of the material of interest. A punch is also inserted in the die cavity and the material is compacted with a hydraulic press. Then, the compact and surrounding die are placed in a dissolution medium as presented in **Figure 1.5**, with the surface of the compact being no less than 1 cm from the bottom of the vessel, and samples are taken at given timepoints. Intrinsic dissolution gives the surface specific dissolution rate of a drug, which can be used in early

development to compare polymorphs and salt forms, evaluate the degree of crystallinity and guide formulation decisions [12].

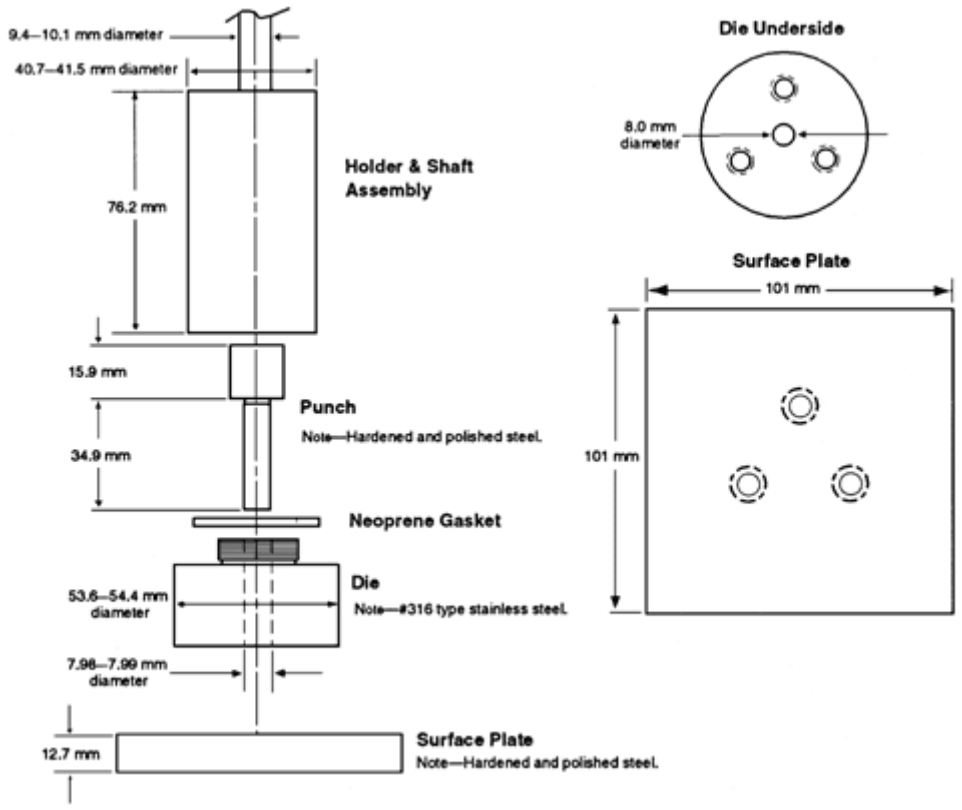

Figure 1.4. Punch and die used to produce the compact for intrinsic dissolution testing. Extracted from Chapter 1087 (Intrinsic dissolution-dissolution testing procedures for rotating disk and stationary disk) of the USP [11].

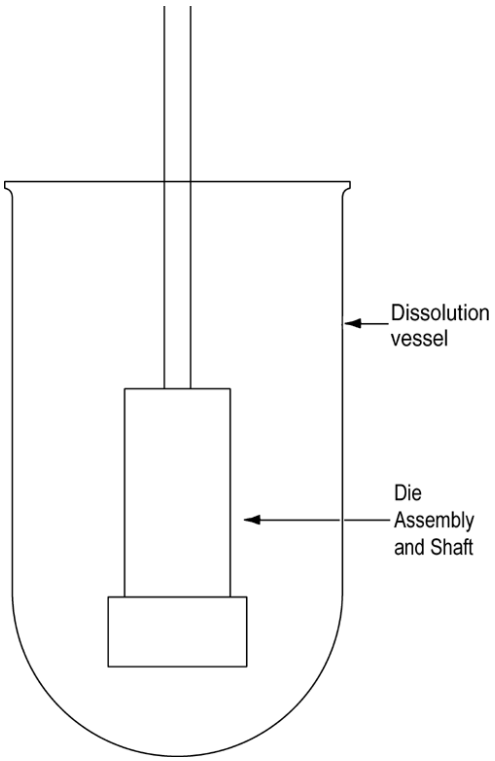

Figure 1.5. Positioning of the rotating die assembly within the dissolution vessel for intrinsic dissolution testing. Extracted from Chapter 1087 (Intrinsic dissolution-dissolution testing procedures for rotating disk and stationary disk) of the USP [11].

The hydrodynamics in the compendial apparatuses represent an added source of variability in *in vitro* dissolution testing [13-15].

1.2.1. Hydrodynamics in the dissolution apparatuses 2 and 4

The hydrodynamic conditions that a tablet is exposed to vary greatly between the FTA and the paddle apparatus, as reviewed by Todaro *et al.* [16].

1.2.1.1. USP apparatus 2

The fluid flow in the paddle apparatus has been characterized by computational fluid dynamics (CFD) and the data validated with experimental visualization techniques. In CFD models, the geometry of the apparatus is defined – and, if included in the model, the geometry of the dosage form is defined as well –, and the boundary conditions are set. A mesh acting as a numerical grid is applied to the fluid body in order to discretise the complex geometry into well-defined cells where the partial differential equations governing fluid flow can be solved by the software.

CFD has been used in a wide range of applications in the pharmaceutical manufacturing process beyond dissolution such as tabletting, die filling, granulation, drying, and disintegration [17].

The dominant velocity component in the paddle apparatus is tangential [16, 18] with two recirculation loops existing below and above the impeller [19]. Above the impeller, fluid is ejected from the impeller upwards next to the wall and back down midway between the wall and the blade [20]. Below the impeller, fluid is pushed downwards next to the wall and back up in the centre of the vessel. There is a dead zone of very low fluid velocity underneath the impeller down to the vessel bottom [19]. This is usually where a tablet is located [14], but, as the tablet is dropped at the beginning of the test it can land in different positions along the vessel bottom or change location during the test [19]. Tablet location will result in different dissolution rates, because of exposure to different velocity fields and shear rates along the vessel bottom [19, 21, 22]. CFD simulations were used to interpret centred versus off-centred tablet dissolution by D'Arcy *et al.* [21] who found that the dissolution rate was increased when tablets were moved 13 mm from the centre of the base. Bai *et al*. [22] also found a correlation between the CFD predicted strain rates in the base of the vessel and the faster dissolution of off-centred disintegrating and non-disintegrating tablets compared to centred tablets. Centred tablets are exposed to the very low fluid flow that occurs under the blade and their dissolution rate is slower. Off-centred tablets are exposed to higher maximum fluid velocities and present faster dissolution profile, due to thinner boundary layers associated with higher local velocities promoting a faster mass transport [19, 21, 22]. Therefore, tablet displacement from the centre can result in a failed quality control (QC) test according to the USP or the Food and Drug Administration (FDA) acceptance criteria.

Minor geometrical variations can alter the typical flow field observed in the dissolution vessel [23]. Bai *et al.* [15], Johansson *et al.* [24] and, more recently, Perivilli *et al.* [25] concluded that the symmetricity of the blade in the vessel had a more significant impact than factors which do not alter vessel symmetry such as clearance, that is the distance between the end of the blade and the bottom of the vessel. When the blade is off-centred, the

low velocity region is disrupted, resulting in a more robust dissolution environment [16, 26]. Wang *et al.* [27] modified the standard USP apparatus 2 so that the impeller was 8 mm off-centre demonstrating faster dissolution rates. Moreover, the resultant dissolution profiles proved to be independent of tablet location, contrary to the compendial apparatus. Similarly, in the PEAK vessel, the low shear rate zone at the bottom of the vessel is replaced by an inverted cone, which is surrounded by a ring of high shear rates that the tablet will be exposed to, such that the dissolution rate is expected to increase [26] even though the recirculation loops and shear rate distribution in the fluid are similar to the standard configuration.

Another alteration of symmetry in the vessel is the presence of a probe to automate the sampling process, which can alter the hydrodynamics leading to higher dissolution rates [28].

Finally, changing the agitation speed could also affect the hydrodynamics and the dissolution rate of tablets. Increasing the agitation speed changes the magnitude of the shear rate but does not improve shear homogeneity [19, 29]. In the region underneath the blade, the velocity profile remains very low independently of the rotation speed. In this area, coning can occur, which is the accumulation of particles near the bottom vessel due to insufficient agitation. Coning can be reduced by increasing the agitation speed because the increase in tangential velocity can cause the particles to move to regions of the vessel where the axial and radial velocities are high enough to lift them [26, 30]. Mathematical equations can be used to predict the minimum rotation speed needed to avoid the coning phenomena for different types of particles [31, 32].

Concern on whether good mixing is achieved in the USP apparatus 2 has also been reported in literature. Stamatopoulos *et al.* [33] showed poor mixing as viscosity was increased in the mini-paddle apparatus, a miniaturized version of the conventional USP 2 paddle apparatus that requires a smaller volume (100 ml) and permits the use of a smaller drug mass. The two recirculation loops and the region of low velocity under the blade observed in the conventional paddle apparatus are also present in the mini-paddle apparatus. The poorer mixing as viscosity increases could be due to a change from turbulent to laminar flow pattern [34] or to the presence

of the two recirculation loops that could generate mixing problems when viscous medium is used [13].

1.2.1.2. USP apparatus 4

Lower Reynolds numbers [35, 36] and lower maximum fluid velocities [37] are found in the FTA compared to the paddle apparatus when operating at standard conditions. Due to the semi-sinusoidal flow profile, fluid velocity is time dependent. There is a discharge phase in which the fluid is introduced into the cell and a suction phase where the inflow velocity is zero.

The flow profile in the FTA has been characterized by visualization techniques such as Magnetic Resonance Imaging (MRI) [38] or Particle Image Velocimetry (PIV) [39]. Hydrodynamics have been studied as a function of flow rate, cell size, pump type, presence of glass beads and location and orientation of a tablet. More uniform conditions were found at lower flow rates with the bigger cell size (22.6 mm).

In the 12 mm cell, axial local velocities increase uniformly through the cell during the discharge phase but are zero close to the wall. During the suction phase, the axial velocities are close to zero and there is re-circulation at the higher flow rates. The flow field is homogeneous when operating at 4 or 8 ml min^{-1}, but heterogeneous at 16 ml min^{-1} [37].

In the 22.6 mm cell, flow velocities are lower and less variable than in the 12 mm cell due to a larger cross-sectional area for the fluid to flow through. When operating at low flow rates (<8 ml min^{-1}), the velocities are negative during the suction phase, indicating downward flow. This is thought to be due to natural convection arising from temperature gradients between the warmer wall and the cooler centre of the cell [40], but CFD simulations have shown the occurrence of flow reversal without any temperature variation [41]. Flow reversal can also arise from natural convection due to a relative increase in medium density around a tablet surface as the tablet dissolves, particularly for a rapidly dissolving substance [41, 42].

When operating with no glass beads, an uncommon configuration, a relatively uniform and symmetric velocity distribution is predicted above the ruby bead during the discharge phase, but the velocity profile is non-uniform and asymmetric during the suction phase [43]. When operating with glass

beads, the flow is more periodic but not completely homogeneous and flow reversal is seen during the suction phase because the fluid is moving against an adverse pressure gradient [44].

Differently oriented tablets are exposed to different hydrodynamics, and this can influence the release rate. In Shiko *et al.* [45] they used a new MRI technique to visualize the three-dimensional flow field around a dissolving tablet. It proved to be heterogeneous, leading to a non-symmetric erosion of a tablet. The faces exposed to a higher velocity showed higher erosion rate, showing the importance of local hydrodynamics in dissolution. Horizontally placed tablets experience higher local axial velocities because of a lower cross-sectional area available for the fluid to flow compared to vertically oriented tablets [38].

Despite the effects of apparatuses' hydrodynamics on dissolution not being fully characterized, compendial apparatuses are used for a variety of applications, which range from QC to biopredictive dissolution testing.

1.3. Applications of *in vitro* dissolution testing

Dissolution tests are applied during preformulation studies, to characterise an API; during formulation development to select appropriate dosage forms and excipients; and in QC to check batch-to-batch consistency, similarity to the original trial batch and effects of product storage [46]. The FDA has set procedures on how to carry out dissolution tests, standard conditions and acceptance criteria [47]. Compendial media as defined by the FDA are typically used for QC purposes.

Although most commonly applied to solid oral dosage forms, it is important to note that dissolution test procedures have been described in the literature for many types of dosage forms, as reviewed by Brown *et al.* [48]. Examples in the literature include an *in vitro* dissolution test developed for lozenges formulations [49, 50] and an *in vitro* test based on the flow-through cell or reciprocating holder equipped with dialysis membranes in different positions for oily suspensions of paracetamol and prednisolone [51].

Dissolution testing has evolved into applications with a more bio-predictive, patient-centric goal [52]. To understand the relevance of *in vitro* dissolution

testing in the bio-predictive field, the definitions of bioavailability and bioequivalence must be clarified.

Bioavailability is the proportion of administered dose of the drug that reaches the systemic circulation unchanged and is available to produce its desired effect. Bioavailability studies are usually performed by measuring the concentration of the drug in the blood after administration of the drug following a non-intravenous dose and an intravenous dose, where the drug is administered directly into the systemic circulation [53].

Bioequivalence (BE) studies are clinical tests designed to compare the performance between two or more drug products [54]. Two medicinal products containing the same active substance are considered bioequivalent if their bioavailability rate and extent after administration in the same molar dose and similar experimental conditions lie within acceptable predefined limits [54, 55]. These limits are set to ensure *in vivo* safety and efficacy. For that, pharmacokinetic (PK) parameters obtained in a clinical study under fasting conditions are compared: the area under the curve (AUC) and the maximum plasma concentration (C_{max}). AUC is related to the total amount of drug absorbed into the systemic circulation. C_{max} is the maximum concentration of drug in plasma reached after the administration of a single dose [56] . For these parameters the 90% confidence interval (CI) for the ratio of the test and reference products should be contained within the acceptance interval of 80 -125% [55].

Apart from demonstrating BE through human studies, BE could potentially be predicted *in silico* reducing the number of clinical trials [57, 58]. As input to said *in silico* models, *in vitro* biopredictive dissolution data is needed as it is expected to increase the likelihood of a successful prediction when compared to dissolution data obtained with compendial media [59].

Dissolution tests can be used to eliminate the need to carry out a BE study for certain drugs through the acquisition of a biowaiver, if the similarity between the reference and test products in terms of bioavailability is sufficiently demonstrated [55]. A biowaiver is a regulatory process that enables the approval of the test drug based on *in vitro* data which replaces a human BE study [60]. Biowaivers reduce the number of clinical studies,

time and costs of development. Biowaivers can be granted for different strength products, provided BE has been demonstrated for the highest strength product or based on the Biopharmaceutics Classification System (BCS) [55].

The BCS is a tool which can help the biowaiver granting process for certain drugs based on their permeability and solubility profile.

1.3.1. Biopharmaceutics classification system (BCS)

BCS is a tool to identify the rate-limiting step in intestinal absorption of the API, on the basis of their aqueous solubility and intestinal permeability (**Table 1.1**) with the aim of improving the efficiency of the drug development process [61].

Table 1.1. Biopharmaceutics Classification System [62].

Class I	**Class II**
High solubility	Low solubility
High permeability	High permeability
Class III	**Class IV**
High solubility	Low solubility
Low permeability	Low permeability

BCS classification was originally developed by Amidon *et al.* [62] as a means to correlate *in vitro* dissolution, solubility and permeability with *in vivo* bioavailability. The originally proposed BCS was refined by narrowing the required solubility pH range from 1.0-7.5 to 1.0-6.8, incorporating biorelevant media in solubility determinations to account for bile salt effects and lowering the high permeability requirement from 90% to 85% absorbed [63]. Further refinements to the BCS yielded the Developability Classification System (DCS) [64], that was then updated to the Refined DCS (rDCS) [65]. The rDCS categorizes drugs based on factors that will influence their absorption like their upper small intestinal solubility rather than gastric solubility (except for weak bases), solubility in biorelevant media instead of compendial USP buffers and dissolution specifications in terms of a

maximum particle size distribution (PSD) above which dissolution becomes the rate-limiting step to oral absorption.

Tsume *et al.* [66] proposed a simple extension of the BCS classes to include sub-specification of acid (a), base (b) and neutral (c) for classes II and IV as a step towards developing more *in vivo* predictive dissolution (IPD). Another development to the BCS was the Biopharmaceutics Drug Disposition Classification System (BDDCS) by Wu and Benet which considers metabolism as a surrogate of permeability due to the difficulties in determining the latter [67, 68]. They propose using the rate of metabolism rather than absorption to classify drugs into class I, as if >90% of the administered dose is metabolized, it implies that the drug has been absorbed.

The BCS has been adopted by the FDA in guidelines for biowaiver granting. According to the FDA [54], a drug substance is considered highly soluble when the highest strength is soluble in ≤250 ml of aqueous media within the pH range of 1 - 6.8 at 37 ± 1°C. A drug substance is considered highly permeable when the systemic bioavailability or the extent of absorption in humans is ≥85% of an administered dose using a mass balance determination or in relation to an intravenous reference dose. An immediate release (IR) drug product is considered rapidly dissolving when a mean of ≥85% of the labelled amount of the drug dissolves within 30 min or very rapidly dissolving when a mean of ≥85% of the labelled amount of the drug dissolves within 15 min, using USP Apparatus 1 at 100 rpm or Apparatus 2 at 50 rpm in a volume of 500 ml (or 900 ml when appropriately justified) in each of the following media: (1) 0.1 N HCl or Simulated Gastric Fluid (SGF) USP without enzymes; (2) a pH 4.5 buffer; and (3) a pH 6.8 buffer or Simulated Intestinal Fluid (SIF) USP without enzymes [47].

Biowaivers can be granted for class I and class III drugs in IR solid oral dosage forms that exhibit rapid or very rapid *in vitro* dissolution using the recommended test methods [54, 63]. Class II drugs, for which dissolution is the rate-limiting step, represent 30% of marketed drugs and 60-70% of the new chemical entities [69], therefore it would be desirable to extend biowaiver applications to this class of drugs, as discussed by Loisios-Konstantinidis *et al*. [70], considering that formulation strategies can

overcome the challenge of poor solubility associated with class II drugs, as reviewed recently by Soliman *et al.* [71].

Ibuprofen was used as a sample drug in this work. It is a weakly acid drug belonging to class II according to the BCS classification [72], with high permeability and pH-dependent solubility, low at pH 1.2 (0.038 mg ml^{-1} [72]) and 4.5 and high at pH 6.8 (3.37 mg ml^{-1} [72]). However, according to the DCS classification, ibuprofen is a class I drug due to its high solubility in the intestine, which is its main site of absorption [64] and it could potentially be granted a biowaiver, as proposed by Potthast *et al.* [72]. Due to its weakly acidic nature, ibuprofen was selected as a good drug candidate with which to study the effects of solubility, fluid velocity and fluid density on *in vitro* drug dissolution.

In order to determine solubility, permeability and dissolution, biorelevant media can be used to overcome some of the limitations associated with compendial media such as the lack of bile salts, and the deviations in buffer capacity, osmolality and surface tension compared to gastrointestinal (GI) fluids [73].

1.3.2. Biorelevant media

Biorelevant media attempt to resemble the physicochemical properties of GI fluids as closely as possible, but they should also be reproducible, economical and easy to analyse [74]. They are used (a) to understand how a drug product will release a drug *in vivo* (b) to help select formulation and dosing conditions (c) to predict formulation and food effects on dissolution (d) to help optimize dosing conditions in PK studies (e) to assess the BE of post-approval formulation changes (f) to increase the likelihood of successful *in vitro-in vivo* correlations (IVIVC) compared to compendial media and (g) to understand the effect of solubilization on amorphous solid dispersion formulations [75, 76].

1.3.2.1. History and composition of biorelevant media

The fact that biorelevant media could increase the accuracy of oral absorption predictions with *in vitro* dissolution tests was proposed in 1998, when media composition for both gastric and intestinal environments in fed and fasted states were proposed [77]. Since their initial proposition, these

media have been revised and updated and snapshot media to represent a time frame after meal ingestion has been suggested [75, 76, 78-81]. The composition and properties of fasted and fed state gastric media (FaSSGF and FeSSGF) and fasted and fed state intestinal media (FaSSIF and FeSSIF) are summarized in **Table 1.2**. Markopoulos *et al.* [82] classified these dissolution media into four levels of increasing complexity, guiding the selection of media depending on API and formulation characteristics: Level 0 are aqueous solutions which pH is adjusted to represent one section of the GIT; in Level I media both pH and buffer capacity are adjusted to reflect physiological values; Level II media includes bile salts and digestion products; Level III media includes enzymes, viscosity effects and luminal hydrodynamics.

Media to simulate fasted and fed state colonic fluids (FaSSCoF and FeSSCoF) which could more closely predict the solubility of poorly soluble compounds in the colon than plain buffers have also been developed and are shown in **Table 1.3** [83].

FaSSIF and FeSSIF were tested with BCS class I and II drugs [77, 78]. Their potential to predict *in vivo* PK profiles compared to compendial media as well as *in vivo* formulation and food effects was assessed with orally administered poorly-soluble lipophilic drugs belonging to BCS class II [84, 85]. In some cases, biorelevant media were demonstrated to perform better than compendial media. For example, the prediction of the *in vivo* performance of a low aqueous solubility drug in the fasted state was enhanced with the use of biorelevant media [86]. Medium proposed by Jantratid *et al.* [87] but with the inclusion of digestive enzymes was tested by Diakidou *et al.* [88] for fed state gastric solubility prediction. Milk digested with pepsin and lipase could predict the fed state solubility of ketoconazole and dipyridamole after 60 min of meal intake, highlighting the importance of biorelevant media and digestion simulation for predicting fed solubility. Dissolution of ibuprofen minitablets in diluted human gastric fluid (HGF) was shown to be similar to dissolution in FaSSGF in recent work presented by Rivera *et al.* [89].

Mann *et al.* [90] and Butler *et al.* [91] concluded that there is high interlaboratory reproducibility when performing dissolution tests in

biorelevant media in the paddle apparatus both in single medium and dual media, that is simulating stomach to intestine transfer. Reppas *et al.* [92] also found good comparability across different laboratories when predicting food effects using biorelevant media with two modified release (MR) products in the USP apparatus 3 and the USP apparatus 4.

Despite the advances and successful applications of biorelevant media, some parameters need further consideration. Viscosity is currently only considered as part of Level III biorelevant media for the fed state based on the complexity levels proposed by Markopoulos *et al*. [82]. The current work aimed to explore whether the incorporation of viscosity enhancing agents (VEAs) to represent the slightly increased viscosity of the fasted state compared to aqueous buffers would affect *in vitro* dissolution results and bioavailability predictions.

Table 1.2. Composition and properties of fasted and fed state simulated gastric and intestinal fluids [81].

Composition	FaSSGF	FeSSGF	FaSSIF-V2	FeSSIF-V2
Sodium taurocholate (mM)	0.08	-	3	10
Lecithin (mM)	0.02	-	0.2	2
Pepsin (mg ml^{-1})	0.1	-	-	-
Hydrochloric acid (mM)	25.1	-	-	-
Glacial acetic acid (mM)	-	17.1	-	-
Sodium acetate (mM)	-	29.8	-	-
Milk/Buffer	-	1:1	-	-
Maleic acid (mM)	-	-	19.12	55.02
Glycerol monooleate (mM)	-	-	-	5
Sodium oleate (mM)	-	-	-	0.8
Sodium hydroxide (mM)	-	-	34.80	81.65
Sodium chloride (mM)	34.2	237.0	68.62	125
Properties				
pH	1.6	5.0	6.5	5.8
Osmolality (mOsm kg^{-1})	120.7± 2.5	400	180±10	390±10
Buffer capacity (mmol L^{-1}/ΔpH)	-	25	10±2	25±2
Surface tension (mN m^{-1})	42.6	52.3±0.3	54.3	40.5±0.2
Recommended volumes (ml)	300	500	200	1000

Table 1.3. Composition and properties of fasted and fed state simulated colonic fluids [83].

Composition	FaSSCoF	FeSSCoF
Buffer species	Tris/Maleates	Tris/Maleates
Proteins (mg ml^{-1})	3	3
Carbohydrates (mg ml^{-1})	0	14
Bile salts (µM)	150	600
Long chain fatty acids (µM)	100	200
Phosphatidyl choline (µM)	300	500
Properties		
pH	7.8	6.0
Osmolality (mOsm kg^{-1})	196	207
Buffer capacity (mmol L^{-1}/ΔpH)	16/26	15/14
Surface tension (mN m^{-1})	51.4	50.4

Another application of *in vitro* dissolution testing is the establishment of *in vitro-in vivo* correlations (IVIVC).

1.3.3. *In vitro-in vivo* correlations (IVIVC)

IVIVCs are predictive mathematical models which define the relationship between an *in vitro* property, usually dissolution rate, and an *in vivo* response or absorption profile [93]. Level A is a linear point-to-point correlation between the *in vitro* dissolution profile and the *in vivo* response such as plasma drug concentration or amount of drug absorbed. Level B compares two summary statistical data points e.g. the mean *in vitro* dissolution time versus mean *in vivo* dissolution time. Level C is a single point relationship between an *in vitro* parameter e.g. time to 50% dissolution with an *in vivo* PK parameter (C_{max}, T_{max}, AUC). Even though level A is considered the gold standard, a survey in 2017 found that for IR products, level C correlations were more common than level A [94].

Some surveys conclude that IVIVCs are mostly used to set dissolution specifications, gather mechanistic understanding and to develop extended

release (ER) formulations [94, 95]. Even though IVIVC development, evaluation and application is presented in a regulatory FDA document [60] and the establishment of IVIVCs is encouraged from a regulatory perspective [96], the rate of success of applications containing IVIVCs is only 40%. Identified areas of improvement included the quality of clinical data (e.g. *in vivo* data has to come from human fasted studies preferably, rather than animal data or fed state human data), the complexity of the dissolution method (compendial *in vitro* setups are normally not able to capture GI conditions and there can be issues with accessibility to more sophisticated dissolution apparatuses); deficiency of time and resources; uncertainty around regulatory acceptance or inability to meet regulatory thresholds and appropriate selection and generation of formulations for development and validation (at least three formulations with different release rates are necessary) [94-96].

Many examples can be found in the literature where IVIVCs were established for different drugs, including ibuprofen. In a recent paper published by Camara-Martinez *et al*. [97], a level A IVIVC was developed for IR ibuprofen tablets by reducing the buffer molarity in *in vitro* dissolution testing to represent the reduced buffering capacity in the GIT. In another recent example, an IVIVC was developed for two other ibuprofen formulations (fast release and liquid gel) by combining *in vitro* release and dissolution data using the non-compendial tiny-TIM method [1] with a PK model [98]. The tiny-TIM dissolution testing device is described in section "1.5. Biorelevant dissolution devices and setups".

In vitro dissolution testing also has a role in the trend towards implementing quality by design (QbD) in the pharmaceutical industry.

1.3.4. Quality by design in the pharmaceutical industry

The traditional approach to pharmaceutical product development has been the design and manufacture of a product upon which end-point testing is carried out. In this manner, it is assessed whether the product meets the set regulatory criteria, such as that defined by the FDA [47]. These criteria are usually strict and rigid, and there is a possibility of batches not meeting them

[1] Information on the tiny-TIM setup can be found in www.thetimcompany.com

because of slight variabilities in the manufacturing process that are poorly understood and require extensive investigation. The concept of pharmaceutical quality was implemented in 2004 as the suitability for therapeutic use and the absence of risks associated with unexpected contamination [99]. The aim of QbD studies is to obtain a product by predefining the final quality characteristics or clinical outcome that it has to meet and gaining a complete understanding of the process and potential sources of variability [100]. QbD emphasises the establishment of a relationship between critical quality attributes (CQAs), critical material attributes (CMAs) and critical process parameters (CPPs) [100, 101]. CQAs refer to the properties of output material whereas CMAs refer to the properties of input material to a defined unit operation such as particle size, dissolution or polymorphic forms. CPPs are manufacturing process parameters that influence the resulting product significantly such as roller force in granulation or compaction pressure in tabletting [102].

QbD can serve to identify a safe space, which is a specification region within which composition and manufacturing variations will not make a significant difference to the *in vivo* bioavailability even though some variation in dissolution performance may occur [58]. Mathematical modelling can support the implementation of QbD in the pharmaceutical industry through safe space design, as reviewed recently by Destro and Barolo [103]. Physiologically based pharmacokinetic modelling (PBPK) can predict the effect of changes in CQAs, CMAs and CPPs on *in vivo* pharmacokinetics [101].

The biopharmaceutics risk assessment roadmap (BioRAM) is an integration of pharmaceutics and QbD [104]. The aim of BioRAM is also to optimise and guide drug development by defining the intended therapeutic outcome to ensure maximal health benefit to the patients [105]. It identifies the drug product attributes and process parameters that are critical to achieving the *in vivo* drug performance, for example, polymorphic transitions, particle size or humidity levels [106]. BioRAM advantages include the detection of manufacturing issues before major clinical trials are carried out as well as improving the efficiency of the drug development process [105].

In vitro dissolution testing for bio-predictive purposes can capture the features of the GIT to some extent, but there are still some gaps that have to be considered, which are reviewed in the next section.

1.4. Limitations of *in vitro* dissolution testing

1.4.1. Buffer capacity

The buffer capacity is the ability of a buffer system to resist the effect of acid and base additions without pH changes. Measured physiological buffer capacities are presented in **Table 1.4**.

The use of USP 50 mM phosphate buffer, with a buffering capacity of 29 mmol $L^{-1}/\Delta pH$, has been questioned as the main buffering species in the intestine is bicarbonate, which has a 5 to 12 times lower buffering capacity. Even the USP SIF (18.4 mmol $L^{-1}/\Delta pH$) and FaSSIF (12 mmol $L^{-1}/\Delta pH$) have higher buffering capacities than the fasted intestinal fluid [107].

The lower buffering capacity of bicarbonate buffer implies that it is not as effective as phosphate buffer at counteracting the reduction of the surface pH that occurs as an acidic drug dissolves, therefore the difference between bulk pH and surface pH is larger *in vivo* than *in vitro*, which might lead to the overprediction of the dissolution rate of weak acids [108, 109]. In a recent publication, Camara-Martinez *et al.* found no differences in ibuprofen release from two tablet formulations when investigating BE in the commonly used 50 mM phosphate buffer and attributed it to the high buffer molarity of the buffer driving the surface pH closer to the bulk pH resulting in low discriminatory power of the test [97].

Lower buffered media and bicarbonate buffer have been proposed to be used in *in vitro* testing to make it more biorelevant [110-113], although, bicarbonate buffer is not used routinely due to the need to sparge CO_2 to maintain the pH, with the subsequent formation of bubbles that can alter hydrodynamics and the volatility of the gas [113, 114]. However, a surrogate concentration of phosphate buffer has been determined in order to match the dissolution of ionizable drugs in bicarbonate buffer and ranges from 1-25 mM, depending on the drug solubility and pKa [113, 115]. It was observed that the lower buffer capacity biorelevant medium was more

discriminating of the dissolution of enteric coated pellets in the FTA. However, a recent report by Matsui *et al*. [116] described an observed over-discrimination in some cases when lower buffer capacity media was used, predicting bio-inequivalence even for a drug where BE had been observed *in vivo*. Even though this is acknowledged, the focus of the current work was not to explore the effect of buffer molarity on dissolution and therefore the most up to date recommendations from USP were followed for media preparation [117].

Table 1.4. Measured physiological characteristics of GI fluids. Values extracted from [118-121].

	Stomach		Duodenum		Colon	
	Fasted	Fed	Fasted	Fed	Fasted	Fed
Buffer capacity (mmol $L^{-1}/\Delta pH$)	7-18	14-28	5.4±0.1	18±0.8	21.4	37.7
pH range	1.4-2.1	4.3-5.4	5.8-6.5	6.0-6.7	-	-
pH median	1.7	5.0	6.1	6.3	7.8	6.0
Surface tension (mN m^{-1})	41.9-45.7	30-31	34.3	26.4	47.9	39.2
Osmolality (mOsm kg^{-1})	140	559	189	372	81±102	224±125
Bile salt concentration (mM)	-	-	3.52	8.91	-	-

1.4.2. GI pH

Measured pH values are presented in **Table 1.4**. The fluid in most GIT regions has a variable pH of up to 2 pH units, which is hard to replicate in *in vitro* dissolution, plus a time-dependent variability, especially in the fed state, where gastric pH levels are restored to fasted state acidic values after

2-4.5 hours [120]. *In vitro* dissolution conditions of pH are usually static and can only represent one location within the GIT, but this can be partly overcome with transfer models, discussed in section 1.5. “Biorelevant dissolution devices and setups”.

1.4.3. Surface tension

Surface tension of the medium has an effect on drug dissolution kinetics [122]. The measured surface tension in the GIT fluids is presented in **Table 1.4**. Surface tension in the colon is lower than water, higher than in the upper small intestine and decreases from fasted to fed state [121]. Surface tension is normally not measured or adjusted in *in vitro* dissolution testing.

1.4.4. Media osmolality

Osmolality affects fluid secretion and volume in the luminal tract thus altering drug dissolution and absorption of low-permeability drugs as exemplified in the recent work by Funai *et al.* [123]. Measured osmolality of GIT fluids is presented in **Table 1.4**. The values of duodenal osmolarity in fasted and fed state closely resemble those in V2 FaSSIF and FeSSIF (180 mOsm kg^{-1} and 390 mOsm kg^{-1}) [119].

1.4.5. Solubilization

Solubilization is the incorporation of an insoluble or partly soluble substance in an aqueous solution with the use of surface-active agents like surfactants [124].

Bile salts are present in both the fasted and fed state, but in higher concentrations in the latter, up to two to four times higher in the duodenum (**Table 1.4**) though with a qualitatively similar composition in both states [118]. This can lead to the solubility in fed state being higher than in fasted state for poorly water-soluble drugs, which was recently investigated *in vitro* with the sample drugs griseofulvin, ketoconazole and ibuprofen by Jamil and Polli [125].

The mechanism by which bile salts influence dissolution can be different even for the same drug families [126]. It can be mediated through increased wetting and exposed surface area or an increased solubilization via micelles. However, an increase in solubility mediated by bile salts does not

necessarily have to be reflected in a proportional increase in dissolution rate and absorption, as dissolution could be delayed because the diffusivity of the larger drug micelles is lower than that of the drug itself and absorption could be reduced due to bile salt micelles trapping the drug [127, 128].

1.4.6. Lack of an absorptive component in *in vitro* dissolution testing

Drug precipitation rates tend to be faster and dissolution rates slower *in vitro* than *in vivo.* One factor involved in this phenomenon is the absence of an absorptive sink in *in vitro* dissolution testing which can remove dissolved drug molecules as dissolution occurs [129]. Attempts to replicate absorption in *in vitro* dissolution testing are discussed in section "1.5. Biorelevant dissolution devices and setups".

1.4.7. Food effects

Co-administration of a drug with a meal can increase or decrease the drug oral absorption affecting its efficacy and safety profile [130]. Food ingestion can delay gastric emptying, increase fluid volume and acid secretion, increase bile salt concentration, increase splanchnic blood flow, vary metabolic enzyme activity, alter GI pH and alter hydrodynamics including viscosity [131].

Food effects can be explored with biorelevant media [132]. It is valuable to be able to predict *in vivo* food effects during the formulation development stages in advance of clinical studies [133]. For now, a clinical food effect is the only method accepted by regulatory authorities to demonstrate the impact of food on absorption, but several methodologies including *in vitro*, *in silico* or preclinical animal studies are being refined for the prediction of food effects, as presented in a recent review by Vinarov *et al*. [134].

A food effect for ibuprofen, the model drug in this work, was observed *in vivo* as the C_{max} for three ibuprofen formulations was consistently lower and appeared later when the dose was administered following a standardized breakfast likely due to larger gastric emptying time (GET) and an elevation of viscosity [135]. Koenigsknecht *et al.* [136] also observed that ibuprofen gastric levels were higher in the fed state due to a higher stomach pH after a meal, and the detection of ibuprofen in the intestine was delayed resulting

in lower plasma concentrations, suggesting that slow gastric emptying and transit dominated the appearance of ibuprofen in plasma.

1.4.8. Hydrodynamics

Hydrodynamic conditions are variable along the GIT, with different fluid volumes, flow profiles and agitation patterns [137].

1.4.8.1. Media volume

Berthelsen *et al.* [138] emphasised the importance of simulating a small biorelevant volume in *in vitro* dissolution testing and *in silico* for the prediction of *in vivo* absorption of a BCS class II drug. The volume of fluids in the fasted stomach is usually only in the order of 30–50 ml, which, with the contribution of 250 ml of co-administered fluid can get to a volume of around 300 ml, which is easier to achieve *in vitro* with the USP 4 or mini-paddle apparatus than with the USP 2 apparatus [87]. After administration of the FDA standard meal, the gastric volume increases, therefore, to simulate the fed stomach *in vitro* a volume of 500 ml would be more suitable [87]. Even without a meal, increasing the volume of administered water can increase the bioavailability of certain drugs [139].

Fluid in the small intestine is present in pockets separated by dry areas filled with gas, therefore dosage forms can be only partially exposed or not exposed at all to the fluid [140]. This situation is hard to replicate in compendial dissolution apparatuses where the dosage form is constantly exposed to the dissolution medium, although there have been some attempts with the reciprocating cylinder dissolution apparatus, recently presented by Wollmer and Klein [141], and the Stress Test device [142].

1.4.8.2. Motility patterns

The migrating motor complex (MMC) is the characteristic motility pattern of the fasted state, which starts in the stomach and travels along the small intestine. It consists of three cyclic phases. Phase I is a quiescent phase of around 60 min where few or no contractions are detected. In phase II contractions of increasing frequency and intensity are recorded over 20 to 30 min and in phase III intense contractions take place for 5 to 10 min [143]. Contractions in phase III are the only ones strong enough to relax and open the pylorus to a diameter large enough to allow the transfer of materials

such as non-digestible solids or dosage forms from the stomach into the intestine [143, 144].

It has been shown how, for ibuprofen, the time to phase III contractions after dose administration *in vivo* is a major determinant of its systemic exposure due to these contractions determining GET and transporting ibuprofen from the stomach (where there is negligible absorption) to the intestine [145]. In fact, Paixao *et al.* [146] found that gastric pH and motility events could explain 63% of the C_{max} variability among individuals after the administration of an ibuprofen tablet.

In the fed state, MMC is stopped and both segmenting and propagating contractions which mix the luminal contents and push them further through the GIT are observed [143]. Peristalsis is the movement of the contents towards the next section of the GIT. In the stomach the peristaltic contractions start in the antrum and move towards the pylorus at a speed of 0.5-5.5 mm s^{-1}, with a mean of 2.7 mm s^{-1} [147]. Peristaltic waves in the small intestine move at a velocity of 5-20 mm s^{-1} [148].

The fluid flows in both fed and fasted states are presented in **Table 1.5**. The values are lower than those normally used in the USP 4 apparatus, but flow rate values do not represent linear velocity as the cross-sectional area of fluid flow is not taken into account.

Table 1.5. Mean fluid flows (ml min^{-1}) from aspirates from healthy human volunteers extracted from [149].

	Fasted	Fed
Jejunum	0.73±0.11	3.00±0.67
Ileum	0.33±0.09	2.35±0.28
Terminal ileum	0.43±0.06	2.09±0.16

1.4.8.3. Pressures

Pressures experienced by the dosage form differ between prandial states [150]. Solid oral dosage forms can be exposed to pressures up to 250-300 mm Hg due to peristaltic activity during gastric emptying and intensive

contractions during phase III of the MMC [144], which correspond to periods of peak velocities up to 0.5 m s^{-1} [143].

These phases of high pressure can negatively affect MR dosage forms which are intended to deliver the drug to later areas of the GIT or to release the drug in a slowed and controlled manner, if the dosage form does not possess the sufficient mechanical stability to withstand such high pressures [143]. The high pressures might cause dose dumping which is the unintended loss of the MR characteristics of a dosage form and a subsequent sharp drug release and increase in absorption within a short period of time [150].

The lack of peristalsis in *in vitro* dissolution setups, which generates *in vivo* hydrodynamic and shear stresses, was found to be a major drawback in replicating tablet disintegration *in vitro* [151]. Attempts to simulate biorelevant pressure events are discussed in section “1.5. Biorelevant dissolution devices and setups”.

1.4.8.4. Residence times

The SmartPill (SmartPill® Corporation, Buffalo, NY, USA) is a cylindrical capsule ingested by a volunteer which contains pressure, pH and temperature sensors and calculates the residence times in each compartment of the GIT based on pH changes.

Residence times of a dosage form in each region of the GIT can be considered to different degrees of accuracy in *in vitro* dissolution testing. For the fasted state, gastric emptying depends on when the drug is ingested in relation to the motility cycle that is operative at the moment of ingestion (see section “1.4.8.2. Motility patterns”), but is thought to occur within one hour [152].

Residence time in the stomach is generally larger in fed than fasted state [150] but it is dependent on (a) the caloric content of the meal, with 2 kcal emptied per minute [153] (b) the meal composition and size, (c) the fat content, as the higher the fat content the more gastric emptying will be delayed, (d) the size and density of the particles or dosage form, as larger dosage forms have longer transit times and (e) whether a drug is dissolved or not, as small particles will travel faster through the GIT than the solid

dosage form [143, 150, 152]. Gastric emptying might be more clinically relevant for enabling formulations, weak bases, highly soluble and permeable drugs which are absorbed from the intestine and not the stomach, and enteric coated products.

Small intestine transit time is less dependent on formulation size and food intake and it is around 3-4 h for both states [143, 152]. Generally, drug absorption occurs in the small intestine due to its high permeability and surface area.

Transit in the colon can vary from hours to days [143, 152], and its low surface area results in lower drug absorption than in the small intestine for many drugs.

Studies have successfully replicated *in vivo* drug transit times with some *in vitro* and *in silico* models [154]. Generally, models consider infinite time for drug absorption, as they assume first-order kinetics of drug concentration change. To challenge the assumption of infinite absorption time, Macheras *et al.* [155, 156] recently developed an absorption model which considers a total transit time in the stomach and small intestine of 4.86 h, and this was defined as the time limit for absorption.

1.4.8.5. Viscosity

Viscosity in the fed state is much higher than in the fasted state. For example, the mean viscosity of the GI fluids in the fed versus fasted state at 100 s^{-1} was elevated 80-800 fold in the stomach and at least 100 fold in the intestine for 3-4 h after a meal [157]. Even in the fasted state, the viscosity of the HGF has been measured to be higher than that of SIF (0.817±0.012 mPa.s [158]) and water (0.700 mPa.s), due to the presence of protein, mucus and lipids, and it is in the range of 1.7-9.3 mPa.s at a shear rate of 50 s^{-1} [3].

Even a slight increase in the viscosity of the medium can affect drug dissolution rate and release from formulations. A lower intrinsic dissolution rate (IDR) of cinnarizine in aspirated HGF versus FaSSGF, whose viscosity is similar to that of water, was observed recently by Pedersen *et al*. [159]. Other examples include the delay in the dissolution of drug released from crushed tablets and suspensions in the presence of thickening agents,

which resulted in a medium viscosity of 1.1 to 1.7 mPa.s, in the paddle apparatus [160, 161] and the two-fold increase in tablet disintegration times with just a small increase in viscosity from 0.817 to 1.062 mPa.s (apple juice) or 3.367 mPa.s (orange juice) [158].

Extensive research has focused on predicting the effect of food on drug absorption *in vitro, in vivo* and *in silico* [131, 162-165]. Although the effect of food and consequent increase of viscosity on oral absorption has been computationally investigated [163-165] there has been less focus on the mechanistic effect of increasing medium viscosity on drug dissolution rate [2].

An increase in viscosity could decrease the dissolution rate through (a) a reduction in drug diffusivity, which is demonstrated in the Stokes-Einstein equation (St-E, (1.1)) [166], and which directly impacts the dissolution rate, as per the Nernst-Brunner equation (1.2) [167, 168] and (b) a reduction in particle relative velocity. On the other hand, an increase in viscosity could increase dispersal and suspension of particles resulting in a greater surface area being exposed to the dissolution medium. The effect of an increase in exposed surface area could partially mitigate against the reduction in dissolution due to reduced diffusivity. Therefore, the magnitude of the impact on dissolution of a moderate medium viscosity increase, such as that relevant to the gastric fasting state, is difficult to predict.

$$D = \frac{k_B T}{6\pi \mu_f R} \tag{1.1}$$

$$\frac{dm}{dt} = \frac{DA(C_S - C_b)}{h} \tag{1.2}$$

where in equation (1.1), D is the diffusion coefficient ($m^2\ s^{-1}$), k_B is the Boltzmann constant ($m^2\ kg\ s^{-2}\ K^{-1}$), T is temperature (K), μ_f is fluid viscosity (Pa.s) and R is the hydrodynamic radius of the particle (m). In equation (1.2), dm/dt is the dissolution rate ($kg\ s^{-1}$), A is the surface area of the particle

(m^2), C_S is solubility (kg m^{-3}), C_b is bulk concentration (kg m^{-3}) and h is the aqueous diffusion boundary layer thickness (m).

An increased viscosity can also reduce the relative velocity due to an increase in drag force, that would in turn increase particle velocity. Moreover, if the increase in viscosity is accompanied by an increase in fluid density, not only the drag force, but also fluid acceleration and buoyancy (the tendency of the particle to float) will increase, ultimately increasing upward particle motion.

To overcome some of the limitations of compendial *in vitro* dissolution testing, apart from biorelevant media, biorelevant dissolution devices and setups have been explored in the literature.

1.5. Biorelevant dissolution devices and setups

Even though apparatuses 3 and 4 allow easy change of the medium composition, volume and hydrodynamics compared to apparatus 2, which is commonly used in QC [133], more sophisticated *in vitro* methods have been developed to include *in vivo* upper GIT relevant hydrodynamics.

The lack of an absorptive component in *in vitro* dissolution can be partly overcome with the use of biphasic models which contain an organic phase to mimic partitioning into the intestinal membrane [169] or with dissolution/permeation setups, such as that described by Kataoka *et al.* [170]. Recent dissolution/permeation setups described in the literature provide an absorptive sink with either cell based (biological) or cell-free (artificial) membrane systems [171-174]. One example is the *in vitro* dissolution absorption system (IDAS2) which contains a cell monolayer to simulate permeation [175]. Dissolution/permeation systems have been shown to improve predictability of *in vivo* data when compared to using only dissolution data [176, 177].

Physio-grad® [2] was developed to overcome the limitation of a single pH value through the whole *in vitro* test and it enables a biorelevant simulation

[2] Information on the Physio-grad® setup can be found in https://physiolution.eu/grad/

of pH gradients by continuous monitoring and adjustment of pH with liquid and gaseous titrants [178].

Some reports conclude that the hydrodynamics in the paddle apparatus are not *in vivo* representative, as the peak forces that a tablet is exposed to are less aggressive in *in vitro* dissolution tests than *in vivo* and the peristaltic contractions which generate shear stresses upon the tablet are not captured *in vitro [91]*. Dissolution tools that are able to simulate peristalsis have been proposed e.g. Dissolution Stress test device [3], introduced by Garbacz *et al.* [142] or the further updated version, the Dynamic Open Flow-Through Test Apparatus [179], which aims to examine the robustness of formulations when exposed to biorelevant dynamic stresses and pressures.

Transfer models, as described by Kostewicz et al. [180], and later called two-stage dissolution, change the medium composition during the course of the test with two vessels representing the stomach and the intestine [181]. In the original transfer model, a peristaltic pump was used to transfer the contents from the stomach to the intestine with first-order kinetics simulating gastric emptying. However, two-stage dissolution tests can also be done by adding the medium simulating the intestinal phase, or a concentrated version of it, directly on top of the gastric medium (or vice versa), with the limitation of not reflecting *in vivo* gastric emptying [181]. Two-stage dissolution is particularly relevant in the case of a weakly basic drug, which has the potential to supersaturate and precipitate when it is transferred from the stomach into the intestine, due to the pH increase, for enabling formulations which are intended to supersaturate in the GIT as a mechanism of improving drug solubility or for MR dosage forms which are intended to deliver the drug to further sections of the GIT or to slowly release it along several sections of the GIT [143]. Some of the transfer models which have been described in the literature are reviewed below.

The TNO intestinal model (TIM-1), is a multicompartmental, dynamic system that uses biorelevant media, volumes, pH and hydrodynamics to simulate the upper GIT [182]. It contains two hollow fibre ultrafiltration modules for dissolved drug removal which account for the absorption in the

[3] Information on the Stress Test device can be found in https://physiolution.eu/stress/

GIT. TIM-1 can also be used to simulate food effects with increasing GETs and bile salt concentrations. The disadvantages of TIM-1 include its complexity and lower throughput compared to the standard apparatuses [183]. Tiny-TIM was developed to circumvent the complexity of TIM-1. It contains one, rather than three, intestinal compartments and has an updated stomach compartment which better reflects the shape and dynamic gastric conditions in humans [91].

In the artificial stomach-duodenum (ASD) [184] fluids flow from a stomach chamber into a duodenum chamber, where measured drug concentration is assumed to be proportional to the amount of drug absorbed. The Gastrointestinal Simulator (GIS) was developed based on the ASD and contains three chambers (stomach, duodenum and jejunum) in which the fluid secretions, gastric and duodenal motilities and GETs can be controlled [185].

The *in vitro* biorelevant gastrointestinal transfer (BioGIT) system simulates drug transfer from the stomach to the upper small intestine with the emptying of contents following first-order kinetics with a half-life of 15 min [186]. Additionally, pH, osmolality, buffer capacity and bile salts concentration can be controlled during the test. The BioGIT system was recently shown to be useful to predict the effect of dose or formulation on exposure in the fasted state for four different poorly soluble APIs [187].

The GastroDuo model simulates biorelevant pressures, peristalsis and gastric emptying as well as pH and temperature [188]. Drug emptying from the stomach as a solution or small particles can be quantified by dynamic UV measurements. GastroDuo can distinguish between formulations and aid formulation development, but it lacks an absorptive component.

In vitro fed state techniques have been developed, such as the Fed Stomach Model (FSM) which attempts to simulate the complex physiology in the fed state considering pressure events, dosage form movement, pH variations and GETs [189]. Food effects can also be explored *in vitro* by a simpler method in which the partitioning of the drug into a lipid-rich phase representing the fed state is measured [190].

Some attempts at developing individualized *in vitro* tests which incorporate variability in GI pH and transfer profiles on drug release has been made with the aim of improving the prediction of *in vivo* efficacy and safety [191, 192].

Parallel to the development of biorelevant dissolution tests, which can help ultimately predict drug bioavailability, the physical models underpinning dissolution have been described in the literature and implemented in dissolution simulation software.

1.6. History of mathematical dissolution models

Noyes and Whitney published the first ever dissolution study and proposed the first model for transport-controlled dissolution (1.3) [193]. They proposed that the rate at which a solid dissolves in its own solution (dC/dt; kg m^{-3} s^{-1}) is proportional to the difference between its saturated solubility (C_S; kg m^{-3}) and its concentration in that solution (C_b; kg m^{-3}) multiplied by a proportionality constant (k_{NW}; s^{-1}).

$$\frac{dC}{dt} = k_{NW}(C_S - C_b) \tag{1.3}$$

Then, Nernst [167] and Brunner [168] proposed that a saturated solution was formed around the solid particle and diffusion occurred from that layer of saturated solution to the bulk solution through a stagnant layer called a diffusion layer. The stagnant layer or aqueous diffusion boundary layer (ADBL) is defined as an unstirred or slowly moving layer of fluid surrounding the solid API particle within which the formation of a saturated solution in the solid/liquid interface is spontaneous and the concentration of solute decreases from saturation to bulk concentration due to solute diffusion (**Figure 1.6**). The diffusion of drug molecules from the stagnant layer to the bulk liquid determines the dissolution rate. The dissolution rate in the Nernst and Brunner model is expressed as per equation (1.2) in section “1.4.8.5. Viscosity”.

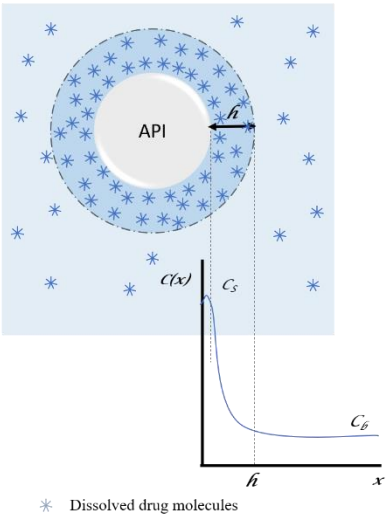

Figure 1.6. Diagrammatic representation of the dissolution of an API in a fluid. Molecules pass from the solid surface of the API to form part of the solution. Dissolved molecules diffuse from the areas of maximum concentration (API's surface) to the areas of least concentration (bulk medium) across a certain distance (x).

Considering agitation and diffusion in the dissolution apparatuses and assuming sink conditions, three equations ((1.4) – (1.6)) were derived by Hixson and Crowell [194], Niebergall [195] and Higuchi and Hiestand [196, 197] to describe particulate dissolution. Sink conditions can be defined as the situation when the solubility is much larger than bulk concentration and therefore bulk concentration can be considered negligible in the models [198] .

$$k_{1/3}\mathrm{t} = W_0^{1/3} - W^{1/3} \qquad k_{1/3}\mathrm{t} = \left(\frac{4\rho\pi}{3}\right)^{1/3} \frac{DC_S}{\rho h} \tag{1.4}$$

$$k_{1/2}\mathrm{t} = W_0^{1/2} - W^{1/2} \qquad k_{1/2}\mathrm{t} = \left(\frac{3\rho\pi}{2}\right)^{1/2} \frac{DC_S}{\rho k'} \tag{1.5}$$

$$k_{2/3}\mathrm{t} = W_0^{2/3} - W^{2/3} \qquad k_{2/3}\mathrm{t} = \left(\frac{4\rho\pi}{3}\right)^{2/3} \frac{2DC_S}{\rho} \tag{1.6}$$

Where W_0 is the particle weight at time 0, W is the particle weight at time t and k are composite constants.

Hixson and Crowell addressed the fact that surface area changes with time for the first time and derived the cube root law to link the rate of dissolution

to concentration, agitation and surface area (1.4) [194]. They stated that the cube root of the solid mass decreases linearly with time, which holds given the assumption that dissolution rate is proportional to the surface area of spherical particles. No assumptions are mentioned in their work in relation to the existence of a boundary layer.

Niebergall *et al.* [195] observed that the dissolution data for size fractions of three compounds were not well described by the cube root law proposed by Hixson and Crowell under an agitation of 500 rpm. They hypothesised it could be due to the cube root law not considering the dependency of the boundary layer thickness on particle size. They proposed a semiempirical expression in which the square-root of the solid mass decreases linearly with time, assuming that the boundary layer thickness is proportional to the square root of the mean volume diameter i.e. h is not constant (1.5).

Higuchi and Hiestand derived a two-thirds root expression which states that the solid mass to the power of two-thirds decreases linearly with time, assuming a constant boundary layer thickness which size is comparable or greater than the particle radius (1.6) [196, 197].

Each of these equations gives adequate fits to a set of dissolution data. These three models did not account for particle shape, as they assumed spherical particles, nor aggregation.

Wang and Flanagan [199] described a semiempirical equation to capture the dissolution rate of a spherical particle taking the curvature of the particle into account, which depended on the relationship between particle size and boundary layer thickness (h), which was assumed to be constant.

Hintz and Johnson [200] modelled the dissolution of polydisperse particles from a rotating disk using the Ranz-Marshall correlation to estimate h as a function of particle size and relative velocity. They derived a critical particle radius of 30 µm, below which the boundary layer thickness equalled particle radius and above which the boundary layer thickness was constant. The critical value was derived from rotating disk dissolution but correlated well with particulate dissolution profiles. De Almeida *et al.* [201] estimated h to be 22 µm for ibuprofen particles in suspension using the Coulter counter technique. In recent work, Andersson *et al.* [202] established a theoretical

relationship between the dependence of the hydrodynamic boundary layer with particle radius and fluid velocity which can be applied under different conditions to understand the mass transfer process during dissolution. Combining dissolution experiments in an aqueous flow medium with CFD simulations, they calculated the hydrodynamic boundary layer for particles of different initial particle sizes (18.8 to 52.3 µm) in four different fluid velocities (46-103 mm s^{-1}), finding a relationship between the hydrodynamic boundary layer thickness (h; m), particle radius (r_p; m) and fluid velocity (U_f; m s^{-1}) of the form $h \propto {r_p}^{3/5}{U_f}^{-2/5}$. This relationship was suggested on the basis of CFD simulations for particles of a radius ranging from 5 – 40 µm in a medium with fluid velocities ranging from 10 to 100 m s^{-1}.

Johnson *et al.* [203] applied the models presented by Wang and Flanagan and Hintz and Johnson but implemented particle size fractions. *h* was estimated from empirical data. This model assumes that the difference between particle density and fluid density is very small, and so all particles are expected to be suspended. This assumption differs from the model presented in the current work, in which it is important to determine particle movement, which depends on the relative velocity between the fluid and the particle.

Sugano *et al.* [204] applied the fluid dynamics theory to calculate the thickness of the hydrodynamic boundary layer. The mass transfer coefficient was calculated based on dimensionless numbers (Reynolds (Re), Schimdt (Sc) and Sherwood (Sh)) that describe particle and fluid properties through the Ranz-Marshall correlation. The Ranz-Marshall correlation was originally derived to describe evaporation rates of pure liquid droplets, and then used to describe the mass transfer from solid spheres under forced convection [205-207]. The computational model presented in this work is also based on the Ranz-Marshall correlation which is described in section "1.6.1. API dissolution simulation in SIMDISSO™".

Wang *et al.* [208] challenged some of the general assumptions made in the classical simulation models that may not be physically correct, the first one being the constant boundary layer thickness. They developed an exact analytical solution describing dissolution, the finite-domain model (FDM).

They further developed the model to include the simulation of the dissolution of polydisperse particles [209]. Another assumption made by the classical simulation models and challenged by these authors is the presence of sink conditions through the so-called confinement effect. Confinement is the increase in bulk concentration because particles are inside a limited physical container or vessel during *in vitro* dissolution, and this will affect the dissolution rate. Confinement can be negligible when bulk concentration is very small compared to solubility. This can happen if the volume available for dissolution is very large. If it is not, bulk concentration is not negligible with respect to solubility and should be considered. Agata *et al.* developed a mathematical model for predicting dissolution of spherical particles under non-sink conditions and applied it to predict the minimum diameter necessary to achieve BE [210]. In the current work, confinement effects were explored computationally by defining a limited volume surrounding the particle, which is available for that particle to dissolve in, before recirculating to the rest of the medium, in both the FTA and paddle apparatuses.

In a recent publication, Pepin *et al.* [211] developed mechanistic *in vitro* USP 2 models that account for dose effect, volume, solubility and micelle size as well as hydrodynamics (paddle rotation speed and medium viscosity) and coning due to both API and excipients, which were validated with *in vitro* dissolution profiles of 18 drugs. The models assumed that wetting is instantaneous, and all the surface is available for dissolution at time zero.

Apart from particulate dissolution in which particles are assumed to be individual spheres, models have been built for other release mechanisms, e.g., diffusion through a polymer layer. Caccavo *et al.* [212] developed a mechanistic mathematical model that was able to describe single pellet behaviour in terms of hydration, drug dissolution, diffusion, release and particle size. The pellets were composed of an inert core, the drug and a polymer layer. This model was extrapolated to mono- and polydisperse ensembles of pellets.

1.6.1. API dissolution simulation in SIMDISSO™

SIMDISSO™ is based on the fluid dynamics theory [204], which considers not only particle-related parameters but also hydrodynamic parameters

such as fluid velocity and viscosity. The software calculates a mass transfer coefficient through the Ranz-Marshall correlation [205, 206] and associates it with solubility and drug surface area to predict the dissolution rate at any moment in time.

The dissolution of a spherical particle can be described by the Nernst-Brunner equation (1.2). In the simulation model presented in this work, the boundary layer thickness (h) and the diffusion coefficient (D) in the Nernst-Brunner equation (1.2) are encompassed as part of the mass transfer coefficient (k, m s^{-1}) ($k = D/h$).

1.6.1.1. Dissolution rate calculation

To obtain the dissolution rate of a single spherical particle for each time step (dm/dt), the mass transfer coefficient (k) has to be estimated. This can be done by calculating the Reynolds number (Re), Schmidt number (Sc) and Sherwood number (Sh) for a particle with equations (1.7) – (1.11).

$$Re = \frac{|U_f - U_p| d_p}{\nu_f} \tag{1.7}$$

$$\nu_f = \frac{\mu_f}{\rho_f} \tag{1.8}$$

$$Sc = \frac{\nu_f}{D} \tag{1.9}$$

$$Sh = 2 + 0.6 Re^{1/2} Sc^{1/3} \tag{1.10}$$

$$Sh = \frac{k d_p}{D} \tag{1.11}$$

Where U_f is fluid velocity (m s^{-1}), U_p is particle velocity (m s^{-1}), d_p is particle diameter (m), ν_f is kinematic viscosity (m^2 s^{-1}), and ρ_f is fluid density (kg m^{-3}). The Ranz-Marshall correlation in equation (1.10) is valid for spheres within a 0 < Re < 300 range [213]. The Re, Sc and Sh numbers are dimensionless parameters used to describe diffusion and convection in the dissolution process [214]. Re in equation (1.7) is the ratio of momentum forces to viscous forces in a fluid in which the particle is moving, Sc in equation (1.9) is the ratio of kinematic viscosity to API molecular diffusion

and Sh in equation (1.11) is the ratio of mass diffusion to molecular diffusion of the API [35].

Once Sh is known, k can be extracted and with that the change in particle diameter from equation (1.12). Using particle number, particle density (ρ_p) (kg m^{-3}), and change in diameter with time, the total mass dissolved can be estimated over each time step and this will result in the generation of a dissolution profile in which percentage dissolved is plotted against time. The equations are solved with Matlab R2022a (MathWorks, Natick Massachusetts, USA) using the solver ode15s.

$$\frac{d(d_p)}{dt} = \frac{-2k(C_s - C_b)}{\rho_f} \tag{1.12}$$

$(U_f - U_p)$ in equation (1.7) refers to the relative velocity which is the difference between fluid and particle velocity. When particle motion is disabled in the code, U_p is set to zero and the particles are exposed to the full fluid velocity U_f. When particle motion is enabled, the particle velocity is calculated for each time step as the integral of their acceleration, *i.e.*, the sum of the forces acting over the particle divided by the apparent mass of the particle (m_p, kg) [1]. In these conditions, the mass transfer is determined by the relative velocity $(U_f - U_p)$ instead of the full fluid velocity U_f. The equations used to calculate those forces, except for the Basset history integral which is considered negligible, and the apparent particle mass are described in equations (1.13) to (1.18) where m_p is the apparent particle mass, F is force (N), g is gravitational acceleration (m s^{-2}) and b is the drag coefficient (N s m^{-1}). The apparent particle mass contains a contribution of the mass of the fluid that is surrounding the particle [213].

$$m_p \frac{dU_p}{dt} = F_{drag} + F_{buoyancy} + F_{fluid\ acceleration} + F_{Basset} \tag{1.13}$$

$$m_p = \rho_p \frac{1}{6}\pi d_p^3 + \frac{1}{2}\rho_f \frac{1}{6}\pi d_p^3 \tag{1.14}$$

$$F_{drag} = b(U_f - U_p) \tag{1.15}$$

$$F_{buoy} = -(\rho_p - \rho_f)\frac{1}{6}\pi d_p^3 g \quad (1.16)$$

$$F_{fluidacc} = \frac{3}{2}\rho_f \frac{1}{6}\pi d_p^3 \frac{dU_f}{dt} \quad (1.17)$$

$$b = 3\pi \mu_f d_p (1 + 0.15Re^{0.687}) \quad (1.18)$$

As mentioned in section "1.2.1. Hydrodynamics in the dissolution apparatuses", the dominant velocity component in the paddle apparatus is tangential [16, 18] and therefore gravity has to be turned off, as SIMDISSO™ is a reduced-order model that can represent only one dimension. Therefore, in the paddle apparatus there is one tangential velocity value input in the simulation (**Figure 1.7**). However, it could be useful to enable gravity in the paddle apparatus in combination with axial fluid velocities to study particle motion and whether sedimentation or floating of the particles occurs in the region of the vessel where opposing axial velocities encounter. Having these motion simulations aids when choosing to enable or disable particle motion. In the FTA, fluid flow is in the axial direction (**Figure 1.7**) and it can be constant or pulsating. As the fluid flow is in the axial direction, the gravitational force and density and buoyance effects are included in the simulation. The pulsating nature of the flow is shown in **Figure 1.8**.

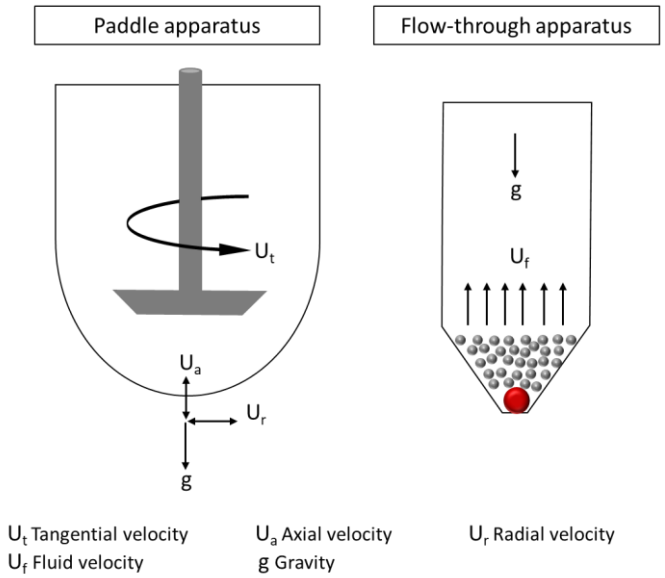

Figure 1.7. Vectorial representation of velocities (m s^{-1}) in the paddle apparatus and the FTA. Tangential velocity is the main velocity component in the paddle apparatus. In the FTA, areas of negative fluid velocity in the experimental cell setup are not accounted for in the diagram as the input fluid velocity is either positive or zero in the simulations, but negative (downward) particle velocity in the cell can be simulated [215].

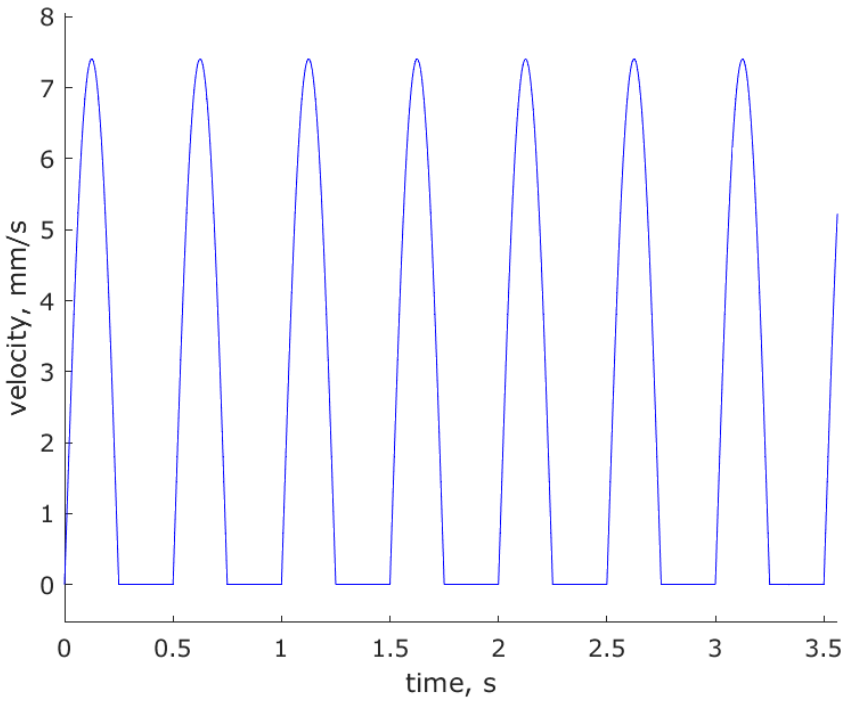

Figure 1.8. Simulated pulsing flow profile in FTA in a 12 mm diameter cell at 16 ml min^{-1} from SIMDISSO™.

In terms of particle diameter (d_p), an average experimentally obtained particle size can be used in SIMDISSO™, however, it is also possible to define different particle size bins to capture a PSD, which is expected to increase the accuracy of the prediction [200, 204]. When a PSD is used, each particle size bin dissolves at a rate based on its surface area and mass, but against a concentration gradient in which the total drug dissolved is calculated with a contribution from every bin. Any potential interactions between particles in the experimental setup are not currently considered in the simulations. As the particles dissolve, a new particle size is calculated for each time step, which will impact surface area and particle velocity, ultimately affecting the mass transfer rate at the next timestep.

Apart from the dissolution profile, other outputs from the simulation can be obtained as a function of time and they include forces acting on the particle, particle and fluid velocities, particle diameter change and concentration in the reservoir, in the cell and near the particle.

1.6.1.2. Bulk concentration calculation

One of the features of SIMDISSO™ is that it can capture the main relevant hydrodynamic effects of the *in vitro* system used. Though it operates in a similar manner for both the paddle apparatus and the FTA, there are substantial differences in the definition of bulk volume and concentration accounting for the particular configuration of each of the apparatuses.

In the FTA, the simulation allows three options to define bulk concentration: cell, reservoir and near-particle volume (NPV) (**Figure 1.9**). If the system is defined as a closed system, which was the selected option for this work, the medium recirculates from the cell into the reservoir and from the reservoir into the cell. If a NPV option is enabled, media flows directly from the reservoir into the NPV and then the mass released flows back into the cell, which is assumed to be ideally mixed. Finally, the new cell concentration is the inlet to the reservoir concentration in the next timestep.

For the paddle apparatus, only two options are available for bulk concentration calculation, whole vessel or NPV, with recirculation between them when the latter is enabled.

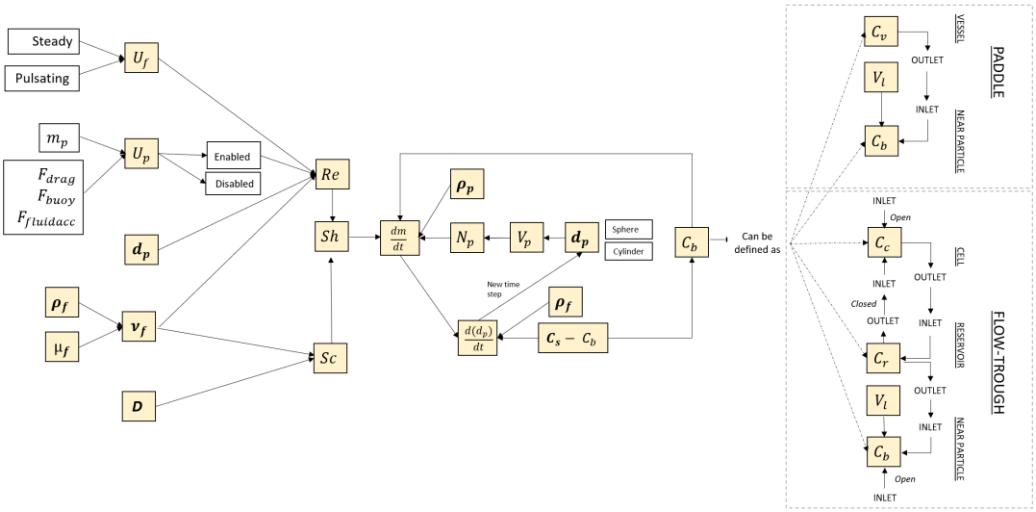

Figure 1.9. Schematic representation of the calculation of the dissolution rate for each timestep in SIMDISSO™ with an insight into how bulk concentration is calculated in each apparatus. C_c – cell concentration (kg m^{-3}), C_r – reservoir concentration (kg m^{-3}), C_v – vessel concentration (kg m^{-3}), V_l – NPV (m^3), V_p – particle volume (m^3), N_p – number of particles. Figure adapted from D'Arcy *et al.* [216].

1.6.1.3. Near-particle volume (NPV) approach in SIMDISSO™

The assumption that the particles have the whole volume of medium instantly available for dissolution can be reasonable in the paddle apparatus, but it may overpredict the dissolution rate in the FTA especially at low flow rates. In the paddle apparatus, unless poor mixing is detected, it is reasonable to consider a homogeneous distribution of drug particles in the dissolution medium and therefore using vessel volume as bulk volume would result in an accurate dissolution profile [217]. Nevertheless, as discussed earlier, there can be some regions of low velocity in the bottom of the vessel [19, 29] or some particular situations where the mixing is poor, for example, when highly viscous media is used [34], that could point to the need for redefining bulk volume as a more local volume to the particle when aiming for a more accurate simulated dissolution profile. In the FTA, this need is exacerbated as different concentrations are likely to be found between both cell and reservoir [16, 37], regardless of the mixing profile, due in part to the possibility for the operator to select different flow rates, pulse frequencies, pump settings, cell sizes and configurations and tablet

orientation. In this apparatus, having the whole reservoir, or even whole cell volume available may overestimate the dissolution rate. Providing a more local volume around the particle can render the simulated dissolution profile more accurate as the drug initially dissolves in a limited volume due to the low local fluid velocity regions and the zero velocity periods of the pulse. Even without considering this local volume, the difference in cell and reservoir concentrations is simulated in SIMDISSO^{TM}.

The possibility of choosing a local volume for dissolution was developed and implemented in SIMDISSO^{TM} for both apparatuses. The radial size of this local volume, called near-particle volume (NPV), is defined as a multiple of the particle radius as can be seen in **Figure 1.10**. In this work one particle radius was selected and compared to using cell volume as the relevant bulk volume for calculating the concentration gradient driving dissolution. In this manner, it is possible to determine which experimental conditions are most influenced by the alternative bulk volume option definition.

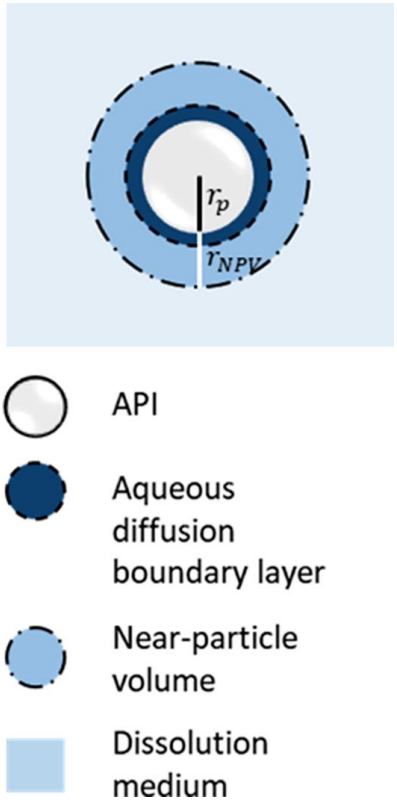

Figure 1.10. Illustration of spherical API particle with radius r_p (m), NPV, with radius extending a distance of one particle radius from the particle surface into the dissolution medium, aqueous diffusion boundary layer and dissolution medium surrounding each particle in the dissolution media. Figure extracted from [218].

By looking at the models describing dissolution, one can identify which are the most relevant parameters affecting dissolution.

1.6.2. Key parameters affecting dissolution

1.6.2.1. Solubility and precipitation

The solubility of a substance is the amount of it that has passed into solution when equilibrium between the solution and the excess undissolved substance is achieved [219] . Solubility defines the concentration gradient which drives dissolution. Dissolution is also driven by the distance over which this concentration gradient occurs, which is influenced by hydrodynamics [73].

When the concentration of drug molecules in solution exceeds its aqueous solubility, it is said to generate a supersaturated solution. This solution is thermodynamically unstable and will revert to the situation of saturation,

leading to the precipitation of the excess drug out of solution through the nucleation and growth mechanism. Nucleation is the formation of a small mass onto which the solid can grow, and growth is the addition of solute to said nucleation site [220]. Precipitation and absorption are competing processes in the GIT [221].

Due to the decrease in aqueous solubility with pH increase, weakly basic drugs supersaturate and can precipitate when transferred from the stomach to the intestine [221]. The rate of precipitation is not only dependent on the intrinsic characteristics of the drug itself, but also on the hydrodynamic conditions [222].

Carlert *et al.* [223] studied precipitation of a basic BCS class II drug *in vitro* with two simple two-step methods and found that the very rapid *in vitro* precipitation was not observed *in vivo*, concluding that simple *in vitro* methods overpredict precipitation *in vivo*.

1.6.2.2. Drug diffusivity

The diffusion coefficient of the solute in the dissolution medium is affected by the viscosity of the dissolution medium, the temperature and the molecular size of the diffusing molecules , as described in the St-E equation (1.1) [166].

As discussed in section “1.4.5. Solubilization”, recent work has shown the diffusivity of the larger drug micelles to be lower than that of the drug itself which could slow dissolution [125, 127].

1.6.2.3. Surface area and particle morphology

The surface area of the API directly influences the dissolution rate, according to the Nernst-Brunner equation (1.2). More particles of a smaller size will present a larger total surface area than the same number of particles of a larger size, therefore the overall dissolution rate will be faster for smaller particles. However, micronization can lead to aggregation of the particles and less surface area being exposed to the dissolution medium [73] due to the attraction forces between molecules in particles being stronger than between drug molecules and water.

Reducing particle diameter during dissolution will also result in a reduction of the Reynolds number, and therefore the mass transfer coefficient will decrease and so will the dissolution rate. As particle size decreases during dissolution, forces acting over the particle will change, altering the relative velocity and increasing the likelihood of particles being suspended and flowing with the fluid, which would, in turn, alter the dissolution rate [2].

Particle morphology is important as it dictates the area available for dissolution. Particle morphology is assumed to be spherical in many models, but this is not necessarily the case *in vitro* or *in vivo*. In the work recently presented by Abrami *et al*. [224, 225], the dissolution of polydisperse particles with three different shapes was simulated.

1.6.2.4. Fluid and particle velocity

Changes in relative velocity between fluid and particle will affect dissolution [215]. Theoretically, if the Ranz-Marshall correlation in equation (1.10) is applied to describe particle dissolution, an increase in fluid velocity would result in an elevation of the Reynolds number in equation (1.7), and the Sherwood number in equation (1.10), which would increase the mass transfer coefficient in equation (1.11) and the dissolution rate, as per the Nernst-Brunner equation (1.2). Moreover, an increase of fluid velocity which improves particle dispersal could enhance the surface area exposed directly increasing the dissolution rate. However, it is likely that the increase in fluid velocity will be accompanied by an increase in particle velocity, depending on particle and fluid density, and therefore the outcome will be more complex and difficult to predict, as it will depend on the relative velocity between fluid and particle in equation (1.7). The exploration of how particle motion affects *in vitro* and *in silico* dissolution was one of the aims of the present work.

1.6.2.5. Bulk concentration and available volume

Increasing bulk concentration decreases the dissolution rate and it is influenced by the volume available for dissolution, as a larger volume will result in a lower bulk concentration, and by the removal of drug molecules through absorption [208].

Bulk concentration can be considered uniform throughout the dissolution volume, or, in sink conditions, it can be considered negligible compared to solubility. In this work, an approach to simulate a non-uniform bulk concentration, the NPV approach was investigated.

1.6.3. Advantages of mechanistic *in vitro* dissolution simulations

Mechanistic dissolution simulations can help select the optimal conditions in which to run *in vitro* tests, reducing time, costs and waste associated with experimental testing [226-228].

Mechanistic models can help formulation scientists to simulate and better understand the effect of varying experimental conditions or CPPs or CMAs on the *in vitro* dissolution profile or drug behaviour [229].

Finally, they can enhance the confidence in physiologically based pharmacokinetic models' predictions by inputting key parameters for dissolution into them [227, 229]. These models are reviewed in the next section.

1.7. *In vivo* absorption modelling: PBPK and PBBM

Physiologically based pharmacokinetic modelling (PBPK) is a computational tool which links physiological and physicochemical factors to predict the *in vivo* pharmacokinetics (PK) of a dosage form [101]. When applied specifically to the dissolution and absorption processes, the term physiologically based biopharmaceutics modelling (PBBM) is commonly used [230]. Both the FDA [101] and the European Medicines Agency (EMA) [231] have issued guidance on how to best use PBPK models.

The concept of PBPK modelling was introduced by Teorell in 1937 [232] with the construction of a five compartment PK model based on physiological parameters. Many commercial software packages have been developed since to predict drug GI absorption, such as GastroPlus® [4], SimCyp™ PBPK Simulator [5] and PK-Sim® [6] [71].

[4] https://www.simulations-plus.com/
[5] https://www.certara.com/software/simcyp-pbpk/
[6] https://www.open-systems-pharmacology.org/

GastroPlus® was used in the current work to predict the PK profiles of orally administered IR ibuprofen tablets. It is based on the advanced compartmental absorption and transit model (ACAT) [233] which predicts the rate and extent of dissolution and absorption in the GI tract by numerically integrating the differential equations describing the processes a drug undergoes in the human body (release, dissolution, precipitation, degradation, absorption, inflow and outflow). It divides the GI tract into nine compartments with a predefined physiology in terms of pH, volume, length, radius, transit times, bile salt concentration, pore size, surface area and absorption scale factor (ASF). The drug can be found as unreleased, undissolved or dissolved form in each simulated compartment, with drug absorption and flow through the GIT occurring simultaneously and the transit of the drug between compartments following first-order kinetics. The ACAT model considers the possibility of absorption from the stomach and/or colon and not only the intestine, the possibility of metabolism and degradation in the gut and the possibility of efflux into the gut due to transporters and concentration gradients instead of unidirectional transport from the gut to the systemic circulation.

Coupling *in vitro* dissolution data with PBPK models can serve to improve the prediction of human PK profiles and to confirm that the *in vitro* conditions used are biopredictive. Examples in the literature have explored several aspects, including the relevance of the *in vitro* buffering capacity, the drug surface pH, the drug particle size and the presence of surfactants for the prediction of *in vivo* drug dissolution and absorption [70, 234, 235].

Dissolution kinetics can be described via the Nernst-Brunner equation, the Wang-Flanagan model or the Z-factor. The Takano Z-factor is a lumped dissolution parameter which combines diffusion coefficient (D, $m^2\ s^{-1}$), particle density (ρ_p, $kg\ m^{-3}$), diffusion layer thickness (h, m) and drug particle radius (r_p, m) as per equation (1.19) and it is estimated by fitting equation (1.20) to experimental dissolution profiles [236]. In equation (1.20), m_d is the mass dissolved (kg), m_u is the mass undissolved (kg) at time 0 or time t, C_l is the concentration in the lumen ($kg\ m^{-3}$) and C_s is as defined in equation (1.1).

$$Z = \frac{3D}{\rho_p h r_p} \tag{1.19}$$

$$\frac{dm_d}{dt} = \mathrm{z} m_{u,0} \left(\frac{m_{u,t}}{m_{u,0}}\right)^{2/3} (C_s - C_l) \tag{1.20}$$

GastroPlus® allows the simulation of absorption from a controlled release (CR) formulation as well as an IR formulation. For a CR formulation, dissolution data can be either input as tabulated data or fitted to a Weibull function of the form (1.21) where max is the maximum amount of drug dissolved, f_1 is the fraction factor, t_{lag} is the lag time to the dissolution onset, b_1 is the shape factor and a_1 is the time scale factor.

$$\%\, Dose\ released = max \left(1 - f_1 \exp\left[\frac{-\left(t - t_{lag}\right)^{b_1}}{a_1}\right]\right) \tag{1.21}$$

These biopredictive tools are used by the pharmaceutical industry to guide drug development decisions [237] reducing the number of clinical trials during the initial stages of drug development, to justify the specifications for the product CQA, to support dissolution method specifications and to support post-approval changes on composition, dissolution specification, manufacturing site or manufacturing process [183]. In fact, from 2008 to 2018, 24 new drug applications to the FDA included PBPK modelling for biopharmaceutics assessment, as recently reviewed by Wu *et al*. [238].

However, there are current limitations to the implementation of PBPK, as presented in **Table 1.6** [239-241].

Table 1.6. Current limitations of PBPK modelling.

Input data	• Selection of input parameters • Adoption of appropriate assumptions • Lack of understanding of *in vivo* influence of formulation excipients
Model refinement	• Model optimization and verification should be supported by comparing the model outputs (C_{max}, T_{max} and AUC) to the same PK parameters from available clinical trials that had not been used for model development
PK data	• Lack of complete information on general abundance of enzymes and the regional and inter-individual variability in their expression • Lack of data on intestinal transporters and first-pass metabolism
Other	• Uncertainty around regulatory support

The rapid growth of these computational tools has led to current use being finely tuned on a case-by-case basis. Attempts have been made to standardise their use. The oral biopharmaceutics tools project (OrBiTo) was a collaborative attempt between academia, industry and research organizations launched in 2012 to (a) establish a database of API data of all BCS classes [242], (b) review and refine simulated GI media reflecting GI composition (c) develop and optimize biorelevant *in vitro* tools for the prediction of *in vivo* behaviour of solid oral dosage forms [91] (d) further characterize *in vivo* GI fluids and understand drug behaviour in them (e) optimize the existing *in silico* biopharmaceutics tools and develop novel ones to improve the accuracy of bioavailability predictions and (f) identify areas of improvement in the prediction of oral absorption.

The performance of three available PBPK software packages was evaluated by comparing observed and simulated PK profiles using more than forty APIs from the OrBiTo database including IR, prolonged or delayed release and intravenous formulations [243]. Average performance was

relatively consistent between software packages. Predictive performance declined from intravenous formulations to oral solution to IR tablet indicating a higher level of error associated with complexity of the delivery system and biopharmaceutics inputs. This was a large-scale simulation exercise and a first step to evaluating modelling strengths and weaknesses. Model refinement was not allowed due to the blinding of *in vivo* data to modellers, which has a negative impact on prediction accuracy. Areas where prediction accuracy was lower or with potential for improvement were identified. For example, the absorption of only 10% of the acidic drugs and 25% of the basic drugs studied was within two-fold of the observed data [244, 245], suggesting there is room for improvement of the prediction of acidic drugs' oral absorption.

PBPK has been applied to different fields of study, summarised in **Table 1.7**.

Table 1.7. Recent applications of PBPK modelling.

Application	References
Drug-drug interactions	Segregur *et al.* [234, 246, 247]*;* Kesisoglou *et al.* [248].
Food effects	Andreas *et al.* [249].
To stablish IVIVCs	Luo *et al.* [250].
To set dissolution specifications and design a dissolution safe space	Paraiso *et al.* [251]; Mohamed *et al.* [252].
To predict PK parameters and bioavailability after oral administration	O´Dwyer *et al.* [253].
For dosing recommendations	Tatipalli *et al.* [254].
To compare formulations	Komasaka *et al.* [255].
Virtual BE (VBE) studies	Kambayashi *et al.* [256]; Laisney *et al.* [257].
To study particle size impact and design a PSD safe space	Pepin *et al.* [258].
To study drug supersaturation and precipitation	Hens *et al.* [259]; Jakubiak *et al.* [260].
To study which GI variables are key determinants for *in vivo* behaviour	Hens *et al.* [261].

As the model drug in this work was ibuprofen, the following two models are presented which predicted *in vivo* ibuprofen systemic and GIT concentrations after administration of an 800 mg IR tablet. PBBM was used by Bermejo *et al*. [262] to predict the systemic concentration of ibuprofen highlighting the importance of including dynamic luminal pH values and motility patterns. Yu *et al.* [263] predicted *in vivo* dissolution profiles of ibuprofen in the GIT of healthy subjects and compared them to measured *in vivo* GIT concentrations. They used a dynamic fluid compartment absorption and transport model to simulate GI volumes and GI fluid transport based on MRI data [264]. The model predicted minimal dissolution

in the stomach (2%), slightly higher in the duodenum (6.3%) and primarily dissolution in the jejunum (63%) and ileum (25%).

PBPK has not only been used to predict absorption of oral dosage forms in the form of IR tablets, but also to predict absorption from enteric coated tablets [265], oral suspensions [109] and other formulations, such as amorphous solid dispersions [266, 267], liposomal formulations [268, 269] and nano-sized formulations [270] and, more recently, to predict absorption from MR dosage forms [271, 272].

PBPK has recently been applied to other routes of administration apart from the oral route, like dermal products [273-275], pulmonary products [276] and parenteral formulations [268, 269] and has been used in different subpopulations such as pregnancy [277], elderly [278], paediatric [279, 280] and diseased states [281, 282], with the later incorporating GI parameters specific to the patient population, such as in the prediction of the *in vivo* performance of levodopa in Parkinson's disease patients [141].

PBPK was used in this work to predict the pharmacokinetics of ibuprofen IR tablets in conditions of increasing viscosity relevant to the fasted state versus the viscosity of compendial media by inputting *in vitro* dissolution profile results and comparing the simulated PK profiles to data from published clinical trials.

Introduction summary

Drug dissolution in the gastrointestinal tract is a crucial step to ensure a drug will reach its site of action at a certain concentration to produce its desired effect. *In vitro* dissolution tests can act as surrogates for studying drug dissolution behaviour prior to carrying out animal and human studies.

Even though dissolution testing has been used for decades, there are still some of areas of development which include discrepancies between the *in vivo* and *in vitro* buffer capacity, solubilization capacity and hydrodynamics (media volume, motility patterns, fluid velocities and fluid viscosity). Some of these, such as the lack of bile salts and the deviations in buffer capacity have been partly corrected with the introduction of biorelevant media and redesigned apparatuses. However, there are some factors which are relatively less focused on, such as fluid velocity and viscosity effects. The current work aimed to explore to what extent the incorporation of viscosity enhancing agents to represent the fasted state and the use different fluid velocity profiles would affect the *in vitro* dissolution of a weakly acidic drug in the flow-through apparatus and the paddle apparatus.

Dissolution profiles can be obtained through *in vitro* testing, but also with computational simulations which mechanistically account for factors such as solubility, diffusivity, surface area, fluid and particle velocity and bulk concentration. Simulating *in vitro* dissolution can help select which conditions to carry out dissolution tests in and provide information on which factors are most relevant to the *in vitro* dissolution of a certain drug. Dissolution models based on transport-controlled dissolution have been developed through the years, starting from the Noyes and Whitney model which was refined by Nernst and Brunner to include the diffusion coefficient, surface area and the boundary layer thickness. The *in silico* model presented in this work, SIMDISSO^{TM} is based on the fluid dynamics theory and the Ranz-Marshall correlation which calculates a mass transfer coefficient based on solubility and drug surface area. Bulk concentration effects were explored computationally in this work by defining a limited volume surrounding the particle which is available for that particle to dissolve into, before recirculating to the rest of the medium, and validated *in vitro* in both the flow-through and paddle apparatuses.

Dissolution profiles obtained through both *in vitro* testing and computational simulations can be input into pharmacokinetic models to predict *in vivo* pharmacokinetics after oral administration of a drug. These models predict drug concentrations in the gastrointestinal tract by dividing it into several compartments. GastroPlus® was used in this work to predict the pharmacokinetics of ibuprofen immediate release tablets by inputting *in vitro* dissolution profiles in conditions of small increases of viscosity relevant to the fasted state and comparing the simulated absorption profiles to those obtained in published clinical trials.

Aims and objectives

The objectives of the current work were:

1. To assess the predictive ability of a computational dissolution simulation code, SIMDISSO™, when defining a local volume available for a particle to dissolve, versus the whole cell or vessel volume in the flow-through apparatus or the paddle apparatus.
2. To evaluate the effect of moderately increasing viscosity on the intrinsic dissolution rate of ibuprofen.
3. To assess the interplay of viscosity, fluid flow and particle motion on ibuprofen particulate and tablet dissolution *in vitro* and *in silico.*
4. To assess the effects of medium viscosity on particle motion with SIMDISSO™ particle motion simulations.
5. To explore the effects of small yet biorelevant increases in viscosity on the simulated pharmacokinetic profile of ibuprofen by inputting *in vitro* dissolution data into GastroPlus® and comparing the simulated profiles to published clinical trials.

Chapter 2. Materials and methods

The materials and methods section presented here was extracted from the following papers:

- Navas-Bachiller, M., Persoons, T., D'Arcy, D.M. (2022). Exploring bulk volume, particle size and particle motion definitions to increase the predictive ability of *in vitro* dissolution simulations. *Eur J Pharm Sci*, **174**, 106185. https://doi.org/10.1016/j.ejps.2022.106185.
- Navas-Bachiller, M., Persoons, T., D'Arcy, D.M. (2023). *In vitro* and *in silico* methods to investigate the effect of moderately increasing medium viscosity and density on ibuprofen dissolution rate. *Eur J Pharm Biopharm,* **193**, 74-88. https://doi.org/10.1016/j.ejpb.2023.10.018

2.1. Materials

Materials	Source
Ibuprofen powder, ≥98%	Glentham Life Sciences Ltd
Ibuprofen tablets (Nurofen® 200 mg)	Reckitt Benckiser Healthcare
Phosphate potassium monobasic, ACS reagent, ≥99.0%	Fisher Scientific
Hydrochloric acid (HCl), ACS reagent, Ph. Eur., 37%	Fisher Scientific
Sodium hydroxide, ACS reagent, pellets, 98%	Thermo Scientific
Polysorbate 20	Sigma-Aldrich
Hydroxypropyl methylcellulose (HPMC), H9262, viscosity 80-120 cP, 2% in H_2O (20^oC) (lit.)	Sigma-Aldrich
Trifluoroacetic acid (TFA) HPLC grade, ≥99.0%	Sigma-Aldrich
Acetonitrile (ACN), HPLC grade, ≥99.9%	Sigma-Aldrich
Sucrose for API dissolution studies, food grade	GEM
Sucrose for tablet dissolution studies, laboratory grade	Scientific Laboratory Supplies
VCaps® Plus Hypromellose empty capsules, size 3	Lonza™
GF/D glass microfiber filters, 25 mm diameter	GE Healthcare Life Sciences Whatman™
0.45 µm Polytetrafluoroethylene (PTFE) filters	Fisher Scientific
HPLC screw vials, 1.5 ml, 9 mm	Fisher Scientific

2.2. Equipment

Viscometer	AND Vibro Viscometer SV-10, A&D Company
Shaking water bath	Precision Reciprocal Shaking Bath Model 25
UV-Vis spectrophotometer	PharmaSpec 1700, Shimadzu
Optical microscope	Olympus BX53 optical microscope, Mason Technologies
Particle size analyser	Mastersizer 3000, Malvern Analytics
Degasser for surface area analysis	SmartPrep degasser, Micromeritics
Surface area analyser	Gemini VI analyser, Micromeritics
Dissolution testing	Agilent 708-DS paddle apparatus
Dissolution testing	SOTAX CE7 smart FTA
Sample quantification	Alliance high pressure liquid chromatography (HPLC), Waters
Sample quantification	250 × 4.6 mm BDS Hypersil™ C18 column, Thermoscientific
Sample quantification	Waters 2996 photodiode array detector

2.3. Experimental methods

All experimental measurements were carried out in triplicate unless otherwise stated and presented as the mean value ± standard deviation (SD).

2.3.1. Media preparation

2.3.1.1. pH 6.8 phosphate buffer (high solubility medium)

0.05 M phosphate buffer pH 6.80 ± 0.05 was prepared and degassed according to the USP [117]. 6.8 g of potassium phosphate monobasic and 112 ml of a 0.2 M NaOH solution per litre were mixed and the volume was made up with Millipore Elix 3 deionised water.

2.3.1.2. 0.1 M HCl (low solubility medium)

0.1 M HCl was prepared by diluting 8.3 ml of 37% HCl per litre of Millipore Elix 3 deionised water.

2.3.1.3. Addition of surfactant

As the SIMDISSO^{TM} simulation is based on the behaviour of individual particles rather than aggregates, Tween 20 was used as a surfactant at a concentration lower than its critical micelle concentration (CMC), 0.06 mg ml^{-1}, to ensure particle dispersal without a significant effect on ibuprofen solubility. 0.003% w/v Tween 20 was present in the media unless otherwise indicated.

2.3.1.4. Media containing viscosity enhancing agents (VEA)

In Chapters 4 and 5, the effects of slightly increasing medium viscosity on the dissolution rate of ibuprofen API (Chapter 4) and ibuprofen tablets (Chapter 5) were investigated.

Either (a) 25% w/v sucrose (Level 2) (b) 59% w/v sucrose (Level 3) (c) 0.3% w/v HPMC (Level 2) or (d) 1.05% w/v HPMC (Level 3) solutions were prepared in pH 6.8 phosphate buffer or 0.1 M HCl.

Sucrose was added directly to the buffer components at room temperature before making up to the final volume while HPMC was added to 1/3 of the total volume of buffer at 90^{o}C. The remaining volume was made up with cold

Millipore Elix 3 deionized water and the solution was allowed to cool under constant stirring.

The viscosity of the solutions was measured at 37^{o}C using an AND Vibro Viscometer SV-10.

2.3.2. Solubility study

120 mg and 30 mg of ibuprofen API were added to 10 ml of 0.05 M phosphate buffer pH 6.8 or 10 ml of 0.1 M HCl, respectively, with and without 25% w/v sucrose, 59% w/v sucrose, 0.3% w/v HPMC or 1.05% w/v HPMC and solubility was measured following the shake flask method [283] (n = 3). The solutions were placed in a shaking water bath at 37^{o}C and 100 rpm. Samples were withdrawn at 1, 5, 24 and 48 hours, filtered through a 0.45 µm PTFE filter and analysed at 222 nm in a UV-Vis spectrophotometer. Results are presented in Chapters 3 (media with no VEA) and 4 (media with VEA).

The solubility in pH 6.8 phosphate buffer and 0.1 M HCl without 0.003% w/v Tween 20 was also measured to determine the effect of the surfactant on the solubility of ibuprofen API.

Two-sided t-tests were carried out in Minitab® Statistical Software (© 2022 Minitab, LLC) to determine whether there was a statistically significant difference between the solubilities of the dissolution media with and without surfactant and VEAs. A confidence level of 95% was selected.

2.3.3. Density study

Density studies were carried out following the method described by D'Arcy and Persoons [1] (n = 3). A density bottle filled with deionised water at 37^{o}C was weighed. Using the known density of water at 37^{o}C (0.993 g cm^{-3}), the volume of liquid that filled the bottle was calculated. Subsequently, the bottle was filled with 0.1 M HCl or pH 6.8 phosphate buffer, with and without 25% w/v sucrose, 59% w/v sucrose, 0.3% w/v HPMC or 1.05% w/v HPMC and the weight was determined, with the density then calculated based on the known weight and volume of the bottle. Results are presented in Chapter 4.

2.3.4. Viscosity versus concentration plots

The dynamic viscosity of a range of sucrose and HPMC solutions was measured at 37ºC using an AND Vibro viscometer SV-10 (n = 3). The apparatus was calibrated with Millipore Elix 3 deionized water at 37ºC, whose viscosity was 0.7 mPa.s. Sucrose and HPMC were dissolved in pH 6.8 phosphate buffer to give final concentrations of 10, 15, 20, 25, 35, 45, 55 and 60% w/v and 0.3, 0.4, 0.5, 0.6, 0.8, 1 and 1.2% w/v, respectively. Solutions with the concentrations of interest were also prepared in 0.1 M HCl to verify that there were no statistically significant differences between viscosity values in both media. Results are presented in Chapter 4.

2.3.5. Optical microscopy

Ibuprofen powder was visualized under an Olympus BX53 optical microscope with a 20x magnification. Results are presented in Chapter 3.

2.3.6. Particle size analysis

Ibuprofen particle size determination (n=3) was carried out using a Mastersizer 3000 in wet mode with the Hydro MV accessory and a measurement time of 10 s. A saturated solution of ibuprofen in pH 6.8 phosphate buffer was used as the dispersant. The refraction index of the particle was 1.52 and the absorption index was 0.010. d50, or the median particle size (MPS), was used as input to the simulations. It is defined as the size in microns below which 50% of the total volume of the particles lies and above which 50% of the total volume of the particles lies. Using the size (µm) versus the percentage volume of particles data extracted from the Mastersizer software (Mastersizer 3000 v3.62), five bins corresponding to 20% of the total volume of particles each were generated. The median size in each of the five bin was calculated in Microsoft Excel. The median sizes for each bin were used as inputs in SIMDISSO™ representing a particle size distribution (PSD). To allocate bins for PSD in SIMDISSO™, 20% of the total simulated mass was allocated to each median size. Results are presented in Chapter 3.

2.3.7. Surface area analysis

Samples (n=2) were degassed at 50ºC overnight under nitrogen gas flow using a SmartPrep degasser. Subsequently, specific surface area was

measured in a Gemini VI analyser following the Brunauer-Emmett-Teller (BET) method by determining the amount of nitrogen adsorbed to the ibuprofen crystals' surface at the relative pressures of 0.05, 0.1, 0.15, 0.2, 0.25 and 0.3. Results are presented in Chapter 3.

2.3.8. Dissolution tests

Dissolution tests were carried out in an Agilent 708-DS paddle apparatus (USP apparatus 2) and a SOTAX CE7 smart FTA (USP apparatus 4) at 37^{o}C (n = 3). Samples were replaced with fresh medium at 37^{o}C after each sampling point in both apparatuses.

2.3.8.1. Dissolution tests in the flow-through apparatus

The ibuprofen API powder mass (5 mg or 50 mg) or ibuprofen tablet was placed on top of the glass beads which filled the conical section of the cell. Each glass bead was 1 mm in diameter and 2.8 mg. The mass of glass beads used was 0.947 g for the 12 mm diameter cell and 6.128 g for the 22.6 mm diameter cell. A GF/D glass microfiber filter with nominal particle retention size of 2.7 µm was placed on top of the cell to retain undissolved particles.

2.3.8.1.1. Ibuprofen active pharmaceutical ingredient

Two average linear fluid velocities were achieved by combining a flow rate of 16 ml min^{-1} and a cell diameter of 12 mm (2.35 mm s^{-1}; high velocity) or a flow rate of 8 ml min^{-1} and a cell diameter of 22.6 mm (0.33 mm s^{-1}; low velocity) in a closed system. The reservoir volume was 200 ml.

Media used included pH 6.8 phosphate buffer and 0.1 M HCl with or without 25% w/v sucrose, 59% w/v sucrose (pH 6.8 phosphate buffer only due to analytical instability of 59% w/v sucrose in 0.1 M HCl), 0.3% w/v HPMC or 1.05% w/v HPMC.

2 ml samples were taken at 2, 4, 8, 15, 30, 45, 60, 90 and 120 min for pH 6.8 phosphate buffer and 10, 20, 40, 60, 90, 150, 210 and 270 min for 0.1 M HCl.

Results are presented in Chapters 3 (dissolution tests in media with no VEA) and 4 (dissolution tests in media with VEA).

2.3.8.1.2. Ibuprofen tablets

Two average linear fluid velocities were achieved by combining a flow rate of 16 ml min^{-1} and a cell diameter of 12 mm (2.35 mm s^{-1}; high velocity) or a flow rate of 16 ml min^{-1} and a cell diameter of 22.6 mm (0.66 mm s^{-1}; low velocity) in a closed system. The reservoir volume was 500 ml.

Either (a) pH 6.8 phosphate buffer with no VEA (PB), (b) pH 6.8 phosphate buffer with 59% w/v sucrose (PB-S) or (c) pH 6.8 phosphate buffer with 1.05% w/v HPMC (PB-H) was used as the dissolution medium. Tests were only carried out in high solubility media (PB) and not in low solubility media (0.1 M HCl) due to most of the dissolution and absorption of ibuprofen occurring in the intestine *in vivo*.

2 ml samples were taken at spaced timepoints up to 90 min (PB, high velocity), 120 min (PB-H, high velocity), 180 min (PB and PB-H, low velocity) and 420 min (PB-S, both velocities). Samples were filtered through 0.45 µm PTFE filters into HPLC vials. Results are presented in Chapter 5.

2.3.8.2. Dissolution tests in the paddle apparatus

3 mg (for 0.1 M HCl) or 50 mg (for pH 6.8 phosphate buffer) of ibuprofen were placed inside a Vcaps® HPMC capsule size 3 and a sinker and added to 500 ml of dissolution medium (pH 6.8 phosphate buffer or 0.1 M HCl, with or without 0.3% w/v HPMC or 1.05% w/v HPMC). Time zero was set as the time when the first capsule was observed to rupture. 3 ml samples were taken at 2, 4, 6, 8, 10, 15, 30, 45 and 60 min for pH 6.8 phosphate buffer and at 10, 20, 40, 60, 90, 120, 180, 240 and 300 min for 0.1 M HCl. Samples were filtered using 0.45 µm PTFE filters and the first millilitre was discarded.

Results are presented in Chapters 3 (dissolution tests in media with no VEA) and 4 (dissolution tests in media with VEA).

2.3.8.3. Intrinsic dissolution

100 mg compacts were prepared inside the rotating cylinder by applying 3 tonnes pressure for 1 min (Perkin Elmer hydraulic press). Tests were carried out in the Agilent 708-DS apparatus at 50 rpm in 500 ml of pH 6.8 phosphate buffer with or without 25% w/v sucrose, 59% w/v sucrose, 0.3% w/v HPMC or 1.05% w/v HPMC, achieving three viscosity levels (0.7 mPa.s, level 1; 1.3-1.4 mPa.s, level 2; 4.5-5.5 mPa.s, level 3). 3 ml samples were taken at

2, 4, 6, 8, 10, 20, 30, 45, 60, 90, 120 min and filtered through 0.45 µm PTFE filters. The resulting intrinsic dissolution profiles are presented in Chapter 4.

2.3.8.4. Analysis of the samples

2.3.8.4.1. Ibuprofen active pharmaceutical ingredient

All samples were analysed by UV–Vis spectrophotometry at 222 nm for ≤5 mg tests or 264 nm for >5 mg tests, due to the higher sensitivity at 222 nm and reduced need for dilution at 264 nm. The calibration curves used to determine the concentration of ibuprofen are presented in Appendix 1.

2.3.8.4.2. Ibuprofen tablets

The quantification method for ibuprofen from the dissolution tests of IR ibuprofen tablets was adapted from Stocker *et al.* [284]. An Alliance HPLC and a 250 × 4.6 mm BDS Hypersil™ C18 column with 5 µm particle size were used. The mobile phase was a 70:30 v/v ACN:water with 0.1% v/v TFA acid mixture pumped at a flow rate of 1 ml min^{-1}. The injection volume was 10 µL, the run time was 10 min and the retention time was 5.4 min. Detection was carried out with a Waters 2996 photodiode array detector at 220 nm. The calibration curves used to determine the concentration of ibuprofen are presented in Appendix 1. The limit of detection (LOD) and limit of quantification (LOQ) was 10.37 µg ml^{-1} and 15.01 µg ml^{-1} (PB), 15.01 µg ml^{-1} and 45.49 µg ml^{-1} (PB-H), 11.90 µg ml^{-1} and 30.04 µg ml^{-1} (PB-S).

2.3.8.5. Diffusion coefficient calculation

Diffusion coefficients for each viscosity level and VEA were calculated through (a) the St-E equation (1.1), introduced in Chapter 1 and reproduced below, and (b) the Levich equation (2.1) [285], which correlates the dissolution rate from a rotating disk with angular velocity, from intrinsic dissolution data.

$$D = \frac{k_B T}{6\pi \mu_f R} \tag{1.1}$$

$$I \approx 1.9 D^{2/3} \nu_f^{-1/6} \omega^{1/2} r_d^{\,2} C_s \tag{2.1}$$

I is total flow of matter from the disk surface (kg s^{-1}), which is determined from each intrinsic dissolution profile, ω is angular velocity (rad s^{-1}), r_d is the disk radius (m), ν_f is kinematic viscosity (m^2 s^{-1}) and C_s is solubility (kg m^{-3}).

A reference experimental diffusion coefficient value extracted from literature (0.80×10^{-9} m^2 s^{-1}) [286] was used to compare the calculated *D* value from the Levich equation for pH 6.8 phosphate buffer with no VEA, to ascertain the accuracy of the method. The Levich-calculated *D* values were used as inputs for the increased-viscosity media simulations.

2.3.9. Dissolution tests characterization

2.3.9.1. Dissolution metrics extracted from dissolution profiles

The time to 85% dissolution in pH 6.8 phosphate buffer (t85) and 50% dissolution in pH 6.8 phosphate buffer and 0.1 M HCl (t50) was extracted from each experimental profile (n=3). t85 and t50 were visually extracted from Microsoft Excel plots of *in vitro* dissolution for the results presented in Chapter 3.

In Chapter 4, t85, t50 and the dissolution rate constant (k_{diss}, s^{-1}) in pH 6.8 phosphate buffer and t50 in 0.1 M HCl were extracted with the curve fitting tool in MATLAB by fitting the data to equation (2.2) in pH 6.8 phosphate buffer and equation (2.3) in 0.1 M HCl for each replicate (where average b <1.0 for each system tested). In equations (2.2) and (2.3), Y_{max} represents the maximum percentage dissolved, t is time and a and b are constants.

Two different equations were used to characterise the dissolution profiles within the ranges observed and to estimate a percentage dissolved at a particular time point within that observed range. As the dissolution in 0.1 M HCl had not reached a plateau in 270 min, the application of equation (2.2) was limited to pH 6.8 phosphate buffer only. Y_{max} in pH 6.8 phosphate buffer was calculated from the observed plateau of the *in vitro* dissolution data as the average percentage dissolved from when variation between two consecutive timepoints at the plateau was less than 5%.

$$f(t) = Y_{max}(1 - e^{-k_{diss}t}) \quad (2.2)$$

$$f(t) = at^b \quad (2.3)$$

2.3.9.2. Characterization of tablet dissolution profiles through Reynolds number calculation

Equations (1.7) and (1.8), introduced in Chapter 1 and reproduced below, were used to calculate the Reynolds number in each of the six experimental conditions. U_p in equation (1.7) was 0 mm s^{-1} and d_p was tablet diameter, which was 0.011 m for all experiments. The Reynolds number was calculated for the tablet dissolution tests and not for the ibuprofen API dissolution tests, as it was used to analyse a potential correlation with the predicted C_{max} and T_{max} values for ibuprofen IR tablets. The calculated Reynolds numbers are presented in Chapter 5.

$$Re = \frac{|U_f - U_p| d_p}{\nu_f} \quad (1.7)$$

$$\nu_f = \frac{\mu_f}{\rho_f} \quad (1.8)$$

2.3.10. Statistical analysis of viscosity, velocity and solubility effects on dissolution metrics for ibuprofen

To study the statistical effect of medium viscosity, fluid velocity and drug solubility on the dissolution rate constant (k_{diss}), t50 and t85 of ibuprofen API, eight factorial design analyses were run in Minitab® Statistical Software (© 2022 Minitab, LLC). Factors and levels are described in **Table 2.1**, based on three replicates per dissolution test. Results were considered statistically significant when p-value <0.05. Results from the statistical analysis are presented in Chapter 4.

Table 2.1. Factors, levels, dissolution metric and significant results (p-value <0.05) for each factorial design. High solubility = pH 6.8 phosphate buffer, low solubility = 0.1 M HCl. * denotes interaction. Sol (solubility), vel (velocity), visc (viscosity).

Test ID	Apparatus	Solubility	Rotation speed (rpm) or Average vel. (mm s^{-1})	Viscosity (mPa.s)	VEA	Metric	Significant result
1	FTA	High, low	0.33 mm s^{-1}, 2.35 mm s^{-1}	Level 1, Level 2	Sucrose, HPMC	t50	Sol Visc Sol*Visc
2	FTA	Low	0.33 mm s^{-1}, 2.35 mm s^{-1}	Level 1, Level 2	Sucrose, HPMC	t50	Visc
3	FTA	High	0.33 mm s^{-1}, 2.35 mm s^{-1}	Level 1, Level 2, Level 3	Sucrose, HPMC	t85	Visc VEA VEA*Visc
4	FTA	High	0.33 mm s^{-1}, 2.35 mm s^{-1}	Level 1, Level 2, Level 3	Sucrose, HPMC	k_{diss}	Visc VEA
5	Paddle	High, low	50 rpm, 100 rpm	Level 1, Level 2, Level 3	HPMC	t50	Sol Vel Sol*Vel Sol*Visc

							Visc Vel*Visc
6	Paddle	Low	50 rpm, 100 rpm	Level 1, Level 2, Level 3	HPMC	t50	Vel Visc Vel*Visc
7	Paddle	High	50 rpm, 100 rpm	Level 1, Level 2, Level 3	HPMC	t85	Vel
8	Paddle	High	50 rpm, 100 rpm	Level 1, Level 2, Level 3	HPMC	k_{diss}	Vel

2.4. SIMDISSO™ simulations

2.4.1. Input parameters for the flow-through apparatus dissolution simulations in SIMIDISSO™

The baseline simulation to assess the predictive ability of three simulation options in SIMDISSO™ was run with the cell volume, the experimentally determined median particle size (MPS: 160 µm) and particle motion enabled. Simulations were assessed for improved predictability by (1) using an NPV instead of the cell volume (2) inputting a PSD instead of a MPS (PSD, 5 bins: 12.7 µm, 81.2 µm, 135.5 µm, 240 µm, 551 µm) and (3) disabling particle motion.

Simulations were run in MATLAB [7] for 5 mg of spherical ibuprofen particles in a simulated flow through cell (closed loop) in high solubility (pH 6.8 phosphate buffer) or low solubility (0.1 M HCl) medium with a fluid viscosity of 0.7 mPa.s (level 1 viscosity) and two fluid velocities in a pulsating flow field: a cell diameter of 12 mm, flow rate of 16 ml min^{-1}, (average linear velocity of 2.35 mm s^{-1}; high velocity) and a cell diameter of 22.6 mm, flow rate of 8 ml min^{-1} (average linear velocity of 0.33 mm s^{-1}; low velocity). The three simulation options (NPV, PSD and particle motion) were also assessed with a mass of 50 mg of ibuprofen in high solubility medium (pH 6.8 phosphate buffer) in level 1 viscosity. Simulation parameters are presented in **Table 2.2**.

[7] MATLAB software information can be found at https://uk.mathworks.com/

Table 2.2. Simulation parameters in SIMDISSO™ for ibuprofen API in aqueous buffers.

Diffusion coefficient ($m^2\ s^{-1}$)	8.00×10^{-10}	
Fluid viscosity (mPa.s)	0.7	
Gravitational acceleration ($m\ s^{-2}$)	9.81	
Pumping mode	Pulsating	
Pump frequency (Hz)	2	
Particle shape	Spherical	
Particle density ($g\ cm^{-3}$)	1.018	
	0.1 M HCl	Phosphate buffer
Solubility ($kg\ cm^{-3}$)	0.064	3.5
Fluid density ($g\ cm^{-3}$)	1.006	1.009

Simulation time was adapted to reflect the *in vitro* dissolution tests in each medium and time steps were 0.004 s. The results of these simulations are presented in Chapter 3.

2.4.1.1. Simulations in increased viscosity medium

To study the effect of viscosity on simulated particulate dissolution, simulations were run for 5 mg of ibuprofen particles in a high fluid velocity scenario (2.35 mm s^{-1}) and a low fluid velocity scenario (0.33 mm s^{-1}) and high solubility (pH 6.8 phosphate buffer) and low solubility (0.1 M HCl) media with different values of viscosity: 0.7 mPa.s (level 1), 1.3 mPa.s (level 2 sucrose), 1.4 mPa.s (level 2 HPMC), 4.5 (level 3 sucrose) and 5.5 mPa.s (level 3 HPMC), corresponding to the HPMC and sucrose concentrations presented in the section “2.3.1.4. Media containing viscosity enhancing agents (VEA)”. Simulations were not run in level 3 sucrose in 0.1 M HCl since the dissolution experiments in level 3 sucrose in the FTA were not included in the study due to analytical instabilities.

The cell volume and a PSD were used, and particle motion was enabled. In these simulations, the code was updated so that a spatial limitation for particle motion in the vertical direction corresponding to the height of the flow-through cell was included. So, particle motion in the vertical direction is restricted and this is incorporated in the relative velocity calculations. Therefore, the effect of enabling or disabling particle motion did not have to be explored.

The solubility, fluid density and diffusion coefficient inputs for each medium viscosity based on experimental data are presented in **Table 2.3**. Solubility and density values were updated from the simulations presented in Chapter 3 to reflect measured *in vitro* solubilities and densities in different viscosity media. Results of these simulations are presented in Chapter 4.

Inputs related to fluid velocities and volumes are presented in **Table 2.4.** The reservoir volume was adjusted so that a total volume of 200 ml including cell and reservoir was generated. A cell height of 66.8 mm was selected for the small cell to reflect the total cell volume, including the tapered upper section, the cell height of the larger cell was 30 mm. It does not include the conical section containing the glass beads, nor regions in the upper cell where the diameter changes, as a constant diameter is required to calculate the instantaneous linear velocity in the cell and the relative particle velocity.

The particle density input was refined from 1.018 g cm^{-3} to 1.1047 g cm^{-3} to reflect the true density of ibuprofen particles measured by helium pycnometry in D'Arcy and Persoons [1].

Table 2.3. Experimentally determined inputs to SIMDISSO™ dissolution simulation code. μ_f, fluid viscosity (mPa.s), D, diffusion coefficient ($m^2\ s^{-1}$), C_s, solubility ($kg\ m^{-3}$), ρ_f, fluid density ($g\ cm^{-3}$).

Media	μ_f	D	C_s	ρ_f
High solubility (pH 6.8 phosphate buffer)	0.7 (Level 1)	8.00×10^{-10}	2.79	0.999
	1.4 (Level 2 HPMC)	5.44×10^{-10}	2.97	1.004
	5.5 (Level 3 HPMC)	1.81×10^{-10}	3.46	1.005
	1.3 (Level 2 sucrose)	4.33×10^{-10}	3.26	1.091
	4.5 (Level 3 sucrose)	1.53×10^{-10}	2.24	1.219
Low solubility (0.1 M HCl)	0.7 (Level 1)	8.00×10^{-10}	0.063	0.994
	1.4 (Level 2 HPMC)	5.44×10^{-10}	0.047	1.000
	5.5 (Level 3 HPMC)	1.81×10^{-10}	0.044	0.997
	1.3 (Level 2 sucrose)	4.33×10^{-10}	0.059	1.088

Table 2.4. Inputs to SIMDISSO™ dissolution simulation code related to flow rate, FR (ml min^{-1}), cell diameter (mm), cell height (mm) and reservoir volume, V_r (ml). For the simulations presented in Chapter 3, reservoir volume was 200 ml.

FR	Cell diameter	Cell height	V_r
8	22.6	30	188
16	12	66.8	192.4

2.4.2. Particle motion simulations in SIMIDISSO™

10-second simulations were run to interpret the initial effect of disabling or enabling particle motion in a closed system flow through cell in 0.1 M HCl with no VEA. Two average linear fluid velocities were used: 0.33 mm s^{-1} and 2.35 mm s^{-1}, to match the experimental flow rates and cell diameters, a mass of 5 mg, an MPS of 160 µm, a reservoir volume of 200 ml, a solubility of 0.064 mg ml^{-1}, a fluid density of 1.006 g cm^{-3}, a particle density of 1.018 g cm^{-3}, a diffusion coefficient of 8 x 10^{-10} m^2 s^{-1} and a fluid density of 0.7 mPa.s in a pulsating fluid flow with a pump frequency of 2 Hz were used as inputs to the simulations. Particle motion and gravity (9.81 m s^{-2}) were enabled. The resulting simulations are presented in Chapter 3. The presented simulations were those obtained when inputting solubility data from the 0.1 M HCl medium, but the same results were obtained for the pH 6.8 phosphate buffer medium, due to an almost equal density, same fluid velocity, same particle properties and minimal dissolution over 10 seconds.

In Chapter 4, the effect of increasing viscosity on simulated particle motion was assessed by running two sets of simulations: (1) 1200 s-simulations for a PSD in 4 scenarios: (a) low velocity – level 1 viscosity, (b) low velocity – level 3 viscosity (5.5 mPa.s), (c) high velocity – level 1 viscosity and (d) high velocity – level 3 viscosity (5.5 mPa.s) and (2) up to 360 s-simulations for a MPS for the five values of viscosity in the two fluid velocity environments. All other inputs were as described in **Table 2.3** and **Table 2.4**.

2.4.3. Statistical assessment of the predictive ability of the particle size distribution versus median particle size approach

For the profiles exploring the effect of PSD on the simulated dissolution of ibuprofen in level 1 viscosity (pH 6.8 phosphate buffer or 0.1 M HCl with no VEA) at two average linear fluid velocities (0.33 mm s^{-1} or 2.35 mm s^{-1}), the experimental dissolution profiles were compared to the simulated MPS and PSD profiles for each time point by calculating the percentage predictive error (PE%) from equation (2.4) and the root mean square error (RMSE) from equation (2.5) to illustrate predictability over the whole profile. Results are presented in Chapter 3.

$$PE\% = \frac{|Simulated\ value - Experimental\ value|}{Experimental\ value} * 100 \quad (2.4)$$

$$RMSE = \sqrt{\frac{1}{n}\sum_{i=1}^{n}(Simulated\ value - Experimental\ value)^2} \quad (2.5)$$

2.4.4. Input parameters for the paddle apparatus dissolution simulations in SIMIDISSO™

Inputs to the simulations in the paddle apparatus are shown in **Table 2.5**. The fluid pumping mode was set to steady as there is no pulsating option for the paddle apparatus, particle motion was enabled and gravity disabled as tangential velocity is the main velocity component in the paddle apparatus [16, 18]. Fluid velocity data were extracted from the literature [14, 30] to be equivalent to a rotational speed of 50 rpm or 100 rpm. Simulations in the paddle apparatus were only run for viscosity level 1 (pH 6.8 phosphate buffer or 0.1 M HCl with no VEAs) and are presented in Chapter 3.

Table 2.5. Experimentally determined (*) and literature extracted (†) inputs to SIMDISSO™ dissolution simulation code for the paddle apparatus. ρ_p, particle density (g cm^{-3}), D, diffusion coefficient (m^2 s^{-1}), μ_f, fluid viscosity (mPa.s), V_r, reservoir volume (ml), m_0, mass (g), d_p, particle diameter (mm), U_p, particle velocity (m s^{-1}), U_f, fluid velocity (m s^{-1}), C_b, bulk concentration C_s, solubility (kg m^{-3}), ρ_f, fluid density (g cm^{-3}), simulation time (min) and timesteps (s).

Constant inputs			Variable inputs		
†	ρ_p	1.018	m_0	0.003	0.050
			d_p	0.160	PSD
			Size bins	1	5
†	D	8 x 10^{-10}	U_p	Enabled	
			† U_f	0.0766 (50 rpm)	0.1476 (100 rpm)
Particle shape		Spherical	C_b calc.	NPV	Cell
†	μ_f	0.7	**Medium properties and solubility**		
Pumping mode		Steady		pH 6.8 phosphate buffer	0.1 M HCl
V_r		500	* C_s	3.5	0.064
			* ρ_f	1.009	1.006
Gravity		Disabled	Simulation time	200	300
			Time steps	0.004	0.004

2.5. GastroPlus® simulations

In Chapter 5, the bioavailability of ibuprofen IR tablets as predicted with GastroPlus® is presented. The dissolution profiles in different viscosity media obtained as described in section "2.3.8.1. Dissolution tests in the apparatus" were used as inputs to the oral model developed in GastroPlus®. In order to develop an intravenous model and validate the oral model, *in vivo* studies from literature were used.

2.5.1. *In vivo* studies

Literature data from one clinical trial was used to develop an intravenous model in order to obtain the distribution and elimination parameters to input in the oral model. The study was a double-blind, randomized, crossover trial in which 12 healthy subjects (25% female) aged 18 to 65 years received either an intravenous injection of 800 mg of ibuprofen infused over 5 to 7 min together with an oral placebo or an oral dose of 800 mg of ibuprofen together with an intravenous placebo [287]. The mean subject weight was 76.9±12.4 kg and the mean subject height was 177.9±6.8 cm. The plasma concentration versus time after the intravenous dose of ibuprofen was digitalized with WebPlotDigitalizer® version 4.6 software to develop the disposition model.

Literature data from two clinical trials where ibuprofen IR tablets were administered orally were used to validate the PK oral model. Both clinical trials were open label, randomized, crossover studies comparing the absorption of different ibuprofen formulations to standard ibuprofen acid tablets. In both trials, two 200 mg standard ibuprofen tablets (Nurofen®) were administered after an overnight fast.

The study by Legg *et al.* [288] (*in vivo* data set A) enrolled 35 healthy adult subjects (48.6% female) between 18 and 45 years of age with a mean body weight of 71.9 kg and a mean height of 173.1 cm.

The study by Dewland *et al*. [289] (*in vivo* data set B) enrolled 22 healthy male and female volunteers between 18 and 50 years of age with a mean body mass index (BMI) of 24.1 kg m^{-2}. The mean body weight was not reported, and it could not be calculated from BMI due to the height not being reported either. Therefore,

the mean body weight used for all oral model simulations was 71.9 kg, as presented in the clinical trial by Legg *et al.* [288], which was similar to the weight in the intravenous data set.

The PK profiles obtained after the administration of two Nurofen® tablets in the fasted state in both clinical trials were digitalized with WebPlotDigitalizer® to extract plasma concentration versus time data and validate the oral model.

The study by Dewland *et al*. [289] presented plots of the PK parameters C_{max}, T_{max}, AUC_{0-t} and $AUC_{0-\infty}$ obtained for each of the 22 individuals. These plots were digitalized to extract the full range of measured PK parameters as a representation of inter-subject variability in order to assess the extent of under or overprediction of PK parameters when inputting the dissolution profiles obtained in the PB-S medium into the GastroPlus® oral model.

2.5.2. Pharmacokinetic model development and verification

GastroPlus® was used as the modelling platform to predict the PK profile of ibuprofen IR tablets.

2.5.2.1. Intravenous model

Disposition parameters (clearance (Cl, ml min^{-1}), volume of distribution (V_c, ml kg^{-1}), half-life ($T_{1/2}$, h), and the transfer rate constants (K_i, h^{-1})) were extracted by fitting published clinical data from the intravenous study carried out by Pavliv *et al*. [287] described in section "2.5.1. *In vivo* studies" to a one-, two- and three-compartment model in PKPlus.

2.5.2.2. Oral model

The input parameters that are common to all simulations are presented in **Table 2.6**. Ibuprofen molecular weight and log P were extracted from Cristofoletti *et al*. [290]. Particle radius was extracted from the work by Cristofoletti *et al.* [235] where an effective PSD was estimated by modelling the *in vitro* dissolution profile of 200 mg of ibuprofen in phosphate buffer at pH 6.7. Particle density corresponded to the true density of ibuprofen particles measured by helium pycnometry [1]. The mean precipitation time was left as the default value provided in the software. The diffusion coefficient was extracted from the work by Healy and Corrigan [286] where it was calculated from the *in vitro* dissolution of

ibuprofen particles in phosphate buffer at pH 7.35. The effective permeability for ibuprofen (P_{eff}; cm s^{-1}) was extracted from Cristofoletti *et al*. [290] where it was back-calculated from the observed absorption rate constant (k_a) of 7.0 h^{-1} after the administration of an oral dose of ibuprofen tablets to 15 subjects by Wagner *et al.* [291]. The fraction unbound to proteins was measured *in vitro* in healthy plasma by Aarons *et al.* [292] and the blood/plasma ratio was measured by Obach *et al.* [293] by incubating the drug in whole blood at ambient temperature for 45 min.

The initial drug dose was 400 mg, corresponding to two 200 mg Nurofen® tablets. 250 ml was used as the dosing volume representing a standard glass of water. Dosage form was selected as controlled release undissolved (CRU) dispersed, which simulates the release of undissolved particles from a tablet, with the unreleased material and drug in solution moving through the simulated GI compartments.

The solubility versus pH profile (**Table 2.7**) was obtained from the ibuprofen monograph published by Potthast *et al.* [72] and was fitted to the built-in pKa-based solubility model to estimate the pKa (4.3) and the solubility factor (SF) (89.5).

An ACAT model was used to simulate absorption. Gut physiology values in each of the nine virtual compartments remained as the default values provided for a healthy fasted human subject. The default human fasted ASF model used was Opt logD Model SA/V 6.1.

Single simulations were carried out using a compartmental PK model in GastroPlus®. The *in vitro* dissolution data from the six dissolution tests of ibuprofen IR tablets carried out under two fluid velocity conditions (2.35 mm s^{-1} and 0.66 mm s^{-1}) and in three media (PB, PB-H, PB-S), as described in section “2.3.8.1. Dissolution tests in the flow-through apparatus”, were used as inputs. Simulation time was 16 h. The predicted plasma concentration versus time profiles are presented in Chapter 5.

The relationship between the resulting simulated PK parameters C_{max} and T_{max} and the Reynolds numbers calculated from the *in vitro* dissolution studies as

described in section “2.3.9.2. Characterization of tablet dissolution profiles through Reynolds number calculation” was investigated in Chapter 5.

Table 2.6. Inputs used in GastroPlus®.

Input	Value	Units	Ref
Molecular formula	$C_{13}H_{18}O_2$		
Molecular weight	206.29	g mol^{-1}	
log P	3.23		[72]
Particle radius	220	µm	[290]
Particle density	1.1047	g ml^{-1}	[1]
Mean precipitation time	900	s	
Diffusion coefficient	0.8 x 10^{-5}	cm^2 s^{-1}	[286]
P_{eff}	17 x 10^{-4}	cm s^{-1}	[290, 291]
Blood/Plasma ratio	0.55		[293]
Fraction unbound to proteins, f_u	1	%	[292]

Table 2.7. Solubility versus pH data extracted from Potthast *et al.* [72].

pH	Solubility (mg ml^{-1})
1	0.038
3	0.043
4.5	0.084
5.5	0.685
6.8	3.37
7.4	3.44

2.5.2.3. In vitro dissolution profiles modelling

The *in vitro* dissolution profiles for ibuprofen tablets were modelled with the Z-factor model described in equation 1.20, introduced in Chapter 1, or a single

Weibull function as described in equation 1.21, introduced in Chapter 1. Fittings were carried out directly in GastroPlus® 9.8.3 (Simulations Plus, Lancaster, CA, USA), in order to obtain inputs for the PK model after oral administration of ibuprofen.

The experimental dissolution profiles modelled were those carried out as described in the subsection "Ibuprofen tablets" of "2.3.8.1. Dissolution tests in the apparatus", that is, in two fluid velocity scenarios (0.66 mm s^{-1} or 2.35 mm s^{-1}) and three viscosity media (PB, PB-H or PB-S). They were fitted to the Z-factor model as obtained from the *in vitro* tests and modified to reduce the lag time. To do so, the profile in PB-high velocity, where the first concentration was measured after 10 min, was selected as the reference. In the rest of the profiles, the first point where ibuprofen was detected at a concentration higher than 5 mg ml^{-1} was set to 10 min and the difference between the real time of the first observation and 10 was subtracted from the subsequent timepoints.

2.5.2.4. In vitro dissolution data inputs

After assessing the model fits to the experimental data, two dissolution data input methods were explored. Firstly, the tabulated data points of percent release versus time from the experimental profiles were directly input into the model, so that the actual amount of drug available for dissolution is determined by interpolation during the simulation. Secondly, the dissolution profiles were fitted to the Weibull function and the Weibull parameters were used as inputs for the PK simulation model after oral administration of ibuprofen tablets.

2.5.3. Intravenous and oral model verification

The fitting of the one-, two- and three-compartment models to the intravenous data presented in the study by Pavliv *et al*. [287] was statistically assessed with the parameters R^2, Schwarz Criterion (SC) and Akaike Information Criterion (AIC) reported in GastroPlus®.

Two statistical analyses were performed in Microsoft Excel (Microsoft Corporation) for the intravenous model: the average fold error (AFE) (equation (2.6)) and absolute average fold error (AAFE) (equation (2.7)).

$$AFE = 10^{\frac{1}{n}\sum_i \log\left(\frac{predicted_i}{observed_i}\right)} \quad (2.6)$$

$$AAFE = 10^{\frac{1}{n}\sum_i \left|\log\left(\frac{predicted_i}{observed_i}\right)\right|} \quad (2.7)$$

In equations (2.6) and (2.7), n is the number of sampling points and i is the sampling point index. For an acceptable prediction, AAFE should be smaller than 2 and AFE should be close to 1, with AAFE <1 indicating underprediction and AAFE >1 indicating overprediction.

The simulated oral PK profiles and PK parameters obtained with both dissolution profile input methods were compared to data from the two clinical trials described in section "2.5.1. *In vivo* studies" where ibuprofen was administered orally [288, 289].

The fold error (FE) (equation (2.8)) was used to compare the predicted C_{max} and $T_{1/2}$ for the intravenous model and C_{max}, T_{max} and AUC for the oral model to the observed data from the clinical studies presented in section "2.5.1. *In vivo* studies". A FE close to 1 indicates an accurate prediction.

$$FE = \frac{predicted\ C_{max}, T_{max}, AUC\ or\ T_{1/2}}{observed\ C_{max}, T_{max}, AUC\ or\ T_{1/2}} \quad (2.8)$$

2.5.4. Virtual bioequivalence studies (VBE)

VBE simulations were performed in GastroPlus® for a sample size of n = 25 healthy fasted adults in one trial. 400 mg of ibuprofen in tablet form were administered with 250 ml of fluids. Dosage form was selected as CRU. The six dissolution profiles for ibuprofen IR tablets obtained with two fluid velocities and three media were input into the model. The dissolution data was directly used as tabulated data. The default coefficients of variation (%CV) for inter-subject variability of the physiological parameters provided in the GastroPlus® database

were applied for each parameter. Simulation time was 16 h. Results from the VBE studies are presented in Chapter 5.

2.5.5. Parameter sensitivity analysis (PSA)

A PSA was performed for the Weibull-related parameter shape factor, particle radius and diffusion coefficient. For the latter two, the dissolution data was input as tabulated data. One PSA was done for each of the six *in vitro* dissolution profiles obtained as described in the subsection "Ibuprofen tablets" of "2.3.8.1. Dissolution tests in the apparatus". The range studied for each parameter is presented in **Table 2.8**. Ten logarithmic spaced values were automatically selected for each variable. The effect of each parameter on the predicted C_{max} and T_{max} for ibuprofen IR tablets is presented in Chapter 5.

Table 2.8. Parameters varied in PSA simulations.

Parameter	Lower bound	Upper Bound
Weibull shape factor	1.32	12.80
Particle radius (µm)	22	2200
Diffusion coefficient $\times 10^5$ ($cm^2\ s^{-1}$)	0.1	1

Chapter 3. Exploring bulk volume, particle size and particle motion definitions to increase the predictive ability of *in vitro* dissolution simulations.

Results, discussion and conclusions presented in the current chapter have been published in the following paper: Navas-Bachiller, M., Persoons, T., D'Arcy, D.M. (2022). Exploring bulk volume, particle size and particle motion definitions to increase the predictive ability of *in vitro* dissolution simulations. *Eur J Pharm Sci*, **174**, 106185. https://doi.org/10.1016/j.ejps.2022.106185.

3.1. Introduction

Many mechanistic simulation models have been developed since the proposal of theoretical equations to describe dissolution [199, 200, 203, 214]. Models like the one presented by Sugano *et al.* [214] and the one presented in the current work consider hydrodynamics in the dissolution apparatuses as a crucial factor for an accurate simulation of drug dissolution. Other models have discussed the influence of bulk volume and bulk concentration definition on dissolution simulation [208].

Dissolution models have to achieve a compromise between the accuracy of the simulation and the computational costs. In this work, dissolution simulations were conducted using a reduced-order model based on the Ranz-Marshall correlation for mass transfer from spherical particles in an in-house non-commercial dissolution software, SIMDISSO^{TM}. The theoretical basis for SIMDISSO^{TM} is outlined in section "1.6.1. API dissolution simulation in SIMDISSO^{TM}". The definition of the relevant volume for dissolution, particle size and particle motion in simulation approaches were explored when simulating the dissolution of ibuprofen API. The simulated profiles were compared to *in vitro* dissolution in the FTA and paddle apparatus in conditions of varying fluid velocities, drug mass and drug solubilities to identify which simulation approaches could better capture the dissolution rate of ibuprofen and in which conditions.

The definition of a local volume to simulate dynamic bulk concentration, the NPV was explored as an illustration of the relevance of local hydrodynamics for dissolution, which might be different from the hydrodynamics in the whole flow

through cell or paddle apparatus vessel at any moment in time due to low local fluid velocity regions. For example, in the paddle apparatus, there can be regions of low velocity in the bottom of the vessel [19, 29]. In the FTA, velocity patterns are homogeneous and depend on flow rate, cell size and differences in fluid density and velocity [38, 41, 45].

The impact of using a PSD versus a MPS was explored in this work as the former is generally expected to be more representative of the *in vitro* situation based on the common polydispersity of the pharmaceutical powders [203, 204], .

The definition of particle motion was considered relevant as particles can be sedimented or suspended *in vitro* at any moment in time depending on the interplay between particle and fluid density and fluid velocity. Particle motion for a moving particle in the FTA is pulsing due to the pulsing flow of the fluid, but more complex velocity patterns have been found [1]. When particle motion is disabled in the code, particles are exposed to fluid velocity, and when particle motion is enabled, particles are exposed to the relative velocity between fluid and particle. Enabling particle motion in two fluid velocity scenarios in the FTA and the implications for drug dissolution were computationally explored.

The aim of this work was to assess the predictive ability of SIMDISSO^{TM} when (1) using the NPV, which extends from the particle surface to a distance of one particle radius, versus the FTA cell volume or the paddle apparatus vessel volume as the relevant instantaneous volume for the dissolution of two drug loadings in a closed system, (2) assessing the effect of inputting a PSD instead of an MPS and (3) exploring the effect of enabling or disabling particle motion, in two media and with two fluid velocity conditions. The applicability of the model was investigated by means of extracting the predicted time to 85% or 50% dissolution and comparing it to the experimental time in each of the three simulated scenarios.

3.2. Results

3.2.1. Solubility study

The solubility study was carried out as described in section "2.3.2. Solubility study".

The solubility of ibuprofen in pH 6.8 phosphate buffer with and without 0.003% w/v Tween 20 (CMC = 0.06 mg ml^{-1}), was 3.5±0.5 mg ml^{-1} and 4.1±0.3 mg ml^{-1}, respectively, after 48 hours of incubation. The pH values of the saturated solutions were 6.05 and 6.10, respectively, which is in accordance with the surface pH of ibuprofen in phosphate buffer reported in the literature [112]. The solubility values with and without surfactant were not statistically significantly different, therefore the value of 3.5 mg ml^{-1} was used in the simulations of dissolution in pH 6.8 phosphate buffer with 0.003% w/v Tween 20. Solubility in 0.1 M HCl with and without 0.003% w/v Tween 20, was 0.063±0.016 mg ml^{-1} and 0.066 ±0.012 mg ml^{-1}, respectively, after 24 hours of incubation, which was in agreement with intrinsic solubility values presented in the literature [113, 294]. Therefore, the calculated value of 0.064 mg ml^{-1} from equation (3.1) [286] was used as input for the simulation.

$$Solubility\ (mg\ ml^{-1}) = 0.064\ (1 + \ 10^{pH-4.39}) \qquad (3.1)$$

3.2.2. Particle size analysis

The experimental d50 value measured as per section "2.3.6. Particle size analysis" was 160±0.197 µm. The particle sizes of the each of the PSD bins were 12.7 µm, 81.2 µm, 135.5 µm, 240 µm and 551 µm.

3.2.3. Dissolution tests in flow-through apparatus (FTA)

Dissolution tests were carried out as described in section "2.3.8.1. Dissolution tests in the flow-through apparatus" and the simulated profiles were obtained in SIMIDISSO™ as per section "2.4.1. Input parameters for the flow-through apparatus dissolution simulations in SIMDISSO™".

3.2.3.1. Cell volume versus near-particle volume (NPV)

The experimental and simulated dissolution profiles of 5 mg of ibuprofen at two average fluid velocities, 2.35 mm s^{-1} and 0.33 mm s^{-1}, in pH 6.8 phosphate buffer and 0.1 M HCl were compared (**Figure 3.1**). Simulated results were obtained using an MPS and enabled particle motion and either the cell volume or the NPV.

The experimental dissolution rate of 5 mg of ibuprofen in pH 6.8 phosphate buffer would be considered rapid (85% within 30 min) by the FDA guidance for BCS class I or III drugs in the paddle apparatus at 50 rpm [47], which was expected due to the high solubility of ibuprofen at pH 6.8. In 0.1 M HCl, after 270 min, only 73% of the ibuprofen was dissolved in the high fluid velocity test and 57% in the low fluid velocity test, due to the low solubility of ibuprofen in 0.1 M HCl and the lack of sink conditions, which were defined as the situation when the solubility value triplicates the maximum bulk concentration value.

The experimental dissolution rates decreased in a lower fluid velocity environment in both media. In pH 6.8 phosphate buffer, the NPV and cell options predicted very rapid dissolution, however use of the NPV suggested velocity effects on dissolution which were not apparent in the simulation using the cell option as the bulk volume. Furthermore, the NPV option was better at predicting t85 than the cell volume option, in both velocities (**Table 3.1**). In 0.1 M HCl, the NPV underpredicted the dissolution rate in both fluid velocities and did not increase the t50 predictive ability. The underprediction from all simulations in 0.1 M HCl (**Figure 3.1**) could be attributed to the assumption of sphericity by the model, whereas the majority of the particles are needle-shaped, as shown by optical microscopy (**Figure 3.2**). However, while the calculated surface area for the 5 mg sample using the MPS (1.80 cm^2) was lower than the BET measured surface area (5.30 cm^2±0.24), the calculated surface area using the PSD (6.15 cm^2) compared well with the BET measured area (5.30 cm^2±0.24). Therefore, the underestimation of surface area resulting from the assumption of spherical particles is likely to have a minor impact in the current work.

The effect of fluid velocity on dissolution rate is due to the local medium being more concentrated in each timestep because of a reduced mass transport rate away from the dissolving surface affecting the local concentration gradient and

slowing down the dissolution process. An effect of the flow rate on dissolution rates has been described before [1], possibly due to a better dispersal of the particles as the flow rate increases as well as the effect on local concentration gradients.

Therefore, an NPV seemed more accurate in predicting dissolution in high solubility than low solubility conditions, although other simulation parameters, such as particle size and particle motion definition can affect the accuracy of the prediction, as will be discussed.

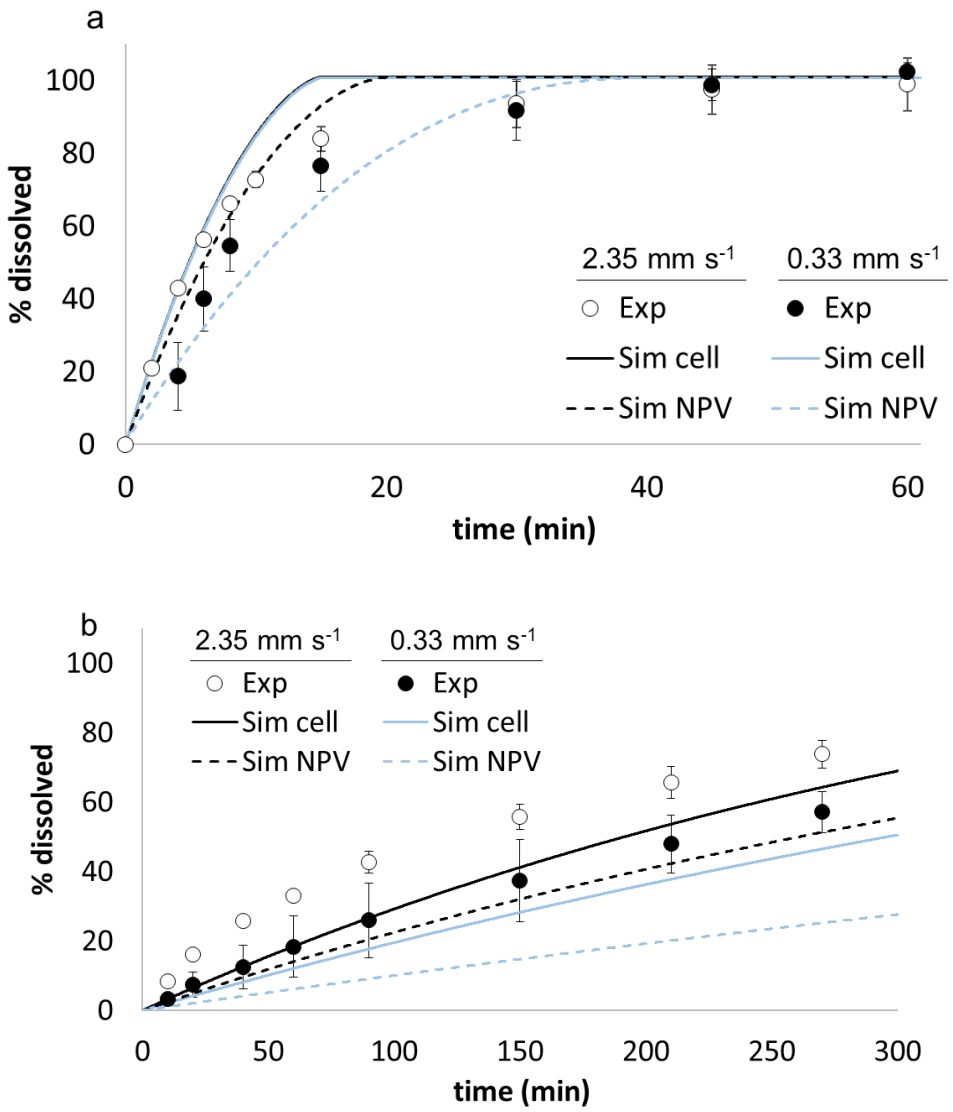

Figure 3.1. Mean experimental (exp) dissolution profiles (±SD) of 5 mg of 160 µm median diameter ibuprofen particles in 200 ml of (a) pH 6.8 phosphate buffer or (b) 0.1 M HCl, with 0.003% w/v Tween 20 at 37ºC in the FTA at two average linear fluid velocities: 2.35 mm s^{-1} (white circles) and 0.33 mm s^{-1} (black circles) (n = 3). Simulated (sim) profiles were obtained with an MPS and particle motion enabled and either cell volume (solid lines) or a NPV (dashed lines) for 2.35 mm s^{-1} (black) and 0.33 mm s^{-1} (blue).

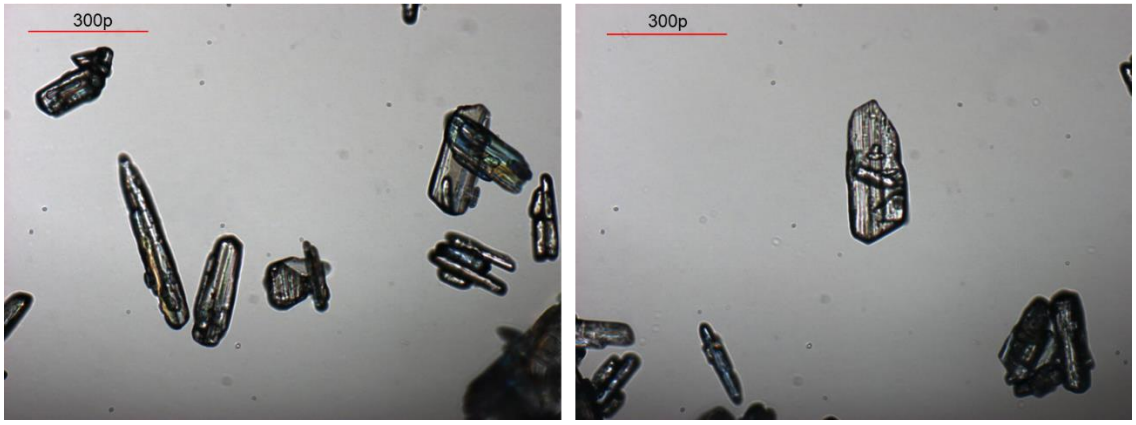

Figure 3.2. Ibuprofen crystals visualized under Olympus BX53 optical microscope with a magnification of x20.

Table 3.1. t85 or t50 (min) in the FTA with a constant 200 ml reservoir volume and gravity enabled. Some of the simulations in the low solubility environment (0.1 M HCl + 0.003% Tween 20, represented by a solubility of 0.064 mg ml^{-1}) did not reach 50% dissolved in 300 min.

Variables							t85 in the FTA	
Test ID	Solubility (mg ml^{-1})	Mass (mg)	Velocity (mm s^{-1})	Bulk volume	Particle size (µm)	Particle motion	Simulated	Experimental
1	3.5	5	2.35	Cell	MPS	On	9.99	16.92±5.51
2	3.5	5	2.35	NPV	MPS	On	12.55	
3	3.5	5	2.35	NPV	PSD	On	18.03	
4	3.5	5	2.35	NPV	PSD	Off	16.11	
5	3.5	5	0.33	Cell	MPS	On	10.09	22.43±4.36
6	3.5	5	0.33	NPV	MPS	On	22.13	
7	3.5	5	0.33	NPV	PSD	On	22.34	
8	3.5	5	0.33	NPV	PSD	Off	30.53	
9	3.5	50	2.35	Cell	MPS	On	10.98	40.89±1.38
10	3.5	50	2.35	NPV	MPS	On	16.05	

11	3.5	50	2.35	NPV	PSD	On	19.98	
12	3.5	50	2.35	NPV	PSD	Off	18.23	
13	3.5	50	0.33	Cell	MPS	On	11.53	69.65±7.01
14	3.5	50	0.33	NPV	MPS	On	37.19	
15	3.5	50	0.33	NPV	PSD	On	30.58	
16	3.5	50	0.33	NPV	PSD	Off	38.30	
							t50 in the FTA	
17	0.064	5	2.35	Cell	MPS	On	282.68	131.01±16.85
18	0.064	5	2.35	NPV	MPS	On	>300	
19	0.064	5	2.35	NPV	PSD	On	223.42	
20	0.064	5	2.35	NPV	PSD	Off	174.50	
21	0.064	5	0.33	Cell	MPS	On	284.30	219.35±44.84
22	0.064	5	0.33	NPV	MPS	On	>300	
23	0.064	5	0.33	NPV	PSD	On	>300	
24	0.064	5	0.33	NPV	PSD	Off	>300	

3.2.3.2. Particle size distribution (PSD) versus median particle size (MPS)

The simulations were run with an NPV, particle motion enabled and either an MPS or a PSD (**Figure 3.3**). Although the shape of the 5 mg dissolution profile in pH 6.8 phosphate buffer resembled the experimental results more closely than when an MPS was used in both velocities (**Figure 3.3**), the PE% and RMSE were larger for the simulations using a PSD (**Figure 3.4a**). This is due to the fast simulated dissolution at early timepoints from the contribution of the small particles (12.7 µm) and the slower simulated dissolution at later timepoints due to the contribution of the larger particles (551 µm).

Moreover, there was a particularly high PE% for early timepoints when a PSD was used in the pH 6.8 phosphate buffer medium, especially in the lower velocity flow field. This could be due to the hydrophobic nature of the ibuprofen particles making them prone to aggregation and therefore behaving as bigger particles at the beginning of the test, even though a small amount of surfactant was used to promote dispersal. An aggregation effect could be considered more likely in the low velocity flow field. Therefore, a PSD could be more useful for drugs not as prone to aggregation as ibuprofen. However, it was as accurate as an MPS when predicting t85 in the low velocity environment and even more accurate than an MPS in high fluid velocity (**Table 3.1**).

In the low solubility media, 0.1 M HCl, a PSD increased the prediction accuracy, reducing the RMSE and PE% to a similar extent in both velocities (**Figure 3.3b** and **Figure 3.4b**). It increased the ability of the simulation to predict the t50 in a high fluid velocity environment, even though the observed time was still exceeded by approximately 92 min (**Table 3.1**).

Overall, PSD improved the predictive accuracy in the low solubility environment, but a notable underprediction was still observed.

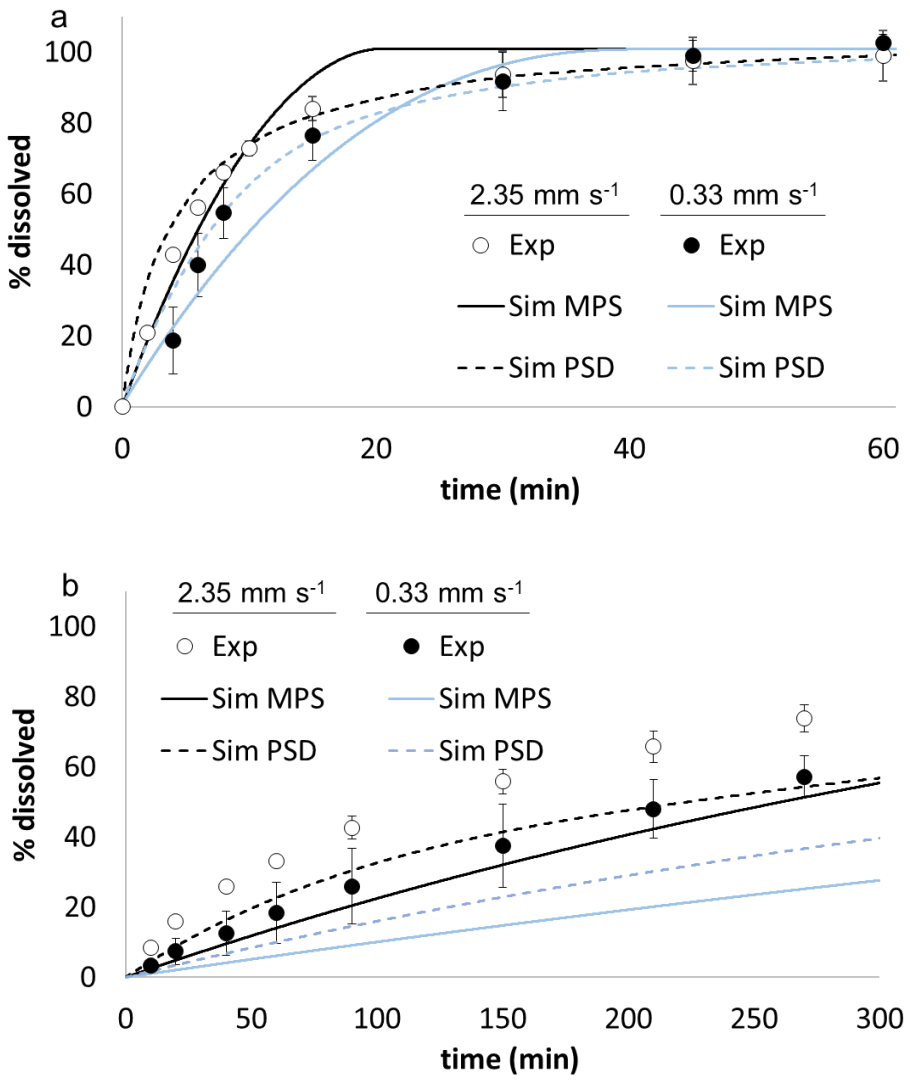

Figure 3.3. Mean experimental (exp) dissolution profiles (±SD) of 5 mg of 160 µm median diameter ibuprofen particles in 200 ml of (a) pH 6.8 phosphate buffer or (b) 0.1 M HCl, with 0.003% w/v Tween 20 at 37ºC in the FTA at two average linear fluid velocities: 2.35 mm s^{-1} (white circles) and 0.33 mm s^{-1} (black circles) (n = 3). Simulated (sim) profiles were obtained with a NPV and particle motion enabled and either an MPS (solid lines) or a PSD (dashed lines) for 2.35 mm s^{-1} (black) and 0.33 mm s^{-1} (blue).

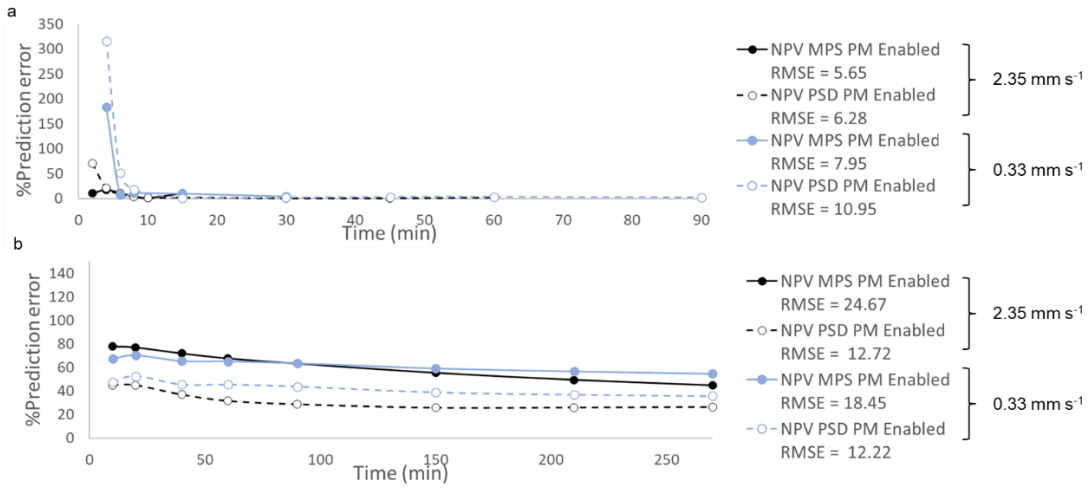

Figure 3.4. PE% versus time profiles and RMSE values of 5 mg of 160 µm median diameter ibuprofen particles in 200 ml of (a) pH 6.8 phosphate buffer or (b) 0.1 M HCl with 0.003% w/v Tween 20 at 37ºC in the FTA at two average linear fluid velocities, 2.35 mm s^{-1} (black) or 0.33 mm s^{-1} (blue). Simulated results were obtained with a NPV, particle motion enabled and either a MPS (solid lines) or a PSD (dashed lines).

3.2.3.3. Particle motion enabled versus disabled

Preliminary particle motion simulations were run as described in "2.4.2 Particle motion simulations in SIMDISSO™" and the results are shown in **Figure 3.5**.

Both velocities present a semi-sinusoidal profile due to the pulsating flow with which the media enters the dissolution cell. Fluid velocities fluctuated between zero and positive values, as defined by the velocity input in the code, with two pulses per second. Particle velocity fluctuated between positive and negative values, which represent upward flow and downward flow, respectively, but the magnitude of the positive values was larger, suggesting particles would move to the top of the cell and be held there at initial stages of dissolution until small enough to move with the fluid. Therefore, these results suggest that particle motion should be disabled, at least during the first instances of dissolution. In light of these results, simulations were run with disabled particle motion in both media.

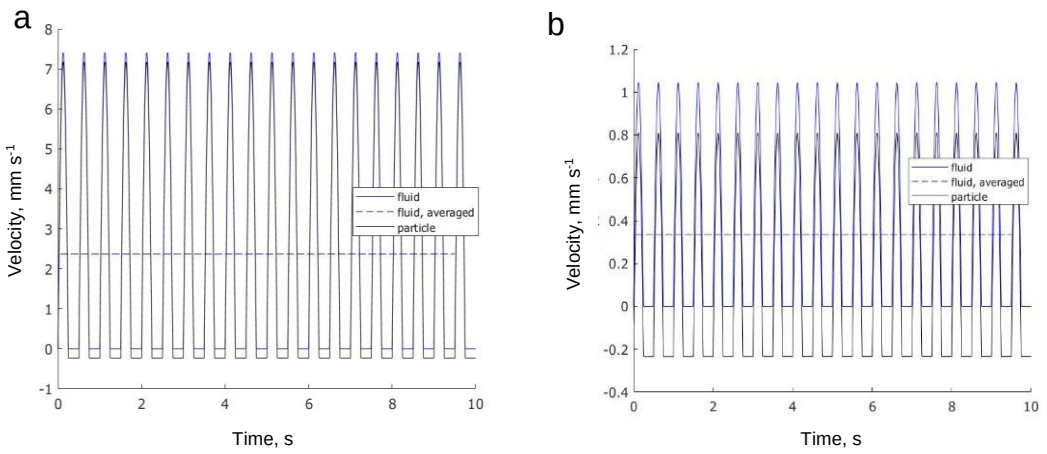

Figure 3.5. Particle motion simulations for 5 mg of 160 µm diameter ibuprofen particles in 200 ml of 0.1 M HCl at 37ºC in the FTA with (a) a flow rate of 16 ml min^{-1} and a cell diameter of 12 mm or (b) a flow rate of 8 ml min^{-1} and a cell diameter of 22.6 mm.

In the case of pH 6.8 phosphate buffer, the results were similar when disabling and enabling particle motion (**Figure 3.6**), and within or very close to the error bars for the 5 mg profile, therefore the usefulness of disabling particle motion was not proven in that particular situation (**Figure 3.6a**).

With respect to the predictive ability of the simulation in pH 6.8 phosphate buffer, it gave an accurate prediction of t85 in a high fluid velocity media, but so did the options with particle motion enabled and an NPV, and in the low fluid velocity situation it predicted a larger t85 than observed (**Table 3.1**).

In the case of 0.1 M HCl, disabling particle motion in a high fluid velocity situation led to the most accurate prediction of the four options and the closest t50 to the observed, but it resulted in an almost superimposable profile as that generated when particle motion was enabled in the case of a low fluid velocity (**Figure 3.6b**). This is because the difference between maximum initial relative velocity (0.225 mm s^{-1}) and maximum initial fluid velocity (1.033 mm s^{-1}) was very small in the low fluid velocity scenario, therefore the velocity that the particle is exposed to is similar when particle motion is enabled or disabled. In the case of a higher fluid velocity, when the particle is exposed to fluid velocity only (maximum 7.398 mm s^{-1}) – that is, when particle motion is disabled – this is of a notably larger magnitude than the relative velocity it is exposed to when particle motion is

enabled (0.235 mm s^{-1}) (**Figure 3.5**), leading to a faster dissolution rate in the former case.

Therefore, disabling particle motion only slightly increased the predictive ability in the low solubility-high velocity conditions simulated in the current work.

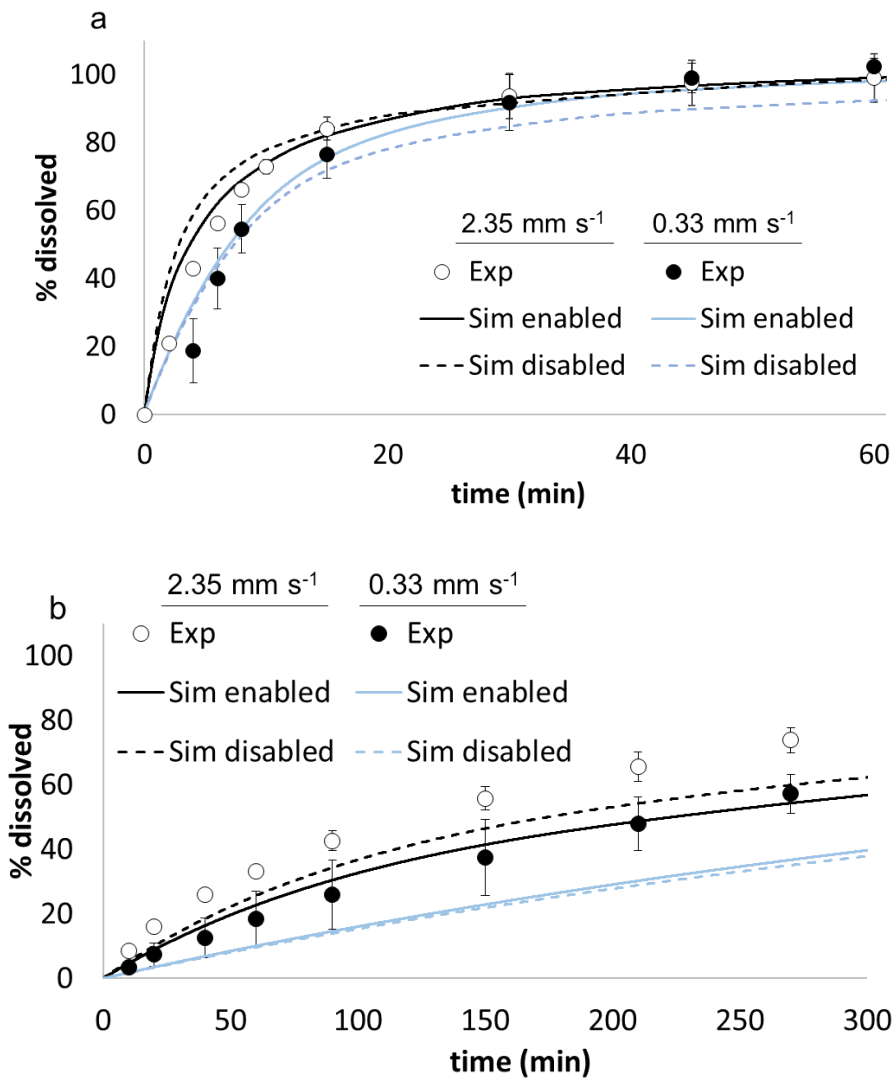

Figure 3.6. Mean experimental (exp) dissolution profiles (±SD) of 5 mg of 160 µm median diameter ibuprofen particles in 200 ml of (a) pH 6.8 phosphate buffer or (b) 0.1 M HCl, with 0.003% w/v Tween 20 at 37°C in the FTA at two average linear fluid velocities: 2.35 mm s^{-1} (white circles) and 0.33 mm s^{-1} (black circles) (n = 3). Simulated (sim) profiles were obtained with a PSD, NPV and particle motion enabled (solid lines) or disabled (dashed lines) for 2.35 mm s^{-1} (black) and 0.33 mm s^{-1} (blue).

3.2.3.4. Predictive ability of the simulation with different drug loadings

All simulation options predicted the dissolution of 5 mg of ibuprofen in pH 6.8 phosphate buffer in the FTA at both velocities reasonably well whereas there was a large overprediction for a mass of 50 mg (**Figure 3.7**), especially for the high velocity environment (**Figure 3.7a**). Even inputting a PSD, with and without particle motion enabled, did not improve the predictions for a mass of 50 mg, compared to inputting an MPS.

Furthermore, all predicted t85 values were lower than the experimental times obtained (**Table 3.1**). This overprediction of the dissolution rate was previously observed with a mass of 10 mg in the FTA when clumping was suspected [1]. The lower predicted t85 values in the current work could be due to visible clumping which was observed to occur in the experimental test, which reduces the surface area exposed to the medium and therefore the dissolution rate. This is not captured by the simulation, which assumes individual spherical particles that do not interact. To ensure particle dispersal. A small amount of surfactant was used in the medium, namely 0.003% w/v Tween 20. This was successful in dispersing the particles without affecting solubility to a great extent when a small mass of ibuprofen was used, but clumping was still visible for the bigger mass of 50 mg. Furthermore, the time to wet the particles at the beginning of the test, resulting in a reduced initial effective surface area for dissolution, may be influencing the overprediction. Wetting issues have been observed previously in the dissolution of ibuprofen API [111]. Therefore, the effect of mass is important in terms of inputting an accurate particle size in the simulation.

In addition to clumping, the saturation with a higher mass can affect the local instantaneous concentration. When using the whole cell volume option in the simulation, combined with an MPS and enabled particle motion, no difference in dissolution rate was predicted between both masses in pH 6.8 phosphate buffer at both velocities. This can be attributed to a very low bulk concentration in the whole reservoir volume of 200 ml entering the cell volume and affecting cell concentration. When an NPV was input in the simulations instead, and the rest of the inputs were maintained, the simulations predicted a difference in the dissolution rate of the two masses in pH 6.8 phosphate buffer, and this difference was larger for a low fluid velocity. This was due to a smaller instantaneous volume

available for the particles to dissolve, and therefore a reduction in the magnitude of the gradient driving dissolution.

When working under sink conditions, as defined by reservoir volume concentration, this observed difference in dissolution between masses is not expected as bulk concentration is assumed to be negligible, however this assumption may be too simplistic for dissolution conditions with low fluid velocity, where the amount of drug transported from the cell into the reservoir is smaller per timestep. Therefore, the fluid local to the dissolving particle might become more concentrated and theoretical sink conditions may not be occurring at all instances in practice.

Overall, even though there was an overprediction in simulated dissolution rates, the relative difference between dissolution rates in each flow field, for a mass of 50 mg, was somewhat captured by the NPV-PSD simulations (70% experimental difference versus 55% simulated difference).

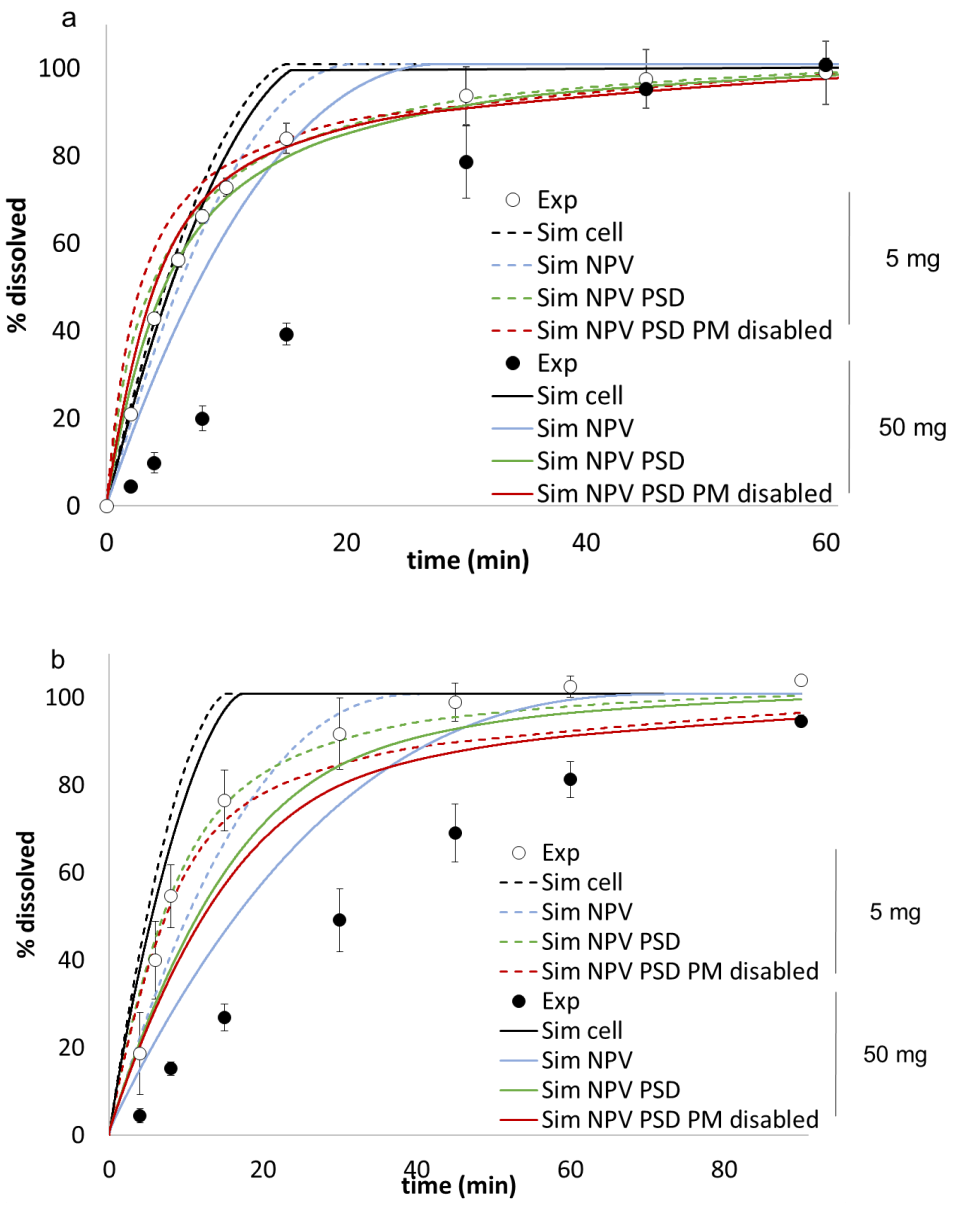

Figure 3.7. Mean experimental (exp) dissolution profiles (±SD) of 5 mg (white circles) and 50 mg (black circles) of 160 µm diameter ibuprofen particles in 200 ml of pH 6.8 phosphate buffer with 0.003% w/v Tween 20 at 37°C in the FTA at two average linear fluid velocities of (a) 2.35 mm s^{-1} and (b) 0.33 mm s^{-1} (n = 3). Simulated (sim) profiles were obtained for 5 mg (dashed lines) and 50 mg (solid lines) with an MPS, particle motion enabled and cell volume (black); an MPS, particle motion enabled and NPV (blue); a PSD, particle motion enabled and NPV (green); a PSD, particle motion disabled and NPV (red).

3.2.4. Dissolution tests in the paddle apparatus

Four tests in the paddle apparatus are presented in **Figure 3.8**: 50 mg in pH 6.8 phosphate buffer at (1) 100 rpm and (2) 50 rpm and 3 mg in 0.1 M HCl at (3) 100 rpm and (4) 50 rpm. The dissolution profiles were obtained as described in section “2.3.8.2. Dissolution tests in the paddle apparatus”.

Again, dissolution in pH 6.8 phosphate buffer was rapid (85% within 30 min) and, in contrast to the FTA, 100% dissolved was observed in the experimental 0.1 M HCl test at 100 rpm due to the presence of sink conditions.

Simulated profiles in the paddle apparatus were obtained as described in section “2.4.4. Input parameters for the paddle apparatus dissolution simulations in SIMDISSO™”.

There was an experimental difference in the dissolution profiles between operating at 50 and 100 rpm in both media that was not reflected in the simulated profiles, where both profiles were superimposable (**Figure 3.8**). This can be due to better dispersion at 100 rpm and observed sedimentation at 50 rpm which would result in the particles being exposed to very different velocities in each case. Dissolution in pH 6.8 phosphate buffer was incomplete after one hour, but it was sufficient to determine t85. Furthermore, notable variability was observed, especially at 50 rpm (**Table 3.2**). The observed sedimented undissolved material at the 1 h time point is likely due to poor initial wetting and subsequent poor dispersal of ibuprofen particles in the low velocity region at the centre of the vessel base. Whereas it is also possible that the relatively high concentration of buffer salts used resulted in the formation and precipitation of sodium or potassium salts of ibuprofen during the dissolution test [111], similar undissolved material was not noted in the FTA tests, suggesting an impact from system hydrodynamics.

In both media, the PSD option seemed more accurate than a MPS from the dissolution profiles in **Figure 3.8**. However, in terms of predictions, a MPS was relatively accurate in predicting <30 min for t85 in pH 6.8 phosphate buffer at a 100 rpm (predicted 14 min versus experimental 8 min), and more accurate than a PSD, due to the slow simulated dissolution of the bigger particles in later stages of dissolution (**Table 3.2**).

Neither an MPS nor a PSD were accurate in predicting the time dissolved at 50 rpm probably because the sedimentation observed during the test was not captured by the simulation, which incorporated only tangential velocity effects. Furthermore, there was no difference in using the cell volume or an NPV for either medium. This can be due to both the fluid velocity and the cross-sectional flow area, which influence how NPV concentration changes over time, being of a higher magnitude in the paddle apparatus simulations than in the FTA.

In 0.1 M HCl, a PSD simulation predicted a closer t50 when compared to an MPS (**Table 3.2**), however both t50 predictions were of a much higher magnitude than the experimental results, as can be observed by the underprediction in **Figure 3.8.**

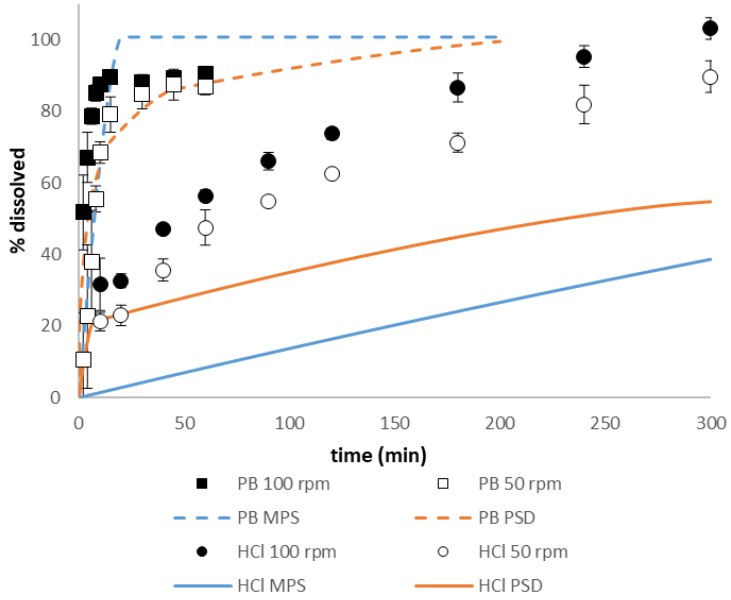

Figure 3.8. Mean experimental dissolution profiles (±SD) of 50 mg of 160 µm median diameter ibuprofen particles in 500 ml of pH 6.8 phosphate buffer (PB) with 0.003% w/v Tween 20 (squares) and 3 mg in 500 ml 0.1 M HCl with 0.003% w/v Tween 20 (circles) at 37ºC in the paddle apparatus at two agitation speeds: 50 rpm (white) and 100 rpm (black) (n = 3). Simulated profiles were obtained with an MPS (blue) or a PSD (orange). Simulated results were obtained using a velocity of 0.1746 m s^{-1}, representing 100 rpm or 0.0766 m s^{-1}, representing 50 rpm (results were superimposable) and cell volume or NPV (results were superimposable). Particle motion was enabled in all simulations.

Table 3.2. t85 or t50 (min) in the paddle apparatus with 500 ml reservoir volume and gravity disabled. Some of the simulations in the low solubility environment (0.1 M HCl + 0.003% w/v Tween 20, represented by a solubility of 0.064 mg ml^{-1}) did not reach 50% dissolved in 300 min.

Variables						t85 in the paddle apparatus		
Test ID	Solubility (mg ml^{-1})	Mass (mg)	Velocity (rpm)	Particle size (µm)	Particle motion	NPV	Vessel volume	Experimental
1	3.5	50	50	MPS	On	14.30	14.05	28.14±16.74
2	3.5	50	50	PSD	On	40.70	40.55	
3	3.5	50	100	MPS	On	14.16	14.05	8.04±6.70
4	3.5	50	100	PSD	On	40.58	40.61	
						t50 in the paddle apparatus		
5	0.064	3	50	MPS	On	-	>300	77.87±5.08
6	0.064	3	50	PSD	On	-	230.46	
7	0.064	3	100	MPS	On	>300	>300	44.59±5.48
8	0.064	3	100	PSD	On	-	230.46	

3.3. Discussion

The predictions were accurate for the rapid dissolution of a low mass of ibuprofen in pH 6.8 phosphate buffer in the FTA, but there was a general underprediction in 0.1 M HCl. This could be due to surface area effects leading to a faster dissolution due to the discrepancy between the actual particle morphology and the assumption of spherical particles in the simulation, however in the current work the simulation using PSD suggested only a minor impact if any from the assumption of sphericity on available surface area. Conversely there was an overprediction of dissolution rate in a high mass system, likely influenced by agglomerated particles observed in the dissolution cell. The observed needle-shaped particle morphology is also likely to contribute to particle agglomeration and caking to a greater extent than would be expected from spherical particles.

In considering dissolution according to the Nernst Brunner equation, flow rate will affect dissolution rate as it will impact the ADBL thickness. In the presented model, using the Ranz-Marshall correlation, the hydrodynamic effect is captured by the Reynolds number, even without considering an NPV. However, defining bulk concentration using NPV better captured the velocity effect.

An NPV volume in the current work was defined as a spherical volume surrounding the particle, which extends a distance of 1 radius from the particle surface. This NPV is a hypothetical situation of a bulk volume which is smaller than the reservoir (or vessel) volume, but how this volume is defined can vary. Any multiple of radii can be input but one was chosen as the smallest NPV thickness that can reasonably be explored as, in a static fluid, due to the asymptotic molecular diffusion effect, the Sherwood number has been demonstrated to equal 2, meaning that the ADBL thickness equals the particle radius [214]. In a moving fluid, where a Re-dependent term is included, the ADBL thickness will decrease although, due to the pulsing flow in the FTA, there can still be periods of near static fluid. Therefore, the thickness of the ADBL will not exceed the NPV thickness at any moment in time. An NPV extending one radius from the particle surface is considered to be the minimum NPV which can be explored if the dissolution medium has periods of static motion. The current work represents an illustration of the effect of a reduced volume in dissolution

simulations as sink conditions might be present globally but not locally, especially in the FTA with a pulsing flow with periods of very low velocity. The results presented indicate that the concept of a more dynamic bulk concentration definition, influenced by both local and reservoir concentrations and transport between both, is potentially useful, both in simulating dissolution in the FTA and in considering the effect of flow rate, pulsation and cell size on experimental results.

The use of a PSD increased the predictive ability of the simulations in a low solubility medium, but it might not always be required, as was shown in the case of a hydrophobic drug such as ibuprofen in a fast dissolution environment, pH 6.8 phosphate buffer, where use of an MPS could be considered sufficiently accurate for many applications. The measured PSD might also not be representative of the effective PSD in the dissolution medium.

Furthermore, it is important to characterize particle motion as, if the difference between fluid velocity and relative velocity is large, as was the case in the high fluid velocity in 0.1 M HCl, this can affect the accuracy of the prediction. SIMDISSO^{TM} takes particle motion into account but there is scope to better explore the simulation of particle motion and local volume to optimally capture the interplay between hydrodynamic effects and local concentration gradients.

Limitations and assumptions include the assumption of individually dissolving spherical particles in the simulation code used for the current work. Therefore, agglomeration of hydrophobic drugs or needle-shaped particles, which were observed experimentally, are not taken into account, and the effect of non-spherical particle morphology on surface area is not captured. The particle size input also has a large influence on the simulated profiles, and particle size measurement methodology and bin allocation will affect the predicted dissolution rates. Finally, particle density, which can impact particle motion and thus the simulated dissolution profiles, was not measured for the current work but extracted from literature, as its effect in ibuprofen dissolution simulations was previously investigated extensively [1].

3.4. Conclusions

The implementation of an NPV available for the particle to dissolve in was compared with the whole FTA cell volume or paddle vessel volume. The NPV was useful to predict effects of velocity differences in a high solubility media in the FTA, accounting for the reduction in the dissolution rate as velocity is reduced. The simulation could capture two very different environments in terms of solubility for the same drug: 0.1 M HCl, where ibuprofen is not very soluble (0.064 mg ml^{-1}), and pH 6.8 phosphate buffer, where ibuprofen is highly soluble (3.5 mg ml^{-1}), even though it underpredicted the dissolution rate in low solubility conditions – in both apparatuses -, especially when the NPV option was used.

In the light of these findings, it could be argued that the cell volume option more accurately captured the experimental profiles in 0.1 M HCl in the FTA, however the underprediction of the NPV option was reduced when other factors were included in the simulation, namely a PSD and disabling particle motion. Therefore, the advantage of cell over NPV cannot be ascertained without further investigation of the confounding effects of other simulation inputs, including effects of particle morphology on exposed surface area.

The PSD option served to increase the predictive ability of the simulations especially in the low solubility medium. In the high solubility medium, the accuracy of the prediction when a PSD was used suggests that in fast dissolution situations use of an MPS could result in a sufficiently accurate simulation, reducing the computational cost.

Whether to have particle motion enabled or disabled can be informed by preliminary simulations which predict particle motion in the first ten seconds of dissolution based on particle mass, particle density and fluid velocity and density. Disabling particle motion was not advantageous in the high solubility medium, but it increased the predictive ability in a high velocity-low solubility scenario pointing towards the need for a good particle motion model in dissolution simulation.

Finally, the current work also presents the predictive ability of SIMDISSO^{TM} as applied to the paddle apparatus. The accuracy of the prediction was reasonable for fast dissolution – high solubility medium, but it underpredicted the dissolution rate in a low solubility situation. This underprediction was probably due to the

relative velocity being too low when only tangential velocity was included, without the impact of axial flow and gravitational effects. Consequently, the different hydrodynamic environment for sedimented versus suspended particles is not considered in the current simulations. This highlights the need to identify optimal hydrodynamic inputs for situations where dissolution is slower.

Chapter 4. *In vitro* and *in silico* methods to investigate the effect of moderately increasing medium viscosity and density on ibuprofen dissolution rate.

Results, discussion and conclusions presented in the current chapter have been published in the following paper: Navas-Bachiller, M., Persoons, T., D'Arcy, D.M. (2023). *In vitro* and *in silico* methods to investigate the effect of moderately increasing medium viscosity and density on ibuprofen dissolution rate. *Eur J Pharm Biopharm,* **193**, 74-88. https://doi.org/10.1016/j.ejpb.2023.10.018

4.1. Introduction

The viscosity of the human gastric fluid (HGF) in the fasted state was measured to be higher than that of water (1.7-9.3 mPa.s versus 0.7 mPa.s) at a shear rate of 50 s^{-1} [3]. The intrinsic dissolution rate (IDR) of the drug cinnarizine in HGF was lower than in FaSSGF, whose viscosity is that of water [159]. Other examples in the literature showed a reduction of drug dissolution and tablet disintegration following small increases of medium viscosity [158, 160, 161]. The viscosity effect might be explained through a reduced drug diffusivity with increased viscosity, as per the Stokes-Einstein (St-E) equation [166] (1.1) which directly impacts the drug dissolution rate in the Nernst-Brunner equation [167, 168] (1.2) and/or through effects on particle suspension and dispersal, as detailed in the Introduction section “1.4.8.5. Viscosity”.

The current work studied the *in vitro* IDR and particulate dissolution rate of ibuprofen in the FTA and paddle apparatus with varying levels of viscosity from 0.7 to 5.5 mPa.s and different fluid velocities in two solubility media with two VEAs, HPMC and sucrose.

Three viscosity levels were explored in the work: 0.7 mPa.s (level 1), 1.3-1.4 mPa.s (level 2) and 4.5-5.5 mPa.s (level 3). 0.7 mPa.s was selected as the viscosity of water, and aqueous buffers, at 37^{o}C. A viscosity of 1.3-1.4 mPa.s was considered as it represents the viscosity of milk [2, 295], which has been used to simulate the gastric fed state [296] and it has been shown to delay water

penetration and disintegration times of tablets by four to five times [297]. This viscosity level is also relevant to parenteral formulations, as the viscosity of plasma is 1.1-1.3 mPa.s [298]. A viscosity range of 4.4-5.5 mPa.s was selected as the mid-range viscosity of the HGF in the fasted state [3].

The resulting experimental dissolution profiles were compared to simulated dissolution profiles in SIMIDISSO^{TM}. *In silico* particle motion was also investigated to understand the effect of increasing medium viscosity on particle suspension and dispersal. A spatial limitation to particle motion was defined in the FTA as the height of the flow-through cell so that once the particle reaches the top or bottom of the cell, it cannot move further. Therefore, motion is restricted in the vertical direction of the specified cell dimensions and the calculated relative velocity value reflects this. There is no requirement to explore the effect of enabling or disabling particle motion as explored in Chapter 3. Particle motion is enabled but limited at the vertical boundaries of the cell. The output of particle motion simulations is in the format of **Figure 4.1**, where the pulsing flow is evident, and the particle vertical location changes with time.

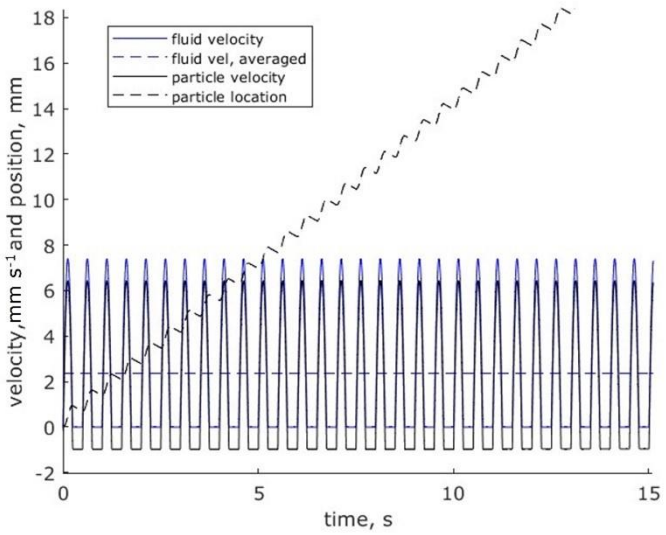

Figure 4.1. 15-second simulation of ibuprofen particle velocity, fluid velocity and particle vertical location in the cell. Particle size: 160 µm, medium: pH 6.8 phosphate buffer, mass: 5 mg, cell diameter: 12 mm, flow rate: 16 ml min^{-1}, viscosity: 1.4 mPa.s.

The aims of this work were to assess the interplay of viscosity and fluid flow on the dissolution rate of ibuprofen both *in vitro* and *in silico*, to assess the ability of the *in silico* simulation to predict effects of viscosity on dissolution and to explore the use of simulated particle motion in interpreting the effect of viscosity on observed and simulated dissolution.

4.2. Results

4.2.1. Viscosity versus concentration plots

Results of the viscosity-concentration plots study which was carried out as described in section “2.3.4 Viscosity versus concentration plots” are presented in **Figure 4.2**. The viscosity of a 25% w/v sucrose solution was 1.41 mPa.s in pH 6.8 phosphate buffer and 1.30 mPa.s in 0.1 M HCl (level 2 viscosity). The concentration of sucrose necessary for a density-adjusted viscosity of 4.5 mPa.s was 59% w/v (level 3 viscosity). From the studies with HPMC, the concentrations needed for viscosities of 1.4 mPa.s (level 2) and 5.5 mPa.s (level 3) were 0.3% w/v and 1.05% w/v, respectively, in both media.

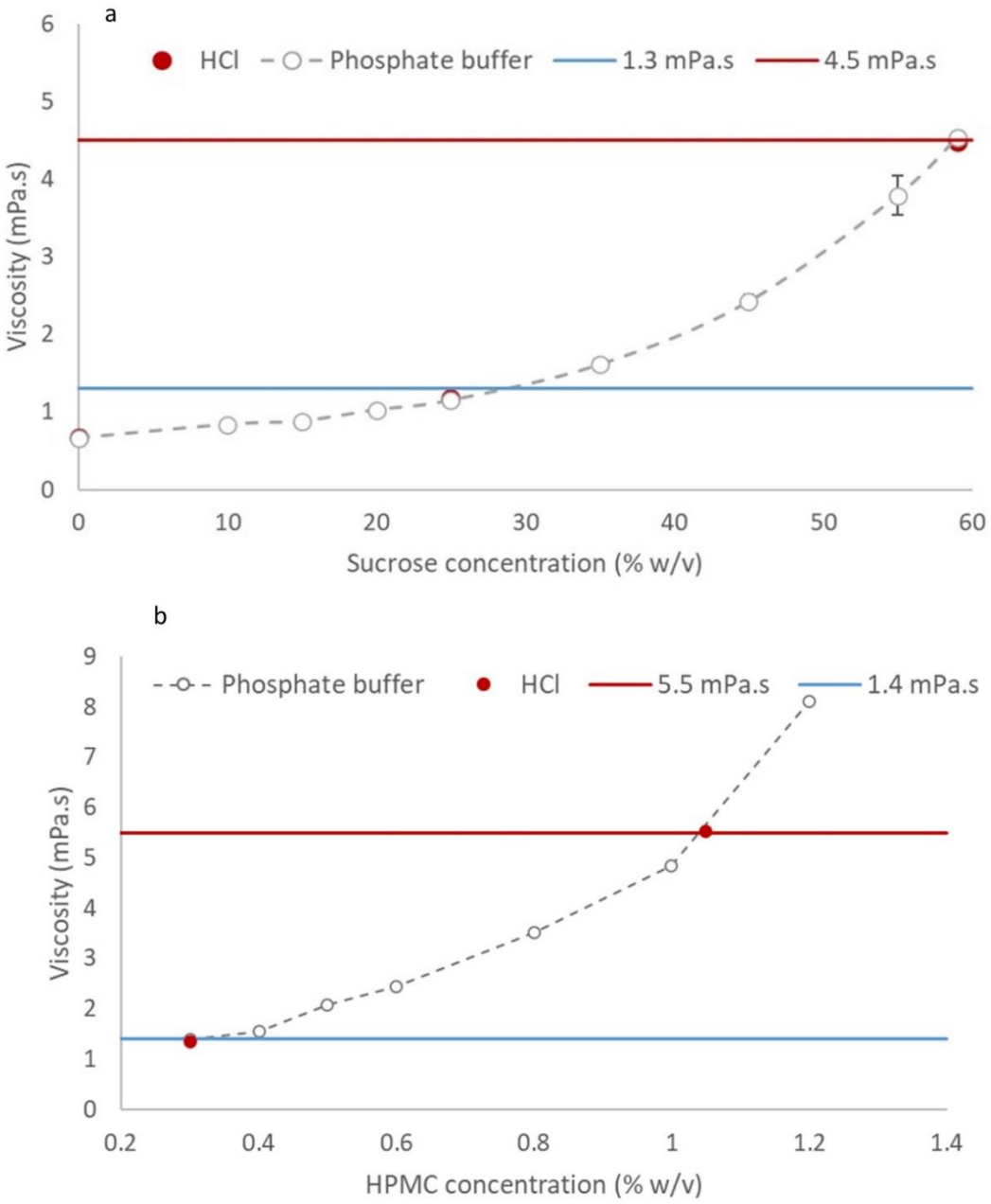

Figure 4.2. Mean fluid viscosity (±SD) in mPa.s versus (a) sucrose or (b) HPMC concentration in pH 6.8 phosphate buffer or 0.1 M HCl (n = 3).

4.2.2. Solubility study

Saturation solubility of ibuprofen measured as described in "2.3.2. Solubility study" for each medium after 24 h is presented in **Table 4.1**. None of the solubility values of media containing a VEA were statically significantly different from media without VEA, however, even though not statistically significant, level 3 HPMC seemed to marginally increase the solubility of ibuprofen.

4.2.3. Density studies

The fluid density of each medium measured as described in "2.3.3. Density study" is presented in **Table 4.1**. Sucrose had a greater impact on density than HPMC at the concentrations used. Each experimentally determined value of density and solubility at 24 h was input in the simulations for each medium (**Table 2.3**).

Table 4.1. Fluid density (g ml^{-1}) and ibuprofen saturation solubility (mg ml^{-1}) after 24 hours of incubation at 37^{o}C and 100 rpm in different media used for dissolution testing (n=3).

	pH 6.8 phosphate buffer		0.1 M HCl	
Viscosity level and VEA	**Fluid density**	**Solubility 24h**	**Fluid density**	**Solubility 24h**
Level 1 (No VEA)	0.999±0.001	2.79±0.31	0.994±0.001	0.063±0.015
Level 2 Sucrose	1.091±0.002	3.26±0.06	1.088±0.002	0.059±0.002
Level 3 Sucrose	1.219±0.002	2.24±0.20	1.221±0.000	0.050±0.007
Level 2 HPMC	1.004±0.000	2.97±0.10	1.000±0.000	0.047±0.002
Level 3 HPMC	1.005±0.001	3.46±0.19	0.997±0.001	0.044±0.004

4.2.4. Intrinsic dissolution and diffusion coefficient

Intrinsic dissolution tests were carried out in media of increasing viscosity as described in section "2.3.8.3. Intrinsic dissolution".

Moderately increasing medium viscosity reduced the IDR of ibuprofen in pH 6.8 phosphate buffer with both VEAs (**Figure 4.3**). The two profiles for each level of viscosity were comparable, although a slightly slower rate can be observed in the level 3 medium when sucrose was used as VEA.

The reduction of the IDR can be explained through the St-E equation (1.1), according to which an increase in viscosity results in a decrease in diffusion coefficient, and the Nernst-Brunner equation (1.2), which correlates a reduced

diffusion coefficient to a decrease in dissolution rate. The theoretical St-E *D* values are presented in **Table 4.2**. The predicted *I* for dissolution, inputting the calculated St-E *D* in the Levich equation, was lower than the observed *I* in intrinsic dissolution tests, in particular for media with HPMC as VEA. Using the Levich equation combined with the observed IDRs to calculate the *D* value enabled incorporation of the slightly higher than expected *D* values, compared to those predicted from equation (2.1) using the St-E *D* values from equation (1.1). The Levich equation accurately predicted the *D* value in pH 6.8 phosphate buffer with no VEA (0.80×10^{-9} m^2 s^{-1}). Moreover, the Levich method predicted *D* values comparable to those experimentally obtained for sucrose level 2 (0.58×10^{-9} m^2 s^{-1} (at 1.03 mPa.s) and 0.38×10^{-9} m^2 s^{-1} (at 1.66 mPa.s)) [285, 286]. Therefore, calculating *D* values using the Levich equation combined with the intrinsic dissolution data was used to estimate *D* for the simulations.

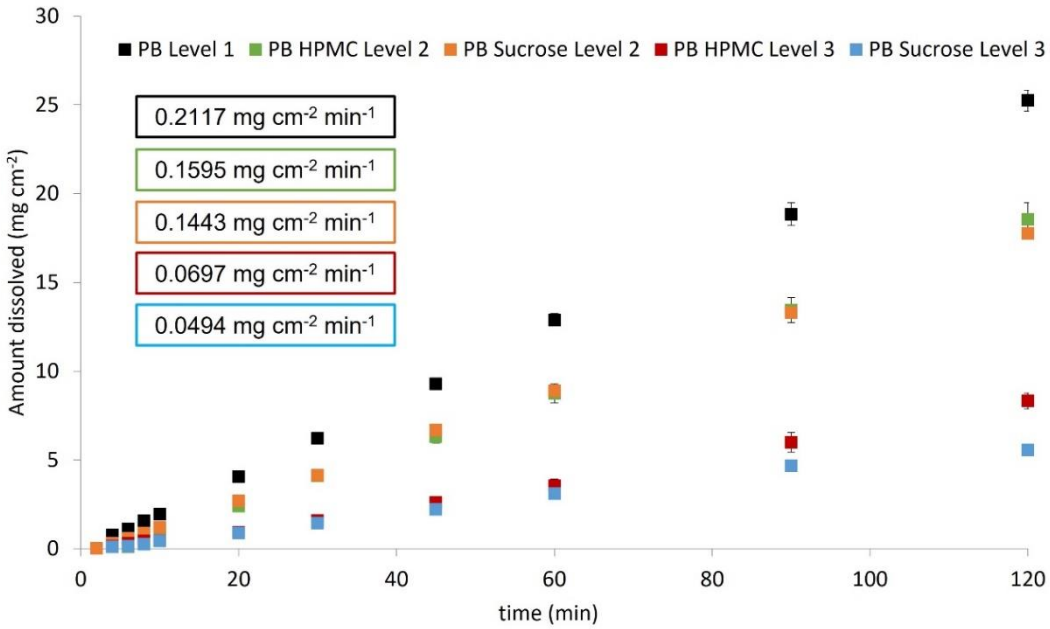

Figure 4.3. Mean intrinsic dissolution profiles (±SD) and dissolution rates (insets) from a rotating disk of ibuprofen in 500 ml of media at 37°C and 50 rpm. PB level 1: black; PB HPMC level 2: green; PB Sucrose level 2: orange; PB HPMC level 3: red; PB Sucrose level 3: blue (n = 3).

Table 4.2. Calculated D using the Levich equation with observed I and calculated D using St-E (n=3). Reference literature value for PB (pH 6.8 phosphate buffer) level 1 D is 0.80 × 10^{-9} m^2 s^{-1} [286]; observed (from intrinsic dissolution studies) and predicted I (through inputting the calculated St-E D in the Levich equation). Table adapted from Navas Bachiller *et al*. [299].

Medium	D±SD from Levich equation using observed I (m^2 s^{-1}) × 10^9	St-E D (m^2 s^{-1}) × 10^9	Observed I (mg min^{-1})	Predicted I with St-E D (mg min^{-1})
PB level 1	0.80±0.065	0.77	0.106	0.103
Sucrose level 2	0.43±0.013	0.42	0.074	0.073
Sucrose level 3	0.15±0.010	0.12	0.025	0.021
HPMC level 2	0.54±0.080	0.39	0.078	0.062
HPMC level 3	0.18±0.025	0.10	0.035	0.023

4.2.5. Observed and simulated dissolution in flow-through apparatus (FTA)

Dissolution tests were carried out as described in section "2.3.8.1. Dissolution tests in the flow-through apparatus" and the simulated profiles were obtained in SIMIDISSO™ as per section "2.4.1. Input parameters for the flow-through apparatus dissolution simulations in SIMDISSO™".

4.2.5.1. Sucrose

In 0.1 M HCl, increasing sucrose concentration resulted in a decrease in the experimental dissolution rate in both fluid velocity environments (**Figure 4.4a1**). At early timepoints (<40 min) both an increase in viscosity and a decrease in velocity resulted in a lower percentage dissolved (**Figure 4.4a2**). In pH 6.8 phosphate buffer, the reduction in dissolution with increasing viscosity was still present but less clear due to the faster dissolution.

Simulated results overestimate the dissolution rate by up to 20–25% dissolved in both pH 6.8 phosphate buffer and 0.1 M HCl, likely due to a simulated faster dissolution of the smaller particles than occurs experimentally (**Figure 4.4a2**).

This suggests that the smallest particles may not have behaved as individual particles but may have aggregated. However, the t50 is well predicted, especially in higher velocity conditions in both pH 6.8 phosphate buffer and 0.1 M HCl, and t85 in pH 6.8 phosphate buffer is reasonably predicted in levels 1 and 2 of viscosity in high fluid velocity (**Table 4.3** and **Table 4.4**). In low velocity conditions, the accuracy of the predictions was lower due to the effect of velocity not being evident in the experimental dissolution tests (**Table 4.3**). In level 3 viscosity the effect of viscosity was over-estimated by the simulations at later timepoints, suggesting a more complex interplay between viscosity and velocity than that simulated. Similarly, in 0.1 M HCl, the prediction of t50 in the high fluid velocity environment was accurate (234 versus 237 min, level 2, sucrose (**Table 4.4**)), however in low fluid velocity, the impact of reducing velocity was overestimated, resulting in the simulated t50 not being achieved in 300 min.

4.2.5.2. HPMC

HPMC had a lesser effect on the dissolution rate than sucrose, as a reduction in the experimental dissolution rate with increased viscosity was only observed in the profiles in 0.1 M HCl (**Figure 4.4b1-2**), and only between level 1 and level 2 viscosity.

In pH 6.8 phosphate buffer, the simulations seem to underpredict the dissolution rate, especially for level 3, leading to an overprediction of t85, but to a larger extent in the low fluid velocity environment (100 min simulated time versus 17 min experimental time) (**Figure 4.4b**, **Table 4.3**). The t50 in HPMC was well predicted overall in pH 6.8 phosphate buffer, apart from in the low velocity environment in level 3 where t50 was also overestimated. There was no observed difference in t50 between level 2 and 3 viscosity, whereas the simulated value suggested a notable increase (5.16 versus 12.29 min (**Table 4.4**)). In 0.1 M HCl, there is also an underprediction of dissolution as viscosity increases, leading to simulated t50 values being over 300 min for level 2 and 3, except for level 2 in the fast fluid velocity (249 min), which still overpredicts the experimental t50 (223 min) (**Figure 4.4b**, **Table 4.4**).

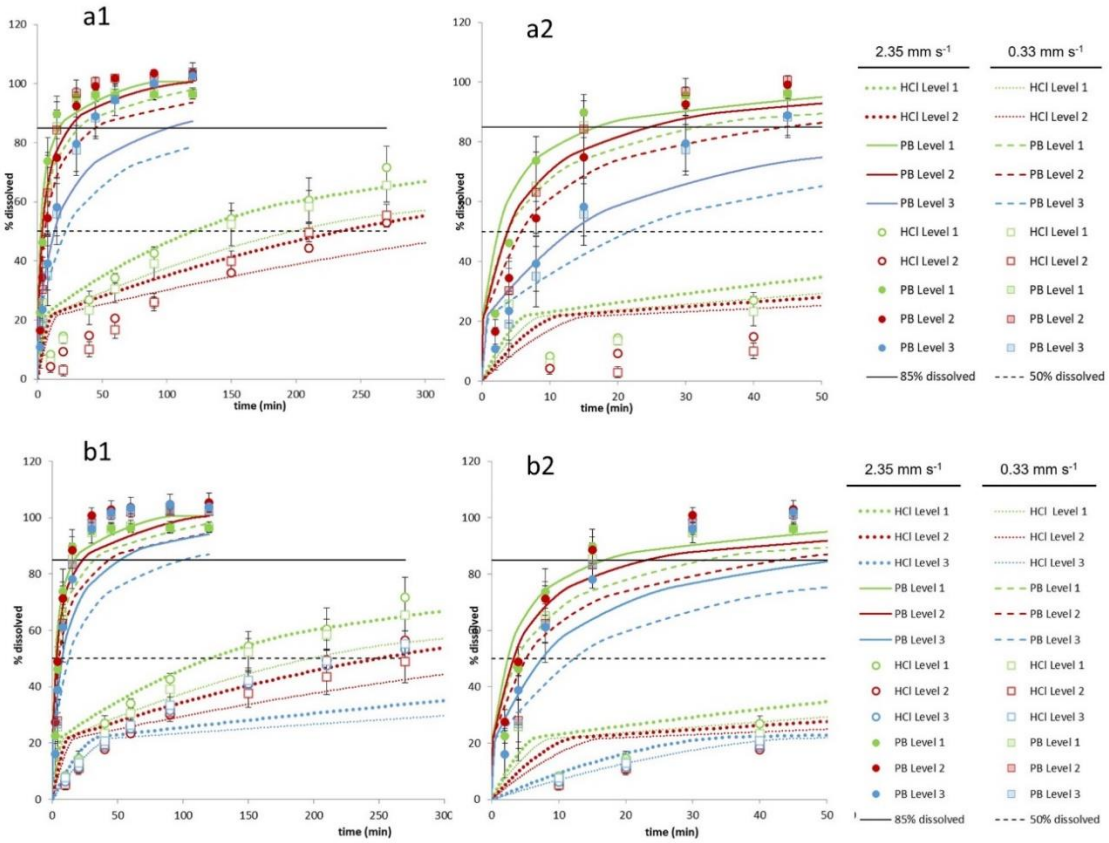

Figure 4.4. Mean experimental dissolution profiles (±SD) of 5 mg of ibuprofen particles in 200 ml of pH 6.8 phosphate buffer (filled icons) or 0.1 M HCl (empty icons) with 0.003% w/v Tween 20 containing (a) sucrose VEA or (b) HPMC VEA at 37ºC in the FTA at two average linear fluid velocities: 0.33 mm s^{-1} (squares) and 2.35 mm s^{-1} (circles) (n = 3). Simulated profiles were generated for 2.35 mm s^{-1} (solid lines – pH 6.8 phosphate buffer; thick dots – 0.1 M HCl) and 0.33 mm s^{-1} (dashed lines – pH 6.8 phosphate buffer; thin dots – 0.1 M HCl). Level 1: green, level 2: red, level 3: blue viscosity levels. Mean observed (±SD) and predicted dissolution profiles at earlier timepoints (≤50 min) are emphasised in Figures a2 and b2.

Table 4.3. Experimental (n=3) and simulated t85 and k_{diss} (pH 6.8 phosphate buffer) in the FTA using a PSD.

	Variables						t85 dissolution in the FTA (min)		
Dissolution Test ID	Solubility (mg ml^{-1})	Mass (mg)	Velocity (mm s^{-1})	VEA	Viscosity (mPa.s)	PS (μm)	Simulated	Experimental	k_{diss} (min^{-1})
1	3.5	5	2.35	-	Level 1	PSD	16.87	12.96±0.91	0.167±0.012
2	3.5	5	2.35	Sucrose	Level 2	PSD	24.73	19.66±3.55	0.092±0.017
3	3.5	5	2.35	Sucrose	Level 3	PSD	101.19	34.72±11.08	0.059±0.022
4	3.5	5	2.35	HPMC	Level 2	PSD	23.17	11.78±1.67	0.143±0.014
5	3.5	5	2.35	HPMC	Level 3	PSD	51.83	16.80±3.54	0.106±0.023
6	3.5	5	0.33	-	Level 1	PSD	31.9	18.53±6.60	0.126±0.031
7	3.5	5	0.33	Sucrose	Level 2	PSD	44.75	17.16±5.68	0.117±0.036
8	3.5	5	0.33	Sucrose	Level 3	PSD	>120	37.88±12.99	0.053±0.012
9	3.5	5	0.33	HPMC	Level 2	PSD	43.25	16.98±2.90	0.108±0.019
10	3.5	5	0.33	HPMC	Level 3	PSD	99.78	17.27±3.09	0.106±0.019

Table 4.4. Experimental (n=3) and simulated t50 in pH 6.8 phosphate buffer and 0.1 M HCl in the FTA using a PSD.

	Variables						t50 dissolution in the FTA (min)	
Dissolution Test ID	Solubility (mg ml^{-1})	Mass (mg)	Velocity (mm s^{-1})	VEA	Viscosity (mPa.s)	PS (µm)	Simulated	Experimental
1	3.5	5	2.35	-	Level 1	PSD	2.44	4.41±0.28
2	3.5	5	2.35	Sucrose	Level 2	PSD	3.81	7.49±1.42
3	3.5	5	2.35	Sucrose	Level 3	PSD	13.13	13.03±4.26
4	3.5	5	2.35	HPMC	Level 2	PSD	3.31	4.58±0.56
5	3.5	5	2.35	HPMC	Level 3	PSD	7.53	6.49±1.37
6	3.5	5	0.33	-	Level 1	PSD	3.84	6.28±2.01
7	3.5	5	0.33	Sucrose	Level 2	PSD	5.84	6.41±2.05
8	3.5	5	0.33	Sucrose	Level 3	PSD	21.75	13.87±4.23
9	3.5	5	0.33	HPMC	Level 2	PSD	5.16	6.39±1.06
10	3.5	5	0.33	HPMC	Level 3	PSD	12.29	6.50±1.10

11	0.064	5	2.35	-	Level 1	PSD	120.34	139.47±12.27
12	0.064	5	2.35	Sucrose	Level 2	PSD	234.08	237.27±20.66
13	0.064	5	2.35	HPMC	Level 2	PSD	249.01	223.51±40.33
14	0.064	5	2.35	HPMC	Level 3	PSD	>300	233.04±24.91
15	0.064	5	0.33	-	Level 1	PSD	196.89	158.04±26.39
16	0.064	5	0.33	Sucrose	Level 2	PSD	>300	221.99±15.01
17	0.064	5	0.33	HPMC	Level 2	PSD	>300	282.61±65.44
18	0.064	5	0.33	HPMC	Level 3	PSD	>300	217.20±28.09

4.2.5.3. Factors affecting dissolution in the flow-through apparatus

Pareto charts are presented as outputs of the statistical analysis of the experimental dissolution data performed in section "2.3.10. Statistical analysis of viscosity, velocity and solubility effects on dissolution metrics for ibuprofen" (**Figure 4.5**). The test ID and significant results originally presented in **Table 2.1** are represented in **Table 4.5** for clarity.

The effect of solubility was significant for t50, with the mean t50 reduced by 189 min when solubility was increased from low (0.1 M HCl) to high (pH 6.8 phosphate buffer) (Test 1).

The effect of viscosity was significant in both 0.1 M HCl, for t50 (Test 2), and pH 6.8 phosphate buffer, for t85 (Test 3), and k_{diss} (Test 4).

The interaction between viscosity and solubility was significant for t50, as increasing viscosity extended t50 to a larger extent in 0.1 M HCl (by 93 min) than in pH 6.8 phosphate buffer (by 1 min) (Test 1).

Carrying out the statistical analysis within each solubility medium allowed determination that the VEA used was significant only in pH 6.8 phosphate buffer, for k_{diss} (Test 3) and t85 (Test 4), and not in 0.1 M HCl for t50 (Test 2), meaning that the effect of increasing viscosity with HPMC or sucrose was statistically similar for t50 in 0.1 M HCl (104 min for HPMC and 80 min for sucrose), but only levels 1 and 2 of viscosity were available for this analysis. Although the VEA used was not significant for t50 in 0.1 M HCl, a different effect at early timepoints (≤40 min) can be noted with dissolution in HPMC being faster than in sucrose for level 2 viscosity (**Figure 4.4a2-b2**).

The interaction between the VEA used and viscosity significantly affected experimental t85 (Test 3) but not k_{diss} (Test 4) in pH 6.8 phosphate buffer. In fact, when viscosity was increased from level 1 to level 2, t85 was increased by 3 min and k_{diss} was decreased by 0.042 min^{-1} in sucrose-containing media, whereas in HPMC-containing media, t85 decreased by 1 min and k_{diss} decreased by 0.021 min^{-1}. This suggests that, for this level of viscosity in pH 6.8 phosphate buffer in the FTA, HPMC has little impact on dissolution whereas sucrose delays it. When a further increase in viscosity was studied (level 3), t85 increased by a further 18 min in sucrose-containing media and 3 min in HPMC-containing media and k_{diss} decreased more in sucrose-

containing media than in HPMC-containing media (0.038 min^{-1} for sucrose and 0.019 min^{-1} for HPMC), indicating that this level of viscosity slows down dissolution for both VEAs, albeit to a larger extent for sucrose.

The effect of fluid velocity was not significant in pH 6.8 phosphate buffer, for t85 (Test 3) and k_{diss} (Test 4), nor 0.1 M HCl, for t50 (Test ID 2), although a trend was observed in 0.1 M HCl in level 2 (sucrose VEA) at early time points (≤40 min).

Overall, as expected, solubility significantly affected t50. The effect of increasing viscosity was more impactful in 0.1 M HCl, as implied by the interaction with solubility. The VEA used was only significant for pH 6.8 phosphate buffer, both for t85 and k_{diss}.

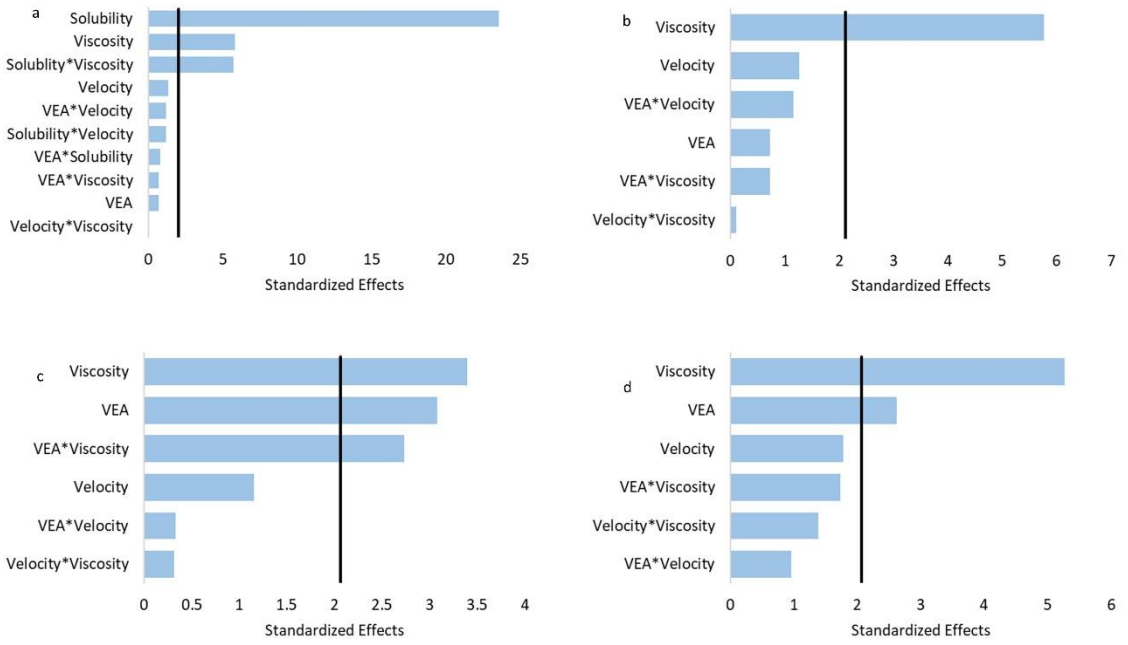

Figure 4.5. Pareto charts of the estimated effects (horizontal bars) of solubility, viscosity, velocity and VEA and their interactions in the FTA on (a) Test ID 1: t50, in pH 6.8 phosphate buffer and 0.1 M HCl, (b) Test ID 2: t50 in 0.1 M HCl, (c) Test ID 3: t85 in pH 6.8 phosphate buffer and (d) Test ID 4: k_{diss} in pH 6.8 phosphate buffer (n = 3). The effect was deemed significant when it overcame the critical value for statistical significance (vertical line).

Table 4.5. Factors, levels, dissolution metric and significant results (p-value <0.05) for each factorial design. High solubility = pH 6.8 phosphate buffer, low solubility = 0.1 M HCl. * denotes interaction. Sol (solubility), vel (velocity), visc (viscosity).

Test ID	Solubility	Average vel. (mm s^{-1})	Viscosity (mPa.s)	VEA	Metric	Significant result
1	High, low	0.33, 2.35	Level 1, Level 2	Sucrose, HPMC	t50	Sol Visc Sol*Visc
2	Low	0.33, 2.35	Level 1, Level 2	Sucrose, HPMC	t50	Visc
3	High	0.33, 2.35	Level 1, Level 2, Level 3	Sucrose, HPMC	t85	Visc VEA VEA*Visc
4	High	0.33, 2.35	Level 1, Level 2, Level 3	Sucrose, HPMC	k_{diss}	Visc VEA

4.2.6. Particle motion simulations

The intrinsic dissolution results showed an effect from both VEAs in pH 6.8 phosphate buffer, whereas HPMC did not show a large influence on the particulate dissolution rate in pH 6.8 phosphate buffer in the FTA; therefore the difference in the effect of VEA on dissolution rate observed in the FTA versus the intrinsic dissolution apparatus must relate to the particles and their wettability and hydrodynamic effects on particle motion.

Particle motion simulations were run as described in section "2.4.2. Particle motion simulations in SIMDISSO^{TM}" and the results are presented in **Figure 4.6** and **Figure 4.7**. Even though the two largest particle size bins were not lifted in 1200 s (**Figure 4.6**), they could experience some upward and downward motion at the base of the cell during the course of a pulse. Increasing viscosity reduced the time it took for particles from a simulated PSD to start lifting from the bottom and to reach the top of the cell in both velocities (**Figure 4.6**). This was further demonstrated by the time that it took for an individual (MPS) particle to reach the top of the cell (**Figure 4.7**), which was reduced as viscosity increased in both velocities, but to a larger extent in the low velocity environment. These results illustrate that increasing viscosity could impact the dissolution rate by improving the dispersal of the drug mass and increasing the surface area exposed to the medium.

In the high fluid velocity environment (**Figure 4.7a**), the average relative velocity of a moving particle decreased with viscosity for both VEAs, however it took less than 120 s for the simulated particles to reach the top of the cell in the five scenarios simulated. Therefore, as these simulations are based on MPS particles, any impact on dissolution from velocities at the bottom of the cell is likely to be relevant for larger particle sizes only. Due to the effect of density on buoyancy, level 3 sucrose simulated relative velocity is negative, as the particle is moving upward faster than the fluid. In the low fluid velocity environment (**Figure 4.7b**), relative velocity was also reduced as viscosity was increased for sucrose, but for HPMC, for the time period simulated, a level 3 viscosity was necessary to lift the particles from the bottom, highlighting the importance of fluid density and buoyancy on particle behaviour.

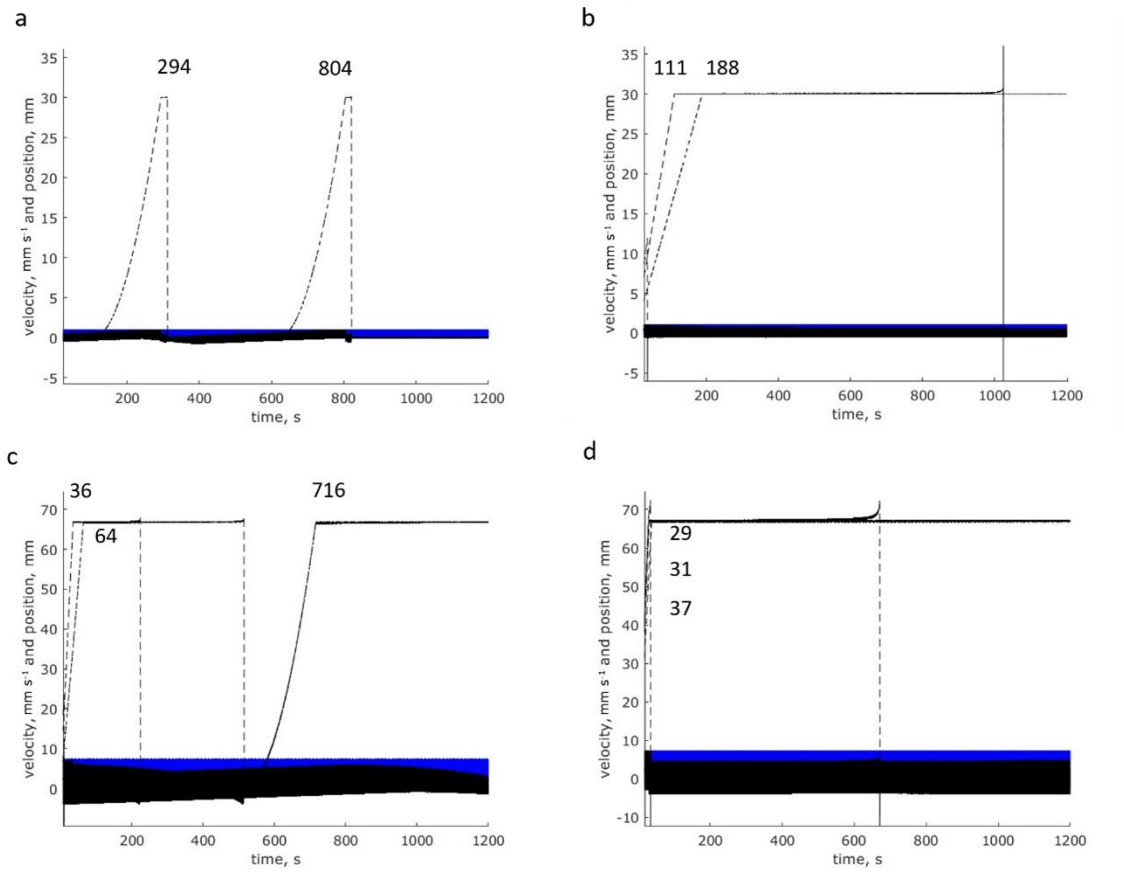

Figure 4.6. 1200 s simulations of fluid velocity, particle velocity and particle location (dashed black lines) for a PSD in a flow-through cell. (a) Low velocity-level 1 viscosity (b) Low velocity-level 3 viscosity (5.5 mPa.s) (c) High velocity-level 1 viscosity (d) High velocity-level 3 viscosity (5.5 mPa.s). Numbers indicate the time when particles from a specific bin reached the top of the cell. The pulses appear as thick blue and black bands at the bottom due to the time being simulated and are not distinguishable as individual pulses.

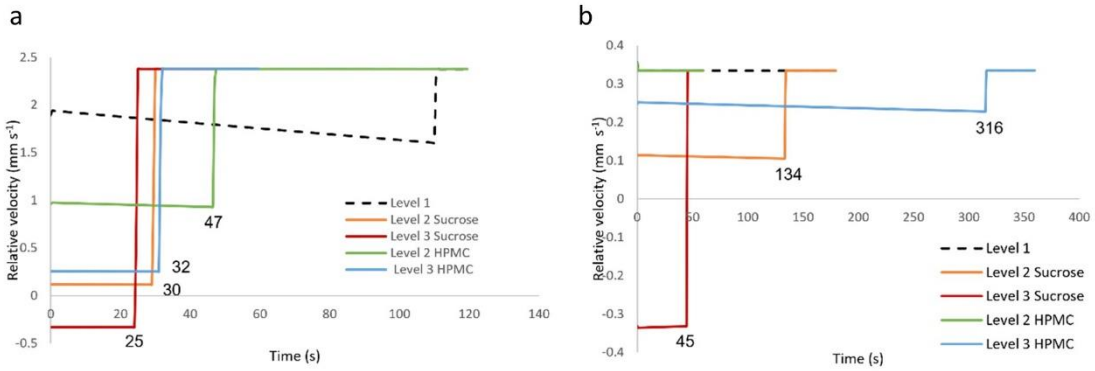

Figure 4.7. Relative velocity (mm s^{-1}) versus time (s) from MPS particle motion simulations. Numbers correspond to the time when particles reached the top of the cell (s). (a) High fluid velocity, (b) low fluid velocity.

4.2.7. Dissolution in the paddle apparatus

Dissolution tests were carried out as described in section "2.3.8.2. Dissolution tests in the paddle apparatus". Only one VEA could be used, HPMC, as with sucrose, the HPMC capsules containing the ibuprofen did not rupture within an hour.

In pH 6.8 phosphate buffer (**Figure 4.8**), the large error bars can be explained due to variability in capsule rupture times, as even though the time for the first capsule to rupture was set as time zero, not all capsules ruptured and released the ibuprofen at the same time, and additionally the exit and dispersal from the capsule of the powder occurred at variable times. As shown in **Figure 4.8** (right), this variability was larger at 50 rpm, pointing to more variability in capsule rupture patterns in low velocity environments.

All the average percentages dissolved at each timepoint were higher at 100 rpm than 50 rpm. Dissolution tests in level 2 viscosity showed a higher percentage dissolved at each timepoint than in level 1 medium. Although this might be influenced by the large variability, it supports the theory of HPMC increasing wettability of ibuprofen (and potentially a marginal effect on solubility at higher HPMC concentrations).

In 0.1 M HCl (**Figure 4.9**), all average percentages dissolved per timepoint at 100 rpm were larger than those at 50 rpm, after the two first timepoints, where variability can be due to different capsule breaking times. At 100 rpm, it is difficult to observe an effect from HPMC, as all profiles are very similar and almost superimposable after the first

two timepoints. At 50 rpm, increasing the concentration of HPMC decreased the dissolution rate, in particular for level 3.

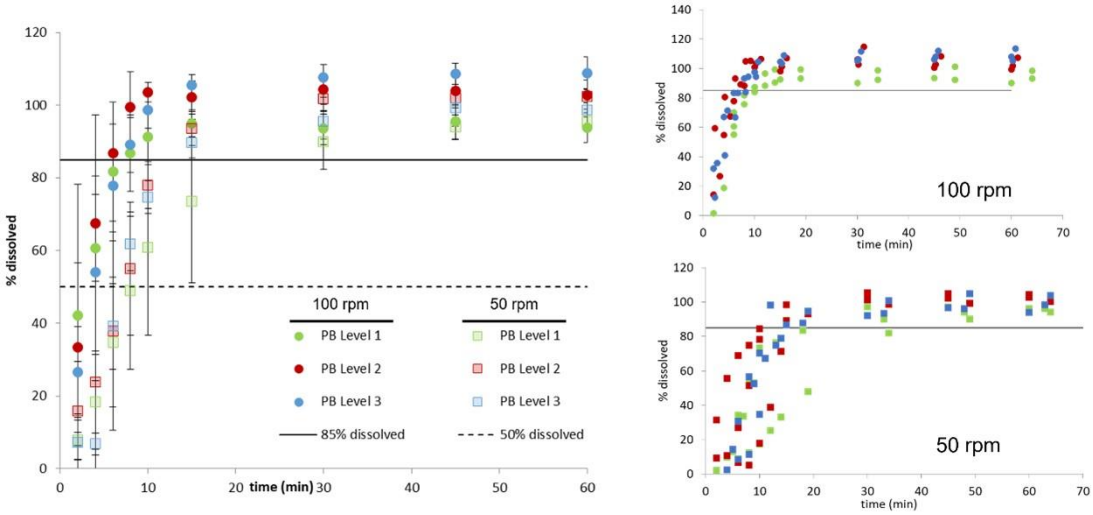

Figure 4.8. Mean experimental dissolution profiles (±SD) of 50 mg of ibuprofen particles in 500 ml of pH 6.8 phosphate buffer or with 0.003% w/v Tween 20 at 37ºC containing HPMC in the paddle apparatus at two rotational speeds: 50 rpm (squares) and 100 rpm (circles), with three replicates averaged (left) and individual datapoints (right) for each level of viscosity, Level 1: green, level 2: red, level 3: blue (n = 3).

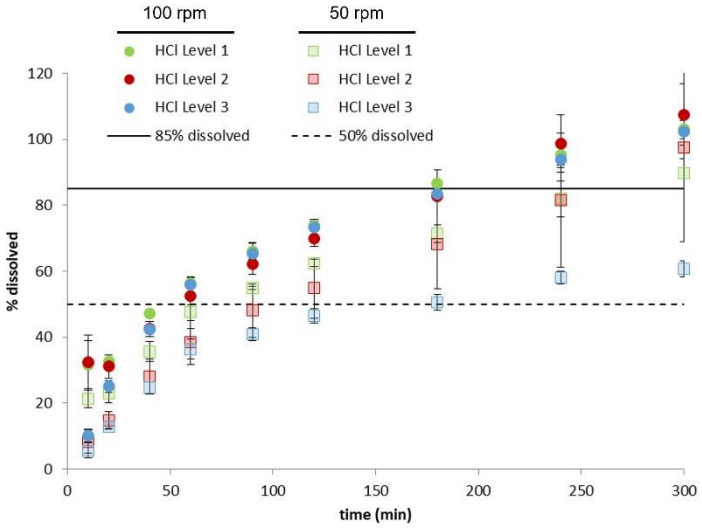

Figure 4.9. Mean experimental dissolution profiles (±SD) of 3 mg of ibuprofen in 500 ml of 0.1 M HCl with 0.003% w/v Tween 20 at 37ºC containing HPMC in the paddle apparatus at two rotational speeds: 50 rpm (squares) and 100 rpm (circles), for each level of viscosity, Level 1: green, level 2: red, level 3: blue (n = 3).

4.2.7.1. Factors affecting dissolution in the paddle apparatus

Pareto charts are presented as outputs of the statistical analysis of the experimental dissolution data performed in section "2.3.10. Statistical analysis of viscosity, velocity and solubility effects on dissolution metrics for ibuprofen" (**Figure 4.10**). The test ID and significant results originally presented in **Table 2.1** are represented in **Table 4.6** for clarity.

As expected, the effect of solubility was significant for t50, with the mean time to 50% dissolved reduced by 83 min when solubility was increased from low (0.1 M HCl) to high (pH 6.8 phosphate buffer) (Test 5).

The effect of velocity was significant for t50 for both higher and lower solubility media, pH 6.8 phosphate buffer and 0.1 M HCl, respectively (Test 5), and also for t85 (Test 7) and k_{diss} (Test 8) in pH 6.8 phosphate buffer. Increasing agitation speed from 50 rpm to 100 rpm reduced the mean t85 from 21 to 8 min and increased k_{diss} from 0.105 min^{-1} to 0.312 min^{-1}.

The interaction between solubility and agitation speed was significant for t50, as increasing the agitation speed reduced t50 to a larger extent in 0.1 M HCl (by 71 min) than in pH 6.8 phosphate buffer (by 5 min) (Test 5), as was expected due to the slower dissolution of ibuprofen in 0.1 M HCl.

Viscosity was significant for t50 in both media (Test 5). The interaction between solubility and viscosity was significant for t50 in both media, as increasing viscosity from level 1 to level 3 increased t50 to a larger extent in 0.1 M HCl (by 57 min) than in pH 6.8 phosphate buffer, where increasing viscosity from level 1 to level 3 decreased t50 (by only 1 min) (Test 5), which was in agreement with the low solubility of ibuprofen in 0.1 M HCl.

Finally, the interaction between agitation speed and viscosity was significant for t50 in both media, meaning that the effect of viscosity was larger in the low agitation environment (Test 5).

While viscosity significantly affected t50 in both solubilities, carrying out separate analysis for each medium showed that viscosity did not affect t85 (Test 7) nor k_{diss} (Test 8) in pH 6.8 phosphate buffer. The same occurred for the interaction between agitation speed and viscosity, which was significant for t50 in both media, but it was not significant for t85 nor k_{diss} in pH 6.8 phosphate buffer. This suggests that as dissolution is almost complete at t85 in pH 6.8 phosphate buffer, it is more difficult to detect the influence of any effect using this metric.

Overall, the effect of solubility was significant for t50, and the effects of velocity and viscosity were larger in 0.1 M HCl than pH 6.8 phosphate buffer, as evidenced by their interaction with solubility.

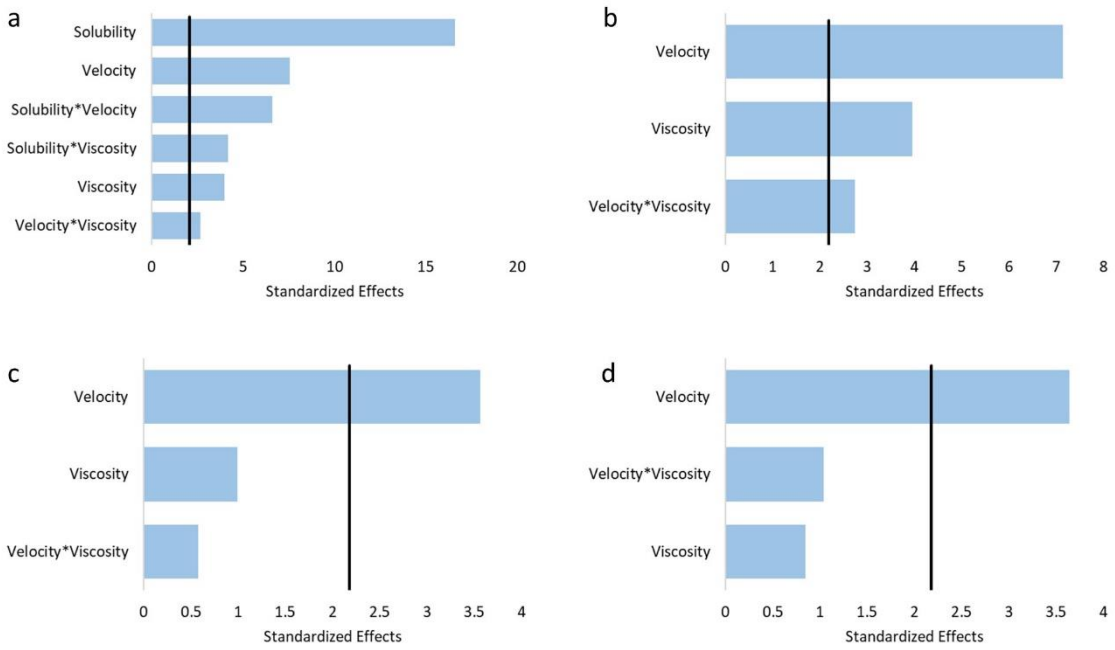

Figure 4.10. Pareto charts of the estimated effects (horizontal bars) of solubility, viscosity and velocity and their interactions in the paddle apparatus on (a) test ID 5: t50 in pH 6.8 phosphate buffer and 0.1 M HCl, (b) test ID 6: t50 in 0.1 M HCl, (c) test ID 7: t85 in pH 6.8 phosphate buffer and (d) test ID 8: k_{diss} in pH 6.8 phosphate buffer (n = 3). The effect was deemed significant when it overcame the critical value for statistical significance (vertical line).

Table 4.6. Factors, levels, dissolution metric and significant results (p-value <0.05) for each factorial design. High solubility = pH 6.8 phosphate buffer, low solubility = 0.1 M HCl. * denotes interaction. Sol (solubility), vel (velocity), visc (viscosity).

Test ID	Solubility	Rotation speed (rpm)	Viscosity (mPa.s)	VEA	Metric	Significant result
5	High, low	50, 100	Level 1, Level 2, Level 3	HPMC	t50	Sol Vel Sol*Vel Sol*Visc Visc Vel*Visc
6	Low	50, 100	Level 1, Level 2, Level 3	HPMC	t50	Vel Visc Vel*Visc
7	High	50, 100	Level 1, Level 2, Level 3	HPMC	t85	Vel
8	High	50, 100	Level 1, Level 2, Level 3	HPMC	k_{diss}	Vel

4.3. Discussion

Results showed how different VEAs influenced the dissolution rate differently. Therefore, not only is the viscosity value important but also the nature of the agent causing that viscosity increase. The different effect of two VEAs for the same value of viscosity has been described previously. Sarisuta and Parrott reported different effects in the dissolution rate of benzoic acid in aqueous solutions containing xanthan gum or non-ionic polymers (methyl cellulose and hydroxypropyl cellulose) [300].

Regardless of its concentration, the presence of sucrose in the FTA decreased the dissolution rate in both media, in particular at early time points. The reduction in dissolution rate by sucrose is thought to be due to the establishment of molecular interactions (hydrogen bonds) between sucrose and water, reducing drug diffusion [301-304] and the reduced relative velocity between particle and fluid, although this would only happen if particles are suspended and not sedimented or retained at the top of the cell. In this regard, PSD particle motion simulations supported the theory of viscosity positively affecting particle suspension, even without any fluid density increase, that is, when HPMC was selected as the VEA and not sucrose. Moreover, in the case of sucrose, the increase in viscosity was correlated to an increase in fluid density. This has an impact on the forces acting on the particle, which determine its velocity. Drag coefficient, buoyancy and fluid acceleration are proportional to fluid density. When fluid density is higher than particle density, which is the case with level 3 viscosity using sucrose as the VEA, buoyancy becomes positive and drag force and fluid acceleration also increase which ultimately results in an increase in upward particle velocity. As fluid velocity is unaltered, an increase in upward particle velocity will decrease the relative velocity for upward motion that the particle is exposed to and reduce the dissolution rate further, up to a point where buoyancy makes the particle faster than the fluid. The present results could serve as a basis for a further study into density effects separately from viscosity, where particle motion simulations provide a useful insight into predicted particle behaviour, especially when considering behaviour over a PSD.

The effect of HPMC on the particulate dissolution rate of ibuprofen was not as clear nor negative as that of sucrose. It has been shown before that for the same concentration of HPMC (0.3% w/v), and viscosity grade (80–120 cP 2% in H_2O at 20^oC)

the amount of drug dissolved - carbamazepine and paracetamol - was higher than that in the same media with no HPMC [305]. This could be due to the reported amphiphilicity and wetting capacity of HPMC which can increase the surface area available for dissolution and hence the dissolution rate [306-308] and/or particle dispersal. The dissolution rate of ethyl p-aminobenzoate has been shown to remain the same in the presence of hydroxypropyl cellulose due to the negligible effect of the polymer on drug diffusivity albeit in a different hydrodynamic system than that presented in this work (constant flow cell versus pulsating flow cell or stirred vessel) and different drug forms (pellet versus particulate) [304]. Moreover, it has been reported that a relative viscosity value of 1.6 of a polymer-containing solution was not likely to affect the dissolution rate of p-aminoethyl benzoate in a laminar flow cell dissolution set-up and that a minimum relative viscosity value of 4.0 is necessary in order to see a reduction in dissolution rate [309]. However, the current work showed a negative effect of HPMC on the IDR (in high solubility media) and on the particulate dissolution rate in low solubility media, in both the FTA and paddle apparatus. A negative effect of HPMC on the dissolution rate has been reported in the literature [164] but the concentration of HPMC used was much higher than in this work, achieving viscosities in the range of 200–600 mPa.s, more representative of the fed state. Therefore, it is difficult to predict the complex effect of viscosity on dissolution when a polymeric VEA is used.

Statistical analysis of dissolution results in the FTA and paddle apparatus showed that viscosity had a larger influence on t50 in low than in high solubility media, in both apparatuses, and additionally velocity had an influence on t50 in the paddle apparatus. This emphasises the importance of a thorough understanding and control of the effect of these two parameters when formulating and testing poorly soluble drugs.

Intrinsic dissolution results indicated a negative effect of viscosity on the dissolution rate eliminating the potential impact of surface area and particle motion effects, for both VEAs, which is in agreement with literature reports in which the decrease in IDR of low solubility drugs - griseofulvin and cinnarizine - for a viscosity range of 1.7–12 mPa.s achieved with 0.2–0.6% w/v HPMC has been described [310]. Determining the intrinsic dissolution results also enabled an assessment of the impact of using a particulate system versus a planar surface on the dissolution behaviour, and the

consequent interplay between particulate behaviour and viscosity of the medium and its effect on dissolution rate.

The applicability of SIMDISSO^{TM} in mechanistically simulating *in vitro* dissolution has been investigated and presented before [1], including in enhanced-viscosity simulations [2]. However, this was the first time that simulated outputs in increased-viscosity media were contrasted with comprehensive experimental dissolution data, enabling investigation into the interrelationship between viscosity, velocity, density, solubility and the VEA used. Simulations in sucrose in the FTA predicted that this increase in viscosity and fluid density would lead to a reduction in the dissolution rate in both flow rates and media, which was observed experimentally. Predictions were more accurate at early time points (≤15 min) in pH 6.8 phosphate buffer at level 1 and level 2–3 (sucrose VEA) and at later timepoints in 0.1 M HCl due to dissolution being slower than in pH 6.8 phosphate buffer, representing a broadly accurate simulation of t50 in all media in the high velocity environment (**Figure 4.4**, **Table 4.4**). Of note, the simulations predicted an effect from velocity which was not observed in the FTA. The transfer of momentum in a flow field is increased as viscosity increases, leading to reduced differences between regions of high and low velocity in the flow field. Therefore, the relevant experimental velocities experienced by the dissolving particles may have been impacted less by the set flow rate than those simulated. In HPMC, the simulated effect was larger than the experimental effect of viscosity on dissolution rate. This points to another factor influencing dissolution in HPMC. Factors not accounted for in the simulation include a potential effect of wettability, a more complex hydrodynamic environment than that simulated, and the potential impact of polymer VEAs on diffusion. Since the dissolution in the high solubility pH 6.8 phosphate buffer environment generally resulted in rapid dissolution (>85% in 30 min), the utility of simulating these rapid dissolution profiles should be considered. However, there is potential value in developing accurate simulations to predict the magnitude of the impact of changes in viscosity and velocity, in particular for those profiles which are at or near the boundary of the acceptable dissolution design space.

Apart from simulating the dissolution profile, the particle motion simulations gave valuable insight into the effect of viscosity on particle dispersal and relative velocity. A spatial limitation for particle motion was newly incorporated into the code and utilized to simulate particle location with time in different viscosity media. The application of

particle motion simulations could be expanded to facilitate selection of dissolution conditions.

In the paddle apparatus, simulations were not performed due to a lack of data around viscosity-induced hydrodynamic changes and the expectation that increasingly viscous media would enhance the complexity of the velocity patterns in the vessel. Combined effects from viscosity on particle dispersal and viscosity-induced transitions to laminar from turbulent flow patterns have been observed in viscous media [34]. Hydrodynamic complexity relating to viscosity has also been shown in the USP 2 mini vessel dissolution apparatus, using planar induced fluorescence for a viscosity range of 13.3–575.6 mPa.s [33].

Some of the limitations of the current work include the assumption of individually dissolving non-interacting spherical particles in the simulation code. Although this means that the effects of particle dispersal on exposed surface area are not simulated, the individual particle motion simulations suggested differences in dispersal behaviour in terms of time for the particle to be lifted from the base as viscosity is increased. The particle displacement stiffness factor was arbitrary and selected to represent a force at the top of the cell while maintaining numerical stability, but it could be further refined. The assumption of sphericity might deviate from the experimental situation, but experimentally determined surface area for the ibuprofen batch used in this work was comparable to the calculated surface area from a PSD as used in the simulations, as described in section “3.2.3.1. Cell volume versus near-particle volume (NPV)” in Chapter 3. In cases of a distinct difference in surface area, other approaches to dissolution simulation can be considered such as the simulation of irregularly shaped drug particles [224, 225]. A further assumption is that of Newtonian fluid behaviour and thus a constant viscosity in the simulated environment. Whereas HPMC solutions are known to exhibit pseudoplastic flow with shear- and concentration-dependent changes in viscosity, the assumption of Newtonian flow is considered reasonable given the low concentrations of the HPMC grade used in the current work and the low overall fluid velocities in the FTA. However, in higher agitation environments deviations from Newtonian behaviour can be expected and a simulation tool may need to include a variable viscosity parameter. A potential limitation of the study is that the particle retention size of the membrane filters on the FTA of 2.7 µm could have allowed the passage of small particles to the reservoir, however this was unlikely due to the median

size of the particles being 160 µm, which suggest most of the dissolution will have occurred before particles of less than 2.7 µm diameter can pass through the filter. Finally, the assumption made in the code for the small cell (high velocity) where the cell diameter is constant along the whole cell – which is not the case experimentally – lead to velocities being overestimated at the top of the cell, but the accuracy of the t50 predictions and t85 in level 1–2 viscosity (sucrose) supports the acceptability of the approximation.

More testing in viscous media could be considered in the *in vitro* stage during drug development and formulation, for example when considering biowaivers [164, 311] as the effect of viscosity is not negligible, especially, but not exclusively, when drugs are taken with food, but also when working towards biopredictive dissolution testing, as there could be a role for small increases in viscosity. Even in the fasted state, the viscosity is higher than that of water or SIF, with recent work by Pedersen *et al.* demonstrating that the increased viscosity of HGF resulted in a reduced IDR of cinnarizine compared to FaSSGF [159]. There could also be unintended small viscosity increases from medium composition which should not be dismissed as irrelevant. Even though increasing the viscosity of Level 1 biorelevant media as presented by Markopoulos *et al*. [82] can help capture one of the factors influencing *in vivo* dissolution rates, other factors such as the presence of bile salts might override the effect of viscosity *in vivo*, at the viscosity level presented in this work, depending on the API characteristics.

A further understanding of viscosity can serve as an input to the development of new generation biorelevant media, where it has been suggested to consider viscosity at the highest/most complex media levels [82, 241, 312].

4.4. Conclusions

Moderate (≤5.5 mPa.s) increases in viscosity over that of water at 37^{o}C were observed to affect the experimental and simulated dissolution rate of ibuprofen particles, in particular in low solubility environments, in both apparatuses. In the FTA, solubility and viscosity significantly affected the dissolution rate. The effect of each VEA on the dissolution rate was different due to their different chemical structures and effects on density and solubility, however, this difference in the effect of the VEA on dissolution was determined to only be statistically significant in pH 6.8 phosphate buffer and not in 0.1 M HCl. Particle motion simulations indicated reduced time to particle suspension with increasing viscosity, suggesting that when viscosity is increased a higher surface area is exposed to the dissolution medium, supporting a larger effect of enhanced viscosity on the intrinsic dissolution from a static disc than on the dissolution from a particulate system. In the paddle apparatus, the effect of solubility and agitation speed were more significant for the dissolution rate than that of viscosity, except for the low solubility-low velocity scenario, where viscosity did have an effect on t50.

Overall, this work demonstrated the value of simulation in probing the mechanistic procedures to identify sources of variation. In the FTA, PSD simulations reasonably predicted the effect of increasing viscosity in dissolution for sucrose, in particular the time to 50% dissolution in the high velocity environment. However, they predicted a larger effect from HPMC than that observed experimentally. This suggests an additional factor contributing to dissolution and countering the effect of viscosity induced by HPMC, highlighting the role of simulation in interrogating the interplay between complex processes.

Chapter 5. Assessing the effect of small increases in medium viscosity on the *in vitro* dissolution and *in vivo* pharmacokinetics of immediate release tablets of a weakly acidic drug through PBPK modelling

5.1. Introduction

In the work by Cristofoletti *et al.* [290] the PK profile after the oral administration of 400 mg of ibuprofen was simulated by modelling the *in vitro* dissolution of ibuprofen free acid particles in the paddle apparatus with the diffusion layer model (DLM). An effective PSD was extracted from the dissolution data and input into an absorption model in SimCyp™ PBPK Simulator [8].

The paddle apparatus was used by Cristofoletti *et al.* [290] to generate dissolution profiles for IR tablets. The current work interrogated the ability of the FTA to generate dissolution profiles which occur within a biorelevant timeframe as the different hydrodynamics that a tablet is exposed to in each apparatus can influence its dissolution rate [16]. Two cell sizes were used to investigate the interplay between fluid velocity and fluid viscosity on the *in vitro* dissolution of ibuprofen IR tablets.

Fluid viscosity had been investigated in Chapter 4 in relation to ibuprofen API dissolution in high and low solubility media in the FTA and paddle apparatus. In order to more closely represent the *in vivo* situation, where a drug product is administered, the effects of the same increases in medium viscosity (up to 5.5 mPa.s) with the same VEAs (sucrose or HPMC) were investigated with ibuprofen IR tablets in pH 6.8 phosphate buffer in the FTA.

The aim of this chapter was to examine the impact of small yet biorelevant increases of medium viscosity relevant to the fasted state on the dissolution rate of a weakly acidic drug – ibuprofen - administered as an IR tablet and the consequent relevance of viscosity to the biopredictive ability of the *in vitro* dissolution profiles when coupled

[8] SimCyp™ PBPK Simulator information at https://www.certara.com/software/simcyp-pbpk/

with GastroPlus®. Three viscosity values, two VEAs and two fluid velocity profiles were used to generate *in vitro* dissolution data in the FTA.

5.2. Results

5.2.1. *In vitro* dissolution tests

Experimental dissolution profiles are shown in **Figure 5.1**. The dissolution of ibuprofen in pH 6.8 phosphate buffer (PB) in high velocity conditions was rapid (85% dissolved in <30 min). Decreasing fluid velocity by increasing cell size resulted in a decrease in the dissolution rate in PB (85% dissolved in 70 min). Both VEAs resulted in a reduction in the dissolution rate, but this was observed to a larger extent when pH 6.8 phosphate buffer with 59% w/v sucrose (PB-S) media was used, despite similar viscosity values of the two VEA-containing media. Increasing viscosity increased the %CV around the percentage dissolved for both VEAs and delayed the time to maximum %CV, possibly due to a delay in tablet disintegration (**5.1**).

Tablet behaviour inside the test cell varied based on the medium used. In PB, the tablets remained on top of the glass beads until complete disintegration in both velocities (**Figure 5.2a** and **Figure 5.2b**). In pH 6.8 phosphate buffer with 1.05% w/v HPMC (PB-H) media, the tablet surface remained in contact with the glass beads in low velocity conditions whereas the tablets were slightly lifted in high velocity conditions (**Figure 5.2c** and **Figure 5.2d**). Moreover, the large variability observed in the percentage dissolved at the 45 min timepoint in high velocity conditions (60% CV) could be explained by the fact that the tablets were at different stages of disintegration in each cell which results in different amounts of the drug being exposed to the dissolution medium (**Figure 5.2e**).

In PB-S the tablets were more buoyant especially in the high velocity scenario (**Figure 5.2g**). Some tablets rotated from a horizontal to a vertical position (**Figure 5.2h**). This could be due to the fluid density of PB-S being higher than that of PB or PB-H (1.2 g cm^{-3} versus 1.0 g cm^{-3}), as reported in Chapter 4. Eventually, due to a reduction in the tablet mass, the tablet was mobilized from the bottom to the top of the cell, where it became attached to the filter (**Figure 5.2i**). This could have prevented the complete release of ibuprofen and could explain the incomplete dissolution after 7 hours.

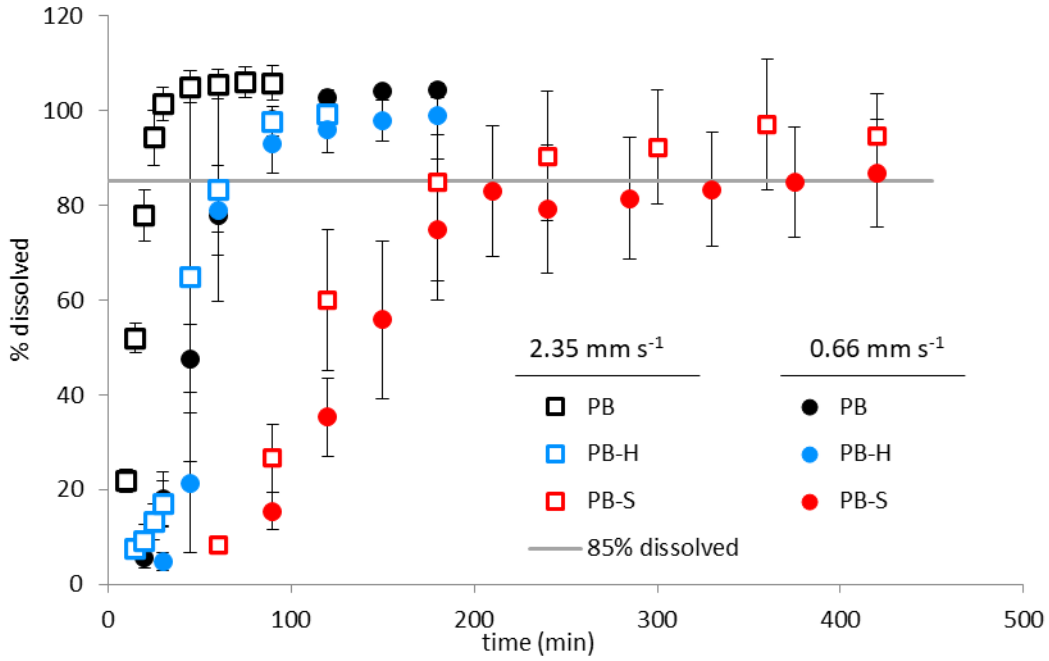

Figure 5.1. Mean experimental dissolution profiles (±SD) of 200 mg ibuprofen tablets in 500 ml of PB (black), PB-H (blue), or PB-S (red) at 37ºC in the FTA at two average linear fluid velocities: 2.35 mm s^{-1}, high velocity (squares) and 0.66 mm s^{-1}, low velocity (circles). All media contained 0.003% w/v Tween 20 (n=3).

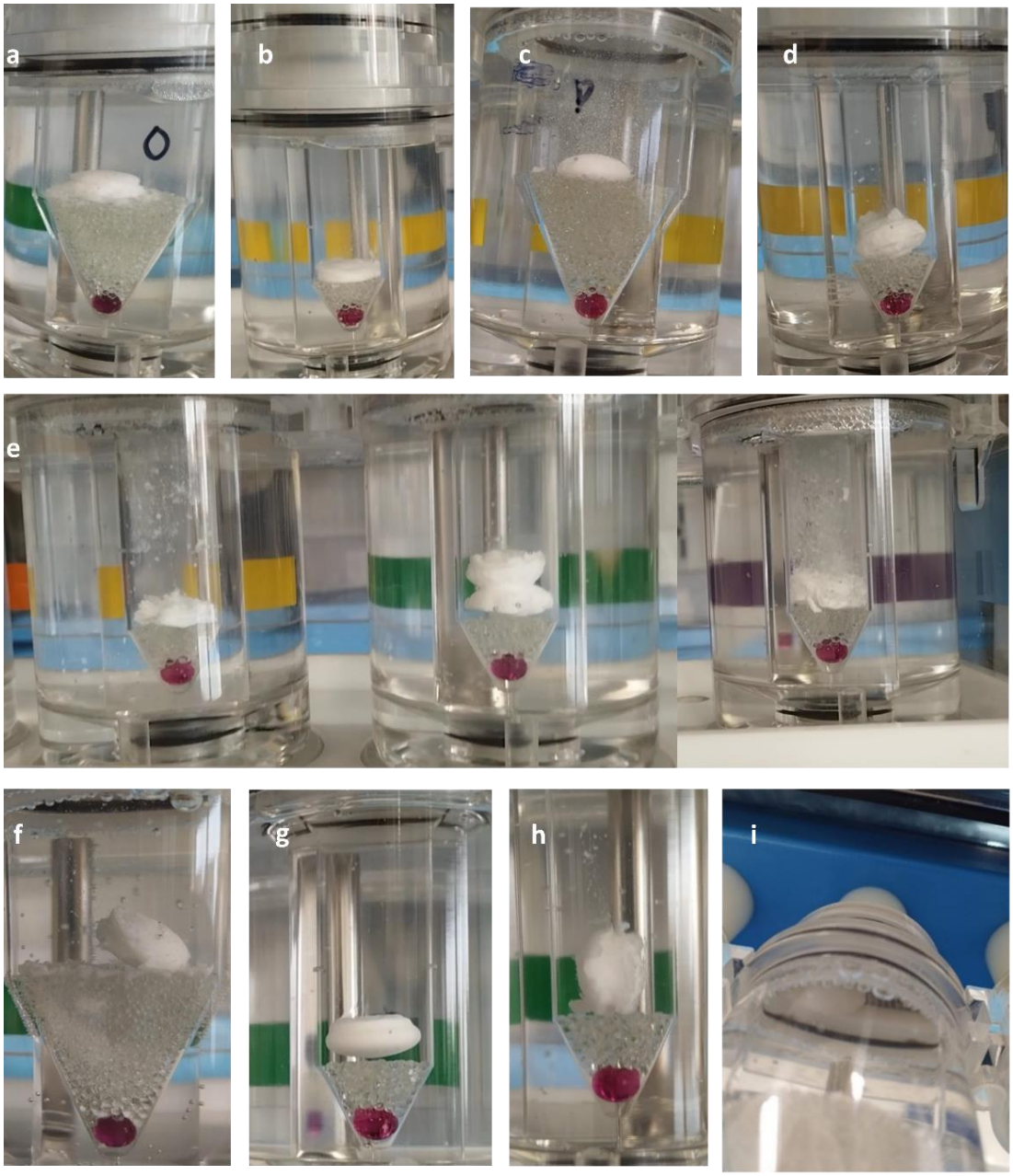

Figure 5.2. Tablets dissolving in the FTA in (a) PB low velocity, (b) PB high velocity, (c) PB-H low velocity, (d) PB-H high velocity, (e) variability in tablet disintegration in PB-H high velocity, (f) PB-S low velocity, (g, h) PB-S high velocity, (i) tablet at the top of the cell in PB-S.

Table 5.1. Minimum (min) and maximum (max) %CV calculated for each triplicate timepoint in two fluid velocities and three media viscosities.

Media velocity	Media viscosity	Min %CV	Max %CV	Time to max %CV (min)
Low	PB	0.77	38.51	20
Low	PB-H	4.05	68.81	45
Low	PB-S	13.04	29.86	150
High	PB	2.99	10.89	10
High	PB-H	2.10	59.85	45
High	PB-S	9.41	26.78	90

5.2.2. *In vitro* dissolution data modelling

The Z-factor fittings to the observed dissolution profiles and lag-time corrected profiles are shown in **Figure 5.3** and **Figure 5.4**, respectively. When fitted directly to the dissolution profiles, the Z-factor only generated a relatively accurate fit when there was a quick onset of dissolution (PB high velocity, **Figure 5.3a**). When adjusted for lag time, the fit in PB-S improved, but the fittings were still generally not very accurate. Based on the poor fittings, the Z-factor option was not used to simulate the PK profiles.

Both the tabulated dissolution data and the Weibull fits to each dissolution profile (**Figure 5.5**) were used to predict the plasma concentration versus time profiles of ibuprofen IR tablets in GastroPlus®.

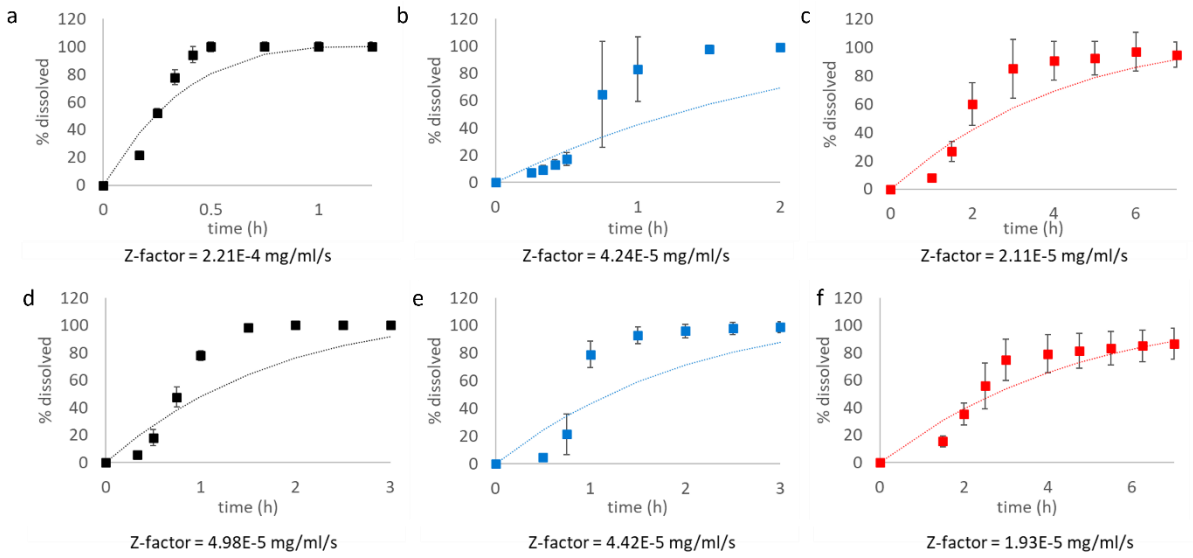

Figure 5.3. Z-factor fittings to mean *in vitro* dissolution profiles (±SD) (n = 3) in GastroPlus® in a high fluid velocity scenario (a-c) and a low fluid velocity scenario (d-f). The *in vitro* dissolution profiles were obtained in PB (black), PB-H (blue) and PB-S (red).

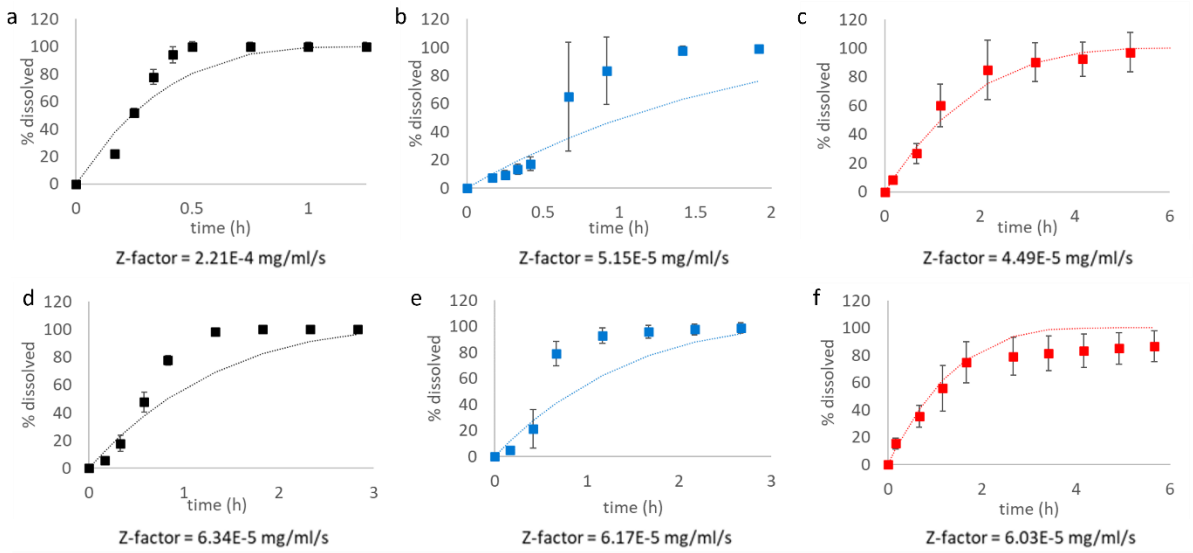

Figure 5.4. Z-factor fittings to mean *in vitro* dissolution profiles (±SD) (n = 3) in GastroPlus® after correcting for lag time in a high fluid velocity scenario (a-c) and a low fluid velocity scenario (d-f). The *in vitro* dissolution profiles were obtained in PB (black), PB-H (blue) and PB-S (red).

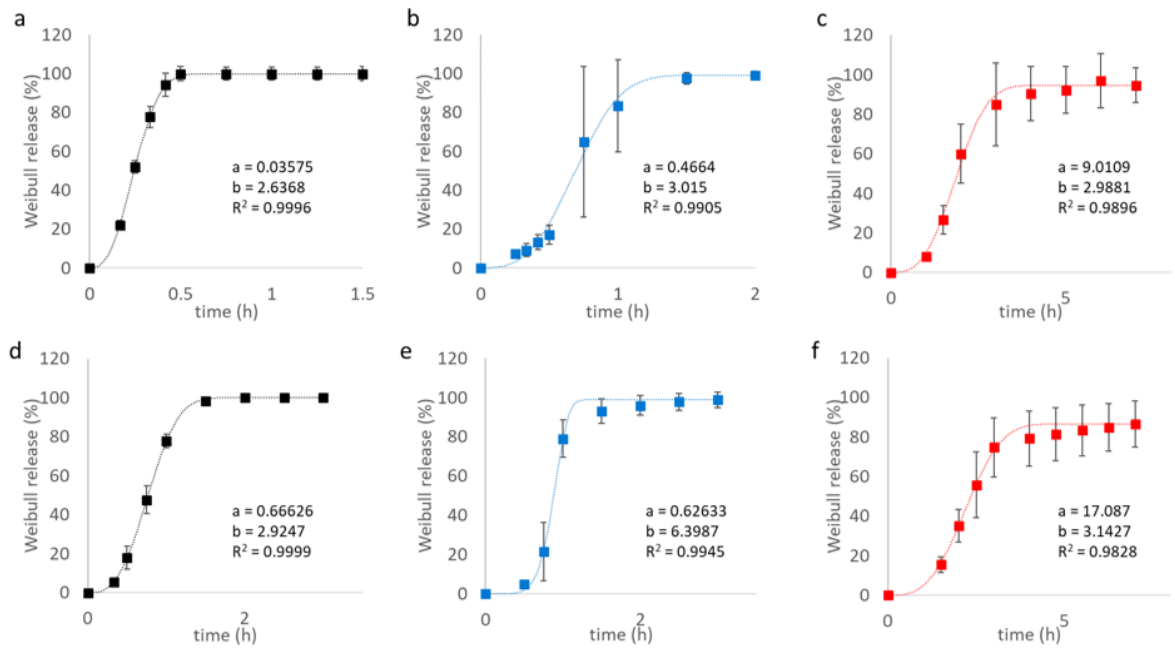

Figure 5.5. Weibull function fitting to mean *in vitro* dissolution profiles (±SD) (n = 3) in GastroPlus® in a high fluid velocity scenario (a-c) and a low fluid velocity scenario (d-f). The *in vitro* dissolution profiles were obtained in PB (black), PB-H (blue) and PB-S (red).

5.2.3. Pharmacokinetic model development and verification

5.2.3.1. Intravenous model development and verification

The plasma concentration versus time profile after the intravenous administration of 800 mg ibuprofen over 5 to 7 min extracted from the *in vivo* studies by Pavliv *et al.* [287] was fitted to one-, two- and three-compartment models in PKPlus. Both two- and three-compartment models with a $1/\hat{y}$ weighting function provided good fits of the model to the data (**Figure 5.6a**), with residuals of a small magnitude (**Figure 5.6b**). The calculated disposition parameters for each model are presented in **Table 5.2**.

Statistical values of R^2, SC, AIC, AFE and AAFE were acceptable for two- and three-compartment models (**Table 5.3**). The predictions of C_{max} and $T_{1/2}$ were in agreement with the data reported by Pavliv *et al.* [287] (**Table 5.4**). Based on the similarity between two- and three- compartment results and the uncertainty (%CV) in the K13 and K31 estimates with the three-compartment model (**Table 5.2**), the two-compartment model was selected, and the estimated disposition parameters obtained from the fit were used for the subsequent extravascular PK simulations (**Table 5.2**).

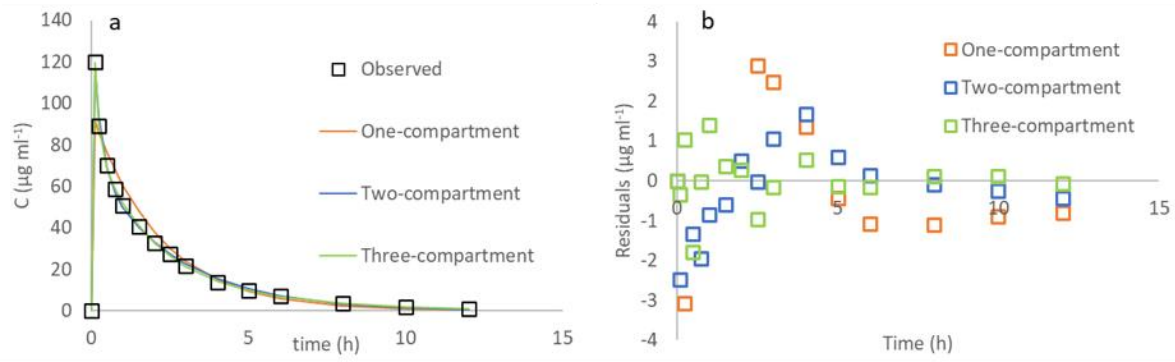

Figure 5.6. Fitted one-, two- and three-compartment models (a) and their residuals (b) to the observed data extracted from the *in vivo* studies by Pavliv *et al*. [287].

Table 5.2. Disposition parameters estimated from Pavliv *et al*. [287] with one-, two- and three-compartment models.

Input	One-comp	%CV	Two-comp	%CV	Three-comp	%CV
Cl/kg (l /h^{-1}/ kg^{-1})	0.051	22.96	0.053	11.75	0.052	6.9
Vc/kg (l /kg^{-1})	0.11	23.55	0.079	10.34	0.074	4.33
T ½ (h)	1.50	32.89	1.83	0.0	2.551	0.0
K10 (h^{-1})	0.461	32.89	0.661	15.65	0.704	8.15
K12 (h^{-1})	-	-	1.456	12.39	2.514	4.64
K21 (h^{-1})	-	-	2.336	39.77	4.489	27.72
K13 (h^{-1})	-	-	-	-	0.110	99.46
K31 (h^{-1})	-	-	-	-	0.382	109.57

Table 5.3. Statistical parameters R^2, SC and AIC calculated in PKPlus for each model. AFE and AAFE for each model calculated in Microsoft Excel.

	R^2	SC	AIC	AFE	AAFE
One-compartment	0.934	7.78	6.24	0.89	1.28
Two-compartment	0.998	-33.37	-36.45	0.97	1.07
Three-compartment	0.999	-54.98	-59.62	1.00	1.03

Table 5.4. Predicted C_{max} and $T_{1/2}$ by each model in PKPlus. FE values, which should be close to 1 for an accurate prediction, are presented in brackets for each value.

	C_{max} (µg ml^{-1})	$T_{1/2}$ (h)
One-compartment	91.2 (0.76)	1.50 (0.75)
Two-compartment	117.6 (0.98)	1.82 (0.91)
Three-compartment	120.0 (1.00)	2.55 (1.28)
Observed data in Pavliv *et al*. [287]	120±13	2.0±0.5

5.2.3.2. Oral model development and verification

The simulated plasma concentration versus time profiles for each *in vitro* dissolution medium are presented in **Figure 5.7**. The FE between the predicted and observed PK parameters was used to analyse the accuracy of the simulations and is presented in **Figure 5.8**. Due to the similarity of the simulated plasma concentration versus time profiles obtained with both dissolution data input methods (tabulated data versus Weibull function), the statistical metrics presented in **Figure 5.8** relate to the profiles obtained with the tabulated data only.

The dissolution profile obtained in PB in high velocity conditions predicted a quick onset of absorption in line with the observed early timepoints from both clinical trials (<1 h) (**Figure 5.7a**). The accurate prediction of the observed early timepoints with PB in high velocity conditions was accompanied by a prediction of T_{max} which was lower than the observed T_{max} and resulted in a FE for T_{max} below 1 (**Figure 5.8b**). However,

the predicted C_{max} values were in line with the observed mean C_{max} values, as demonstrated by a FE of 1.08 for data set A – extracted from the clinical study by Legg *et al*. [288] – and 1.11 for data set B – extracted from the clinical study by Dewland *et al*. [289] – (**Figure 5.8a**).

When fluid velocity was reduced in the FTA in PB medium, an underprediction of the early timepoints was observed, but T_{max} was closer to the observed values (**Figure 5.7a**). This was reflected in a T_{max} FE which was closer to 1 (**Figure 5.8b**). The accurate prediction of C_{max} in high velocity conditions was also observed in low velocity conditions as the C_{max} FE was also close to 1 (**Figure 5.8a**).

The plasma concentration versus time predictions were similar for both velocities when inputting the dissolution profiles obtained in PB-H (**Figure 5.7b**) due to the similarities in the *in vitro* dissolution profiles (**Figure 5.1**). The C_{max} and T_{max} FE in PB-H for both velocities were close to 1, suggesting accurate predictions of these metrics when HPMC was used as a VEA in both fluid velocity scenarios (**Figure 5.8a** and **Figure 5.8b**).

When *in vitro* medium viscosity was increased with sucrose, there was a larger underprediction of the early timepoints and a delayed T_{max} in both velocity scenarios (**Figure 5.7c**). In fact, the predicted T_{max} values were above 3 hours and outside the observed range of T_{max} values in the *in vivo* data set B [289] (0.57 h – 3.00 h). The simulated C_{max} values were lower than the observed mean C_{max} in both velocities, but they were within the range of observed values in data set B [289], which presented large variability (15.37 µg ml^{-1} – 45.71 µg ml^{-1}). These deviations in predicted C_{max} and T_{max} from the observed values corresponded to FEs which were furthest from 1 out of the three media studied (**Figure 5.8a** and **Figure 5.8b**).

The range of predicted AUC_{0-t} and $AUC_{0-\infty}$ was 89.9-104.7 µg h ml^{-1} and 90.6-105.0 µg h ml^{-1}, respectively, with the lowest values corresponding to PB-S medium in a low velocity scenario. All values were lower than observed mean values in the *in vivo* data set A [288] (AUC_{0-t} = 142.6 µg h ml^{-1} and $AUC_{0-\infty}$ = 144.3 µg h ml^{-1}) and B [289] (AUC_{0-t} = 121.8 µg h ml^{-1} and $AUC_{0-\infty}$ = 125.1 µg h ml^{-1}).

The input dissolution profiles in each of the six *in vitro* conditions resulted in a narrow range of predicted AUC_{0-t} and $AUC_{0-\infty}$ values, which was reflected in the small range for the calculated FE (0.69-0.86). In all cases, the FE for AUC_{0-t} and $AUC_{0-\infty}$ was

slightly below 1 (**Figure 5.8c** and **Figure 5.8d**). The FE for AUC_{0-t} and $AUC_{0-\infty}$ was closer to 1 for the data set B due to the *in vivo* AUC_{0-t} and $AUC_{0-\infty}$ values being smaller than in data set A and closer to the predicted values.

Nevertheless, all the predicted AUC_{0-t} and $AUC_{0-\infty}$ values were within the observed range in data set B [289] (AUC_{0-t} = 88.73-168.85 µg h ml^{-1} and $AUC_{0-\infty}$ = 89.11-178.03 µg h ml^{-1}).

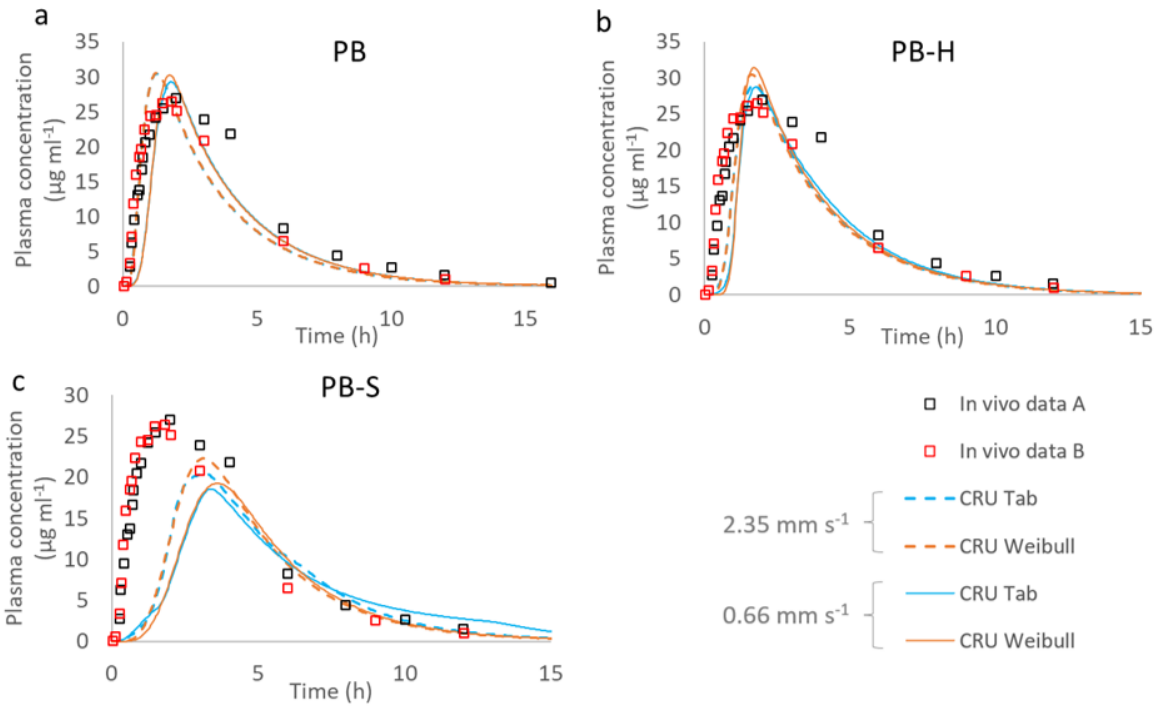

Figure 5.7. GastroPlus® predicted plasma concentration versus time profile inputting mean *in vitro* dissolution profiles (n = 3) obtained in three different media (a) PB, (b) PB-H, (c) PB-S, two fluid velocities (high velocity, 2.35 mm s^{-1} – dashed lines; low velocity, 0.66 mm s^{-1} – continuous lines) and two data input methods (CRU Tabulated (blue) and CRU Weibull (orange)), compared to literature data from data set A [288] (black squares) and data set B [289] (red squares).

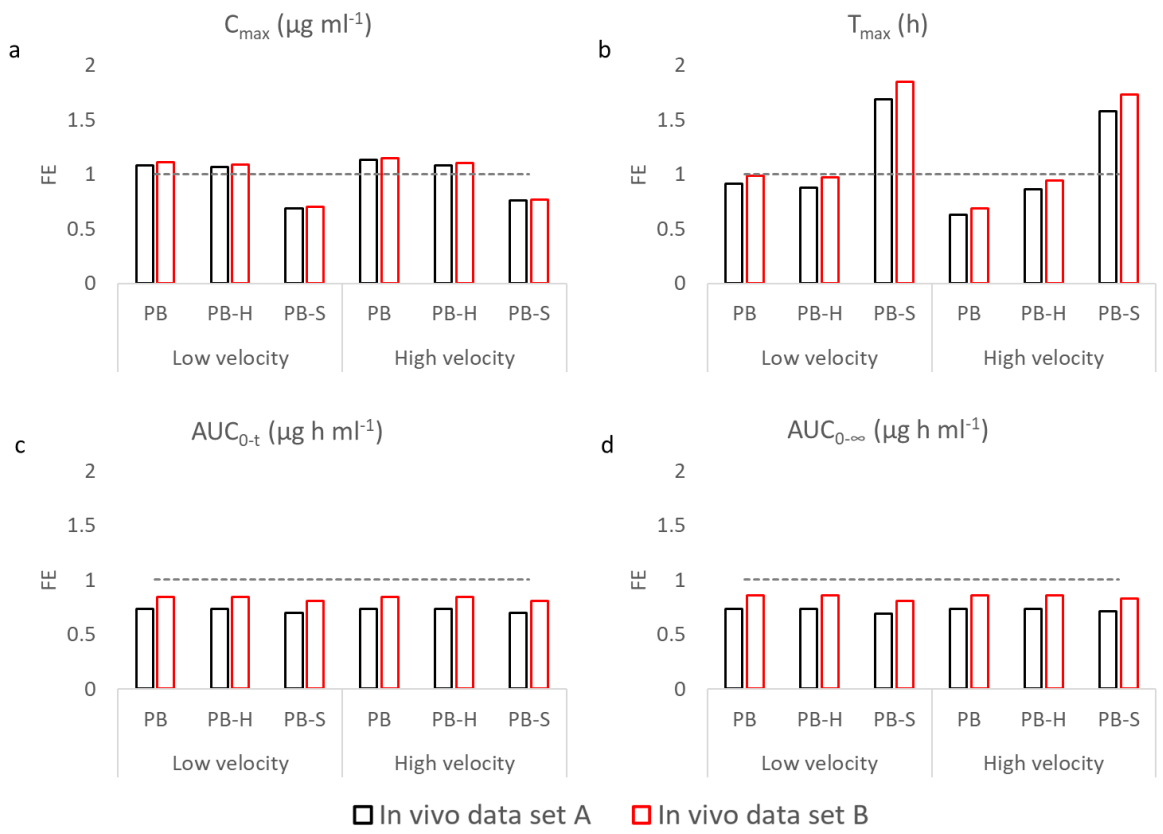

Figure 5.8. (a) C_{max}, (b) T_{max}, (c) AUC_{0-t} (d) $AUC_{0-\infty}$ FE between the GastroPlus® predicted PK parameters versus the observed PK parameters in data set A [288] (black) or data set B [289] (red). An FE of 1 is depicted as a grey dashed line.

5.2.3.3. Pharmacokinetic parameters versus Reynolds number

The calculated Reynolds number for each dissolution experiment is presented in **Table 5.5**. As expected, lower Reynolds numbers were obtained for media containing VEAs, due to their higher viscosity, and in the low velocity conditions.

A correlation was observed between lower Reynolds numbers and lower predicted C_{max} values as well as lower Reynolds numbers and higher predicted T_{max} values (**Figure 5.9**), however the range of C_{max} values was small in **Figure 5.9a**. The observed relations between the Reynolds number and the PK parameters were different for each VEA with a higher impact of the Reynolds number on the PK parameters in PB-S than PB-H.

Some limitations are encountered when considering the relationship between the Reynolds number and the PK parameters. The relative motion of the tablet or

fragments is not considered in the Reynolds calculation, and tablet motion was observed in the dissolution tests, mainly in the higher density medium (PB-S) and in higher velocity situations (**Figure 5.2**). The density of the PB-S medium was higher than that of the PB and PB-H media and, although fluid density is considered when calculating the Reynolds number, the impact of buoyancy on the relative velocity would need to be explicitly calculated. Finally, any potential impacts of VEAs on wetting and tablet disintegration are not taken into account in the Reynolds number calculation. This could be relevant for HPMC due to its amphiphilic nature.

Despite the limitations, there is value in investigating the impact of different Reynolds numbers in the predicted PK parameters, which was different depending on the VEA used.

Table 5.5. Calculated Reynolds numbers for each dissolution test in different conditions of velocity (low velocity (0.66 mm s^{-1}); and high velocity (2.35 mm s^{-1})) and viscosity (PB (0.7 mPa.s), PB-H (5.5 mPa.s) and PB-S (4.5 mPa.s)).

Media velocity	Media viscosity	Re $\times 10^6$
Low	PB	10.36
Low	PB-H	1.62
Low	PB-S	1.60
High	PB	36.89
High	PB-H	5.77
High	PB-S	5.72

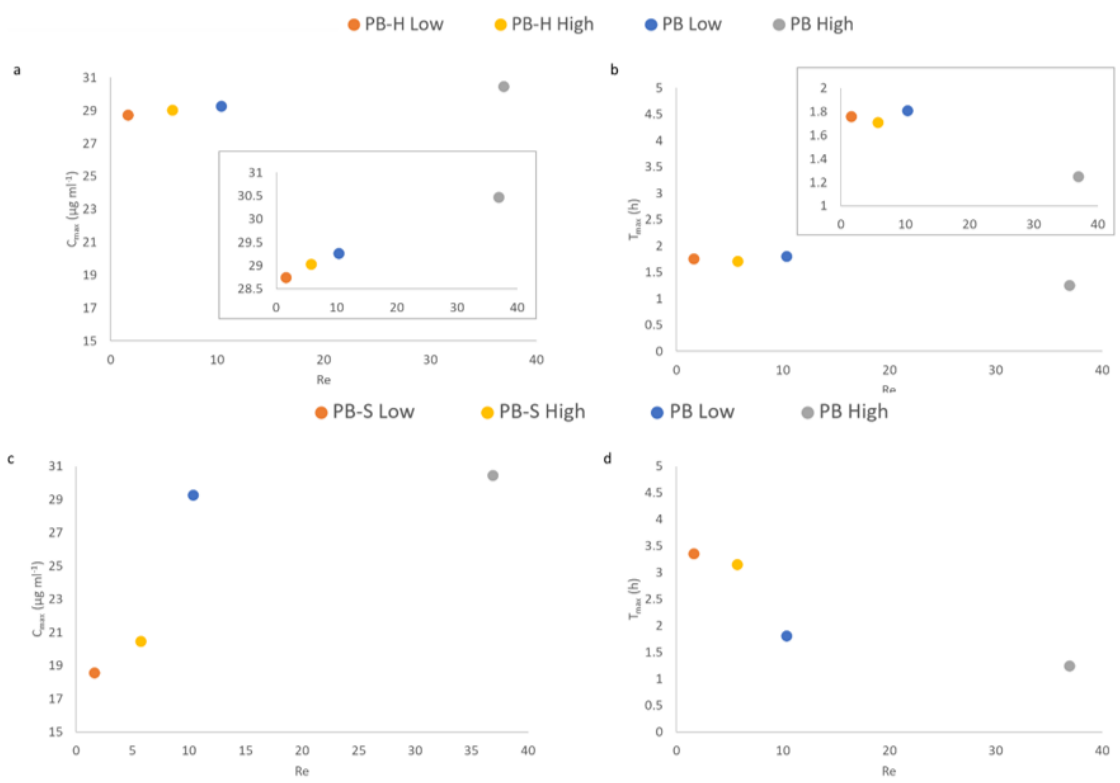

Figure 5.9. C_{max} (a, c) and T_{max} (b, d) versus Reynolds number in PB and PB-H (a, b) and PB and PB-S (c, d) in low (0.66 mm s^{-1}) and high (2.35 mm s^{-1}) velocity conditions. Insets in (a) and (b) with a reduced Y axis are presented for ease of interpretation.

5.2.3.4. *Virtual bioequivalence studies (VBE)*

VBE studies were carried out to confirm the predictive ability of the simulations when the *in vitro* dissolution rates were input and to investigate the extent of underprediction of the early timepoints when simulated variability was taken into account. The resulting profiles for each *in vitro* medium are presented in **Figure 5.10**.

The ability of the PK simulations to accurately predict the ibuprofen concentrations at early timepoints when using the *in vitro* dissolution profiles generated in PB medium in high velocity conditions was reiterated in the VBE simulations (**Figure 5.10a**). As observed in the single simulations (**Figure 5.7**), absorption was delayed as medium viscosity was increased, to a larger extent in PB-S, which resulted in later predicted T_{max} values.

The observed data around T_{max} (1.5-2.5 h) and at later timepoints (>6 h) fell within the predicted 90% CI in PB in a low velocity scenario and PB-H in both velocity scenarios but not in PB in high velocity conditions, nor in PB-S media.

C_{max} was found to be equivalent to the observed data from both clinical trials in GastroPlus® in PB and PB-H in both velocities, but it was not equivalent in PB-S. Therefore, the different effects of each VEA on the *in vitro* dissolution rate of ibuprofen were also reflected in different impacts on the plasma concentration versus time profiles when simulated variability was considered. The observed data points for the *in vivo* data set B [289] were better captured by the simulations due to the two high concentrations in the *in vivo* data set A [288] at 3 h and 4 h that were consistently outside the 90% CI in all simulations, but, even though variability around the PK parameters could be extracted from one of the clinical trials, the variability around each clinically measured datapoint was not available.

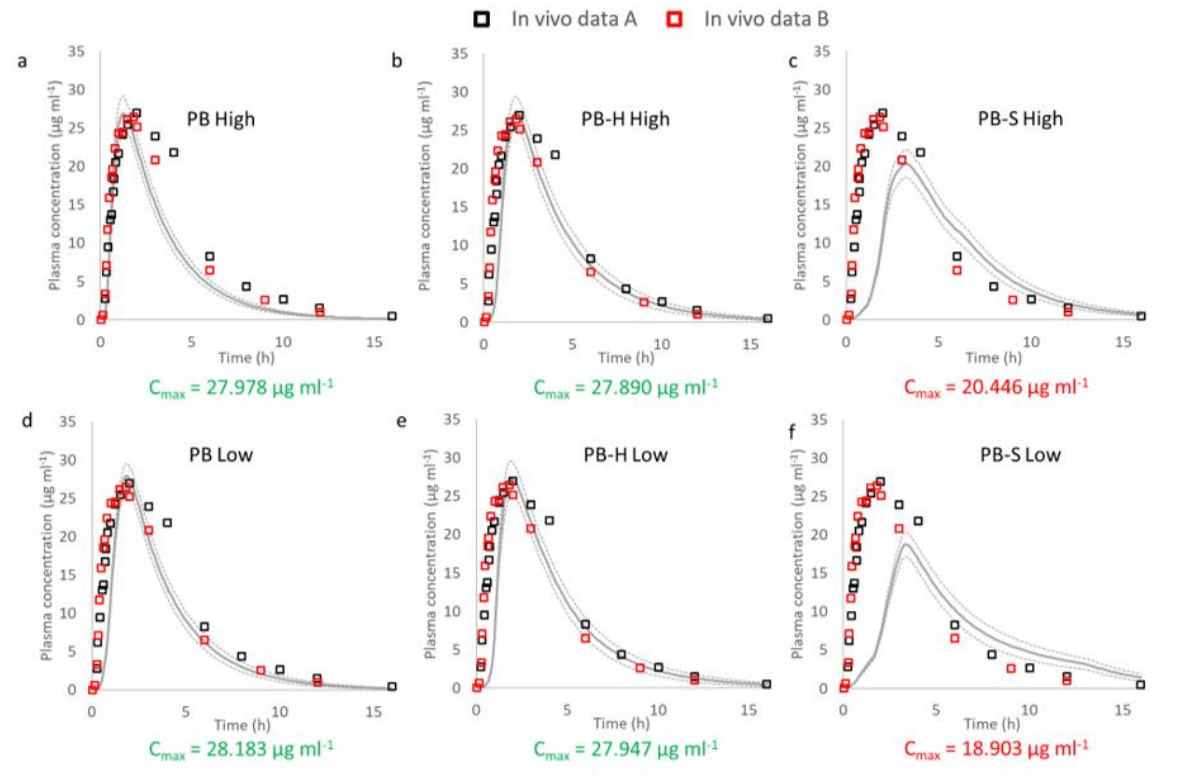

Figure 5.10. Mean plasma concentration (continuous grey line) and 90% CI (dashed grey line) versus time simulated in GastroPlus®. The mean *in vitro* dissolution profiles input were those obtained in PB (a, d), PB-H, (b, e) and PB-S (c, f) and two fluid velocity conditions (high velocity, 2.35 mm s^{-1} – upper; low velocity, 0.66 mm s^{-1} – lower) (n = 3). Mean C_{max} values are coloured green if meeting bioequivalent criteria and red if not meeting bioequivalent criteria. Literature plasma concentration versus time data from the *in vivo* data sets A [288] and B [289] are included for comparison.

5.2.3.5. Parameter sensitivity analysis (PSA)

PSA was performed to understand how the critical variables Weibull shape factor, diffusion coefficient and particle size affected the predictions of C_{max}, T_{max} and AUC differently for each medium viscosity.

Weibull shape factor changes did not affect T_{max} nor C_{max} in PB and PB-H but they did in PB-S (**Figure 5.11a** and **Figure 5.11b**). The shape factor for sucrose for the single simulations was around 3 for both velocities, indicating sigmoidal curves of the dissolution profiles. A shape factor above 3 resulting from a faster *in vitro* dissolution in PB-S medium, would have resulted in a lower predicted T_{max} and a higher predicted C_{max} in PB-S, reaching similar values to those obtained in PB and PB-H. This suggests

that a dissolution test where faster dissolution in PB-S is achieved could be considered a more biorelevant dissolution test, as it would result in predicted plasma concentration time profiles which are closer to the *in vivo* data sets A [288] and B [289] used as reference in the current work.

The diffusion coefficient input in the plasma concentration versus time simulations was 0.8 x 10^{-5} cm^2 s^{-1} for all simulations, which was used to calculate the dissolution rate of drug particles when released from the dosage form. The PSA results suggest that a decrease in the diffusion coefficient below 0.5 x 10^{-5} cm^2 s^{-1} would lead to a larger T_{max} and a lower C_{max} (**Figure 5.11c** and **Figure 5.11d**). A lower diffusion coefficient for ibuprofen was calculated from intrinsic dissolution studies in media containing HPMC and sucrose at the same concentration as used in the current work (0.15 – 0.18 x 10^{-5} cm^2 s^{-1}) compared to the diffusion coefficient of ibuprofen in PB with no VEAs (0.80 x 10^{-5} cm^2 s^{-1}), as presented in section "4.2.4. Intrinsic dissolution and diffusion coefficient" in Chapter 4. Therefore, an intentional or unintentional increase in medium viscosity could impact the absorption profile through a reduced diffusion coefficient.

The effect of particle size on C_{max} and T_{max} was different depending on the VEA used (**Figure 5.11e** and **Figure 5.11f**). As different tablet and particle motion patterns might mean there are different effective PSDs present in the *in vitro* set up, it could be important to determine the effective PSD that is present in each viscosity medium. Imaging techniques such as shadowgraph imaging could help determine particle size, motion and velocity changes with time in each viscosity medium. In fact, shadowgraph imaging was employed before to illustrate the retention of particles in suspension in a 1.4 mPa.s viscosity medium compared to water [2].

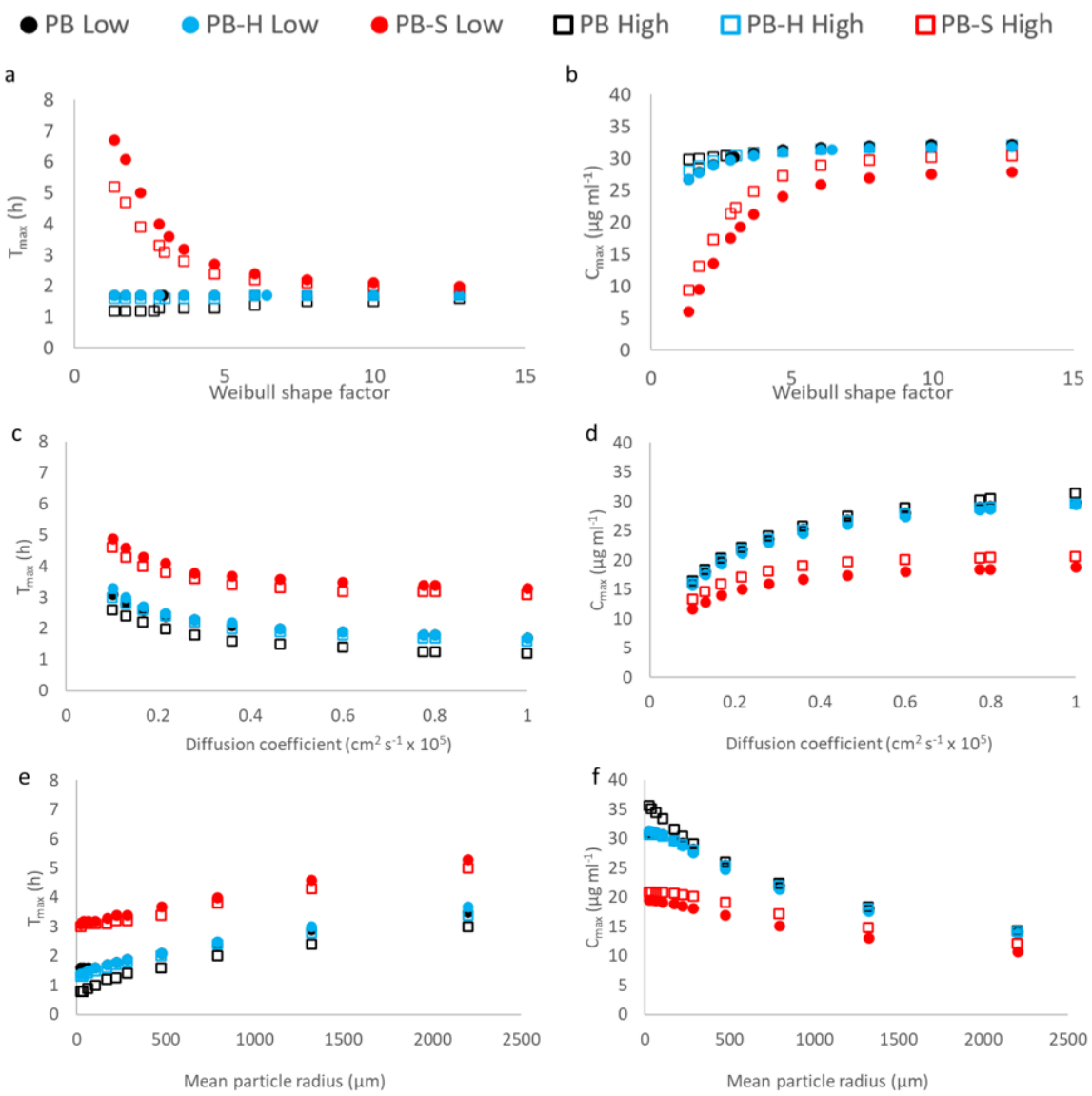

Figure 5.11. T_{max} (left) and C_{max} (right) changes when varying (a, b) the Weibull shape factor from 1 to 12, (c, d) the diffusion coefficient from 0.1 to 1.0 x 10^{-5} cm^2 s^{-1} or (e, f) the mean particle radius from 22 to 2200 µm (right) in PB (black), PB-H (blue) and PB-S (red) in high velocity conditions (squares) or low velocity conditions (circles).

5.3. Discussion

Hydrodynamic changes induced by different fluid velocity patterns in *in vitro* dissolution testing can have large effects on drug dissolution [41, 43]. Shiko *et al.* [38, 45] demonstrated that heterogeneous flow profiles in the FTA that depended on cell size, flow rate and tablet orientation affected tablet erosion and drug dissolution. The faster dissolution of ibuprofen IR tablets when fluid velocity was increased by means of reducing cell size and maintaining a flow rate of 16 ml min^{-1} was evident in the current work in pH 6.8 phosphate buffer medium, which might be due to a better dispersal of the tablet contents and a higher mass transfer rate away from the particle surface when cell diameter is reduced [38].

In chapter 4, a reduced IDR of ibuprofen in the presence of either HPMC or sucrose in the media at the same concentrations was observed. A negative effect of sucrose-containing medium was also observed on ibuprofen API dissolution in the FTA with average linear fluid velocities ranging from 0.33 mm s^{-1} to 2.35 mm s^{-1} in media representing either the intestinal or the gastric pH, but this effect was not so evident with HPMC. This is in agreement with the observations from the current chapter, which studied the release and dissolution of ibuprofen IR tablets rather than ibuprofen API. Even though a slower dissolution of ibuprofen from IR tablets was observed with both VEAs, the dissolution rate was reduced to a larger extent in sucrose-containing medium than in HPMC-containing medium, despite the media having similar viscosity values (4.5 – 5.5 mPa.s). This could be underpinned by their different chemical properties, e.g. the amphiphilicity of HPMC [306, 307] and the water-binding properties of sucrose [302], and the higher fluid density achieved in PB-S, which was reflected in the increased buoyance of the tablets *in vitro*.

In vitro dissolution data was modelled to be incorporated as an input to the extravascular PK model. A publication from the OrBiTo working group discussed the usefulness of *in vitro* dissolution test data and best approaches for incorporating it into PBPK models [237] suggesting that empirical models such as the Weibull function are useful for complex formulations but are less sensitive to physiological regional differences and within and between subject variability. Although the formulation used in this study was not complex (IR tablet) the slow disintegration *in vitro* in the conditions studied together with the slow dissolution in conditions of higher viscosity prompted

the investigation of inputting and modelling the dissolution data as a CR formulation. In the current work, the Z-factor model, which was developed based on the dissolution of crushed tablets to circumvent the step of disintegration [236] did not provide the best fits when intact tablets were used, as it does not account for a disintegration lag time, as discussed by Hofsäss and Dressman [313]. Therefore, the dissolution data was input into the model directly as tabulated data or fitted to a single Weibull function.

The different effect of each VEA on the dissolution rate of ibuprofen IR tablets was reflected in a lower predictive ability of the plasma concentration versus time profiles when the dissolution profiles in PB-S medium were input instead of those obtained in PB-H medium. VBE studies which served to confirm the predictive ability when simulated variability was considered, suggested BE of C_{max} in PB and PB-H at both velocities. Although slightly increasing medium viscosity with HPMC did not impact C_{max} BE, it did impact the prediction accuracy at the early timepoints.

Analgesics like ibuprofen require a quick onset of action, which is associated with a short T_{max}, and therefore it is highly valuable to predict T_{max} correctly. It was observed that T_{max} was delayed to different extents depending on the VEA used. In fact, the predicted T_{max} in PB-S was outside the full range of observed values in the *in vivo* data set B [289]. Moreover, the T_{max} delay in higher viscosity medium was accompanied by an underprediction of the early timepoints. This showcased the difficulty of accurately predicting T_{max} without underpredicting the early timepoints, despite the presence of low fluid velocities in the FTA. Given the observed effects of sucrose, HPMC and no VEA, and fluid velocity, further work could include the manipulation of viscosity and VEA in *in vitro* dissolution tests to capture the early time points but delay C_{max}.

PSA illustrated how critical variables affected PK parameters differently depending on the VEA used. Different values of *in vitro* viscosity or density which result in a faster dissolution in PB-S might generate predicted PK parameters closer to those obtained when inputting data obtained in PB and PB-H media. Moreover, viscosity mediated changes in diffusion coefficient and effective PSD might affect the PK parameters, therefore it is important to characterize these two parameters when medium viscosity is increased, for example through imaging techniques [2].

The different effects of each VEA on drug dissolution and predicted absorption, together with the Reynolds number results suggest that there is a complex interplay

of factors affecting drug dissolution from tablets in the higher viscosity media. Not only has medium viscosity an impact on tablet dissolution but also other factors, like the VEA used, the fluid density, tablet motion and the potential wetting effect of VEAs on tablet disintegration could affect drug dissolution and absorption of tablets of a similar size and density as that presented in this work.

The current work proposes that considering biorelevant viscosity in the fasted state when selecting the most appropriate *in vitro* biopredictive dissolution test could be acceptable, as it can have a small impact on the PK parameters. In addition, the dissolution behaviour should be characterized, and special attention should be paid to fluid density and tablet motion when intentionally or unintentionally altering medium viscosity. It was also demonstrated that the FTA can be used to generate dissolution profiles occurring in a broadly biorelevant timeframe for IR tablets, as it can potentially achieve biorelevant fluid velocities.

The work presented here has some limitations that could impact the accuracy of the predictions. The disposition parameters were obtained from a different published clinical trial than the clinical trials used to validate the simulations and differences between the studied cohorts could impact the resulting simulations.

In vitro dissolution was carried out at a pH of 6.8, which is representative of the intestinal pH. A two-stage dissolution, with a simulated gastric and intestinal compartment could have led to slightly different predicted profiles. However, as dissolution and absorption of ibuprofen in the stomach are expected to be negligible compared to the intestine [263] and precipitation when transiting from stomach to intestine is not expected for weak acids, a two-stage dissolution was not considered a priority of this work. To build on the current work and with a focus on an accurate prediction of concentrations at very early time points, a two-stage dissolution test could be the next step to develop a more biorelevant model.

The availability of inter-subject variability data around mean PK parameters can help contextualize the effect of small changes, such as a small increase of medium viscosity or slightly different fluid velocities on the bioavailability of a drug. For the two clinical trials used to compare to the simulations in the current work, variability around the early timepoints of the plasma concentration versus time profiles was not reported. This could have helped assess the extent of underprediction when medium viscosity

was increased. However, the full range of measured PK parameters was reported for one of the clinical trials [289]. The predicted PK parameters in the current work were within the observed range, except for T_{max} in PB-S, suggesting that the studied *in vitro* viscosity range could be an acceptable representation of the conditions of the fasted GI tract.

Lastly, the present work examined the effect of medium viscosity and fluid velocity on the dissolution and absorption of one weakly acidic drug in an IR dosage form. Further work could study the impact of medium viscosity on neutral or weakly basic drugs and more complex formulations.

5.4. Conclusions

Moderate increases in medium viscosity (≤5.5 mPa.s) relevant to the fasted state can be considered as they might slightly affect the plasma concentration versus time of an orally administered drug. Moreover, dissolution profiles occurring in a broadly biorelevant timeframe can be generated in the FTA. Media containing different VEAs, which result in different Reynolds numbers, can affect the observed drug dissolution and simulated bioavailability differently, suggesting not only that media viscosity is important, but also other factors such as fluid density, wetting effects or the movement of the dosage form. Therefore, the dissolution behaviour of a drug in increased medium viscosity should be characterized, even when the viscosity increase is moderate, reflecting the viscosity of the fasted state, and special attention should be paid to fluid density, tablet motion, drug diffusivity and the effective PSD.

Chapter 6. General discussion

6.1. *In vitro* hydrodynamic effects

Hydrodynamic effects are an added source of variability for the dissolution rate of poorly soluble drugs [13]. The differences between *in vitro* and *in vivo* hydrodynamics in terms of the velocities and shear rates that dosage forms are exposed to could complicate the development of tests that are more representative of the *in vivo* situation [61]. The importance of *in vivo* hydrodynamics should not be underestimated as *in vivo* motility patterns and GETs might be governing drug dissolution and absorption from IR products and overriding the effect of solubility or viscosity. Motility patterns can determine when a drug is transferred from the stomach to the intestine. This could be relevant for weakly basic drugs which can precipitate upon transfer to the intestine. For example, Psachoulias *et al*. [314, 315] evaluated the *in vivo* precipitation of ketoconazole and dipyridamole and developed an *in vitro* predictive model based on a three-compartment setup. GET can also be determinant for weakly acidic drugs as they will readily dissolve and be absorbed in the intestine [316]. For ibuprofen, the drug studied in the current work, a correlation was observed between the time to the next phase III contraction of the MMC which influences GET and C_{max} and T_{max} variability as once ibuprofen is transferred from the stomach to the intestine it can start dissolving and being absorbed [145, 146].

Given the influence that hydrodynamic conditions can have on drug dissolution rate, it is important to (a) acquire a deeper understanding of *in vivo* hydrodynamics [52] and (b) study how *in vitro* hydrodynamics affect the mass transfer mechanism from the surface of the drug particles. Although both *in vitro* and *in vivo* hydrodynamic studies are of relevance, the effect of *in vitro* hydrodynamics on the dissolution of a model drug – ibuprofen – was the focus of the current work.

Ibuprofen was selected as the study drug as it is a weakly acidic drug that belongs to the BCS class II [62] and the DCS class I [64], which means its dissolution under different pH conditions and the interplay of hydrodynamic factors such as fluid velocity, viscosity and density could be explored. Also, the granting of biowaivers for some BCS class II drugs based on the prediction of BE with *in vitro* data has been discussed in the literature [70], therefore it is important to get a better understanding of which factors affect dissolution data for this type of drug.

6.1.1. Fluid velocity effects in the paddle apparatus and the flow-through apparatus

With the aim of getting a better understanding of hydrodynamic effects on ibuprofen particulate dissolution and dissolution from an ibuprofen IR tablet, one of the factors studied in the current work was fluid velocity, by means of changing flow rate and cell size in the FTA and agitation speed in the paddle apparatus, as it could affect the dissolution rate of poorly soluble drugs.

The hydrodynamic conditions in the paddle apparatus are complex. Flow is dominated by a tangential component [14] with low radial velocities and both positive and negative axial velocities [18]. Two recirculating loops are present below and above the impeller [20] as well as a zone of very low fluid velocity between the end of the impeller and the bottom of the vessel [19].

In the current work, decreasing the agitation speed in the paddle apparatus reduced the dissolution rate of ibuprofen API powder contained in HPMC capsules in both high and low solubility media. Many examples can be found on the literature illustrating the effect of the agitation speed on drug dissolution. O'Farrell *et al.* [317] showed that the drug release and dissolution from theophylline tablets increased with increasing agitation speeds (25, 50, 100 rpm) and Salehi *et al.* [36] showed an increase in drug dissolution rate with increasing agitation speed from 50 to 200 rpm and corresponding increases in volume average shear rates and fluid velocities.

In this apparatus, an increase in the agitation speed leads to an increase in local fluid velocity, except for the region in between the end of the impeller and the vessel bottom, where the velocity remains low. The higher local fluid velocity can result in an increase in the mass transport rate away from the dissolving surface and an increase in the dissolution rate [30]. There might also be higher particle dispersal at higher fluid velocities, increasing the surface area available for dissolution. Moreover, at lower agitation speeds coning is more likely to occur, which can reduce the dissolution rate due to a lower surface area exposed to the medium [26, 30] and lower local velocities that the particles are exposed to compared to suspended particles [211]. In the studies by Salehi *et al*. [36] and Uebbing *et al*. [301] coning was observed at 50 rpm and below and an equation was proposed in the literature to determine the lowest agitation speed needed to prevent coning, which will depend on particle size and fluid density [31, 34].

In the FTA, the flow profile is heterogeneous [38] and, due to the pulsating nature of the flow, fluid velocity is time-dependent, with periods of very low or zero velocity. In general, lower velocities are present in the FTA than in the paddle apparatus [16, 37]. Moreover, due to these lower velocity conditions, the contribution of natural convection due to density gradients between the saturated and bulk solutions might be important [41].

In the current work, in the FTA, higher linear average fluid velocities were achieved by increasing the flow rate or decreasing the cell diameter. In the smaller cell (12.6 mm), temporary higher velocities are achieved as there is a lower cross-sectional area for the fluid to flow through than in the larger cell (26 mm). Decreasing fluid velocity in the FTA resulted in a reduced dissolution rate of ibuprofen API in both high and low solubility conditions, as presented in Chapter 3, and ibuprofen tablets in the high solubility environment, as observed in Chapter 4. Tablet dissolution was only investigated in high solubility media so the effect of increasing flow rate on low solubility media was not determined. An effect of flow rate in the FTA was shown before [215], where increasing the flow rate from 8 to 16 or 32 ml min^{-1} in the 22.6 mm cell increased the dissolution rate of the poorly soluble drug danazol [318] and increasing the flow rate from 10.4 to 51.2 ml min^{-1} in the 12 mm cell statistically significantly increased the dissolution rate from salicylic acid tablets [35]. Moreover, when the 22.6 mm cell size was used in the second study, all salicylic acid dissolution rates were statistically significantly lower than in the 12 mm cell for each flow rate studied [35].

The effect of flow rate in the FTA on drug dissolution is possibly due to higher mass transfer as velocity increases, which affects the local concentration gradients, and a better dispersal of the particles as the flow rate increases.

The lowest linear average fluid velocity explored in the FTA with API powder was 0.33 mm s^{-1} which was achieved by combining a flow rate of 8 ml min^{-1} and a cell diameter of 22.6 mm. This velocity resulted in a very slow and variable dissolution with tablets in the FTA in pH 6.8 phosphate buffer medium (70% dissolved in 5 h), as presented in Appendix 2, which was too slow to be used for PK prediction purposes. Therefore, the lowest linear average fluid velocity with ibuprofen tablets was increased to 0.66

mm s^{-1} achieved by combining a flow rate of 16 ml min^{-1} and a cell diameter of 22.6 mm.

The importance of local velocities on the dissolution rate has been highlighted for tablets, as Shiko *et al.* [38, 45] demonstrated through MRI that the faces of the tablet exposed to a higher velocity in the FTA had a higher erosion rate. Horizontally placed tablets, such as those in this work, experience higher local axial velocities because of a lower cross-sectional area available for the fluid to flow compared to vertically oriented tablets [38]. The effect of tablet position is also observed in the paddle apparatus, were off-centred tablets experience the highest shear rates and present faster dissolution profiles, due to thinner boundary layers associated with higher local velocities promoting a faster mass transport, whereas centred tablets are exposed to the very low fluid flow that occurs under the blade and their dissolution rate is slower [19, 21, 22]. Moreover, different surfaces of the same tablet are exposed to different velocities and shear rates in the paddle apparatus which results in different erosion and dissolution rates, highlighting the importance of local hydrodynamics on tablet dissolution [217].

6.1.2. *In vivo* hydrodynamics

Fluid flow *in vivo* is complex and intermittent during fasting states and depends on the MMC patterns [149]. In the fed state, stomach peristaltic contractions present a mean velocity of 2.7 mm s^{-1} [147] and, in the small intestine, peristaltic waves propagate at a maximum velocity of 5 to 20 mm s^{-1} [148]. However, fluid motion is not continuous in the intestinal tract, with phases of high and low velocities, periods of rest and retrograde transport [319].

Hydrodynamics have also been studied in the proximal colon. One research group generated dissolution data in a modified *in vitro* setup simulating the lower intestine, which consisted of a two-stage one-compartment mini-paddle apparatus and a reduced agitation speed to simulate the intensity of hydrodynamics in the lower intestine. They then used the generated dissolution data to predict oral absorption and plasma profiles of three low-solubility drugs in a PBPK model [320-322]. Another group used the MRI-measured motility patterns and pressures in the human ascending colon to develop both an *in vitro* computer-controlled dynamic colon model (DCM) [317, 323-

325] and an *in silico* model of the proximal colon [326] which helped understand how hydrodynamics in the colon might affect drug release.

When comparing *in vivo* and *in vitro* hydrodynamics in the dissolution apparatuses, it was seen that the hydrodynamic parameters (maximum shear rate and fluid velocity) in the paddle apparatus under different rotational speeds are orders of magnitude higher compared to the *in vivo* situation which can result in the overestimation of *in vivo* dissolution [36]. The relevant hydrodynamic characteristics of the paddle, basket and flow-through apparatuses were reviewed in detail by Todaro *et al.* [16].

In the paddle apparatus at 50 rpm the average velocity was 76.2 mm s^{-1} and at 100 rpm, 153.3 mm s^{-1} [36]. Besides, the peak forces that the tablets are exposed to are less aggressive *in vitro* than *in vivo* and peristaltic contractions which generate shear stresses upon the tablet are not captured *in vitro* [91, 151]. There have been recent attempts to incorporate gentle mechanical stress in the paddle apparatus, for example with the use of cotton balls added to the paddle vessel [327]. Even without considering mechanical stress, it has been shown that agitation speeds lower than those commonly used (20 rpm) might generate more biorelevant velocities in the bottom of the paddle [42]. Despite its limitations, the paddle apparatus has been successfully used to establish IVIVCs [328, 329].

The FTA can simulate lower and more biorelevant velocities than the paddle apparatus when operating at 8 ml min^{-1}, as demonstrated by the establishment of an IVIVC for the poorly soluble drug danazol at said flow rate and a 22.6 mm cell [318]. Moreover, Cammarn *et al.* [35] showed that the dissolution rates in the paddle apparatus at 100 rpm would only be matched by the FTA operating with parameters that generate very high average fluid velocities and the highest Reynolds numbers, that is a flow rate of 52 ml min^{-1} which is not a standard operating flow rate, with a cell size of 12 mm and with tablets in the horizontal position. Plus, the FTA can use volumes that are more relevant to both the fed and fasted states in the intestine [312, 330] considering that the simulation of smaller volumes is sometimes necessary for a good prediction of *in vivo* performance [138], for example in the paediatric population [280]. For this particular population, the mini-paddle apparatus has also been used to represent the smaller GI fluid volumes [331, 332].

6.1.3. Medium viscosity effects on ibuprofen dissolution

Another factor that can potentially impact drug dissolution, which was studied in this work, is medium viscosity. Viscosity can affect drug dissolution through an altered diffusion coefficient and particle dispersal and suspension effects.

Viscosity has been considered in terms of mediating negative food effects through inhibition of disintegration of a dosage form, prevention of drug release or reduction of drug diffusivity from the dosage form to the GIT membrane [82, 131, 333, 334], although an improved description of the effect of increased viscosity on *in vivo* hydrodynamics is necessary [335]. It was observed that the most common effect of high meal viscosity is an increase in the T_{max} values of drugs [296]. *In vitro* dissolution data in phosphate buffer with a cellulose additive VEA improved the prediction of a negative food effect for the *in vivo* dissolution of tropsium chloride in PBPK [334]. Ibuprofen, the drug studied in this work, also showed a food effect, as its levels were found to be higher in plasma in the fasted than the fed state. The levels of ibuprofen in the stomach were found to be higher after a meal due to a higher stomach pH, which also resulted in delayed concentrations in the intestine [136].

Even though not as pronounced as in the fed state, the viscosity of the HGF in the fasted state was shown to be slightly higher than that of water (1.7-9.3 mPa.s versus 0.7 mPa.s) at a shear rate of 50 s^{-1} due to the presence of mucus, lipids and proteins [3]. Moreover, it was shown that the IDR of cinnarizine in HGF was lower than in FaSSGF, whose viscosity is that of water [159].

Other examples have shown that just a small increase in viscosity from 0.817 to 1.062 mPa.s (apple juice) or 3.367 mPa.s (orange juice) led to a two-fold decrease in disintegration times [158]. Also, the dissolution of crushed paracetamol tablets was delayed in dissolution media whose viscosity was 1.1-1.7 mPa.s which was achieved with thickening agents [160, 161]. It is possible that even excipients like surfactants in a tablet increase the medium viscosity around the API and retard drug dissolution [309, 336].

Currently, viscosity in *in vitro* dissolution testing is only considered in the highest level of complexity for biorelevant media in the classification presented by Markopoulos *et al.* [82] and it is generally only considered for the fed state.

Biorelevant media intend to more closely match the composition and properties of the GI fluids including the pH, buffer capacity, osmolarity, surface tension, bile salt concentration and volume [77, 81, 87, 152] in order to understand how a drug will be released and dissolve *in vivo*. Colonic biorelevant media have also been developed to study the dissolution of drugs intended to be delivered to the lower intestine [83]. Biorelevant media has been shown to improve PK profile predictions compared to compendial media [85] and increase the likelihood of a successful IVIVC in particular scenarios [330, 337], however a compromise between the complexity of the media and the accuracy of the prediction of *in vivo* dissolution rates or bioavailability has to be achieved. The use of a VEA added to compendial media might be useful to represent the increased viscosity of the GI tract in fasted state without an overcomplication of the media. This would allow isolation of the effects of small increases of viscosity *in vitro* on the dissolution rate of drug API and tablet formulations.

In the current work, small increases of viscosity up to 5.5 mPa.s relevant to the fasted state were explored in *in vitro* dissolution tests in both the FTA and paddle apparatus for ibuprofen API and IR tablets.

Increasing viscosity reduced the IDR of ibuprofen in pH 6.8 phosphate buffer containing up to 1.05% w/v HPMC and 59% w/v sucrose compared to pH 6.8 phosphate buffer with no VEAs, whose viscosity was 0.7 mPa.s. The reduction of the dissolution rate was observed for ibuprofen API in the FTA in pH 6.8 phosphate buffer and 0.1 M HCl with sucrose. This was also the case for ibuprofen IR tablets in the FTA in pH 6.8 phosphate buffer containing sucrose. HPMC did decrease the IDR of ibuprofen in pH 6.8 phosphate buffer but had not such a big impact on the particulate dissolution of ibuprofen API or ibuprofen IR tablets. This suggests that the VEA has effects on particle motion and hydrodynamics and that the effect of each VEA on the dissolution rate of ibuprofen was different in the FTA, despite similar viscosity values.

In the paddle apparatus, only HPMC could be explored, as sucrose prevented the release of ibuprofen from the capsules for at least one hour. The presence of HPMC in the media in the paddle apparatus had small yet statistically significant effects on ibuprofen API dissolution in low velocity - low solubility media. It was shown in previous reports that the presence of VEAs in the media can reduce the efficiency of agitation

in stirred apparatuses which can result in a reduced flow and shear rate in the areas surrounding the dissolving particles [303, 304]. In the mini-paddle apparatus, the fluid flow patterns were altered in increased viscosity media [33], which could affect the velocities that the particles are exposed to and mediate a negative effect of viscosity in the dissolution rate.

It has been reported that the dissolution rate is not a simple function of fluid viscosity, as it varies with the VEA used [300, 303, 304, 334]. This was also observed in the current work. The different effects of each VEA might be mediated by differences in media density, osmolarity, different effects of each VEA on particle motion and velocities that particles are exposed to or differences in wettability exerted by each VEA.

Including sucrose in the media increased fluid density which can explain the larger reduction of the dissolution rate mediated by sucrose when compared to HPMC. The larger reduction of the dissolution rate could be due to a decrease in the relative velocity in sucrose medium from an increased buoyancy force. Moreover, the water diffusivity in sucrose solutions was reported to be lower than in HPMC solutions, which might be derived from the formation of hydrogen bonds between sucrose and water molecules [301, 302] and could reduce the dissolution rate further. In the case of tablets, it was observed previously that disintegration times were longer as sucrose concentration increased [302].

The effect of HPMC on drug dissolution rate has generated contradictory results so far, which depend on the drug studied and the concentration of HPMC. On the one hand, a negative effect of HPMC on tablet disintegration and dissolution rate of atenolol has been reported in the literature [164] but the concentration of HPMC used was much higher than in this work, achieving viscosities in the range of 200–600 mPa.s, more representative of the fed state. Also, a high viscosity achieved with 1.4% w/v HPMC (110 mPa.s) reduced or delayed drug dissolution for drugs of all BCS classes, and more so for classes II and IV [333]. On the other hand, when a small concentration of HPMC was present in the medium, more suspended carbamazepine particles were observed than when no VEA was used, using shadowgraph imaging [2]. 0.3% w/v HPMC solutions also showed higher amounts of carbamazepine and paracetamol released than media with no VEA, which could be due to the wetting

properties of HPMC or the increased suspension [305]. The hydrophilicity of water-soluble polymers like HPMC might increase wettability of the drug and counteract the effects of increased viscosity on the dissolution rate [306, 307]. Therefore, the effect of HPMC-containing media on drug dissolution might be different depending on the polymer concentration and the physicochemical characteristics of the drug.

6.1.4. Interplay between fluid velocity, medium viscosity and drug solubility

An interplay between fluid viscosity and velocity was expected due to the decrease in the transfer of momentum as viscosity increases. This could result in a reduction in the differences between regions of high and low velocity within the cell, and more homogeneous velocity magnitudes present throughout the cell for a given flow rate. So, when viscosity is increased, particles are expected to be less impacted by the set flow rate and cell size. The computational work by Schutt *et al.* [338] shows how the combination of different motility patterns and fluid viscosities exerts different shear stresses on a sample tablet, resulting in different drug release rates and different drug distributions along the colon.

In the current work, a statistically significant interaction between agitation speed and viscosity was observed in the paddle apparatus for the time to 50% dissolution of ibuprofen API in both high and low solubility media, suggesting that the effect of viscosity was larger in lower agitation speeds. Moreover, a statistically significant interaction between viscosity and solubility on the time to 50% dissolution of ibuprofen API was found in both apparatuses, with a larger influence of viscosity in low than high solubility conditions. This shows the importance of understanding and controlling the effects and interplay of fluid velocity and medium viscosity, especially in low solubility media, when testing and developing formulations for poorly soluble drugs.

The effects of a high viscosity of the medium on the dissolution rate has been considered previously in the literature to explain food effects [164]. However, the effects of smaller increases in medium viscosity on drug dissolution have not been investigated. Moderate increases in medium viscosity could be relevant as a representation of the viscosity of the human gastric fluids in the fasted state [3], or if a dosage form is to be taken with juice, which could slightly increase the GI fluids viscosity [158], and because local viscosity around a dosage form could increase due to the presence of excipients like surfactants [309]. This work has demonstrated that

even moderate increases in medium viscosity (below 5.5 mPa.s) could potentially impact the dissolution of a drug – albeit, this work focused on ibuprofen dissolution, as an API powder and as an IR tablet, so the effect for other drugs' dissolution behaviour cannot be inferred.

Another point demonstrated in this work is that despite achieving similar values of viscosity, the effect on drug dissolution and bioavailability differed depending on the VEA used. The reasons behind this discrepancy were previously analysed, but this suggests that in some instances a particular VEA might have a large impact on the dissolution of a drug whereas a different VEA might not.

With the current data, it is not possible to make a broad recommendation that VEAs should be consistently included in dissolution media, until more knowledge has been generated about how moderate increases of viscosity affect other candidate drugs and whether the effects are relevant when combined with other factors which might override the effect of a small increase of viscosity, such as the presence of bile salts in the medium. Moreover, it is possible that a VEA at a low concentration might not have a large impact on the dissolution rate or bioavailability of a drug, as was observed with HPMC in this work. The investigation of other drugs with different physicochemical characteristics to ibuprofen would allow a relationship to be established between the VEA used and the drug dissolution behaviour, to ascertain whether a particular VEA has the same positive or negative effect on the dissolution of a broad range of drugs.

6.1.5. Factors impacting the dissolution rate beyond viscosity

Even though it was not the focus of this work, it is acknowledged that much has been investigated in relation to bile salts presence in the media and the media buffering capacity, both being flagged as important parameters for dissolution that may be considered *in vitro* for improved *in vivo* predictions [86, 107]. Bile salts could increase the solubility of poorly soluble drugs through micelle encapsulation, but this could result in slower dissolution rates due to the lower diffusivity of micelles [125] and reduced absorption due to drug entrapment in micelles [127, 177].

The buffering capacity of both compendial media and biorelevant media was found to be higher than the buffering capacity *in vivo* due to the use of phosphate buffer instead of bicarbonate buffer, which is predominant *in vivo* [108-112]. This might result in a faster dissolution of weak acids *in vitro* due to the surface pH being higher than *in vivo*

as the drug dissolves. Bicarbonate buffer has been used *in vitro* to represent the lower buffering capacity of the intestinal fluids [327]. But, because of the challenges encountered when using bicarbonate buffer *in vitro*, phosphate buffers of a lower concentration have been proposed to match the *in vivo* buffering capacity [113, 115]. However, in some cases, using media of a lower buffer capacity results in overdiscriminating tests and predictions of bio-inequivalence when BE had been observed *in vivo* [116]. In the current work, the most updated buffering capacity recommended by the USP was used (50 mM). These research interests could be investigated in combination with small medium viscosity increases, to assess the relative influence of viscosity on drug dissolution when considered against other relevant factors, such as bile salts and media buffering capacity.

Another research topic has revolved around the presence of an absorptive sink *in vitro* that can represent *in vivo* absorption simultaneously with drug dissolution and the effects of drug removal on supersaturation and permeation with the use of a dissolution/permeation setup [171-173, 339]. This might increase the translatability of dissolution and precipitation rates to *in vivo* data through oral absorption modelling [175] and the accuracy of the prediction of dose and food effects [176]. Absorptive sinks *in vitro* have also been implemented with an organic layer like decanol in which the dissolved drug partitions into to simulate drug absorption [340]. This was not investigated in the current work, but could be an addition to it, as the effect of fluid velocity and viscosity on dissolution rate might be more or less relevant when an absorptive sink is present.

As fluid velocity and medium viscosity changes affected *in vitro* drug dissolution rates of ibuprofen API powder and IR tablets, an accurate simulation of both hydrodynamic factors was considered important.

6.2. Mechanistic dissolution simulations

The advantages of mechanistic simulations were outlined by Pathak *et al.* [226] and they include an understanding of factors affecting drug dissolution, a basis for selection of *in vitro* dissolution conditions, a means of exploring the effect of manufacturing changes on the dissolution of poorly soluble drugs [200], and an input generation method for PK modelling and simulation.

Much work has been done on developing mechanistic dissolution models [199, 200, 203, 208, 209, 211, 214, 341] which are built from theoretical mathematic equations that predict the dissolution rate of a drug based on particle and fluid related parameters. However, it is not possible for the simulation model to capture all the factors affecting dissolution and their spatiotemporal variability so a compromise must be made between the complexity and the accuracy of the model.

The early models focused on defining the boundary layer thickness and its relationship with particle size. Some of them defined it as a constant value [199] while others determined that it was a time-dependent parameter that changes with particle size up to a threshold value above which it remains constant [200]. In SIMDISSO^{TM}, the boundary layer thickness is encompassed and calculated as part of the mass transfer coefficient together with diffusivity, therefore it is not necessary to empirically estimate and input a value of h.

The current work explored three *in silico* approaches to potentially improve the predictive ability of mechanistic dissolution simulations in SIMDISSO^{TM}, which were the definition of an NPV versus the FTA cell volume or the paddle vessel volume, the use of a PSD versus an MPS and the effect of enabling versus disabling particle motion.

6.2.1. Bulk volume definition in mechanistic dissolution models

The importance of the definition of a bulk volume was proposed by Wang *et al.* [208], as sometimes when the fluid volume is small or the drug is poorly permeable and not being quickly removed from the GIT, the increase in bulk concentration might slow down or halt dissolution due to saturation of the medium.

Sink conditions in which bulk concentration is much lower than solubility are often assumed when mechanistic dissolution models are used [193, 194, 199]. The importance of simulating dissolution under non-sink conditions in some situations has been highlighted by the application of simulation models to situations where bulk concentration is higher [210, 342]. In the current work, different definitions of bulk volume *in silico* were investigated. The volume available to simulate dynamic bulk concentration was defined as either the whole flow-through cell or vessel volume in the paddle apparatus or the NPV, a reduced volume intended to exemplify the importance of local hydrodynamics in drug dissolution, which can be different to global

hydrodynamics in either apparatus. An NPV was explored based on the assumption of an instantaneous distribution of drug mass in the dissolution apparatus potentially not being accurate, especially when low local fluid velocities are found in the FTA [16] and in the paddle apparatus between the end of the paddle blade and the bottom of the vessel [19].

The NPV predicted effects of fluid velocity differences on dissolution in the high solubility medium in the FTA but had no effect on predictive ability in the paddle apparatus. The NPV more accurately predicted t85 in the high solubility medium than when the cell volume was used in high and low fluid velocity conditions when combined with a MPS and enabled particle motion. This was thought to be due to a slower simulated dissolution rate which was closer to the observed *in vitro* dissolution rate as detailed in Chapter 3.

In the current work, an overall advantage of defining a NPV in dissolution simulations was not observed. This option is theoretically more accurate than the generally assumed condition in which the drug dissolves and instantaneously diffuses across the whole cell volume (in the FTA) or vessel volume (paddle apparatus), but it might be the case that (a) sufficient accuracy is achieved without the implementation of this option (b) other factors such as solubility or particle size have a larger impact than the local volume definition on the accuracy of a simulation. Therefore, more studies of the applicability of the NPV volume under different conditions are needed before a general recommendation on the NPV usage can be made.

In vivo sink conditions might be present for BCS class II due to the high permeability and quick absorption reducing the bulk concentration in the intestinal tract. However, the NPV option or the simulation of a smaller volume where dynamic bulk concentration is calculated could be useful for BCS Class IV drugs where sink conditions *in vivo* might not be achieved due to a lower permeability, and dissolution might be occurring closer to saturation conditions.

One of the advantages of SIMDISSO^{TM} is that it can capture the different hydrodynamic conditions of each dissolution apparatus by incorporating the relative velocity in the term Re. However, the simulations in the paddle apparatus were not as accurate as in the FTA suggesting higher hydrodynamic complexity than simulated. Only one direction of velocity can be simulated. The tangential direction velocity was

selected as it is the main velocity component in the paddle apparatus [16, 18]. This in turn meant that the velocities in the axial and radial directions could not be included in the simulations. Gravitational effects could not be simulated either due to this limitation. In addition, differences between the velocities that sedimented versus suspended particles are exposed to are not currently captured by the code. All of this could explain the lower simulated dissolution than observed.

6.2.2. Effective particle size and particle morphology in dissolution simulations

The selection of an effective particle size for dissolution simulation can be challenging. Models which considered a PSD reported an improved accuracy of the simulation model [200, 204, 209, 341]. However, it has been discussed before that the input of a PSD is not always representative of the drug surface area available for dissolution [211] due to drug morphologies deviating from sphericity and the tendency to form agglomerates as particle size is reduced through manufacturing processes like milling or the hydrophobicity and cohesiveness of the drug increases [343].

This study supports a higher accuracy of the predicted dissolution profiles when a PSD is used, based on the fact that most pharmaceutical API powders are not monodispersed. Nonetheless, it was seen that in some cases an MPS could be sufficient for an accurate simulation of dissolution metrics like t85, reducing computational costs.

Also, a PSD simulation has the potential to overpredict API dissolution at the earlier stages in high solubility media, as shown in the current work. This overprediction of early dissolution was also seen in higher viscosity media for ibuprofen API up to the point of 20-25% dissolution in both high and low solubility conditions in the FTA as presented in Chapter 4. The faster simulated dissolution could be due to the simulated smaller particles contributing to a faster early dissolution than observed. Particle aggregation *in vitro* was suggested as the reason for this overprediction based on the hydrophobicity of ibuprofen. Particle agglomeration effects were also observed when API mass was increased from 5 mg to 50 mg, which resulted in an overprediction of dissolution rate in all simulated profiles with the three options explored (NPV, PSD, enabling or disabling particle motion). Other examples of a potential effect of agglomeration on drug dissolution rate have been described in literature. A lower than predicted dissolution rate was observed when the mass of drug was increased from 5

mg to 10 mg and clumping was suspected [1]. Polli *et al.* [342] also reported an effect of increasing drug dose but only in low solubility media.

Even though low concentration of surfactants below their CMC have been reported to result in better disaggregation of aggregated particles [344], a small amount of non-ionic surfactant (0.003% w/v Tween 20), which was purposely selected to not affect the solubility of ibuprofen in low nor high solubility media, was not sufficient to ensure particle dispersal when a mass of 50 mg was studied in the current work. Therefore, the use of a PSD in mechanistic dissolution simulations could be more useful for drugs which are not as prone to aggregation as ibuprofen and for lower drug doses.

Shadowgraph imaging is a useful tool to observe particle behaviour during dissolution in terms of particle motion, velocity and size changes versus time and it can help explain differences between predicted and observed dissolution rates in terms of particle aggregation. Apart from less surface area exposed, if particles are agglomerating at the bottom of the cell they will be exposed to different fluid velocities and local concentrations than if they are suspended and moving with the fluid [345]. Other imaging techniques, like surface dissolution UV imaging have helped assess the dissolution and precipitation of drugs in pure and amorphous forms [222]. Imaging techniques could aid in the selection of an appropriate effective PSD to input into dissolution models.

Particle aggregation and clumping are challenging to incorporate in a mechanistic dissolution simulation, but the effective particle size could be increased to reflect these phenomena.

Apart from particle size, another challenge faced by mechanistic simulations is the definition of particle shape and the assumption of sphericity, which might underestimate the dissolution rate due to an underestimation of the available surface area.

One of the assumptions generally made when applying mechanistic models to simulate drug dissolution is that of particle sphericity. Moreover, the particles remain spherical with time, that is, there are no morphology changes during the dissolution test [199, 200, 210]. Nonetheless, spherical particles might not always be found *in vitro* or *in vivo* [211]. Abrami *et al.* [224, 225] simulated the dissolution of particles with different shapes, including an irregular shape, and determined that particle shape is

important as long as it influences the area available for dissolution. In the current work, the assumption of spherical particles may not be correct based on the microscopy results where needle-shaped particles are observed, as presented in Chapter 3 and this could partly explain the discrepancies between the observed and simulated dissolution rate of ibuprofen in low solubility medium. However, confirmatory BET studies indicated that the measured surface area (5.3 cm^2 ± 0.24) compared well to the calculated surface area when a PSD was simulated (6.2 cm^2).

Another assumption is that of particle surface smoothness. A porous surface would have a much greater surface area than a smooth surface with the impact on dissolution depending on the total number of pores, the pore shape and the pore size distribution. Several techniques can be deployed to characterise the pore architecture of a pharmaceutical particle, such as helium pycnometry, mercury porosimetry, or nuclear magnetic resonance (NMR) [346]. In the current work, the true density of ibuprofen particles – that is the density of the solid part of the particle – obtained in helium pycnometer studies was input in the simulations [1].

Another general approach to mechanistic dissolution modelling is to assume that all surface area is available for dissolution from time 0, and that wetting and particle dispersal are instantaneous [211]. This might depend on the fluid velocity and density, particle density, and the presence of wetting agents and surfactants in the media. Pepin *et al.* [211] highlighted the difficulty of mechanistically predicting the impact of poor wetting on the early dissolution rate at this stage, which could be relevant for hydrophobic drugs.

When the API is administered in a dosage form like a tablet, not all of the surface will be available for dissolution instantaneously, as this will depend on tablet disintegration. Considering water uptake into a tablet matrix as a driver of disintegration, water uptake was modelled with Fick's second law of diffusion to represent the disintegration process [347], but modelling the complex process of disintegration can be challenging. Modelling disintegration is expected to be particularly relevant for slowly disintegrating tablets. Besides, the incorporation of a disintegration rate can increase the accuracy of bioavailability models, as occurred for two poorly soluble weakly basic drugs in tablet form, which disintegration rates were extracted from empirical models [348].

6.2.3. Particle motion definition in dissolution models

One of the major advantages of SIMDISSO^{TM} is the possibility of simulating particle motion within the flow-through cell, as a combination of the forces acting upon the particle and its mass. The relative velocity between the particle and the fluid contributes to the simulated dissolution rate, through the Re term in the Ranz-Marshall correlation.

It is important to determine whether particles are suspended or sedimented, because this can ultimately influence the dissolution rate, and which fluid velocities are necessary to achieve particle suspension. In some cases, models have been applied with the assumption that the difference in density between the fluid and the particle is negligible and particles will be suspended [203, 214], but this might not be the case, for example, for particles of high porosity, whose density might be lower than that of the fluid or, as seen in this work, in higher viscosity media with sucrose, which resulted in a higher fluid density. In the current model, it is important to determine whether particles are sedimented or moving upwards with the fluid or downwards and at what velocity they are doing so.

Particle motion was shown to follow complex patterns in the FTA with shadowgraph imaging previously [215]. Short particle motion simulations in SIMDISSO^{TM} can suggest whether to enable or disable particle motion based on particle mass, particle density, and fluid density and velocity.

The particle motion simulations in Chapter 3 showed that the magnitude of positive particle velocity values was larger than that of negative velocity values – in the first ten seconds of the simulation at least –, which suggests that particles would be lifted to the top of the cell and remain there until they are small enough to move with the fluid. In Chapter 3, the effects of enabling versus disabling particle motion in SIMDISSO^{TM} for the whole duration of the test were investigated. This reflects a potential limitation as particle motion can change with time *in vitro* due to a decreasing particle size. To capture the *in vitro* situation more accurately, a spatial limitation was implemented and tested in the higher viscosity simulations presented in Chapter 4. It was defined as the height of the flow-through cell so that when the particle reaches the top or the bottom of the cell, it cannot move further in the vertical direction. This motion restriction is reflected in the calculated relative velocity.

Of the three simulation approaches studied (cell volume versus NPV, MPS versus PSD and disabled versus enabled particle motion), particle motion definition was the least impactful on the dissolution rate of ibuprofen API in high solubility media, in either of the velocity conditions studied.

Disabling particle motion marginally increased the prediction accuracy in low solubility-high velocity media when a PSD and NPV were used. This is explained by the difference between fluid and particle velocity that ultimately affects the velocity that particles are exposed to. This difference was large in the high velocity conditions (average fluid velocity of 2.35 mm s^{-1}) but not in the low velocity conditions (average fluid velocity of 0.33 mm s^{-1}), as presented in Chapter 3.

Even though the difference in the simulated dissolution profiles when enabling or disabling particle motion was not large, there is still value in simulating particle motion. For example, in instances of higher fluid velocity, there could be a large difference on the velocity that a particle is exposed to depending on whether it is sedimented, trapped at the top of the cell or suspended with the fluid, and this can affect its dissolution rate. An underprediction of the velocity that a particle is exposed to, by means of assuming the particle is moving with the fluid could result in a predicted dissolution rate that is lower than that observed *in vitro*. Moreover, if a wider PSD is present in the test cell, the definition of particle motion could be more relevant, as there might be more pronounced differences in particle motion between the smaller and larger particles for larger periods of time. Given the complexity of the flow field and fluid velocities in the FTA [16], the study of relative velocity is considered important for an accurate dissolution simulation and should be assessed on a case-by-case basis.

6.2.4. Dissolution simulations in moderately increased viscosity media

SIMIDISSO™ was also used to explore the predictive ability of a mechanistic dissolution simulation code when medium viscosity was slightly increased, and validated with *in vitro* data for the first time, building on the work by D'Arcy and Persoons where simulations in enhanced-viscosity media were explored [2]. The reduction in the *in vitro* dissolution rate with sucrose was accurately simulated in SIMDISSO™ at high velocities. However, the simulations predicted a larger effect than observed from HPMC, suggesting some experimental factor might not be captured in the simulation.

Moreover, the simulations were valuable to study particle motion differences depending on viscosity. The simulated profiles suggested reduced particle lifting times as viscosity was increased. This indicates that the velocities that particles are exposed to in different viscosity media can be different and that an increase in viscosity could impact the dissolution rate by improving drug mass dispersal and available drug surface area. The effect of medium viscosity on particle motion was more pronounced when it was accompanied by an increase in fluid density, as was the case with sucrose in this work.

In both apparatuses, mechanistic simulations of ibuprofen API dissolution were reasonable for the high solubility environment but underpredicted dissolution in the low solubility environment. However, some of the simulated inputs considered - disabling particle motion and inputting a PSD instead of a MPS - increased the predictive ability of the simulations of API ibuprofen dissolution in low solubility media in the FTA. This suggests some *in vitro* factor in the low solubility media is not captured by the simulation. However, as most of the dissolution and absorption of ibuprofen is expected to occur in the intestine [145] due to its low solubility in the stomach and the higher surface area for absorption in the intestine, one could argue that an accurate simulation in the media representing the intestine could be more useful than in the media representing the stomach for weakly acidic drugs. An accurate simulation of intestinal conditions could also be useful for weakly basic drugs which might precipitate as they transition to an environment with an elevated pH [223]. The success of different precipitation inhibiting strategies which has been assessed with *in vitro* dissolution transfer models [349] could potentially be predicted with an accurate simulation of intestinal conditions.

6.2.5. Recent approaches to dissolution simulation

The development of mechanistic models of dissolution continues to be of relevance as exemplified by models recently proposed in the literature. Salehi *et al*. [36] developed a hierarchical mass transfer drug dissolution model which incorporates drug properties, GIT fluid properties and fluid hydrodynamics to simulate drug dissolution in a compendial dissolution vessel. In the model, particle radius change with time is dependent on the Sherwood number for the particle, which represents the ratio of convective to diffusive mass transport rate. Mass transport is also determined by the PSD, the drug solubility and surface pH, the drug diffusivity and the bulk

concentration and bulk pH. The model was validated with *in vitro* dissolution data for ibuprofen, haloperidol and felodipine. The dissolving particle's shape is assumed to be spherical and the particles on each bin size are assumed to be homogeneously distributed across the medium. The equation used to calculate the shear contribution to the Sherwood number is only valid for Re 0 to 10 and S^* (the shear Peclet number) 0 to 500. S^* is the ratio of flow effects to diffusivity effects and is calculated as sr_p/D where s is flow shear rate (s^{-1}) at the particle of radius r_p (m), and D is mass diffusivity ($m^2\ s^{-1}$). This limitation could make the simulation of the dissolution of larger particles less accurate.

Another mass transport model was presented by the same research group [350] which was used to study the effect of incorporating acidic pH modifiers to dosage forms containing weakly basic drugs. This formulation approach is utilized to improve GIT solubility and dissolution of weakly basic drugs in a stomach with an elevated pH as a consequence of proton-pump inhibitors coadministration or hypochloridria disease conditions. The model allows the selection of the most appropriate pH modifier depending on the drug's physicochemical characteristics to optimize *in vivo* drug solubility and dissolution. The main assumption is the rapid dissolution of the pH modifiers, which are present in the bulk medium from the beginning of the API dissolution process.

In a more recent paper from the same research group, Sinko *et al*. [351] built a particle size, dose-dependent dissolution and permeation model which considers drug dissolution within the concentration boundary layer that is formed in the adjacent region to a semipermeable membrane. They used ibuprofen suspensions of three different PSDs as the model drug and validated the model with an *in vitro* dissolution-permeation setup. The dissolution of spherical ibuprofen particles was also calculated with the Sherwood number model, accounting for confinement or dissolved drug accumulation in the vicinity of the undissolved particle. Potential limitations of the model included the assumption that mass transport is unidirectional across a semipermeable membrane, the semipermeable surface does not affect dissolution kinetics, the solid dissolving is spherical, and the particles are homogeneously distributed in the dissolution vessel.

There have also been recent dissolution modelling attempts coupled with CFD to predict fluid flows and mass transfer rates in the commonly used dissolution apparatuses. Some examples include the CFD model developed by Liu *et al*. [352] which is based on an *in vitro* dissolution study of a benzoic acid tablet in a beaker and stirrer system, the model built by Kubinski *et al*. [353] which considers relevant hydrodynamics in the paddle and basket apparatuses at different rotation speeds and media volumes commonly used in drug development for erosion-based formulations, and the model described by Lou and Hageman [354] which illustrates the velocity distribution across the paddle apparatus and its effect on the dissolution and release from a polymer-controlled sustained release tablet. CFD simulations have also been applied recently to the FTA. For example, Yoshida *et al*. [355] combined CFD and PIV to study fluid flows and the effect of air bubbles on the dissolution of disintegrating and non-disintegrating tablets in the FTA. CFD helped illustrate the different dissolution rate of prednisolone tablets depending on particle distribution through the cell due to the particles being exposed to different fluid velocities depending on their location on the cell. One of the main limitations of CFD models is the generation of an acceptable mesh and the definition of acceptable boundary conditions to generate a sufficiently accurate solution [17]. Numerical solutions to dissolution based on the Noyes-Whitney equation have also been applied, as exemplified by the work of Yokoyama *et al*. [356, 357]. A three-dimensional cellular automata model was applied to the disintegration and dissolution of a mefenamic acid tablet in which the tablet geometry is discretized into individual grids from each of which drug release is calculated. As with CFD models, in the cellular automata model, the definition of the number of grids that the tablet geometry is divided into has to allow for a sufficiently accurate mass transfer calculation without capturing the whole complexity of a solid-liquid contact interface.

6.3. PBPK simulations

The current work investigates the effects of *in vitro* dissolution parameters (fluid velocity, fluid viscosity, VEA) on the prediction of the plasma concentration profile of ibuprofen following the oral administration of ibuprofen IR tablets as well as the different approaches for incorporating FTA-generated dissolution data in GastroPlus®.

The incorporation of PBPK modelling and simulation in new drug applications submitted to the FDA has been increasing since 2008 [238]. PBPK guidelines have

been published by the FDA [101] and the EMA [231] and there have been attempts at harmonizing and refining the use of PBPK models, for example by the Orbito Working Group [358], as PBPK models tend to be fine-tuned on a case-by-case basis. The same can be said for the dissolution methods used to generate data to inform said models. Even though the FDA has concluded that dissolution testing is a key modelling input for PBPK, the appropriate *in vitro* method to predict drug absorption can be widely variable as it depends on the specific research question, the stage of drug development, equipment availability and the type of drug substance and formulation [253].

The integration of *in vitro* dissolution data into *in vivo* absorption models can increase the accuracy of the prediction of the performance of a formulation in the body [237], and it can also verify if the dissolution method used is biorelevant [183]. However, there are still aspects to further consider in terms of the biorelevance of *in vitro* dissolution tests such as hydrodynamics, or accounting for permeation, and more information is needed on GIT volumes, forces and pressures in healthy and diseased populations to build into the *in silico* models [237].

Integrating *in vitro* dissolution with *in vivo* absorption prediction could be considered within the QbD framework which emphasises the understanding and control of processes during drug development in order to obtain a final product that meets some predefined characteristics [100, 359]. Mathematical models substantiated with *in vitro* inputs could serve to identify key factors affecting drug bioavailability that could be controlled during drug development such as dissolution [252], permeability and solubility [177], supersaturation ratio and precipitation rate constant [360] or PSD [258], or to set the final product characteristics, for example, the percentage dissolved *in vitro* versus time necessary to achieve BE [70, 251, 257].

In the current work, the dissolution profiles in sucrose-containing medium corresponded with the least accurate predictions of C_{max}, T_{max} and the early timepoints, suggesting this VEA might not be a suitable surrogate to represent the slightly increased medium viscosity of the fasted GI fluids. However, obtaining different values of *in vitro* viscosity or density in sucrose-containing media could generate different PK profiles, which resemble those obtained in HPMC-containing medium, as suggested by PSA studies. On the other hand, when the dissolution profiles in HPMC-containing

medium were input into the model, the predictions of C_{max} and T_{max} were considered accurate in both fluid velocity scenarios studied, with FEs close to 1. However, it is important to note that it is difficult to isolate the effect of fluid viscosity on the observed dissolution rates and predicted PK profiles and that the effects of each VEA on tablet motion, particle wetting and fluid density warrant further consideration. This is relevant when purposely altering medium viscosity but also when the increase in viscosity is unintentional. This could derive from the presence of certain excipients like surfactants which can locally increase medium viscosity if present at a high concentration [336].

Other works in the literature have investigated several *in vitro* dissolution features and data treatments with a focus on both improving *in vivo* behaviour predictions and the selection of *in vitro* biorelevant conditions. Klumpp *et al.* [361] evaluated the influence of media composition (FaSSGF, FaSSIF V1, V2 and V3), dissolution test type (single-stage or two-stage in USP II) and dissolution data input method into PBPK (observed release profile or dissolution rate model versus mechanistic model or diffusion layer model (DLM)) for simulating the *in vivo* plasma profile of IR formulations of glibenclamide and dipyridamole. They found that in general, two-stage testing, fitting the data with the DLM and a dynamic pH selection was consistently accurate. Litou *et al.* [270] investigated the utility of biorelevant *in vitro* setups and media to predict the *in vivo* performance of two tablets of an amorphous solid dispersion formulation in the fed state and combined that data and literature data into PBPK modelling to identify the key parameters affecting the drug's pharmacokinetics. They found a disagreement between predicted versus observed precipitation rates. Litou *et al.* [270] developed a PBPK model to simulate the *in vivo* performance of nano-sized poorly soluble API capsules implementing *in vitro* dissolution, solubility and transfer studies data and found out that although nano-sizing the API improves its *in vivo* performance, intestinal solubility still remained a barrier to bioavailability and that an accurate simulation of GET was relevant in this case.

These studies, and the work presented here, methodically investigate factors relating to the *in vitro* dissolution testing itself and the best practices in data treatment before inputting them into an absorption model.

6.3.1. Virtual bioequivalence (VBE) studies

VBE studies were carried out as part of this work. Currently, human studies are viewed as the major type of evidence to demonstrate BE [57]. Refining and validating PBPK models is a step towards generating more confidence in VBE predictions [362]. VBE studies using *in silico* models could serve as alternatives to time-consuming *in vivo* comparative BE studies for poorly soluble drugs [256] or permeation controlled absorption drugs [257]. Moreover, they can be useful in contextualizing the impact of dissolution parameters such as media viscosity on PK predictions as they incorporate variability around physiological parameters.

In the current work, VBE studies illustrated that the presence of HPMC in the dissolution media would not impact C_{max} BE, whereas the presence of sucrose did not result in bioequivalent C_{max} values. Other examples can be found in the literature where PBBM models have been used to predict VBE. Kambayashi *et al*. [256] predicted BE of dosage forms with different *in vitro* dissolution behaviour containing two poorly soluble drugs inputting *in vitro* biorelevant data into Stella software. Laisney *et al*. [257] used PBBM to determine VBE between a tablet and capsule formulation of a weakly basic drug (ribociclib) in both healthy and cancer patients. In the study by Laisney *et al*. [257], VBE trials inputting virtual batches with slower dissolution rates were used to define an *in vitro* bioequivalent safe space.

The potential for VBE analysis is acknowledged in these studies, together with the need to further study and characterize the GI physiology to increase the accuracy and confidence in the PK predictions for a virtual population. Moreover, VBE can be applied to different patient cohorts provided that data on physiological variability is available for model building.

6.3.2. Flow-through apparatus dissolution profiles and transfer models for pharmacokinetic predictions

Dissolution profiles occurring in a biorelevant timeframe were generated in the FTA in the current work and implemented into GastroPlus®. As discussed previously, the FTA can generate fluid flows and Reynolds numbers which are closer to those found in the human GIT [16].

The paddle apparatus has generally been used to generate biorelevant dissolution data to be used as inputs to PBPK models, although some reports in the literature which have utilized the FTA instead can be found. Ibarra *et al*. [363] used FTA-generated dissolution profiles of three carvedilol products to predict the *in vivo* pharmacokinetics in a virtual population. In order to simulate the fasted GIT, the formulations were originally exposed to acidic medium at a high flow rate for 30 min to represent the stomach, followed by exposure to phosphate buffer at a low flow rate for 150 min. The authors highlighted the need to carry out *in vivo* BE studies for this particular drug, based on the predicted non-BE of commonly marketed forms of carvedilol in the Uruguayan market.

Kushwah et al. [364] built a PBPK model to predict the bioavailability of rivaroxaban from Xarelto IR tablets. The model was informed with *in vitro* solubility, permeability and dynamic dissolution data, which was generated in the FTA. In this work, the tablets were also exposed to two consecutive media to represent transfer of the dosage form from the stomach to the intestine - FaSSGF for 30 min and FaSSIF for 5.5 h. The FTA was also used to generate dissolution profiles which were relevant to the fed state.

The current work represents an additional example of the use of the FTA to generate biorelevant dissolution data to be used as inputs to PBPK models.

Other two-stage *in vitro* models which did not use the FTA, but other dissolution setups have been performed to generate dissolution inputs for PBPK models of basic drugs. This is considered of relevance as basic drugs are prone to precipitation when transferred from the stomach to the intestine [226]. For example, the BioGIT system which simulates drug transfer from the stomach to the upper intestine was able to predict the impact of dose and formulation on early exposure for eight low solubility compounds [187, 365]. However, transfer models could be subject to further improvements, as Carlert *et al.* [223] observed that *in vitro* two-stage models using FaSSGF and FaSSIF tended to overpredict *in vivo* precipitation rates, probably due to the absence of an absorptive sink [129]. For weakly basic drugs, it is important to input accurate precipitation parameters in the model [227]. This is also the case for the salt forms of weakly acidic drugs. In the work by Zöller *et al*. [366] the supersaturation and precipitation behaviour of two ibuprofen salts was different depending on the apparatus used (paddle apparatus versus µDISS Profiler™) and the pH of the media.

Therefore, a two-stage dissolution system that incorporates an absorptive sink might be necessary for accurate precipitation parameters to be input into PBPK models of weakly basic drugs and salt forms of weakly acidic drugs.

It could be argued that weakly acidic drugs, for which precipitation when transferred from the stomach to the intestine is not expected, do not necessitate such accurate precipitation parameters in the model. Instead, for these drugs an accurate prediction of GET could be considered more relevant, as GET will determine when the solubility, dissolution rate and absorption rate of the acidic drug is expected to rise as a response to the pH increase in the GIT.

In the current work, dissolution inputs to GastroPlus® were generated in pH 6.8 phosphate buffer media only, representing the intestinal pH. It was shown in the literature that a pre-treatment in acidic conditions to simulate the *in vivo* environment was relevant for the salt forms of ibuprofen in terms of capturing their faster oral absorption [111]. Even though the current work did not use tablets containing ibuprofen salts, it might still be relevant to study the effect of exposure to an acidic environment prior to dissolution in pH 6.8 phosphate buffer, considering the observed underprediction of the early timepoints of the plasma concentration profiles. The impact of an acidic pre-treatment on the PK profile of ibuprofen tablets in different viscosity scenarios could be simulated with the model presented in the current work.

6.3.3. Parameter sensitivity analysis (PSA)

PSA can be used to assess which parameters are more relevant to include in *in vitro* biopredictive tests and which variables are more likely to influence the *in vivo* behaviour of a formulation [183, 261]. In the current work, the effects of viscosity on the parameters C_{max} and T_{max} through altered diffusion coefficients and effective PSDs were highlighted in a PSA study. Other works have used PSA to demonstrate the relevance of parameters such as GET, intestinal solubility, or effective permeability for an accurate simulation [251, 270]. PSA has also been used to determine the optimal percentage dissolved of montelukast to achieve a target plasma concentration profile [279]. In the work by Mukherjee *et al*. [367], PSA was used to study the effect of hypothetical dissolution scenarios generating different dissolution rates on the plasma concentration profile of the drug elagolix.

PBPK models coupled with biorelevant dissolution testing could be used to refine and select the most appropriate *in vitro* dissolution conditions to obtain a target *in vitro* dissolution profile. For example, in the current work there was a compromise between an accurate prediction of T_{max} and an accurate prediction of the early timepoints (<1 h). It is suggested that selective changes to *in vitro* fluid velocities and viscosity values, or the use of different VEAs, could optimize the predictions of the early timepoints while delaying C_{max} to closely compare to the *in vivo* values. This is relevant in light of the importance of an accurate prediction of T_{max}, particularly for analgesic drugs like ibuprofen, but also for other types of drugs, like hypnotics used for the treatment of insomnia [251].

In order to develop accurate PBPK models, it is imperative to understand *in vivo* and *in vitro* hydrodynamics and how they affect drug dissolution and absorption. Working towards the refinement of these models can bring many advantages, such as speeding up development times, and reducing costs associated with clinical trials.

Chapter 7. Conclusions

The effect of hydrodynamic parameters – i.e., fluid velocity and medium viscosity – on the dissolution rate of ibuprofen powder and immediate release ibuprofen tablets was investigated in the paddle apparatus and the flow-through apparatus. The dissolution profiles of ibuprofen immediate release tablets generated in the flow-through apparatus in different medium viscosity conditions served to inform a predictive pharmacokinetic model in GastroPlus®. The in-house dissolution simulation code SIMDISSO™ was used to predict the dissolution rate of ibuprofen particles in the flow-through apparatus and in the paddle apparatus, with three different approaches being explored in relation to bulk volume, particle size and particle motion. Moreover, the applicability of SIMDISSO™ to simulate dissolution in higher medium-viscosity environments was assessed.

- The current work added to the body of evidence that shows that increasing fluid velocity in the *in vitro* dissolution apparatuses through an increased agitation speed in the paddle apparatus and an increased flow rate or decreased cell size in the flow-through apparatus increases the *in vitro* dissolution rate of Biopharmaceutics System Classification class II drugs.
- The flow-through apparatus was used to generate dissolution profiles for an immediate release tablet that served as an input to a pharmacokinetic model, representing an example of the use of this apparatus for a biopredictive application. In the case presented here, moderately increasing medium viscosity with HPMC led to predicted bioequivalence of ibuprofen C_{max} between medium containing 1.05% w/v HPMC and medium without this viscosity enhancing agent in the two fluid velocity conditions examined.
- SIMDISSO™ simulations could predict the differences in dissolution rate of ibuprofen particles in different solubility media, although there was a general underprediction in 0.1 M HCl, which was reduced when factors like particle size distribution and particle motion were adjusted. This suggests there is scope for better simulating dissolution in a low solubility environment.

- The computational studies also showed the relevance of an accurate simulation of local hydrodynamics for dissolution simulation, which was illustrated with the implementation of a near-particle volume in the flow-through apparatus.
- This study also considers the importance of the selection of an effective particle size to input into mechanistic dissolution models. It was observed that in some scenarios, a median particle size might be sufficiently accurate in predicting dissolution metrics like the time to 85% dissolution. Using a particle size distribution might improve the accuracy of the predicted dissolution profiles, but it might also overpredict early dissolution. This was hypothesised to be due to agglomerates behaving as bigger particles *in vitro*, with a reduced surface area exposed, which would not be captured by the simulation code. Therefore, to capture agglomeration effects inputting an accurate effective particle size distribution is considered relevant.
- In the paddle apparatus, the complexity of simulating hydrodynamics with a reduced-order model were manifested by the poorer predictions in this apparatus than in the flow-through apparatus. Only one velocity component can be input in the code and the different velocities that particles are exposed to depending on whether they are suspended or sedimented are not currently considered but could be further steps to refine SIMDISSO^{TM}. Even though the simulations in the flow-through apparatus were relatively accurate when compared to paddle apparatus simulations, there is still scope for improvement of the simulation in particular scenarios like low solubility media.
- One of the advantages of SIMDISSO^{TM} is the possibility of performing short particle motion simulations which can give insight into the effects of dissolution parameter changes on particle velocity. Particle motion simulations aided in the selection of whether to enable or disable particle motion for the full simulation in the simulations presented in Chapter 3, based on the relative velocity between particle and fluid velocity. A spatial limitation defined as the height of the cell to limit particle motion in the vertical direction was implemented in Chapter 4 to better represent the *in vitro* situation. This eliminates the need to enable or disable particle motion, as it is automatically disabled at the cell upper and lower boundaries.

- Moderate increases in medium viscosity (≤5.5 mPa.s) were shown to affect particulate drug dissolution, intrinsic drug dissolution and drug dissolution from immediate release tablets to different extents depending on the viscosity enhancing agent used, medium solubility and apparatus used. Both HPMC and sucrose reduced the intrinsic dissolution rate of ibuprofen. The particulate dissolution rate of ibuprofen was also reduced in the flow-through apparatus in sucrose-containing medium, but this was not so evident in HPMC-containing medium. The reduction of the dissolution rate of ibuprofen from immediate release tablets was also more prominent in sucrose-containing media than in HPMC-containing media, in both fluid velocity environments studied in the flow-through apparatus.
- The simulations in SIMDISSO^{TM} could capture the effect of sucrose on ibuprofen particulate dissolution but overpredicted the effect of HPMC suggesting other factors, like wetting or impacts of viscosity enhancing agents on fluid velocity are not currently captured by the simulations.
- Particle motion simulations carried out in SIMDISSO^{TM} were useful to illustrate the effect of an increased medium viscosity and fluid density on particle velocity. Reduced times for particles from a particle size distribution to start lifting and reach the top of the cell were observed when viscosity was increased. This could partly explain the observed difference between intrinsic dissolution, where HPMC reduced the dissolution rate, and particulate dissolution in both the flow-through apparatus and paddle apparatus, where the effect of HPMC was not so evident.
- The complexity of isolating the effect of small increases of viscosity on the *in vitro* dissolution rate was manifested, as the presence of viscosity enhancing agents in the media might impact other factors that affect dissolution such as fluid velocities and shear rates, particle motion, wettability and fluid density, and the impact might be different depending on the viscosity enhancing agent used, as demonstrated in this work. Further work with different viscosity enhancing agent, drugs belonging to different Biopharmaceutics System Classification classes and different formulations is needed to continue to build a body of knowledge that suggests which conditions are most affected by small increases

of medium viscosity and how this impacts oral absorption predictions and drug bioavailability.

- The results presented here show that intentional or unintentional viscosity increases could impact a drug dissolution profile and that variables like diffusion coefficient, effective particle size distribution and particle motion should be characterized in a medium-dependent basis.

Chapter 8. Future work

The present work examined the effect of medium viscosity and fluid velocity on the *in vitro* dissolution and predicted bioavailability of one weakly acidic drug in an immediate release dosage form and an API form. The mechanistic simulation of the dissolution of ibuprofen particles under different experimental conditions of solubility, fluid velocity and fluid density was investigated in SIMIDISSO^{TM} and areas of improvement were identified.

1. The effect of moderate increases in medium viscosity (≤5.5 mPa.s) using sucrose and HPMC as viscosity enhancing agents could be explored with other class II drugs according to the Biopharmaceutics Classification System like ketoconazole, a weakly basic drug, or carbamazepine, a neutral drug. The study of class II drugs is considered relevant due to the increase of poorly soluble drugs being developed in recent years. The majority (60-70%) of the drugs in pipeline in 2018 belonged to class II, and together with class IV drugs, they represented up to 90% of the drugs in the development pipeline [69].
2. A design of experiments approach could be used to study the relative influence of moderate increases of viscosity versus other factors affecting drug dissolution such as bile salt concentration or buffer capacity. This would allow the interplay and relative effects of each of these important parameters to be studied. Ibuprofen or the above-mentioned drugs might be used as a sample drug for this study.
3. To further understand the effect of medium viscosity increases on fluid velocities and shear rates, imaging techniques such as particle imaging velocimetry or flow visualization with dyes could be used. Another imaging technique, shadowgraph imaging, is suggested as a means to study viscosity effects on particle suspension, particle motion and particle size changes with time. Shadowgraph imaging has already been used for this purpose with carbamazepine in HPMC-containing medium, proving it a useful technique to characterize viscosity effects on dissolution.
4. Shadowgraph imaging could also aid in the selection of an effective particle size for dissolution simulation models. This is expected to mitigate the limitation

encountered in this work relating to the selection of an effective particle size when agglomeration is observed or suspected.

5. The limitation of a simulated spherical particle shape described in the current work could be challenged with the simulation of other particles shapes in SIMDISSO^{TM}. This could help contextualize the importance of particle shape definition in the case of ibuprofen particles, in light of the surface area studies, which do not suggest a large difference between the experimental and simulated surface area when a particle size distribution is used for the ibuprofen powder used in the current work. The use of more realistic particle shapes is expected to be of particular relevance in low solubility media, where the simulations were found to be of a lower accuracy.
6. When investigating medium viscosity effects, a large impact of fluid density on drug dissolution was identified both *in vitro* and through mechanistic simulations. A separate study to isolate density effects on drug dissolution should be considered with the use of SIMDISSO^{TM} which can study density and viscosity effects separately. This might be difficult to achieve *in vitro* as generally an increase in fluid density of the dissolution media will be accompanied by an increase in fluid viscosity.
7. In the current work, the plasma concentration versus time profile after the administration of an ibuprofen immediate release tablet formulation was simulated. Ibuprofen is a weakly acidic drug but the effect of medium viscosity on the release from and dissolution of other formulations should be considered as the complexity of the formulation is expected to decrease the accuracy of the prediction and be more reliant on the quality of the input data [244]. Based on the successful implementation of flow-through apparatus-generated dissolution profiles for ibuprofen tablets into a bioavailability simulation model, dissolution data with a class II weakly basic drug such as ketoconazole or neutral drugs such as carbamazepine could be generated in the flow-through apparatus and incorporated into a PBPK model. On the one hand, this would help with the assessment of the impact of moderately increasing medium viscosity on the predicted bioavailability of other drugs with different physicochemical characteristics than ibuprofen. On the other hand, it might be relevant for the further confirmation of the usefulness of the flow-through apparatus to generate biopredictive dissolution profiles.

References

1. D'Arcy D, M., Persoons, T. (2011). Mechanistic modelling and mechanistic monitoring: simulation and shadowgraph imaging of particulate dissolution in the flow-through apparatus. *J Pharm Sci*, **100** (3), 1102-1115. https://doi.org/10.1002/jps.22337
2. D'Arcy, D.M., Persoons, T. (2019). Understanding the Potential for Dissolution Simulation to Explore the Effects of Medium Viscosity on Particulate Dissolution. *AAPS PharmSciTech*, **20** (2), 47. https://doi.org/10.1208/s12249-018-1260-4
3. Pedersen, P.B., Vilmann, P., Bar-Shalom, D., Mullertz, A., Baldursdottir, S. (2013). Characterization of fasted human gastric fluid for relevant rheological parameters and gastric lipase activities. *Eur J Pharm Biopharm*, **85** (3 Pt B), 958-965. https://doi.org/10.1016/j.ejpb.2013.05.007
4. Thomas, F. (2019). The Fundamentals of Dissolution Testing. *Pharm Tech*, **43** (10), 44-47.
5. Siepmann, J., Siepmann, F. (2013). Mathematical modeling of drug dissolution. *Int J Pharm*, **453** (1), 12-24. https://doi.org/10.1016/j.ijpharm.2013.04.044
6. United States Pharmacopoeia. (2020). ⟨711⟩ Dissolution.
7. European Pharmacopoeia 5.0. (2005). Dissolution tests for solid dosage forms.
8. International Pharmaceutical Federation (FIP). (1981). FIP guidelines for dissolution testing of solid oral products.
9. Fotaki, N. (2011). Flow-Through Cell Apparatus (USP Apparatus 4): Operation and Features. *Dissolution Technol*, **18** (4), 46-49. https://doi.org/10.14227/dt180411p46
10. Fotaki, N., Reppas, C. (2005). The Flow Through Cell Methodology in the Evaluation of Intralumenal Drug Release Characteristics. *Dissolution Technol*, **12** (2), 17-21. https://doi.org/10.14227/dt120205p17
11. Unites States Pharmacopoeia. (2020). ⟨1087⟩ Intrinsic dissolution - dissolution testing procedures for rotating disk and stationary disk.
12. Bergstrom, C.A.S., Box, K., Holm, R., Matthews, W., McAllister, M., Mullertz, A., Rades, T., Schafer, K.J., Teleki, A. (2019). Biorelevant intrinsic dissolution profiling in early drug development: Fundamental, methodological, and

industrial aspects. *Eur J Pharm Biopharm*, **139**, 101-114. https://doi.org/10.1016/j.ejpb.2019.03.011

13. Kukura, J., Arratia, P.E., Szalai, E.S., Muzzio, F.J. (2003). Engineering tools for understanding the hydrodynamics of dissolution tests. *Drug Dev Ind Pharm*, **29** (2), 231-239. https://doi.org/10.1081/ddc-120016731
14. Bai, G., Armenante, P.M., Plank, R.V., Gentzler, M., Ford, K., Harmon, P. (2007). Hydrodynamic investigation of USP dissolution test apparatus II. *J Pharm Sci*, **96** (9), 2327-2349. https://doi.org/10.1002/jps.20818
15. Bai, G., Armenante, P.M. (2008). Velocity distribution and shear rate variability resulting from changes in the impeller location in the USP dissolution testing apparatus II. *Pharm Res*, **25** (2), 320-336. https://doi.org/10.1007/s11095-007-9477-z
16. Todaro, V., Persoons, T., Grove, G., Healy, A.M., D'Arcy, D.M. (2017). Characterization and Simulation of Hydrodynamics in the Paddle, Basket and Flow-Through Dissolution Testing Apparatuses - A Review. *Dissolution Technol*, **24** (3), 24-36. https://doi.org/10.14227/dt240317p24
17. Hemamanjushree, S., Tippavajhala, V.K. (2020). Simulation of Unit Operations in Formulation Development of Tablets Using Computational Fluid Dynamics. *AAPS PharmSciTech*, **21** (3), 103-116. https://doi.org/10.1208/s12249-020-1635-1
18. McCarthy, L.G., Kosiol, C., Healy, A.M., Bradley, G., Sexton, J.C., Corrigan, O.I. (2003). Simulating the hydrodynamic conditions in the United States Pharmacopeia paddle dissolution apparatus. *AAPS PharmSciTech*, **4** (2), E22. https://doi.org/10.1208/pt040222
19. Kukura, J., Baxter, J.L., Muzzio, F.J. (2004). Shear distribution and variability in the USP Apparatus 2 under turbulent conditions. *Int J Pharm*, **279** (1-2), 9-17. https://doi.org/10.1016/j.ijpharm.2004.03.033
20. Ameur, H., Bouzit, M. (2013). 3D hydrodynamics and shear rates' variability in the United States Pharmacopeia Paddle Dissolution Apparatus. *Int J Pharm*, **452** (1-2), 42-51. https://doi.org/10.1016/j.ijpharm.2013.04.049
21. D'Arcy, D.M., Corrigan, O.I., Healy, A.M. (2005). Hydrodynamic simulation (computational fluid dynamics) of asymmetrically positioned tablets in the paddle dissolution apparatus: impact on dissolution rate and variability. *J Pharm Pharmacol*, **57**, 1-8. https://doi.org/10.1211/jpp.57.10.0002

22. Bai, G., Armenante, P.M. (2009). Hydrodynamic, mass transfer, and dissolution effects induced by tablet location during dissolution testing. *J Pharm Sci*, **98** (4), 1511-1531. https://doi.org/10.1002/jps.21512
23. Baxter, J.L., Kukura, J., Muzzio, F.J. (2006). Shear-induced variability in the United States Pharmacopeia Apparatus 2: modifications to the existing system. *AAPS J*, **7** (4), E857-864. https://doi.org/10.1208/aapsj070483
24. Johansson, K.E., Plum, J., Mosleh, M., Madsen, C.M., Rades, T., Mullertz, A. (2018). Characterization of the Hydrodynamics in a Miniaturized Dissolution Apparatus. *J Pharm Sci*, **107** (4), 1095-1103. https://doi.org/10.1016/j.xphs.2017.11.022
25. Perivilli, S., Walfish, S., Stippler, E., Liddell, M.R. (2022). Impact of Select Geometric and Operational Parameters on Hydrodynamics in Dissolution Apparatus 2 (Paddle Apparatus): A Design of Experiments Analysis Based on Computational Fluid Dynamics Simulations. *Pharm Res*, **39** (5), 919-934. https://doi.org/10.1007/s11095-022-03272-4
26. Mirza, T., Joshi, Y., Liu, Q., Vivilecchia, R. (2005). Evaluation of Dissolution Hydrodynamics in the USP, Peak™ and Flat-Bottom Vessels Using Different Solubility Drugs. *Dissolution Technol*, **1** (1), 11-16. https://doi.org/10.14227/dt120105p11
27. Wang, Y., Armenante, P.M. (2012). A novel off-center paddle impeller (OPI) dissolution testing system for reproducible dissolution testing of solid dosage forms. *J Pharm Sci*, **101** (2), 746-760. https://doi.org/10.1002/jps.22783
28. Zhang, Y., Bredael, G., Armenante, P.M. (2013). Dissolution of prednisone tablets in the presence of an arch-shaped fiber optic probe in a USP dissolution testing apparatus 2. *J Pharm Sci*, **102** (8), 2718-2729. https://doi.org/10.1002/jps.23651
29. Baxter, J.L., Kukura, J., Muzzio, F.J. (2005). Hydrodynamics-induced variability in the USP apparatus II dissolution test. *Int J Pharm*, **292** (1-2), 17-28. https://doi.org/10.1016/j.ijpharm.2004.08.003
30. Bai, G., Wang, Y., Armenante, P.M. (2011). Velocity profiles and shear strain rate variability in the USP Dissolution Testing Apparatus 2 at different impeller agitation speeds. *Int J Pharm*, **403** (1-2), 1-14. https://doi.org/10.1016/j.ijpharm.2010.09.022

31. Higuchi, M., Yoshihashi, Y., Tarada, K., Sugano, K. (2014). Minimum rotation speed to prevent coning phenomena in compendium paddle dissolution apparatus. *Eur J Pharm Sci*, **65**, 74-78. https://doi.org/10.1016/j.ejps.2014.09.010
32. Higuchi, M., Nishida, S., Yoshihashi, Y., Tarada, K., Sugano, K. (2015). Prediction of coning phenomena for irregular particles in paddle dissolution test. *Eur J Pharm Sci*, **76**, 213-216. https://doi.org/10.1016/j.ejps.2015.05.019
33. Stamatopoulos, K., Batchelor, H.K., Alberini, F., Ramsay, J., Simmons, M.J.H. (2015). Understanding the impact of media viscosity on dissolution of a highly water soluble drug within a USP 2 mini vessel dissolution apparatus using an optical planar induced fluorescence (PLIF) method. *Int J Pharm*, **495** (1), 362-373. https://doi.org/10.1016/j.ijpharm.2015.09.002
34. Higuchi, M., Terada, K., Sugano, K. (2015). Coning phenomena under laminar flow. *Eur J Pharm Sci*, **80**, 53-55. https://doi.org/10.1016/j.ejps.2015.08.004
35. Cammarn, S.R., Sakr, A. (2000). Predicting dissolution via hydrodynamics: salicylic acid tablets in flow through cell dissolution. *Int J Pharm*, **201** (2), 199-209. https://doi.org/10.1016/s0378-5173(00)00415-4
36. Salehi, N., Al-Gousous, J., Mudie, D.M., Amidon, G.L., Ziff, R.M., Amidon, G.E. (2020). Hierarchical Mass Transfer Analysis of Drug Particle Dissolution, Highlighting the Hydrodynamics, pH, Particle Size, and Buffer Effects for the Dissolution of Ionizable and Nonionizable Drugs in a Compendial Dissolution Vessel. *Mol Pharm*, **17** (10), 3870-3884. https://doi.org/10.1021/acs.molpharmaceut.0c00614
37. D'Arcy, D.M., Liu, B., Bradley, G., Healy, A.M., Corrigan, O.I. (2010). Hydrodynamic and species transfer simulations in the USP 4 dissolution apparatus: considerations for dissolution in a low velocity pulsing flow. *Pharm Res*, **27** (2), 246-258. https://doi.org/10.1007/s11095-009-0010-4
38. Shiko, G., Gladden, L.F., Sederman, A.J., Connolly, P.C., Butler, J.M. (2011). MRI studies of the hydrodynamics in a USP 4 dissolution testing cell. *J Pharm Sci*, **100** (3), 976-991. https://doi.org/10.1002/jps.22343
39. Yoshida, H., Kuwana, A., Shibata, H., Izutsu, K., Goda, Y. (2015). Particle Image Velocimetry Evaluation of Fluid Flow Profiles in USP 4 Flow-Through Dissolution Cells. *Pharm Res*, **32** (9), 2950-2959. https://doi.org/10.1007/s11095-015-1676-4

40. Yoshida, H., Kuwana, A., Shibata, H., Izutsu, K., Goda, Y. (2016). Effects of Pump Pulsation on Hydrodynamic Properties and Dissolution Profiles in Flow-Through Dissolution Systems (USP 4). *Pharm Res*, **33** (6), 1327-1336. https://doi.org/10.1007/s11095-016-1874-8
41. D'Arcy, D.M., Liu, B., Corrigan, O.I. (2011). Investigating the effect of solubility and density gradients on local hydrodynamics and drug dissolution in the USP 4 dissolution apparatus. *Int J Pharm*, **419** (1-2), 175-185. https://doi.org/10.1016/j.ijpharm.2011.07.048
42. D'Arcy, D.M., Healy, A.M., Corrigan, O.I. (2009). Towards determining appropriate hydrodynamic conditions for in vitro in vivo correlations using computational fluid dynamics. *Eur J Pharm Sci*, **37** (3-4), 291-299. https://doi.org/10.1016/j.ejps.2009.02.016
43. Kakhi, M. (2009). Mathematical modeling of the fluid dynamics in the flow-through cell. *Int J Pharm*, **376** (1-2), 22-40. https://doi.org/10.1016/j.ijpharm.2009.04.012
44. Kakhi, M. (2009). Classification of the flow regimes in the flow-through cell. *Eur J Pharm Sci*, **37** (5), 531-544. https://doi.org/10.1016/j.ejps.2009.04.003
45. Shiko, G., Sederman, A.J., Gladden, L.F. (2012). MRI technique for the snapshot imaging of quantitative velocity maps using RARE. *J Magn Reson*, **216**, 183-191. https://doi.org/10.1016/j.jmr.2012.01.021
46. Anand, O., Yu, L.X., Conner, D.P., Davit, B.M. (2011). Dissolution testing for generic drugs: an FDA perspective. *AAPS J*, **13** (3), 328-335. https://doi.org/10.1208/s12248-011-9272-y
47. U.S. Department of Health and Human Services Food and Drug Administration Center for Drug Evaluation and Research (CDER). (2018). Dissolution Testing and Acceptance Criteria for Immediate-Release Solid Oral Dosage Form Drug Products Containing High Solubility Drug Substances.
48. Brown, C.K., Friedel, H.D., Barker, A.R., Buhse, L.F., Keitel, S., Cecil, T.L., Kraemer, J., Morris, J.M., Reppas, C., Stickelmeyer, M.P., Yomota, C., Shah, V.P. (2011). FIP/AAPS joint workshop report: dissolution/in vitro release testing of novel/special dosage forms. *AAPS PharmSciTech*, **12** (2), 782-794. https://doi.org/10.1208/s12249-011-9634-x
49. Tietz, K., Gutknecht, S.I., Klein, S. (2018). Bioequivalence of locally acting lozenges: Evaluation of critical in vivo parameters and first steps towards a bio-

predictive in vitro test method. *Eur J Pharm Biopharm*, **123**, 71-83. https://doi.org/10.1016/j.ejpb.2017.11.011

50. Tietz, K., Gutknecht, S.I., Klein, S. (2018). Predicting local drug availability of locally acting lozenges: From method design to a linear level A IVIVC. *Eur J Pharm Biopharm*, **133**, 269-276. https://doi.org/10.1016/j.ejpb.2018.10.015
51. Probst, M., Schmidt, M., Tietz, K., Klein, S., Weitschies, W., Seidlitz, A. (2017). In vitro dissolution testing of parenteral aqueous solutions and oily suspensions of paracetamol and prednisolone. *Int J Pharm*, **532** (1), 519-527. https://doi.org/10.1016/j.ijpharm.2017.09.052
52. Otsuka, K., Shono, Y., Dressman, J. (2013). Coupling biorelevant dissolution methods with physiologically based pharmacokinetic modelling to forecast in-vivo performance of solid oral dosage forms. *J Pharm Pharmacol*, **65** (7), 937-952. https://doi.org/10.1111/jphp.12059
53. Pharmacopoeia, U.S. (2020). ⟨1090⟩ Assessment of solid oral drug product performance and interchangeability, bioavailability, bioequivalence, and dissolution.
54. U.S. Department of Health and Human Services Food and Drug Administration Center for Drug Evaluation and Research (CDER). (2017). Waiver of In Vivo Bioavailability and Bioequivalence Studies for Immediate-Release Solid Oral Dosage Forms Based on a Biopharmaceutics Classification System. Guidance for Industry.
55. European Medicines Agency (EMA). (2010). Guideline on the investigation of bioequivalence.
56. Urso, R., Blardi, P., Giorgi, G. (2002). A short introduction to pharmacokinetics. *Eur Rev Med Pharmacol Sci*, **6**, 33-44.
57. Amidon, K.S., Langguth, P., Lennernas, H., Yu, L., Amidon, G.L. (2011). Bioequivalence of oral products and the biopharmaceutics classification system: science, regulation, and public policy. *Clin Pharmacol Ther*, **90** (3), 467-470. https://doi.org/10.1038/clpt.2011.109
58. Abend, A., Heimbach, T., Cohen, M., Kesisoglou, F., Pepin, X., Suarez-Sharp, S. (2018). Dissolution and Translational Modeling Strategies Enabling Patient-Centric Drug Product Development: the M-CERSI Workshop Summary Report. *AAPS J*, **20** (3), 60. https://doi.org/10.1208/s12248-018-0213-x

59. Tuszyński, P.K., Szlęk, J., Polak, S., Jachowicz, R., Mendyk, A. (2018). In Vitro-In Vivo Correlation (IVIVC): From Current Achievements Towards the Future. *Dissolution Technol*, **25** (3), 20-27. https://doi.org/10.14227/dt250318p20
60. U.S. Department of Health and Human Services Food and Drug Administration Center for Drug Evaluation and Research (CDER). (1997). Extended Release Oral Dosage Forms: Development, Evaluation, and Application of In Vitro/In Vivo Correlations.
61. Charalabidis, A., Sfouni, M., Bergstrom, C., Macheras, P. (2019). The Biopharmaceutics Classification System (BCS) and the Biopharmaceutics Drug Disposition Classification System (BDDCS): Beyond guidelines. *Int J Pharm*, **566**, 264-281. https://doi.org/10.1016/j.ijpharm.2019.05.041
62. Amidon, G.L., Lennernäs, H., Shah, V.P., Crison, J.R. (1995). A theoretical basis for a biopharmaceutic drug classification: the correlation of in vitro drug product dissolution and in vivo bioavailability. *Pharm Res*, **12** (3), 413-420. https://doi.org/10.1023/a:1016212804288
63. Yu, L.X., Amidon, G.L., Polli, J.E., Zhao, H., Mehta, M.U., Conner, D.P., Shah, V.P., Lesko, L.J., Chen, M.L., Lee, V.H., Hussain, A.S. (2002). Biopharmaceutics classification system: the scientific basis for biowaiver extensions. *Pharm Res*, **19** (7), 921-925. https://doi.org/10.1023/a:1016473601633
64. Butler, J.M., Dressman, J.B. (2010). The developability classification system: application of biopharmaceutics concepts to formulation development. *J Pharm Sci*, **99** (12), 4940-4954. https://doi.org/10.1002/jps.22217
65. Rosenberger, J., Butler, J., Dressman, J. (2018). A Refined Developability Classification System. *J Pharm Sci*, **107** (8), 2020-2032. https://doi.org/10.1016/j.xphs.2018.03.030
66. Tsume, Y., Mudie, D.M., Langguth, P., Amidon, G.E., Amidon, G.L. (2014). The Biopharmaceutics Classification System: subclasses for in vivo predictive dissolution (IPD) methodology and IVIVC. *Eur J Pharm Sci*, **57**, 152-163. https://doi.org/10.1016/j.ejps.2014.01.009
67. Benet, L.Z., Amidon, G.L., Barends, D.M., Lennernas, H., Polli, J.E., Shah, V.P., Stavchansky, S.A., Yu, L.X. (2008). The use of BDDCS in classifying the permeability of marketed drugs. *Pharm Res*, **25** (3), 483-438. https://doi.org/10.1007/s11095-007-9523-x

68. Wu, C.Y., Benet, L.Z. (2005). Predicting drug disposition via application of BCS: transport/absorption/ elimination interplay and development of a biopharmaceutics drug disposition classification system. *Pharm Res*, **22** (1), 11-23. https://doi.org/10.1007/s11095-004-9004-4

69. Ting, J.M., Porter, W.W., 3rd, Mecca, J.M., Bates, F.S., Reineke, T.M. (2018). Advances in Polymer Design for Enhancing Oral Drug Solubility and Delivery. *Bioconjug Chem*, **29** (4), 939-952. https://doi.org/10.1021/acs.bioconjchem.7b00646

70. Loisios-Konstantinidis, I., Cristofoletti, R., Fotaki, N., Turner, D.B., Dressman, J. (2020). Establishing virtual bioequivalence and clinically relevant specifications using in vitro biorelevant dissolution testing and physiologically-based population pharmacokinetic modeling. case example: Naproxen. *Eur J Pharm Sci*, **143**, 105170. https://doi.org/10.1016/j.ejps.2019.105170

71. Soliman, M.E., Adewumi, A.T., Akawa, O.B., Subair, T.I., Okunlola, F.O., Akinsuku, O.E., Khan, S. (2022). Simulation Models for Prediction of Bioavailability of Medicinal Drugs-the Interface Between Experiment and Computation. *AAPS PharmSciTech*, **23** (3), 86. https://doi.org/10.1208/s12249-022-02229-5

72. Potthast, H., Dressman, J.B., Junginger, H.E., Midha, K.K., Oeser, H., Shah, V.P., Vogelpoel, H., Barends, D.M. (2005). Biowaiver monographs for immediate release solid oral dosage forms: ibuprofen. *J Pharm Sci*, **94** (10), 2121-2131. https://doi.org/10.1002/jps.20444

73. Hörter, D., Dressman, J.B. (2001). Influence of physicochemical properties on dissolution of drugs in the gastrointestinal tract. *Adv Drug Deliv Rev*, **46** (1-3), 75-87. https://doi.org/10.1016/s0169-409x(00)00130-7

74. Fuchs, A., Dressman, J.B. (2014). Composition and physicochemical properties of fasted-state human duodenal and jejunal fluid: a critical evaluation of the available data. *J Pharm Sci*, **103** (11), 3398-3411. https://doi.org/10.1002/jps.24183

75. Dressman, J. (2014). Evolution of Dissolution Media Over the Last Twenty Years. *Dissolution Technol*, **21** (3), 6-10. https://doi.org/10.14227/dt210314p6

76. Marques, M. (2004). Dissolution Media Simulating Fasted and Fed States. *Dissolution Technol*, **11** (2). https://doi.org/10.14227/dt110204p16

77. Galia, E., Nicolaides, E., Horter, D., Lobenberg, R., Reppas, C., Dressman, J.B. (1998). Evaluation of various dissolution media for predicting In vivo performance of class I and II drugs. *Pharm Res*, **15** (5), 698-705. https://doi.org/10.1023/A:1011910801212

78. Dressman, J.B., Reppas, C. (2000). In vitro-in vivo correlations for lipophilic, poorly water-soluble drugs. *Eur J Pharm Sci*, **11**, S73-S80. https://doi.org/10.1016/S0928-0987(00)00181-0

79. Vertzoni, M., Fotaki, N., Kostewicz, E., Stippler, E., Leuner, C., Nicolaides, E., Dressman, J., Reppas, C. (2004). Dissolution media simulating the intralumenal composition of the small intestine: physiological issues and practical aspects. *J Pharm Pharmacol*, **56** (4), 453-462. https://doi.org/10.1211/0022357022935

80. Vertzoni, M., Dressman, J., Butler, J., Hempenstall, J., Reppas, C. (2005). Simulation of fasting gastric conditions and its importance for the in vivo dissolution of lipophilic compounds. *Eur J Pharm Biopharm*, **60** (3), 413-417. https://doi.org/10.1016/j.ejpb.2005.03.002

81. Jantratid, E., Dressman, J. (2009). Biorelevant Dissolution Media Simulating the Proximal Human Gastrointestinal Tract: An Update. *Dissolution Technol*, **16** (3), 21-25. https://doi.org/10.14227/dt160309p21

82. Markopoulos, C., Andreas, C.J., Vertzoni, M., Dressman, J., Reppas, C. (2015). In-vitro simulation of luminal conditions for evaluation of performance of oral drug products: Choosing the appropriate test media. *Eur J Pharm Biopharm*, **93**, 173-182. https://doi.org/10.1016/j.ejpb.2015.03.009

83. Vertzoni, M., Diakidou, A., Chatzilias, M., Soderlind, E., Abrahamsson, B., Dressman, J.B., Reppas, C. (2010). Biorelevant media to simulate fluids in the ascending colon of humans and their usefulness in predicting intracolonic drug solubility. *Pharm Res*, **27** (10), 2187-2196. https://doi.org/10.1007/s11095-010-0223-6

84. Nicolaides, E., Galia, E., Efthymiopoulos, C., Dressman, J.B., Reppas, C. (1999). Forecasting the in vivo performance of four low solubility drugs from their in vitro dissolution data. *Pharm Res*, **16** (12), 1876-1882. https://doi.org/10.1023/a:1018959511323

85. Nicolaides, E., Symillides, M., Dressman, J.B., Reppas, C. (2001). Biorelevant Dissolution Testing to Predict the Plasma Profile of Lipophilic Drugs After Oral

Administration. *Pharm Res*, **18** (3), 380-388. https://doi.org/10.1023/a:1011071401306

86. Löbenberg, R., Krämer, J., Shah, V.P., Amidon, G.L., Dressman, J.B. (2000). Dissolution testing as a prognostic tool for oral drug absorption: dissolution behavior of glibenclamide. *Pharm Res*, **17** (4), 439-444. https://doi.org/10.1023/a:1007529020774
87. Jantratid, E., Janssen, N., Reppas, C., Dressman, J.B. (2008). Dissolution media simulating conditions in the proximal human gastrointestinal tract: an update. *Pharm Res*, **25** (7), 1663-1676. https://doi.org/10.1007/s11095-008-9569-4
88. Diakidou, A., Vertzoni, M., Dressman, J., Reppas, C. (2009). Estimation of intragastric drug solubility in the fed state: comparison of various media with data in aspirates. *Biopharm Drug Dispos*, **30** (6), 318-325. https://doi.org/10.1002/bdd.670
89. Rivera, K.R., Pessi, J., Andersson, V., Gustafsson, H., Gluud, L.L., Buckley, S.T. (2023). Characterizing interspecies differences in gastric fluid properties to improve understanding of in vivo oral drug formulation performance. *Eur J Pharm Sci*, **183**, 106386. https://doi.org/10.1016/j.ejps.2023.106386
90. Mann, J., Dressman, J., Rosenblatt, K., Ashworth, L., Muenster, U., Frank, K., Hutchins, P., Williams, J., Klumpp, L., Wielockx, K., Berben, P., Augustijns, P., Holm, R., Hofmann, M., Patel, S., Beato, S., Ojala, K., Tomaszewska, I., Bruel, J.L., Butler, J. (2017). Validation of Dissolution Testing with Biorelevant Media: An OrBiTo Study. *Mol Pharm*, **14** (12), 4192-4201. https://doi.org/10.1021/acs.molpharmaceut.7b00198
91. Butler, J., Hens, B., Vertzoni, M., Brouwers, J., Berben, P., Dressman, J., Andreas, C.J., Schaefer, K.J., Mann, J., McAllister, M., Jamei, M., Kostewicz, E., Kesisoglou, F., Langguth, P., Minekus, M., Mullertz, A., Schilderink, R., Koziolek, M., Jedamzik, P., Weitschies, W., Reppas, C., Augustijns, P. (2019). In vitro models for the prediction of in vivo performance of oral dosage forms: Recent progress from partnership through the IMI OrBiTo collaboration. *Eur J Pharm Biopharm*, **136**, 70-83. https://doi.org/10.1016/j.ejpb.2018.12.010
92. Reppas, C., Vrettos, N.N., Dressman, J., Andreas, C.J., Miyaji, Y., Brown, J., Etherson, K., Hanley, S., Karkossa, F., Karlsson, E., Klein, S., Maier, G.M., McAllister, M., Mistry, N., Rosenblatt, K., Schafer, K.J., Smith, K.L.,

Tomaszewska, I., Williams, J., Winge, F., Vertzoni, M. (2020). Dissolution testing of modified release products with biorelevant media: An OrBiTo ring study using the USP apparatus III and IV. *Eur J Pharm Biopharm*, **156**, 40-49. https://doi.org/10.1016/j.ejpb.2020.08.025

93. Cardot, J.M., Beyssac, E., Alric, M. (2007). In Vitro–In Vivo Correlation: Importance of Dissolution in IVIVC. *Dissolution Technol*, **14** (1), 15-19. https://doi.org/10.14227/dt140107p15

94. Nguyen, M.A., Flanagan, T., Brewster, M., Kesisoglou, F., Beato, S., Biewenga, J., Crison, J., Holm, R., Li, R., Mannaert, E., McAllister, M., Mueller-Zsigmondy, M., Muenster, U., Ojala, K., Page, S., Parr, A., Rossenu, S., Timmins, P., Van Peer, A., Vermeulen, A., Langguth, P. (2017). A survey on IVIVC/IVIVR development in the pharmaceutical industry - Past experience and current perspectives. *Eur J Pharm Sci*, **102**, 1-13. https://doi.org/10.1016/j.ejps.2017.02.029

95. Fotaki, N., Gray, V., Kesisoglou, F., Mayock, S., Mirza, T., Salt, A., Selen, A. (2013). Survey Results for In Vitro-In Vivo Correlations (IVIVC): Critical Variables for Success. *Dissolution Technol*, **20** (2), 48-50. https://doi.org/10.14227/dt200213p48

96. Suarez-Sharp, S., Li, M., Duan, J., Shah, H., Seo, P. (2016). Regulatory Experience with In Vivo In Vitro Correlations (IVIVC) in New Drug Applications. *AAPS J*, **18** (6), 1379-1390. https://doi.org/10.1208/s12248-016-9966-2

97. Camara-Martinez, I., Blechar, J.A., Ruiz-Picazo, A., Garcia-Arieta, A., Calandria, C., Merino-Sanjuan, V., Langguth, P., Gonzalez-Alvarez, M., Bermejo, M., Al-Gousous, J., Gonzalez-Alvarez, I. (2022). Level A IVIVC for immediate release tablets confirms in vivo predictive dissolution testing for ibuprofen. *Int J Pharm*, **614**, 121415. https://doi.org/10.1016/j.ijpharm.2021.121415

98. Chiang, P.C., Liu, J., Nagapudi, K., Wu, R., Dolton, M.J., Salehi, N., Amidon, G. (2022). Evaluating the IVIVC by Combining Tiny-tim Outputs and Compartmental PK Model to Predict Oral Exposure for Different Formulations of Ibuprofen. *J Pharm Sci*, **111** (7), 2018-2029. https://doi.org/10.1016/j.xphs.2022.01.024

99. Woodcock, J. (2004). The concept of pharmaceutical quality. *Am Pharm Rev*, **7**, 10-15.

100. Zhang, L., Mao, S. (2017). Application of quality by design in the current drug development. *Asian J Pharm Sci*, **12** (1), 1-8. https://doi.org/10.1016/j.ajps.2016.07.006
101. U.S. Department of Health and Human Services Food and Drug Administration Center for Drug Evaluation and Research (CDER). (2020). The Use of Physiologically Based Pharmacokinetic Analyses-Biopharmaceutics Applications for Oral Drug Product Development, Manufacturing Changes, and Controls. Guidance for Industry.
102. Matji, A., Donato, N., Gagol, A., Morales, E., Carvajal, L., Serrano, D.R., Worku, Z.A., Healy, A.M., Torrado, J.J. (2019). Predicting the critical quality attributes of ibuprofen tablets via modelling of process parameters for roller compaction and tabletting. *Int J Pharm*, **565**, 209-218. https://doi.org/10.1016/j.ijpharm.2019.05.011
103. Destro, F., Barolo, M. (2022). A review on the modernization of pharmaceutical development and manufacturing - Trends, perspectives, and the role of mathematical modeling. *Int J Pharm*, **620**, 121715. https://doi.org/10.1016/j.ijpharm.2022.121715
104. Selen, A., Dickinson, P.A., Mullertz, A., Crison, J.R., Mistry, H.B., Cruanes, M.T., Martinez, M.N., Lennernas, H., Wigal, T.L., Swinney, D.C., Polli, J.E., Serajuddin, A.T.M., Cook, J.A., Dressman, J.B. (2014). The biopharmaceutics risk assessment roadmap for optimizing clinical drug product performance. *J Pharm Sci*, **103** (11), 3377-3397. https://doi.org/10.1002/jps.24162
105. Dickinson, P.A., Kesisoglou, F., Flanagan, T., Martinez, M.N., Mistry, H.B., Crison, J.R., Polli, J.E., Cruanes, M.T., Serajuddin, A.T.M., Mullertz, A., Cook, J.A., Selen, A. (2016). Optimizing Clinical Drug Product Performance: Applying Biopharmaceutics Risk Assessment Roadmap (BioRAM) and the BioRAM Scoring Grid. *J Pharm Sci*, **105** (11), 3243-3255. https://doi.org/10.1016/j.xphs.2016.07.024
106. Charoo, N.A., Cristofoletti, R., Kim, S.K. (2017). Integrating biopharmaceutics risk assessment and in vivo absorption model in formulation development of BCS class I drug using the QbD approach. *Drug Dev Ind Pharm*, **43** (4), 668-677. https://doi.org/10.1080/03639045.2016.1278013
107. Amaral Silva, D., Al-Gousous, J., Davies, N.M., Bou Chacra, N., Webster, G.K., Lipka, E., Amidon, G., Lobenberg, R. (2019). Simulated, biorelevant, clinically

relevant or physiologically relevant dissolution media: The hidden role of bicarbonate buffer. *Eur J Pharm Biopharm*, **142**, 8-19. https://doi.org/10.1016/j.ejpb.2019.06.006

108. Al-Gousous, J., Salehi, N., Amidon, G.E., Ziff, R.M., Langguth, P., Amidon, G.L. (2019). Mass Transport Analysis of Bicarbonate Buffer: Effect of the CO(2)-H(2)CO(3) Hydration-Dehydration Kinetics in the Fluid Boundary Layer and the Apparent Effective p K(a) Controlling Dissolution of Acids and Bases. *Mol Pharm*, **16** (6), 2626-2635. https://doi.org/10.1021/acs.molpharmaceut.9b00187

109. Hofmann, M., Garcia, M.A., Al-Gousous, J., Ruiz-Picazo, A., Thieringer, F., Nguyen, M.A., Mansson, W., Galle, P.R., Langguth, P. (2020). In vitro prediction of in vivo absorption of ibuprofen from suspensions through rational choice of dissolution conditions. *Eur J Pharm Biopharm*, **149**, 229-237. https://doi.org/10.1016/j.ejpb.2020.02.009

110. Al-Gousous, J., Ruan, H., Blechar, J.A., Sun, K.X., Salehi, N., Langguth, P., Job, N.M., Lipka, E., Loebenberg, R., Bermejo, M., Amidon, G.E., Amidon, G.L. (2019). Mechanistic analysis and experimental verification of bicarbonate-controlled enteric coat dissolution: Potential in vivo implications. *Eur J Pharm Biopharm*, **139**, 47-58. https://doi.org/10.1016/j.ejpb.2019.03.012

111. Cristofoletti, R., Dressman, J.B. (2017). Dissolution Methods to Increasing Discriminatory Power of In Vitro Dissolution Testing for Ibuprofen Free Acid and Its Salts. *J Pharm Sci*, **106** (1), 92-99. https://doi.org/10.1016/j.xphs.2016.06.001

112. Cristofoletti, R., Dressman, J.B. (2016). Matching phosphate and maleate buffer systems for dissolution of weak acids: Equivalence in terms of buffer capacity of bulk solution or surface pH? *Eur J Pharm Biopharm*, **103**, 104-108. https://doi.org/10.1016/j.ejpb.2016.03.024

113. Krieg, B.J., Taghavi, S.M., Amidon, G.L., Amidon, G.E. (2015). In Vivo Predictive Dissolution: Comparing the Effect of Bicarbonate and Phosphate Buffer on the Dissolution of Weak Acids and Weak Bases. *J Pharm Sci*, **104** (9), 2894-2904. https://doi.org/10.1002/jps.24460

114. Tsume, Y., Patel, S., Fotaki, N., Bergström, C., Amidon, G.L., Brasseur, J.G., Mudie, D.M., Sun, D., Bermejo, M., Gao, P., Zhu, W., Sperry, D.C., Vertzoni, M., Parrott, N., Lionberger, R., Kambayashi, A., Hermans, A., Lu, X., Amidon,

G.E. (2018). In Vivo Predictive Dissolution and Simulation Workshop Report: Facilitating the Development of Oral Drug Formulation and the Prediction of Oral Bioperformance. *AAPS J*, **20** (6), 100. https://doi.org/10.1208/s12248-018-0260-3

115. Sheng, J.J., McNamara, D.P., Amidon, G.L. (2009). Toward an In Vivo dissolution methodology: A comparison of phosphate and bicarbonate buffers. *Mol Pharm*, **6** (1), 29-39. https://doi.org/10.1021/mp800148u
116. Matsui, K., Nakamichi, K., Nakatani, M., Yoshida, H., Yamashita, S., Yokota, S. (2023). Lowly-buffered biorelevant dissolution testing is not necessarily biopredictive of human bioequivalence study outcome: Relationship between dissolution and pharmacokinetics. *Int J Pharm*, **631**, 122531. https://doi.org/10.1016/j.ijpharm.2022.122531
117. United States Pharmacopoeia. (2020). Buffer solutions.
118. Kalantzi, L., Goumas, K., Kalioras, V., Abrahamsson, B., Dressman, J.B., Reppas, C. (2006). Characterization of the human upper gastrointestinal contents under conditions simulating bioavailability/bioequivalence studies. *Pharm Res*, **23** (1), 165-176. https://doi.org/10.1007/s11095-005-8476-1
119. Dahlgren, D., Venczel, M., Ridoux, J.P., Skjold, C., Mullertz, A., Holm, R., Augustijns, P., Hellstrom, P.M., Lennernas, H. (2021). Fasted and fed state human duodenal fluids: Characterization, drug solubility, and comparison to simulated fluids and with human bioavailability. *Eur J Pharm Biopharm*, **163**, 240-251. https://doi.org/10.1016/j.ejpb.2021.04.005
120. Dressman, J.B., Berardi, R.R., Dermentzoglou, L.C., Russell, T.L., Schmaltz, S.P., Barnett, J.L., Jarvenpaa, K.M. (1990). Upper gastrointestinal (GI) pH in young, healthy men and women. *Pharm Res*, **7** (7), 756-761. https://doi.org/10.1023/a:1015827908309
121. Diakidou, A., Vertzoni, M., Goumas, K., Soderlind, E., Abrahamsson, B., Dressman, J., Reppas, C. (2009). Characterization of the contents of ascending colon to which drugs are exposed after oral administration to healthy adults. *Pharm Res*, **26** (9), 2141-2151. https://doi.org/10.1007/s11095-009-9927-x
122. Finholt, P., Solvang, S. (1968). Dissolution kinetics of drugs in human gastric juice--the role of surface tension. *J Pharm Sci*, **57** (8), 1322-1326. https://doi.org/10.1002/jps.2600570809

123. Funai, Y., Takemura, M., Inoue, K., Shirasaka, Y. (2022). Effect of ingested fluid volume and solution osmolality on intestinal drug absorption: Impact on drug interaction with beverages. *Eur J Pharm Sci*, **172**, 106136. https://doi.org/10.1016/j.ejps.2022.106136
124. Tadros, T.F. (2003). Surfactants, Industrial Applications. *Encyclopedia of Physical Science and Technology*, 423-438.
125. Jamil, R., Polli, J.E. (2022). Prediction of In Vitro Drug Dissolution into Fed-state Biorelevant Media: Contributions of Solubility Enhancement and Relatively Low Colloid Diffusivity. *Eur J Pharm Sci*, **173**, 106179. https://doi.org/10.1016/j.ejps.2022.106179
126. Bakatselou, V., Oppenheim, R.C., Dressman, J.B. (1991). Solubilization and wetting effects of bile salts on the dissolution of steroids. *Pharm Res*, **8** (12), 1461-1469. https://doi.org/10.1023/a:1015877929381
127. Nur Oktay, A., Polli, J.E. (2022). Comparison of a single pharmaceutical surfactant versus intestinal biorelevant media for etravirine dissolution: Role and impact of micelle diffusivity. *Int J Pharm*, **624**, 122015. https://doi.org/10.1016/j.ijpharm.2022.122015
128. Sheng, J.J., Kasim, N.A., Chandrasekharan, R., Amidon, G.L. (2006). Solubilization and dissolution of insoluble weak acid, ketoprofen: effects of pH combined with surfactant. *Eur J Pharm Sci*, **29** (3-4), 306-314. https://doi.org/10.1016/j.ejps.2006.06.006
129. Tsume, Y., Igawa, N., Drelich, A.J., Amidon, G.E., Amidon, G.L. (2018). The Combination of GIS and Biphasic to Better Predict In Vivo Dissolution of BCS Class IIb Drugs, Ketoconazole and Raloxifene. *J Pharm Sci*, **107** (1), 307-316. https://doi.org/10.1016/j.xphs.2017.09.002
130. U.S. Department of Health and Human Services Food and Drug Administration Center for Drug Evaluation and Research (CDER). (2022). Assessing the Effects of Food on Drugs in INDs and NDAs. Clinical Pharmacology Considerations. Guidance for Industry.
131. O'Shea, J.P., Holm, R., O'Driscoll, C.M., Griffin, B.T. (2019). Food for thought: formulating away the food effect - a PEARRL review. *J Pharm Pharmacol*, **71** (4), 510-535. https://doi.org/10.1111/jphp.12957
132. Andreas, C.J., Chen, Y.C., Markopoulos, C., Reppas, C., Dressman, J. (2015). In vitro biorelevant models for evaluating modified release mesalamine

products to forecast the effect of formulation and meal intake on drug release. *Eur J Pharm Biopharm*, **97** (Pt A), 39-50. https://doi.org/10.1016/j.ejpb.2015.09.002

133. Andreas, C.J., Tomaszewska, I., Muenster, U., van der Mey, D., Mueck, W., Dressman, J.B. (2016). Can dosage form-dependent food effects be predicted using biorelevant dissolution tests? Case example extended release nifedipine. *Eur J Pharm Biopharm*, **105**, 193-202. https://doi.org/10.1016/j.ejpb.2016.06.010
134. Vinarov, Z., Butler, J., Kesisoglou, F., Koziolek, M., Augustijns, P. (2023). Assessment of food effects during clinical development. *Int J Pharm*, **635**, 122758. https://doi.org/10.1016/j.ijpharm.2023.122758
135. Klueglich, M., Ring, A., Scheuerer, S., Trommeshauser, D., Schuijt, C., Liepold, B., Berndl, G. (2005). Ibuprofen extrudate, a novel, rapidly dissolving ibuprofen formulation: relative bioavailability compared to ibuprofen lysinate and regular ibuprofen, and food effect on all formulations. *J Clin Pharmacol*, **45** (9), 1055-1061. https://doi.org/10.1177/0091270005279579
136. Koenigsknecht, M.J., Baker, J.R., Wen, B., Frances, A., Zhang, H., Yu, A., Zhao, T., Tsume, Y., Pai, M.P., Bleske, B.E., Zhang, X., Lionberger, R., Lee, A., Amidon, G.L., Hasler, W.L., Sun, D. (2017). In Vivo Dissolution and Systemic Absorption of Immediate Release Ibuprofen in Human Gastrointestinal Tract under Fed and Fasted Conditions. *Mol Pharm*, **14** (12), 4295-4304. https://doi.org/10.1021/acs.molpharmaceut.7b00425
137. Wang, K., Amidon, G.L., Smith, D.E. (2023). Physiological Dynamics in the Upper Gastrointestinal Tract and the Development of Gastrointestinal Absorption Models for the Immediate-Release Oral Dosage Forms in Healthy Adult Human. *Pharm Res*, **40** (11), 2607-2626. https://doi.org/10.1007/s11095-023-03597-8
138. Berthelsen, R., Sjogren, E., Jacobsen, J., Kristensen, J., Holm, R., Abrahamsson, B., Mullertz, A. (2014). Combining in vitro and in silico methods for better prediction of surfactant effects on the absorption of poorly water soluble drugs-a fenofibrate case example. *Int J Pharm*, **473** (1-2), 356-365. https://doi.org/10.1016/j.ijpharm.2014.06.060
139. Sunesen, V.H., Vedelsdal, R., Kristensen, H.G., Christrup, L., Mullertz, A. (2005). Effect of liquid volume and food intake on the absolute bioavailability of

danazol, a poorly soluble drug. *Eur J Pharm Sci*, **24** (4), 297-303. https://doi.org/10.1016/j.ejps.2004.11.005

140. Mudie, D.M., Murray, K., Hoad, C.L., Pritchard, S.E., Garnett, M.C., Amidon, G.L., Gowland, P.A., Spiller, R.C., Amidon, G.E., Marciani, L. (2014). Quantification of gastrointestinal liquid volumes and distribution following a 240 mL dose of water in the fasted state. *Mol Pharm*, **11** (9), 3039-3047. https://doi.org/10.1021/mp500210c
141. Wollmer, E., Klein, S. (2022). Patient-specific in vitro drug release testing coupled with in silico PBPK modeling to forecast the in vivo performance of oral extended-release levodopa formulations in Parkinson's disease patients. *Eur J Pharm Biopharm*, **180**, 101-118. https://doi.org/10.1016/j.ejpb.2022.09.015
142. Garbacz, G., Golke, B., Wedemeyer, R.S., Axell, M., Soderlind, E., Abrahamsson, B., Weitschies, W. (2009). Comparison of dissolution profiles obtained from nifedipine extended release once a day products using different dissolution test apparatuses. *Eur J Pharm Sci*, **38** (2), 147-155. https://doi.org/10.1016/j.ejps.2009.06.010
143. Garbacz, G., Klein, S. (2012). Dissolution testing of oral modified-release dosage forms. *J Pharm Pharmacol*, **64** (7), 944-968. https://doi.org/10.1111/j.2042-7158.2012.01477.x
144. Cassilly, D., Kantor, S., Knight, L.C., Maurer, A.H., Fisher, R.S., Semler, J., Parkman, H.P. (2008). Gastric emptying of a non-digestible solid: assessment with simultaneous SmartPill pH and pressure capsule, antroduodenal manometry, gastric emptying scintigraphy. *Neurogastroenterol Motil*, **20** (4), 311-319. https://doi.org/10.1111/j.1365-2982.2007.01061.x
145. Bermejo, M., Paixao, P., Hens, B., Tsume, Y., Koenigsknecht, M.J., Baker, J.R., Hasler, W.L., Lionberger, R., Fan, J., Dickens, J., Shedden, K., Wen, B., Wysocki, J., Lobenberg, R., Lee, A., Frances, A., Amidon, G.E., Yu, A., Salehi, N., Talattof, A., Benninghoff, G., Sun, D., Kuminek, G., Cavanagh, K.L., Rodriguez-Hornedo, N., Amidon, G.L. (2018). Linking the Gastrointestinal Behavior of Ibuprofen with the Systemic Exposure between and within Humans-Part 1: Fasted State Conditions. *Mol Pharm*, **15** (12), 5454-5467. https://doi.org/10.1021/acs.molpharmaceut.8b00515
146. Paixao, P., Bermejo, M., Hens, B., Tsume, Y., Dickens, J., Shedden, K., Salehi, N., Koenigsknecht, M.J., Baker, J.R., Hasler, W.L., Lionberger, R., Fan, J.,

Wysocki, J., Wen, B., Lee, A., Frances, A., Amidon, G.E., Yu, A., Benninghoff, G., Lobenberg, R., Talattof, A., Sun, D., Amidon, G.L. (2018). Linking the Gastrointestinal Behavior of Ibuprofen with the Systemic Exposure between and within Humans-Part 2: Fed State. *Mol Pharm*, **15** (12), 5468-5478. https://doi.org/10.1021/acs.molpharmaceut.8b00736

147. Kwiatek, M.A., Steingoetter, A., Pal, A., Menne, D., Brasseur, J.G., Hebbard, G.S., Boesiger, P., Thumshirn, M., Fried, M., Schwizer, W. (2006). Quantification of distal antral contractile motility in healthy human stomach with magnetic resonance imaging. *J Magn Reson Imaging*, **24** (5), 1101-1109. https://doi.org/10.1002/jmri.20738
148. Tripathi, D., Anwar Beg, O. (2014). Peristaltic propulsion of generalized Burgers' fluids through a non-uniform porous medium: a study of chyme dynamics through the diseased intestine. *Math Biosci*, **248**, 67-77. https://doi.org/10.1016/j.mbs.2013.11.006
149. Kerlin, P., Zinsmeister, A., Phillips, S. (1982). Relationship of motility to flow of contents in the human small intestine. *Gastroenterol*, **82** (4), 701-706. https://doi.org/10.1016/0016-5085(82)90314-6
150. Koziolek, M., Kostewicz, E., Vertzoni, M. (2018). Physiological Considerations and In Vitro Strategies for Evaluating the Influence of Food on Drug Release from Extended-Release Formulations. *AAPS PharmSciTech*, **19** (7), 2885-2897. https://doi.org/10.1208/s12249-018-1159-0
151. Kindgen, S., Wachtel, H., Abrahamsson, B., Langguth, P. (2015). Computational Fluid Dynamics Simulation of Hydrodynamics and Stresses in the PhEur/USP Disintegration Tester Under Fed and Fasted Fluid Characteristics. *J Pharm Sci*, **104** (9), 2956-2968. https://doi.org/10.1002/jps.24511
152. Dressman, J.B., Amidon, G.L., Reppas, C., Shah, V.P. (1998). Dissolution testing as a prognostic tool for oral drug absorption: Immediate release dosage form. *Pharm Res*, **15** (1), 11-22. https://doi.org/10.1023/a:1011984216775
153. Brener, W., Hendrix, T.R., McHugh, P.R. (1983). Regulation of the Gastric Emptying of Glucose. *Gastroenterol*, **85** (1), 76-82. https://doi.org/10.1016/s0016-5085(83)80232-7
154. Hens, B., Brouwers, J., Anneveld, B., Corsetti, M., Symillides, M., Vertzoni, M., Reppas, C., Turner, D.B., Augustijns, P. (2014). Gastrointestinal transfer: in

vivo evaluation and implementation in in vitro and in silico predictive tools. *Eur J Pharm Sci*, **63**, 233-242. https://doi.org/10.1016/j.ejps.2014.07.008

155. Macheras, P., Chryssafidis, P. (2020). Revising Pharmacokinetics of Oral Drug Absorption: I Models Based on Biopharmaceutical/Physiological and Finite Absorption Time Concepts. *Pharm Res*, **37** (10), 187. https://doi.org/10.1007/s11095-020-02894-w

156. Chryssafidis, P., Tsekouras, A.A., Macheras, P. (2022). Re-writing Oral Pharmacokinetics Using Physiologically Based Finite Time Pharmacokinetic (PBFTPK) Models. *Pharm Res*, **39** (4), 691-701. https://doi.org/10.1007/s11095-022-03230-0

157. Pentafragka, C., Vertzoni, M., Dressman, J., Symillides, M., Goumas, K., Reppas, C. (2020). Characteristics of contents in the upper gastrointestinal lumen after a standard high-calorie high-fat meal and implications for the in vitro drug product performance testing conditions. *Eur J Pharm Sci*, **155**, 105535. https://doi.org/10.1016/j.ejps.2020.105535

158. Radwan, A., Wagner, M., Amidon, G.L., Langguth, P. (2014). Bio-predictive tablet disintegration: effect of water diffusivity, fluid flow, food composition and test conditions. *Eur J Pharm Sci*, **57**, 273-279. https://doi.org/10.1016/j.ejps.2013.08.038

159. Pedersen, P.B., Berthelsen, R., Rades, T., Jorgensen, S.A., Vilmann, P., Bar-Shalom, D., Baldursdottir, S., Mullertz, A. (2022). Physico-chemical characterization of aspirated and simulated human gastric fluids to study their influence on the intrinsic dissolution rate of cinnarizine. *Int J Pharm*, **622**, 121856. https://doi.org/10.1016/j.ijpharm.2022.121856

160. Manrique, Y.J., Sparkes, A.M., Cichero, J.A., Stokes, J.R., Nissen, L.M., Steadman, K.J. (2016). Oral medication delivery in impaired swallowing: thickening liquid medications for safe swallowing alters dissolution characteristics. *Drug Dev Ind Pharm*, **42** (9), 1537-1544. https://doi.org/10.3109/03639045.2016.1151033

161. Manrique, Y.J., Lee, D.J., Islam, F., Nissen, L.M., Cichero, J.A.Y., Stokes, J.R., Steadman, K.J. (2014). Crushed Tablets: Does the Administration of Food Vehicles and Thickened Fluids to Aid Medication Swallowing Alter Drug Release? *J Pharm Pharm Sci*, **17** (2), 207-219. https://doi.org/https://doi.org/10.18433/J39W3V

162. Abrahamsson, B., Albery, T., Eriksson, A., Gustafsson, I., Sjoberg, M. (2004). Food effects on tablet disintegration. *Eur J Pharm Sci*, **22** (2-3), 165-172. https://doi.org/10.1016/j.ejps.2004.03.004

163. Paraiso, R.L.M., Watanabe, A., Andreas, C.J., Turner, D., Zane, P., Dressman, J. (2019). In-vitro-in-silico investigation of the negative food effect of zolpidem when administered as immediate-release tablets. *J Pharm Pharmacol*, **71** (11), 1663-1676. https://doi.org/10.1111/jphp.13161

164. Cvijic, S., Parojcic, J., Langguth, P. (2014). Viscosity-mediated negative food effect on oral absorption of poorly-permeable drugs with an absorption window in the proximal intestine: In vitro experimental simulation and computational verification. *Eur J Pharm Sci*, **61**, 40-53. https://doi.org/10.1016/j.ejps.2014.04.008

165. Radwan, A., Zaid, A.N., Jaradat, N., Odeh, Y. (2017). Food effect: The combined effect of media pH and viscosity on the gastrointestinal absorption of ciprofloxacin tablet. *Eur J Pharm Sci*, **101**, 100-106. https://doi.org/10.1016/j.ejps.2017.01.030

166. Einstein, A. (1905). Über die von der molekularkinetischen Theorie der Wärme geforderte Bewegung von in ruhenden Flüssigkeiten suspendierten Teilchen. *Annalen der Physik*, **322** (8), 549-560. https://doi.org/https://doi.org/10.1002/andp.19053220806

167. Nernst, W. (1904). Theorie der Reaktionsgeschwindigkeit in heterogenen Systemen. *Z Phys Chem*, **47U** (1), 52-55. https://doi.org/10.1515/zpch-1904-4704

168. Brunner, E. (1904). Reaktionsgeschwindigkeit in heterogenen Systemen. *Z Phys Chem*, **47U** (1), 56-102. https://doi.org/10.1515/zpch-1904-4705

169. Phillips, D.J., Pygall, S.R., Cooper, V.B., Mann, J.C. (2012). Overcoming sink limitations in dissolution testing: a review of traditional methods and the potential utility of biphasic systems. *J Pharm Pharmacol*, **64** (11), 1549-1559. https://doi.org/10.1111/j.2042-7158.2012.01523.x

170. Kataoka, M., Masaoka, Y., Yamazaki, Y., Sakane, T., Sezaki, H., Yamashita, S. (2003). In vitro system to evaluate oral absorption of poorly water-soluble drugs: simultaneous analysis on dissolution and permeation of drugs. *Pharm Res*, **10**, 1674-1680. https://doi.org/10.1023/a:1026107906191

171. Adhikari, A., Seo, P.R., Polli, J.E. (2023). Dissolution-Hollow Fiber Membrane (D-HFM) System to Anticipate Biopharmaceutics Risk of Tablets and Capsules. *J Pharm Sci*, **112** (3), 751-759. https://doi.org/10.1016/j.xphs.2022.09.030

172. Holzem, F.L., Weck, A., Schaffland, J.P., Stillhart, C., Klein, S., Bauer-Brandl, A., Brandl, M. (2022). Biopredictive capability assessment of two dissolution/permeation assays, microFLUX and PermeaLoop, using supersaturating formulations of Posaconazole. *Eur J Pharm Sci*, **176**, 106260. https://doi.org/10.1016/j.ejps.2022.106260

173. Lentz, K.A., Plum, J., Steffansen, B., Arvidsson, P.O., Omkvist, D.H., Pedersen, A.J., Sennbro, C.J., Pedersen, G.P., Jacobsen, J. (2021). Predicting in vivo performance of fenofibrate amorphous solid dispersions using in vitro non-sink dissolution and dissolution permeation setup. *Int J Pharm*, **610**, 121174. https://doi.org/10.1016/j.ijpharm.2021.121174

174. Eriksen, J.B., Christiansen, J.J., Bauer-Brandl, A., Ruponen, M., Rautio, J., Brandl, M. (2023). In-vitro dynamic dissolution/bioconversion/permeation of fosamprenavir using a novel tool with an artificial biomimetic permeation barrier and microdialysis-sampling. *Eur J Pharm Sci*, **181**, 106366. https://doi.org/10.1016/j.ejps.2022.106366

175. Li, J., Spivey, N., Silchenko, S., Gonzalez-Alvarez, I., Bermejo, M., Hidalgo, I.J. (2021). A differential equation based modelling approach to predict supersaturation and in vivo absorption from in vitro dissolution-absorption system (idas2) data. *Eur J Pharm Biopharm*, **165**, 1-12. https://doi.org/10.1016/j.ejpb.2021.05.003

176. Kataoka, M., Itsubata, S., Masaoka, Y., Sakuma, S., Yamashita, S. (2011). In vitro dissolution/permeation system to predict the oral absorption of poorly water-soluble drugs: effect of food and dose strength on it. *Biol Pharm Bull*, **34** (3), 401-407. https://doi.org/10.1248/bpb.34.401

177. Buch, P., Holm, P., Thomassen, J.Q., Scherer, D., Kataoka, M., Yamashita, S., Langguth, P. (2010). IVIVR in oral absorption for fenofibrate immediate release tablets using dissolution and dissolution permeation methods. *Pharmazie*, **65** (10), 723-728. https://doi.org/10.1691/ph.2011.0114

178. Garbacz, G., Kolodziej, B., Koziolek, M., Weitschies, W., Klein, S. (2014). A dynamic system for the simulation of fasting luminal pH-gradients using

hydrogen carbonate buffers for dissolution testing of ionisable compounds. *Eur J Pharm Sci*, **51**, 224-231. https://doi.org/10.1016/j.ejps.2013.09.020

179. Garbacz, G., Cade, D., Benameur, H., Weitschies, W. (2014). Bio-relevant dissolution testing of hard capsules prepared from different shell materials using the dynamic open flow through test apparatus. *Eur J Pharm Sci*, **57**, 264-272. https://doi.org/10.1016/j.ejps.2013.08.039
180. Kostewicz, E.S., Wunderlich, M., Brauns, U., Becker, R., Bock, T., Dressman, J.B. (2004). Predicting the precipitation of poorly soluble weak bases upon entry in the small intestine. *J Pharm Pharmacol*, **56** (1), 43-51. https://doi.org/10.1211/0022357022511
181. Fiolka, T., Dressman, J. (2018). Development, current applications and future roles of biorelevant two-stage in vitro testing in drug development. *J Pharm Pharmacol*, **70** (3), 335-348. https://doi.org/10.1111/jphp.12875
182. Barker, R., Abrahamsson, B., Kruusmagi, M. (2014). Application and validation of an advanced gastrointestinal in vitro model for the evaluation of drug product performance in pharmaceutical development. *J Pharm Sci*, **103** (11), 3704-3712. https://doi.org/10.1002/jps.24177
183. Gray, V.A., Mann, J.C., Barker, R., Pepin, X.J.H. (2020). The Case for Physiologically Based Biopharmaceutics Modelling (PBBM): What do Dissolution Scientists Need to Know? *Dissolution Technol*, **27** (3), 6-19. https://doi.org/10.14227/dt270320p6
184. Carino, S.R., Sperry, D.C., Hawley, M. (2006). Relative bioavailability estimation of carbamazepine crystal forms using an artificial stomach-duodenum model. *J Pharm Sci*, **95** (1), 116-125. https://doi.org/10.1002/jps.20495
185. Takeuchi, S., Tsume, Y., Amidon, G.E., Amidon, G.L. (2014). Evaluation of a three compartment in vitro gastrointestinal simulator dissolution apparatus to predict in vivo dissolution. *J Pharm Sci*, **103** (11), 3416-3422. https://doi.org/10.1002/jps.24112
186. Kourentas, A., Vertzoni, M., Stavrinoudakis, N., Symillidis, A., Brouwers, J., Augustijns, P., Reppas, C., Symillides, M. (2016). An in vitro biorelevant gastrointestinal transfer (BioGIT) system for forecasting concentrations in the fasted upper small intestine: Design, implementation, and evaluation. *Eur J Pharm Sci*, **82**, 106-114. https://doi.org/10.1016/j.ejps.2015.11.012

187. Kostantini, C., Spilioti, E., Bevernage, J., Ceulemans, J., Hansmann, S., Hellemans, K., Jede, C., Kourentas, A., Reggane, M., Shah, L., Wagner, C., Reppas, C., Vertzoni, M. (2023). Usefulness of the BioGIT system in screening for differences in early exposure in the fasted state on an a priori basis. *Int J Pharm*, **634**, 122670. https://doi.org/10.1016/j.ijpharm.2023.122670

188. Schick, P., Sager, M., Wegner, F., Wiedmann, M., Schapperer, E., Weitschies, W., Koziolek, M. (2019). Application of the GastroDuo as an in Vitro Dissolution Tool To Simulate the Gastric Emptying of the Postprandial Stomach. *Mol Pharm*, **16** (11), 4651-4660. https://doi.org/10.1021/acs.molpharmaceut.9b00799

189. Koziolek, M., Gorke, K., Neumann, M., Garbacz, G., Weitschies, W. (2014). Development of a bio-relevant dissolution test device simulating mechanical aspects present in the fed stomach. *Eur J Pharm Sci*, **57**, 250-256. https://doi.org/10.1016/j.ejps.2013.09.004

190. Baxevanis, F., Zarmpi, P., Kuiper, J., Fotaki, N. (2020). Investigation of drug partition kinetics to fat in simulated fed state gastric conditions based on drug properties. *Eur J Pharm Sci*, **146**, 105263. https://doi.org/10.1016/j.ejps.2020.105263

191. Karkossa, F., Klein, S. (2018). A Biopredictive In Vitro Comparison of Oral Locally Acting Mesalazine Formulations by a Novel Dissolution Model for Assessing Intraluminal Drug Release in Individual Subjects. *J Pharm Sci*, **107** (6), 1680-1689. https://doi.org/10.1016/j.xphs.2018.02.016

192. Karkossa, F., Klein, S. (2019). Individualized in vitro and in silico methods for predicting in vivo performance of enteric-coated tablets containing a narrow therapeutic index drug. *Eur J Pharm Biopharm*, **135**, 13-24. https://doi.org/10.1016/j.ejpb.2018.12.004

193. Noyes, A.A., Whitney, W.R. (1897). The rate of solution of solid substances in their own solutions. *J Am Chem Soc*, **19**, 930-934. https://doi.org/10.1021/ja02086a003

194. Hixson, A.W., Crowell, J.H. (1931). Dependence of Reaction Velocity upon surface and Agitation. *Ind Eng Chem*, **23** (8), 923-931. https://doi.org/10.1021/ie50260a018

195. Niebergall, P.J., Milosovixh, G., Goyan, J.E. (1936). Dissolution rate studies II: Dissolution of particles under conditions of agitation. *J Pharm Sci*, **52**, 236-241. https://doi.org/10.1002/jps.2600520310
196. Higuchi, W.I., Hiestand, E.N. (1963). Dissolution rates of finely divided drug powders I: Effect of a distribution of particle sizes in a diffusion-controlled process. *J Pharm Sci*, **52**, 67-71. https://doi.org/10.1002/jps.2600520114
197. Higuchi, W.I., Hiestand, E.N. (1963). Dissolution rates of finely divided drug powders II: Micronized methylprednisolone. *J Pharm Sci*, **52**, 162-164. https://doi.org/10.1002/jps.2600520213
198. Siew, A. (2016). Factors to Consider in Dissolution Testing. *Pharm Tech*, **11** (12).
199. Wang, J., Flanagan, D.R. (1999). General solution for diffusion-controlled dissolution of spherical particles. 1. Theory. *J Pharm Sci*, **88** (7), 731-738. https://doi.org/10.1021/js980236p
200. Hintz, R.J., Johnson, K.C. (1989). The effect of particle size distribution on dissolution rate and oral absorption. *Int J Pharm*, **51** (1), 9-17. https://doi.org/10.1016/0378-5173(89)90069-0
201. de Almeida, L.P., Simöes, S., Brito, P., Portugal, A., Figueiredo, M. (1997). Modeling dissolution of sparingly soluble multisized powders. *J Pharm Sci*, **86** (6), 726-732. https://doi.org/10.1021/js960417w
202. Andersson, S.B.E., Frenning, G., Alderborn, G., Grasjo, J. (2022). Effect of fluid velocity and particle size on the hydrodynamic diffusion layer thickness. *Eur J Pharm Biopharm*, **180**, 1-10. https://doi.org/10.1016/j.ejpb.2022.09.016
203. Johnson, K.C. (2012). Comparison of methods for predicting dissolution and the theoretical implications of particle-size-dependent solubility. *J Pharm Sci*, **101** (2), 681-689. https://doi.org/10.1002/jps.22778
204. Okazaki, A., Mano, T., Sugano, K. (2008). Theoretical dissolution model of poly-disperse drug particles in biorelevant media. *J Pharm Sci*, **97** (5), 1843-1852. https://doi.org/10.1002/jps.21070
205. Ranz, W.E., Marshall, W.R. (1952). Evaporation from drops: Part 1 *Chem Eng Prog*, **48** (3), 141-146.
206. Ranz, W.E., Marshall, W.R. (1952). Evaporation from drops: Part 2. *Chem Eng Prog*, **48** (4), 173-180.

207. Sheng, J.J., Sirois, P.J., Dressman, J.B., Amidon, G.L. (2008). Particle diffusional layer thickness in a USP dissolution apparatus II: a combined function of particle size and paddle speed. *J Pharm Sci*, **97** (11), 4815-4829. https://doi.org/10.1002/jps.21345
208. Wang, Y., Abrahamsson, B., Lindfors, L., Brasseur, J.G. (2012). Comparison and analysis of theoretical models for diffusion-controlled dissolution. *Mol Pharm*, **9** (5), 1052-1066. https://doi.org/10.1021/mp2002818
209. Wang, Y., Abrahamsson, B., Lindfors, L., Brasseur, J.G. (2015). Analysis of Diffusion-Controlled Dissolution from Polydisperse Collections of Drug Particles with an Assessed Mathematical Model. *J Pharm Sci*, **104** (9), 2998-3017. https://doi.org/10.1002/jps.24472
210. Agata, Y., Iwao, Y., Miyagishima, A., Itai, S. (2010). Novel mathematical model for predicting the dissolution profile of spherical particles under non-sink conditions. *Chem Pharm Bull (Tokyo)*, **58** (4), 511-515. https://doi.org/10.1248/cpb.58.511
211. Pepin, X., Goetschy, M., Abrahmsen-Alami, S. (2022). Mechanistic Models for USP2 Dissolution Apparatus, Including Fluid Hydrodynamics and Sedimentation. *J Pharm Sci*, **111** (1), 185-196. https://doi.org/10.1016/j.xphs.2021.10.006
212. Caccavo, D., Lamberti, G., Cafaro, M.M., Barba, A.A., Kazlauske, J., Larsson, A. (2017). Mathematical modelling of the drug release from an ensemble of coated pellets. *Br J Pharmacol*, **174** (12), 1797-1809. https://doi.org/10.1111/bph.13776
213. Melling, A. (1997). Tracer particles and seeding for particle image velocimetry. *Meas Sci Technol*, **8** (12), 1406. https://doi.org/10.1088/0957-0233/8/12/005
214. Sugano, K. (2008). Theoretical comparison of hydrodynamic diffusion layer models used for dissolution simulation in drug discovery and development. *Int J Pharm*, **363** (1-2), 73-77. https://doi.org/10.1016/j.ijpharm.2008.07.002
215. D'Arcy, D.M., Liu, B., Persoons, T., Corrigan, O.I. (2011). Hydrodynamic Complexity Induced by the Pulsing Flow Field in USP Dissolution Apparatus 4. *Dissolution Technol*, **18** (4), 6-13. https://doi.org/10.14227/dt180411p6
216. D'Arcy, D.M., Pham, T.T.V., Navas Bachiller, M., Fotaki, N., Persoons, T. (2020). Using in silico process simulation tools in pharmacy education:

Considerations for pivoting to online learning. *Pharm Ed*, **20** (2), 124-135. https://doi.org/10.46542/pe.2020.202.124135

217. McCarthy, L.G., Bradley, G., Sexton, J.C., Corrigan, O.I., Healy, A.M. (2004). Computational Fluid Dynamics Modeling of the Paddle Dissolution Apparatus: Agitation Rate, Mixing Patterns, and Fluid Velocities. *AAPS PharmSciTech*, **5** (2), 50-59. https://doi.org/10.1208/pt050231
218. Navas-Bachiller, M., Persoons, T., D'Arcy, D.M. (2022). Exploring bulk volume, particle size and particle motion definitions to increase the predictive ability of in vitro dissolution simulations. *Eur J Pharm Sci*, **174**, 106185. https://doi.org/10.1016/j.ejps.2022.106185
219. Pharmacopoeia, U.S. (2020). ⟨1236⟩ Solubility measurements.
220. Price, D.J., Ditzinger, F., Koehl, N.J., Jankovic, S., Tsakiridou, G., Nair, A., Holm, R., Kuentz, M., Dressman, J.B., Saal, C. (2019). Approaches to increase mechanistic understanding and aid in the selection of precipitation inhibitors for supersaturating formulations - a PEARRL review. *J Pharm Pharmacol*, **71** (4), 483-509. https://doi.org/10.1111/jphp.12927
221. O'Dwyer, P.J., Litou, C., Box, K.J., Dressman, J.B., Kostewicz, E.S., Kuentz, M., Reppas, C. (2019). In vitro methods to assess drug precipitation in the fasted small intestine - a PEARRL review. *J Pharm Pharmacol*, **71** (4), 536-556. https://doi.org/10.1111/jphp.12951
222. Long, C.M., Tang, K., Chokshi, H., Fotaki, N. (2019). Surface Dissolution UV Imaging for Investigation of Dissolution of Poorly Soluble Drugs and Their Amorphous Formulation. *AAPS PharmSciTech*, **20** (3), 113. https://doi.org/10.1208/s12249-019-1317-z
223. Carlert, S., Palsson, A., Hanisch, G., von Corswant, C., Nilsson, C., Lindfors, L., Lennernas, H., Abrahamsson, B. (2010). Predicting intestinal precipitation--a case example for a basic BCS class II drug. *Pharm Res*, **27** (10), 2119-2130. https://doi.org/10.1007/s11095-010-0213-8
224. Abrami, M., Grassi, M., Masiello, D., Pontrelli, G. (2022). Dissolution of irregularly-shaped drug particles: mathematical modelling. *Eur J Pharm Biopharm*, **177**, 199-210. https://doi.org/10.1016/j.ejpb.2022.06.012
225. Abrami, M., Grassi, L., di Vittorio, R., Hasa, D., Perissutti, B., Voinovich, D., Grassi, G., Colombo, I., Grassi, M. (2020). Dissolution of an ensemble of differently shaped poly-dispersed drug particles undergoing solubility reduction:

mathematical modelling. *ADMET DMPK*, **8** (3), 297-313. https://doi.org/10.5599/admet.841

226. Pathak, S.M., Ruff, A., Kostewicz, E.S., Patel, N., Turner, D.B., Jamei, M. (2017). Model-Based Analysis of Biopharmaceutic Experiments To Improve Mechanistic Oral Absorption Modeling: An Integrated in Vitro in Vivo Extrapolation Perspective Using Ketoconazole as a Model Drug. *Mol Pharm*, **14** (12), 4305-4320. https://doi.org/10.1021/acs.molpharmaceut.7b00406
227. Pathak, S.M., Schaefer, K.J., Jamei, M., Turner, D.B. (2019). Biopharmaceutic IVIVE-Mechanistic Modeling of Single- and Two-Phase In Vitro Experiments to Obtain Drug-Specific Parameters for Incorporation Into PBPK Models. *J Pharm Sci*, **108** (4), 1604-1618. https://doi.org/10.1016/j.xphs.2018.11.034
228. Duque, M.D., Issa, M.G., Silva, D.A., Barbosa, E.J., Löbenberg, R., Ferraz, H.G. (2018). In Silico Simulation of Dissolution Profiles for Development of Extended-Release Doxazosin Tablets. *Dissolution Technol*, **25** (4), 14-21. https://doi.org/10.14227/dt250418p14
229. Loisios-Konstantinidis, I., Dressman, J. (2021). Physiologically Based Pharmacokinetic/Pharmacodynamic Modeling to Support Waivers of In Vivo Clinical Studies: Current Status, Challenges, and Opportunities. *Mol Pharm*, **18** (1), 1-17. https://doi.org/10.1021/acs.molpharmaceut.0c00903
230. A collaboration by FDA | CDER Office of Pharmaceutical Quality (OPQ), Small Business and Industry Assistance (SBIA), and University of Maryland CERSI. (2019). WORKSHOP: Current State and Future Expectations of Translational Modeling Strategies to Support Drug Product Development, Manufacturing Changes and Controls.
231. European Medicines Agency (EMA). (2019). Guideline on the reporting of physiologically based pharmacokinetic (PBPK) modelling and simulation.
232. Teorell, T. (1937). Kinetics of distribution of substances administered to the body, I: the extravascular modes of administration. *Arch Int Pharmacodynamie Ther* **57**, 205-225.
233. Yu, L.X., Amidon, G.L. (1999). A compartmental absorption and transit model for estimating oral drug absorption. *Int J Pharm*, **186** (2), 119-125. https://doi.org/10.1016/s0378-5173(99)00147-7
234. Segregur, D., Mann, J., Moir, A., Karlsson, E.M., Dressman, J. (2021). Prediction of plasma profiles of a weakly basic drug after administration of

omeprazole using PBPK modeling. *Eur J Pharm Sci*, **158**, 105656. https://doi.org/10.1016/j.ejps.2020.105656

235. Cristofoletti, R., Hens, B., Patel, N., Esteban, V.V., Schmidt, S., Dressman, J. (2019). Integrating Drug- and Formulation-Related Properties With Gastrointestinal Tract Variability Using a Product-Specific Particle Size Approach: Case Example Ibuprofen. *J Pharm Sci*, **108** (12), 3842-3847. https://doi.org/10.1016/j.xphs.2019.09.012
236. Takano, R., Sugano, K., Higashida, A., Hayashi, Y., Machida, M., Aso, Y., Yamashita, S. (2006). Oral absorption of poorly water-soluble drugs: computer simulation of fraction absorbed in humans from a miniscale dissolution test. *Pharm Res*, **23** (6), 1144-1156. https://doi.org/10.1007/s11095-006-0162-4
237. Jamei, M., Abrahamsson, B., Brown, J., Bevernage, J., Bolger, M.B., Heimbach, T., Karlsson, E., Kotzagiorgis, E., Lindahl, A., McAllister, M., Mullin, J.M., Pepin, X., Tistaert, C., Turner, D.B., Kesisoglou, F. (2020). Current status and future opportunities for incorporation of dissolution data in PBPK modeling for pharmaceutical development and regulatory applications: OrBiTo consortium commentary. *Eur J Pharm Biopharm*, **155**, 55-68. https://doi.org/10.1016/j.ejpb.2020.08.005
238. Wu, F., Shah, H., Li, M., Duan, P., Zhao, P., Suarez, S., Raines, K., Zhao, Y., Wang, M., Lin, H.P., Duan, J., Yu, L., Seo, P. (2021). Biopharmaceutics Applications of Physiologically Based Pharmacokinetic Absorption Modeling and Simulation in Regulatory Submissions to the U.S. Food and Drug Administration for New Drugs. *AAPS J*, **23** (2), 31. https://doi.org/10.1208/s12248-021-00564-2
239. Kostewicz, E.S., Aarons, L., Bergstrand, M., Bolger, M.B., Galetin, A., Hatley, O., Jamei, M., Lloyd, R., Pepin, X., Rostami-Hodjegan, A., Sjogren, E., Tannergren, C., Turner, D.B., Wagner, C., Weitschies, W., Dressman, J. (2014). PBPK models for the prediction of in vivo performance of oral dosage forms. *Eur J Pharm Sci*, **57**, 300-321. https://doi.org/10.1016/j.ejps.2013.09.008
240. Perry, C., Davis, G., Conner, T.M., Zhang, T. (2020). Utilization of Physiologically Based Pharmacokinetic Modeling in Clinical Pharmacology and Therapeutics: an Overview. *Curr Pharmacol Rep*, **6** (3), 71-84. https://doi.org/10.1007/s40495-020-00212-x

241. O'Dwyer, P.J., Box, K.J., Dressman, J., Griffin, B.T., Henze, L.J., Litou, C., Pentafragka, C., Statelova, M., Vertzoni, M., Reppas, C. (2021). Oral biopharmaceutics tools: recent progress from partnership through the Pharmaceutical Education and Research with Regulatory Links collaboration. *J Pharm Pharmacol*, **73** (4), 437-446. https://doi.org/10.1093/jpp/rgaa055

242. Margolskee, A., Darwich, A.S., Pepin, X., Pathak, S.M., Bolger, M.B., Aarons, L., Rostami-Hodjegan, A., Angstenberger, J., Graf, F., Laplanche, L., Muller, T., Carlert, S., Daga, P., Murphy, D., Tannergren, C., Yasin, M., Greschat-Schade, S., Muck, W., Muenster, U., van der Mey, D., Frank, K.J., Lloyd, R., Adriaenssen, L., Bevernage, J., De Zwart, L., Swerts, D., Tistaert, C., Van Den Bergh, A., Van Peer, A., Beato, S., Nguyen-Trung, A.T., Bennett, J., McAllister, M., Wong, M., Zane, P., Ollier, C., Vicat, P., Kolhmann, M., Marker, A., Brun, P., Mazuir, F., Beilles, S., Venczel, M., Boulenc, X., Loos, P., Lennernas, H., Abrahamsson, B. (2017). IMI - oral biopharmaceutics tools project - evaluation of bottom-up PBPK prediction success part 1: Characterisation of the OrBiTo database of compounds. *Eur J Pharm Sci*, **96**, 598-609. https://doi.org/10.1016/j.ejps.2016.09.027

243. Margolskee, A., Darwich, A.S., Pepin, X., Aarons, L., Galetin, A., Rostami-Hodjegan, A., Carlert, S., Hammarberg, M., Hilgendorf, C., Johansson, P., Karlsson, E., Murphy, D., Tannergren, C., Thorn, H., Yasin, M., Mazuir, F., Nicolas, O., Ramusovic, S., Xu, C., Pathak, S.M., Korjamo, T., Laru, J., Malkki, J., Pappinen, S., Tuunainen, J., Dressman, J., Hansmann, S., Kostewicz, E., He, H., Heimbach, T., Wu, F., Hoft, C., Laplanche, L., Pang, Y., Bolger, M.B., Huehn, E., Lukacova, V., Mullin, J.M., Szeto, K.X., Costales, C., Lin, J., McAllister, M., Modi, S., Rotter, C., Varma, M., Wong, M., Mitra, A., Bevernage, J., Biewenga, J., Van Peer, A., Lloyd, R., Shardlow, C., Langguth, P., Mishenzon, I., Nguyen, M.A., Brown, J., Lennernas, H., Abrahamsson, B. (2017). IMI - Oral biopharmaceutics tools project - Evaluation of bottom-up PBPK prediction success part 2: An introduction to the simulation exercise and overview of results. *Eur J Pharm Sci*, **96**, 610-625. https://doi.org/10.1016/j.ejps.2016.10.036

244. Darwich, A.S., Margolskee, A., Pepin, X., Aarons, L., Galetin, A., Rostami-Hodjegan, A., Carlert, S., Hammarberg, M., Hilgendorf, C., Johansson, P., Karlsson, E., Murphy, D., Tannergren, C., Thorn, H., Yasin, M., Mazuir, F.,

Nicolas, O., Ramusovic, S., Xu, C., Pathak, S.M., Korjamo, T., Laru, J., Malkki, J., Pappinen, S., Tuunainen, J., Dressman, J., Hansmann, S., Kostewicz, E., He, H., Heimbach, T., Wu, F., Hoft, C., Pang, Y., Bolger, M.B., Huehn, E., Lukacova, V., Mullin, J.M., Szeto, K.X., Costales, C., Lin, J., McAllister, M., Modi, S., Rotter, C., Varma, M., Wong, M., Mitra, A., Bevernage, J., Biewenga, J., Van Peer, A., Lloyd, R., Shardlow, C., Langguth, P., Mishenzon, I., Nguyen, M.A., Brown, J., Lennernas, H., Abrahamsson, B. (2017). IMI - Oral biopharmaceutics tools project - Evaluation of bottom-up PBPK prediction success part 3: Identifying gaps in system parameters by analysing In Silico performance across different compound classes. *Eur J Pharm Sci*, **96**, 626-642. https://doi.org/10.1016/j.ejps.2016.09.037

245. Ahmad, A., Pepin, X., Aarons, L., Wang, Y., Darwich, A.S., Wood, J.M., Tannergren, C., Karlsson, E., Patterson, C., Thorn, H., Ruston, L., Mattinson, A., Carlert, S., Berg, S., Murphy, D., Engman, H., Laru, J., Barker, R., Flanagan, T., Abrahamsson, B., Budhdeo, S., Franek, F., Moir, A., Hanisch, G., Pathak, S.M., Turner, D., Jamei, M., Brown, J., Good, D., Vaidhyanathan, S., Jackson, C., Nicolas, O., Beilles, S., Nguefack, J.F., Louit, G., Henrion, L., Ollier, C., Boulu, L., Xu, C., Heimbach, T., Ren, X., Lin, W., Nguyen-Trung, A.T., Zhang, J., He, H., Wu, F., Bolger, M.B., Mullin, J.M., van Osdol, B., Szeto, K., Korjamo, T., Pappinen, S., Tuunainen, J., Zhu, W., Xia, B., Daublain, P., Wong, S., Varma, M.V.S., Modi, S., Schafer, K.J., Schmid, K., Lloyd, R., Patel, A., Tistaert, C., Bevernage, J., Nguyen, M.A., Lindley, D., Carr, R., Rostami-Hodjegan, A. (2020). IMI - Oral biopharmaceutics tools project - Evaluation of bottom-up PBPK prediction success part 4: Prediction accuracy and software comparisons with improved data and modelling strategies. *Eur J Pharm Biopharm*, **156**, 50-63. https://doi.org/10.1016/j.ejpb.2020.08.006

246. Segregur, D., Barker, R., Mann, J., Moir, A., Karlsson, E.M., Turner, D.B., Arora, S., Dressman, J. (2021). Evaluating the impact of acid-reducing agents on drug absorption using biorelevant in vitro tools and PBPK modeling - case example dipyridamole. *Eur J Pharm Sci*, **160**, 105750. https://doi.org/10.1016/j.ejps.2021.105750

247. Segregur, D., Mann, J., Moir, A., Karlsson, E.M., Dressman, J. (2022). Biorelevant in vitro Tools and in silico Modeling to Assess pH-Dependent Drug-drug Interactions for Salts of Weak Acids: Case Example Potassium

Raltegravir. *J Pharm Sci*, **111** (2), 517-528. https://doi.org/10.1016/j.xphs.2021.09.037

248. Kesisoglou, F., Vertzoni, M., Reppas, C. (2018). Physiologically Based Absorption Modeling of Salts of Weak Bases Based on Data in Hypochlorhydric and Achlorhydric Biorelevant Media. *AAPS PharmSciTech*, **19** (7), 2851-2858. https://doi.org/10.1208/s12249-018-1059-3

249. Andreas, C.J., Pepin, X., Markopoulos, C., Vertzoni, M., Reppas, C., Dressman, J.B. (2017). Mechanistic investigation of the negative food effect of modified release zolpidem. *Eur J Pharm Sci*, **102**, 284-298. https://doi.org/10.1016/j.ejps.2017.03.011

250. Luo, L., Thakral, N.K., Schwabe, R., Li, L., Chen, S. (2022). Using Tiny-TIM Dissolution and In Silico Simulation to Accelerate Oral Product Development of a BCS Class II Compound. *AAPS PharmSciTech*, **23** (6), 185. https://doi.org/10.1208/s12249-022-02343-4

251. Paraiso, R.L.M., Rose, R.H., Fotaki, N., McAllister, M., Dressman, J.B. (2020). The use of PBPK/PD to establish clinically relevant dissolution specifications for zolpidem immediate release tablets. *Eur J Pharm Sci*, **155**, 105534. https://doi.org/10.1016/j.ejps.2020.105534

252. Mohamed, M.F., Winzenborg, I., Othman, A.A., Marroum, P. (2022). Utility of Modeling and Simulation Approach to Support the Clinical Relevance of Dissolution Specifications: a Case Study from Upadacitinib Development. *AAPS J*, **24** (2), 39. https://doi.org/10.1208/s12248-022-00681-6

253. O'Dwyer, P.J., Box, K.J., Imanidis, G., Vertzoni, M., Reppas, C. (2022). On the usefulness of four in vitro methods in assessing the intraluminal performance of poorly soluble, ionisable compounds in the fasted state. *Eur J Pharm Sci*, **168**, 106034. https://doi.org/10.1016/j.ejps.2021.106034

254. Tatipalli, M., Siripuram, V.K., Long, T., Shuster, D., Bernstein, G., Martineau, P., Cook, K.A., Cristofoletti, R., Schmidt, S., Vozmediano, V. (2021). Model-Informed Optimization of a Pediatric Clinical Pharmacokinetic Trial of a New Spironolactone Liquid Formulation. *Pharmaceutics*, **13** (6). https://doi.org/10.3390/pharmaceutics13060849

255. Komasaka, T., Dressman, J. (2021). Simulation of oral absorption from non-bioequivalent dosage forms of the salt of raltegravir, a poorly soluble acidic drug, using a physiologically based biopharmaceutical modeling (PBBM)

approach. *Eur J Pharm Sci*, **157**, 105630. https://doi.org/10.1016/j.ejps.2020.105630

256. Kambayashi, A., Dressman, J.B. (2022). Towards Virtual Bioequivalence Studies for Oral Dosage Forms Containing Poorly Water-Soluble Drugs: A Physiologically Based Biopharmaceutics Modeling (PBBM) Approach. *J Pharm Sci*, **111** (1), 135-145. https://doi.org/10.1016/j.xphs.2021.08.008

257. Laisney, M., Heimbach, T., Mueller-Zsigmondy, M., Blumenstein, L., Costa, R., Ji, Y. (2022). Physiologically Based Biopharmaceutics Modeling to Demonstrate Virtual Bioequivalence and Bioequivalence Safe-space for Ribociclib which has Permeation Rate-controlled Absorption. *J Pharm Sci*, **111** (1), 274-284. https://doi.org/10.1016/j.xphs.2021.10.017

258. Pepin, X.J., Flanagan, T.R., Holt, D.J., Eidelman, A., Treacy, D., Rowlings, C.E. (2016). Justification of Drug Product Dissolution Rate and Drug Substance Particle Size Specifications Based on Absorption PBPK Modeling for Lesinurad Immediate Release Tablets. *Mol Pharm*, **13** (9), 3256-3269. https://doi.org/10.1021/acs.molpharmaceut.6b00497

259. Hens, B., Pathak, S.M., Mitra, A., Patel, N., Liu, B., Patel, S., Jamei, M., Brouwers, J., Augustijns, P., Turner, D.B. (2017). In Silico Modeling Approach for the Evaluation of Gastrointestinal Dissolution, Supersaturation, and Precipitation of Posaconazole. *Mol Pharm*, **14** (12), 4321-4333. https://doi.org/10.1021/acs.molpharmaceut.7b00396

260. Jakubiak, P., Wagner, B., Grimm, H.P., Petrig-Schaffland, J., Schuler, F., Alvarez-Sanchez, R. (2016). Development of a Unified Dissolution and Precipitation Model and Its Use for the Prediction of Oral Drug Absorption. *Mol Pharm*, **13** (2), 586-598. https://doi.org/10.1021/acs.molpharmaceut.5b00808

261. Hens, B., Talattof, A., Paixao, P., Bermejo, M., Tsume, Y., Lobenberg, R., Amidon, G.L. (2018). Measuring the Impact of Gastrointestinal Variables on the Systemic Outcome of Two Suspensions of Posaconazole by a PBPK Model. *AAPS J*, **20** (3), 57. https://doi.org/10.1208/s12248-018-0217-6

262. Bermejo, M., Hens, B., Dickens, J., Mudie, D., Paixao, P., Tsume, Y., Shedden, K., Amidon, G.L. (2020). A Mechanistic Physiologically-Based Biopharmaceutics Modeling (PBBM) Approach to Assess the In Vivo Performance of an Orally Administered Drug Product: From IVIVC to IVIVP. *Pharmaceutics*, **12** (1). https://doi.org/10.3390/pharmaceutics12010074

263. Yu, A., Koenigsknecht, M.J., Hens, B., Baker, J.R., Wen, B., Jackson, T.L., Pai, M.P., Hasler, W., Amidon, G.L., Sun, D. (2019). Mechanistic Deconvolution of Oral Absorption Model with Dynamic Gastrointestinal Fluid to Predict Regional Rate and Extent of GI Drug Dissolution. *AAPS J*, **22** (1), 3. https://doi.org/10.1208/s12248-019-0385-z

264. Yu, A., Jackson, T., Tsume, Y., Koenigsknecht, M., Wysocki, J., Marciani, L., Amidon, G.L., Frances, A., Baker, J.R., Hasler, W., Wen, B., Pai, A., Sun, D. (2017). Mechanistic Fluid Transport Model to Estimate Gastrointestinal Fluid Volume and Its Dynamic Change Over Time. *AAPS J*, **19** (6), 1682-1690. https://doi.org/10.1208/s12248-017-0145-x

265. Al-Gousous, J., Amidon, G.L., Langguth, P. (2016). Toward Biopredictive Dissolution for Enteric Coated Dosage Forms. *Mol Pharm*, **13** (6), 1927-1936. https://doi.org/10.1021/acs.molpharmaceut.6b00077

266. Litou, C., Turner, D.B., Holmstock, N., Ceulemans, J., Box, K.J., Kostewicz, E., Kuentz, M., Holm, R., Dressman, J. (2020). Combining biorelevant in vitro and in silico tools to investigate the in vivo performance of the amorphous solid dispersion formulation of etravirine in the fed state. *Eur J Pharm Sci*, **149**, 105297. https://doi.org/10.1016/j.ejps.2020.105297

267. Kambayashi, A., Kiyota, T., Fujiwara, M., Dressman, J.B. (2019). PBPK modeling coupled with biorelevant dissolution to forecast the oral performance of amorphous solid dispersion formulations. *Eur J Pharm Sci*, **135**, 83-90. https://doi.org/10.1016/j.ejps.2019.05.013

268. Diaz de Leon-Ortega, R., D'Arcy, D.M., Fotaki, N. (2020). In vitro conditions for performance evaluation of products for intravascular administration: Developing appropriate test media using Amphotericin B as a model drug. *Eur J Pharm Sci*, **143**, 1051-1074. https://doi.org/10.1016/j.ejps.2019.105174

269. Diaz de Leon-Ortega, R., D'Arcy, D.M., Lamprou, D.A., Xue, W.F., Fotaki, N. (2021). In vitro in vivo relations for the parenteral liposomal formulation of Amphotericin B: A biorelevant and clinically relevant approach. *Eur J Pharm Biopharm*, **159**, 188-197. https://doi.org/10.1016/j.ejpb.2020.07.025

270. Litou, C., Patel, N., Turner, D.B., Kostewicz, E., Kuentz, M., Box, K.J., Dressman, J. (2019). Combining biorelevant in vitro and in silico tools to simulate and better understand the in vivo performance of a nano-sized

formulation of aprepitant in the fasted and fed states. *Eur J Pharm Sci*, **138**, 105031. https://doi.org/10.1016/j.ejps.2019.105031

271. Subhani, S., Kim, C., Muniz, P., Rodriguez, M., van Os, S., Suarez, E., Cristofoletti, R., Schmidt, S., Vozmediano, V. (2022). Application of physiologically based absorption and pharmacokinetic modeling in the development process of oral modified release generic products. *Eur J Pharm Biopharm*, **176**, 87-94. https://doi.org/10.1016/j.ejpb.2022.05.007
272. Madny, M.A., Deshpande, P., Tumuluri, V., Borde, P., Sangana, R. (2022). Physiologically Based Biopharmaceutics Model of Vildagliptin Modified Release (MR) Tablets to Predict In Vivo Performance and Establish Clinically Relevant Dissolution Specifications. *AAPS PharmSciTech*, **23** (4), 108. https://doi.org/10.1208/s12249-022-02264-2
273. Tsakalozou, E., Babiskin, A., Zhao, L. (2021). Physiologically-based pharmacokinetic modeling to support bioequivalence and approval of generic products: A case for diclofenac sodium topical gel, 1. *CPT Pharmacometrics Syst Pharmacol*, **10** (5), 399-411. https://doi.org/10.1002/psp4.12600
274. Patel, N., Clarke, J.F., Salem, F., Abdulla, T., Martins, F., Arora, S., Tsakalozou, E., Hodgkinson, A., Arjmandi-Tash, O., Cristea, S., Ghosh, P., Alam, K., Raney, S.G., Jamei, M., Polak, S. (2022). Multi-phase multi-layer mechanistic dermal absorption (MPML MechDermA) model to predict local and systemic exposure of drug products applied on skin. *CPT Pharmacometrics Syst Pharmacol*, **11** (8), 1060-1084. https://doi.org/10.1002/psp4.12814
275. Mittapelly, N., Polak, S. (2022). Modelling and simulation approaches to support formulation optimization, clinical development and regulatory assessment of the topically applied formulations - Nimesulide solution gel case study. *Eur J Pharm Biopharm*, **178**, 140-149. https://doi.org/10.1016/j.ejpb.2022.08.005
276. Tang, C., Ou-Yang, C.X., Chen, W.J., Zou, C., Huang, J., Cui, C., Yang, S., Guo, C., Yang, X.Y., Lin, Y., Pei, Q., Yang, G.P. (2022). Prediction of pharmacokinetic parameters of inhaled indacaterol formulation in healthy volunteers using physiologically-based pharmacokinetic (PBPK) model. *Eur J Pharm Sci*, **168**, 106055. https://doi.org/10.1016/j.ejps.2021.106055
277. Chen, J., You, X., Wu, W., Guo, G., Lin, R., Ke, M., Huang, P., Lin, C. (2023). Application of PBPK modeling in predicting maternal and fetal

pharmacokinetics of levetiracetam during pregnancy. *Eur J Pharm Sci*, **181**, 106349. https://doi.org/10.1016/j.ejps.2022.106349

278. Sia, J.E.V., Lai, X., Wu, X., Zhang, F., Li, H., Cui, C., Liu, D. (2023). Physiologically-based pharmacokinetic modeling to predict drug-drug interactions of dabigatran etexilate and rivaroxaban in the Chinese older adults. *Eur J Pharm Sci*, **182**, 106376. https://doi.org/10.1016/j.ejps.2023.106376
279. Guimaraes, M., Vertzoni, M., Fotaki, N. (2022). Performance Evaluation of Montelukast Pediatric Formulations: Part II - a PBPK Modelling Approach. *AAPS J*, **24** (1), 27. https://doi.org/10.1208/s12248-021-00662-1
280. Pawar, G., Wu, F., Zhao, L., Fang, L., Burckart, G.J., Feng, K., Mousa, Y.M., Al Shoyaib, A., Jones, M.C., Batchelor, H.K. (2023). Integration of Biorelevant Pediatric Dissolution Methodology into PBPK Modeling to Predict In Vivo Performance and Bioequivalence of Generic Drugs in Pediatric Populations: a Carbamazepine Case Study. *AAPS J*, **25** (4), 67. https://doi.org/10.1208/s12248-023-00826-1
281. Rasool, M.F., Ali, S., Khalid, S., Khalid, R., Majeed, A., Imran, I., Saeed, H., Usman, M., Ali, M., Alali, A.S., AlAsmari, A.F., Ali, N., Asiri, A.M., Alasmari, F., Alqahtani, F. (2021). Development and evaluation of physiologically based pharmacokinetic drug-disease models for predicting captopril pharmacokinetics in chronic diseases. *Sci Rep*, **11** (1), 85-89. https://doi.org/10.1038/s41598-021-88154-2
282. Zhao, H., Wei, Y., He, K., Zhao, X., Mu, H., Wen, Q. (2022). Prediction of janagliflozin pharmacokinetics in type 2 diabetes mellitus patients with liver cirrhosis or renal impairment using a physiologically based pharmacokinetic model. *Eur J Pharm Sci*, **179**, 106298. https://doi.org/10.1016/j.ejps.2022.106298
283. Alsenz, J., Kansy, M. (2007). High throughput solubility measurement in drug discovery and development. *Adv Drug Deliv Rev*, **59** (7), 546-567. https://doi.org/10.1016/j.addr.2007.05.007
284. Stocker, M.W., Healy, A.M., Ferguson, S. (2020). Spray Encapsulation as a Formulation Strategy for Drug-Based Room Temperature Ionic Liquids: Exploiting Drug-Polymer Immiscibility to Enable Processing for Solid Dosage Forms. *Mol Pharm*, **17** (9), 3412-3424. https://doi.org/10.1021/acs.molpharmaceut.0c00467

285. Levich, V.G., *Physicochemical Hydrodynamics*. 2nd edition ed. 1962: Prentice-Halls, Englewood Cliffs, N.J., 1962.
286. Healy, A.M., Corrigan, O.I. (1992). Predicting the dissolution rate of ibuprofen-acidic excipient compressed mixtures in reactive media. *Int J Pharm*, **84**, 167-173. https://doi.org/https://doi.org/10.1016/0378-5173(92)90057-9
287. Pavliv, L., Voss, B., Rock, A. (2011). Pharmacokinetics, safety, and tolerability of a rapid infusion of i.v. ibuprofen in healthy adults. *Am J Health Syst Pharm*, **68** (1), 47-51. https://doi.org/10.2146/ajhp100120
288. Legg, T.J., Laurent, A.L., Leyva, R., Kellstein, D. (2014). Ibuprofen sodium is absorbed faster than standard Ibuprofen tablets: results of two open-label, randomized, crossover pharmacokinetic studies. *Drugs R D*, **14** (4), 283-290. https://doi.org/10.1007/s40268-014-0070-8
289. Dewland, P.M., Reader, S., Berry, P. (2009). Bioavailability of ibuprofen following oral administration of standard ibuprofen, sodium ibuprofen or ibuprofen acid incorporating poloxamer in healthy volunteers. *BMC Clin Pharmacol*, **9**, 19. https://doi.org/10.1186/1472-6904-9-19
290. Cristofoletti, R., Dressman, J.B. (2016). Bridging the Gap Between In Vitro Dissolution and the Time Course of Ibuprofen-Mediating Pain Relief. *J Pharm Sci*, **105** (12), 3658-3667. https://doi.org/10.1016/j.xphs.2016.08.024
291. Wagner, J.G., Albert, K.S., Szpunar, G.J., Lockwood, G.F. (1984). Pharmacokinetics of ibuprofen in man IV: Absorption and disposition. *J Pharmacokinet Pharmacodyn*, **12** (4), 381-399. https://doi.org/10.1007/BF01062664
292. Aarons, L., Grennan, D.M., Siddiqui, M. (1983). The binding of ibuprofen to plasma proteins. *Eur J Clin Pharmacol*, **25** (6), 815-818. https://doi.org/10.1007/BF00542526
293. Obach, R.S. (1999). Prediction of human clearance of twenty-nine drugs from hepatic microsomal intrinsic clearance data: An examination of in vitro half-life approach and nonspecific binding to microsomes. *Drug Metab Dispos*, **27** (11), 1350-1359.
294. Levis, K.A., Lane, M.E., Corrigan, O.I. (2003). Effect of buffer media composition on the solubility and effective permeability coefficient of ibuprofen. *Int J Pharm*, **253** (1-2), 49-59. https://doi.org/10.1016/s0378-5173(02)00645-2

295. Klein, S., Butler, J., Hempenstall, J.M., Reppas, C., Dressman, J.B. (2004). Media to simulate the postprandial stomach I. Matching the physicochemical characteristics of standard breakfasts. *J Pharm Pharmacol*, **56** (5), 605-610. https://doi.org/10.1211/0022357023367
296. Baxevanis, F., Kuiper, J., Fotaki, N. (2016). Fed-state gastric media and drug analysis techniques: Current status and points to consider. *Eur J Pharm Biopharm*, **107**, 234-248. https://doi.org/10.1016/j.ejpb.2016.07.013
297. Anwar, S., Fell, J.T., Dickinson, P.A. (2005). An investigation of the disintegration of tablets in biorelevant media. *Int J Pharm*, **290** (1-2), 121-127. https://doi.org/10.1016/j.ijpharm.2004.11.023
298. Késmárky, G., Kenyeres, P., Rábai, M., Tóth, K. (2008). Plasma viscosity: A forgotten variable. *Clin Hemorheol Microcirc*, **39**, 243-246. https://doi.org/10.3233/CH-2008-1088
299. Navas Bachiller, M., Persoons, T., Healy, A.M., D'Arcy, D.M. (2022). Assessing the effect of moderately increasing medium viscosity on the intrinsic dissolution rate and diffusion coefficient of ibuprofen particles. *Br J Pharm*, **7** (2). https://doi.org/10.5920/bjpharm.1130
300. Sarisuta, N., Parrott, E.L. (1982). Relationship of Dissolution Rate to Viscosity of Polymeric Solutions. *J Pharm Sci*, **71** (12), 1375-1380. https://doi.org/https://doi.org/10.1002/jps.2600711216
301. Uebbing, L., Klumpp, L., Webster, G.K., Lobenberg, R. (2017). Justification of disintegration testing beyond current FDA criteria using in vitro and in silico models. *Drug Des Devel Ther*, **11**, 1163-1174. https://doi.org/10.2147/DDDT.S131213
302. Radwan, A., Ebert, S., Amar, A., Munnemann, K., Wagner, M., Amidon, G.L., Langguth, P. (2013). Mechanistic understanding of food effects: water diffusivity in gastrointestinal tract is an important parameter for the prediction of disintegration of solid oral dosage forms. *Mol Pharm*, **10** (6), 2283-2290. https://doi.org/10.1021/mp3006209
303. Shah, A.C., Nelson, K.G. (1987). Mass transport in dissolution kinetics. II: Convective diffusion to assess role of viscosity under conditions of gravitational flow. *J Pharm Sci*, **76** (12), 910-913. https://doi.org/10.1002/jps.2600761214
304. Nelson, K.G., Shah, A.C. (1987). Mass transport in dissolution kinetics I: Convective diffusion to assess the role of fluid viscosity under forced flow

conditions. *J Pharm Sci*, **76** (10), 799-802. https://doi.org/https://doi.org/10.1002/jps.2600761010

305. Darby, G. (2018). Investigating the Effect of Flow Rate and Medium Viscosity on Particulate Dispersion and Dissolution in the USP 4 Flow-Through Dissolution Apparatus., **MSc Dissertation**.
306. Shi, N.Q., Jin, Y., Zhang, Y., Che, X.X., Xiao, X., Cui, G.H., Chen, Y.Z., Feng, B., Li, Z.Q., Qi, X.R. (2018). The Influence of Cellulosic Polymer's Variables on Dissolution/Solubility of Amorphous Felodipine and Crystallization Inhibition from a Supersaturated State. *AAPS PharmSciTech*, **20** (1), 12. https://doi.org/10.1208/s12249-018-1266-y
307. Javeer, S., Amin, P. (2014). Solubility and dissolution enhancement of HPMC - based solid dispersions of carbamazepine by hot-melt extrusion technique. *Asian J Pharm*, **8** (2). https://doi.org/10.4103/0973-8398.134950
308. Tundisi, L.L., Mostaco, G.B., Carricondo, P.C., Petri, D.F.S. (2021). Hydroxypropyl methylcellulose: Physicochemical properties and ocular drug delivery formulations. *Eur J Pharm Sci*, **159**, 105736. https://doi.org/10.1016/j.ejps.2021.105736
309. Shah, N.B., Sheth, B.B. (1976). Effect of Polymers on Dissolution from Drug Suspensions. *J Pharm Sci*, **65** (11), 1618-1623. https://doi.org/https://doi.org/10.1002/jps.2600651114
310. Nielsen, A.L., Pedersen, P.B., Baldursdottir, S., Müllertz, A. (2012). Impact of physiologically relevant viscosity on intrinsic dissolution rate of poorly soluble compounds in simulated gastric media.
311. Zaheer, K., Langguth, P. (2018). Formulation strategy towards minimizing viscosity mediated negative food effect on disintegration and dissolution of immediate release tablets. *Drug Dev Ind Pharm*, **44** (3), 444-451. https://doi.org/10.1080/03639045.2017.1397685
312. Klein, S. (2010). The use of biorelevant dissolution media to forecast the in vivo performance of a drug. *AAPS J*, **12** (3), 397-406. https://doi.org/10.1208/s12248-010-9203-3
313. Hofsass, M.A., Dressman, J. (2020). Suitability of the z-Factor for Dissolution Simulation of Solid Oral Dosage Forms: Potential Pitfalls and Refinements. *J Pharm Sci*, **109** (9), 2735-2745. https://doi.org/10.1016/j.xphs.2020.05.019

314. Psachoulias, D., Vertzoni, M., Goumas, K., Kalioras, V., Beato, S., Butler, J., Reppas, C. (2011). Precipitation in and supersaturation of contents of the upper small intestine after administration of two weak bases to fasted adults. *Pharm Res*, **28** (12), 3145-3158. https://doi.org/10.1007/s11095-011-0506-6

315. Psachoulias, D., Vertzoni, M., Butler, J., Busby, D., Symillides, M., Dressman, J., Reppas, C. (2012). An in vitro methodology for forecasting luminal concentrations and precipitation of highly permeable lipophilic weak bases in the fasted upper small intestine. *Pharm Res*, **29** (12), 3486-3498. https://doi.org/10.1007/s11095-012-0844-z

316. Li, M., Zhang, X., Wu, D., Anand, O., Chen, H., Raines, K., Yu, L. (2021). Understanding In Vivo Dissolution of Immediate Release (IR) Solid Oral Drug Products Containing Weak Acid BCS Class 2 (BCS Class 2a) Drugs. *AAPS J*, **23** (6), 113. https://doi.org/10.1208/s12248-021-00639-0

317. O'Farrell, C., Simmons, M.J.H., Batchelor, H.K., Stamatopoulos, K. (2022). The Effect of Biorelevant Hydrodynamic Conditions on Drug Dissolution from Extended-Release Tablets in the Dynamic Colon Model. *Pharmaceutics*, **14** (10). https://doi.org/10.3390/pharmaceutics14102193

318. Sunesen, V.H., Pedersen, B.L., Kristensen, H.G., Mullertz, A. (2005). In vivo in vitro correlations for a poorly soluble drug, danazol, using the flow-through dissolution method with biorelevant dissolution media. *Eur J Pharm Sci*, **24** (4), 305-313. https://doi.org/10.1016/j.ejps.2004.11.007

319. Weitschies, W., Blume, H., Monnikes, H. (2010). Magnetic marker monitoring: high resolution real-time tracking of oral solid dosage forms in the gastrointestinal tract. *Eur J Pharm Biopharm*, **74** (1), 93-101. https://doi.org/10.1016/j.ejpb.2009.07.007

320. Georgaka, D., Butler, J., Kesisoglou, F., Reppas, C., Vertzoni, M. (2017). Evaluation of Dissolution in the Lower Intestine and Its Impact on the Absorption Process of High Dose Low Solubility Drugs. *Mol Pharm*, **14** (12), 4181-4191. https://doi.org/10.1021/acs.molpharmaceut.6b01129

321. Markopoulos, C., Vertzoni, M., Symillides, M., Kesisoglou, F., Reppas, C. (2015). Two-Stage Single-Compartment Models to Evaluate Dissolution in the Lower Intestine. *J Pharm Sci*, **104** (9), 2986-2997. https://doi.org/10.1002/jps.24485

322. Reppas, C., Karatza, E., Goumas, C., Markopoulos, C., Vertzoni, M. (2015). Characterization of Contents of Distal Ileum and Cecum to Which Drugs/Drug Products are Exposed During Bioavailability/Bioequivalence Studies in Healthy Adults. *Pharm Res*, **32** (10), 3338-3349. https://doi.org/10.1007/s11095-015-1710-6

323. Stamatopoulos, K., Batchelor, H.K., Simmons, M.J.H. (2016). Dissolution profile of theophylline modified release tablets, using a biorelevant Dynamic Colon Model (DCM). *Eur J Pharm Biopharm*, **108**, 9-17. https://doi.org/10.1016/j.ejpb.2016.08.004

324. Stamatopoulos, K., Karandikar, S., Goldstein, M., O'Farrell, C., Marciani, L., Sulaiman, S., Hoad, C.L., Simmons, M.J.H., Batchelor, H.K. (2020). Dynamic Colon Model (DCM): A Cine-MRI Informed Biorelevant In Vitro Model of the Human Proximal Large Intestine Characterized by Positron Imaging Techniques. *Pharmaceutics*, **12** (7). https://doi.org/10.3390/pharmaceutics12070659

325. O'Farrell, C., Hoad, C.L., Stamatopoulos, K., Marciani, L., Sulaiman, S., Simmons, M.J.H., Batchelor, H.K. (2021). Luminal Fluid Motion Inside an In Vitro Dissolution Model of the Human Ascending Colon Assessed Using Magnetic Resonance Imaging. *Pharmaceutics*, **13** (10). https://doi.org/10.3390/pharmaceutics13101545

326. Schutt, M., Stamatopoulos, K., Simmons, M.J.H., Batchelor, H.K., Alexiadis, A. (2020). Modelling and simulation of the hydrodynamics and mixing profiles in the human proximal colon using Discrete Multiphysics. *Comput Biol Med*, **121**, 103819. https://doi.org/10.1016/j.compbiomed.2020.103819

327. Ikuta, S., Nakagawa, H., Kai, T., Sugano, K. (2024). Bicarbonate buffer dissolution test with gentle mechanistic stress for bioequivalence prediction of enteric-coated pellet formulations. *Eur J Pharm Sci*, **192**, 106622. https://doi.org/10.1016/j.ejps.2023.106622

328. Gonzalez-Garcia, I., Mangas-Sanjuan, V., Merino-Sanjuan, M., Alvarez-Alvarez, C., Diaz-Garzon Marco, J., Rodriguez-Bonnin, M.A., Langguth, T., Torrado-Duran, J.J., Langguth, P., Garcia-Arieta, A., Bermejo, M. (2017). IVIVC approach based on carbamazepine bioequivalence studies combination. *Pharmazie*, **72** (8), 449-455. https://doi.org/10.1691/ph.2017.7011

329. Mercuri, A., Pagliari, M., Baxevanis, F., Fares, R., Fotaki, N. (2017). Understanding and predicting the impact of critical dissolution variables for nifedipine immediate release capsules by multivariate data analysis. *Int J Pharm*, **518** (1-2), 41-49. https://doi.org/10.1016/j.ijpharm.2016.12.034

330. Kleberg, K., Jacobsen, J., Mullertz, A. (2010). Characterising the behaviour of poorly water soluble drugs in the intestine: application of biorelevant media for solubility, dissolution and transport studies. *J Pharm Pharmacol*, **62** (11), 1656-1668. https://doi.org/10.1111/j.2042-7158.2010.01023.x

331. Guimaraes, M., Somville, P., Vertzoni, M., Fotaki, N. (2022). Performance Evaluation of Montelukast Pediatric Formulations: Part I-Age-Related In Vitro Conditions. *AAPS J*, **24** (1), 26. https://doi.org/10.1208/s12248-021-00661-2

332. Martir, J., Flanagan, T., Mann, J., Fotaki, N. (2020). Impact of Food and Drink Administration Vehicles on Paediatric Formulation Performance Part 2: Dissolution of Montelukast Sodium and Mesalazine Formulations. *AAPS PharmSciTech*, **21** (7), 287. https://doi.org/10.1208/s12249-020-01815-9

333. Silchenko, S., Nessah, N., Li, J., Li, L.B., Huang, Y., Owen, A.J., Hidalgo, I.J. (2020). In vitro dissolution absorption system (IDAS2): Use for the prediction of food viscosity effects on drug dissolution and absorption from oral solid dosage forms. *Eur J Pharm Sci*, **143**, 105164. https://doi.org/10.1016/j.ejps.2019.105164

334. Radwan, A., Amidon, G.L., Langguth, P. (2012). Mechanistic investigation of food effect on disintegration and dissolution of BCS class III compound solid formulations: the importance of viscosity. *Biopharm Drug Dispos*, **33** (7), 403-416. https://doi.org/10.1002/bdd.1798

335. Wagner, C., Kesisoglou, F., Pepin, X.J.H., Parrott, N., Emami Riedmaier, A. (2021). Use of Physiologically Based Pharmacokinetic Modeling for Predicting Drug-Food Interactions: Recommendations for Improving Predictive Performance of Low Confidence Food Effect Models. *AAPS J*, **23** (4), 85. https://doi.org/10.1208/s12248-021-00601-0

336. Braun, R.J., Parrott, E.L. (1972). Influence of viscosity and solubilization on dissolution rate. *J Pharm Sci*, **61** (2), 175-178. https://doi.org/10.1002/jps.2600610206

337. Lue, B.M., Nielsen, F.S., Magnussen, T., Schou, H.M., Kristensen, K., Jacobsen, L.O., Mullertz, A. (2008). Using biorelevant dissolution to obtain

IVIVC of solid dosage forms containing a poorly-soluble model compound. *Eur J Pharm Biopharm*, **69** (2), 648-657. https://doi.org/10.1016/j.ejpb.2007.12.013

338. Schutt, M., Stamatopoulos, K., Batchelor, H.K., Simmons, M.J.H., Alexiadis, A. (2021). Modelling and Simulation of the Drug Release from a Solid Dosage Form in the Human Ascending Colon: The Influence of Different Motility Patterns and Fluid Viscosities. *Pharmaceutics*, **13** (6). https://doi.org/10.3390/pharmaceutics13060859
339. Adhikari, A., Seo, P.R., Polli, J.E. (2022). Characterization of Dissolution-Permeation System using Hollow Fiber Membrane Module and Utility to Predict in Vivo Drug Permeation Across BCS Classes. *J Pharm Sci*, **111** (11), 3075-3087. https://doi.org/10.1016/j.xphs.2022.07.002
340. O'Dwyer, P.J., Box, K.J., Koehl, N.J., Bennett-Lenane, H., Reppas, C., Holm, R., Kuentz, M., Griffin, B.T. (2020). Novel Biphasic Lipolysis Method To Predict in Vivo Performance of Lipid-Based Formulations. *Mol Pharm*, **17** (9), 3342-3352. https://doi.org/10.1021/acs.molpharmaceut.0c00427
341. van der Zwaan, I., Frenning, G. (2023). A new modelling approach for dissolution of polydisperse powders. *Int J Pharm*, **633**, 122626. https://doi.org/10.1016/j.ijpharm.2023.122626
342. Polli, J.E. (2022). A Simple One-Parameter Percent Dissolved Versus Time Dissolution Equation that Accommodates Sink and Non-sink Conditions via Drug Solubility and Dissolution Volume. *AAPS J*, **25** (1), 1. https://doi.org/10.1208/s12248-022-00765-3
343. Varghese, S., Ghoroi, C. (2017). Improving the wetting and dissolution of ibuprofen using solventless co-milling. *Int J Pharm*, **533** (1), 145-155. https://doi.org/10.1016/j.ijpharm.2017.09.062
344. Lindfors, L., Jonsson, M., Weibull, E., Brasseur, J.G., Abrahamsson, B. (2015). Hydrodynamic Effects on Drug Dissolution and Deaggregation in the Small Intestine-A Study with Felodipine as a Model Drug. *J Pharm Sci*, **104** (9), 2969-2976. https://doi.org/10.1002/jps.24487
345. Serrano, D.R., Persoons, T., D'Arcy, D.M., Galiana, C., Dea-Ayuela, M.A., Healy, A.M. (2016). Modelling and shadowgraph imaging of cocrystal dissolution and assessment of in vitro antimicrobial activity for sulfadimidine/4-aminosalicylic acid cocrystals. *Eur J Pharm Sci*, **89**, 125-136. https://doi.org/10.1016/j.ejps.2016.04.030

346. Markl, D., Strobel, A., Schlossnikl, R., Botker, J., Bawuah, P., Ridgway, C., Rantanen, J., Rades, T., Gane, P., Peiponen, K.E., Zeitler, J.A. (2018). Characterisation of pore structures of pharmaceutical tablets: A review. *Int J Pharm*, **538** (1-2), 188-214. https://doi.org/10.1016/j.ijpharm.2018.01.017

347. So, C., Narang, A.S., Mao, C. (2021). Modeling the Tablet Disintegration Process Using the Finite Difference Method. *J Pharm Sci*, **110** (11), 3614-3622. https://doi.org/10.1016/j.xphs.2021.07.001

348. Nakamura, K., Kambayashi, A., Onoue, S. (2022). Quantitative assessment of disintegration rate is important for predicting the oral absorption of solid dosage forms containing poorly soluble weak base drugs. *Eur J Pharm Biopharm*, **180**, 23-32. https://doi.org/10.1016/j.ejpb.2022.09.017

349. Taupitz, T., Dressman, J.B., Klein, S. (2013). In vitro tools for evaluating novel dosage forms of poorly soluble, weakly basic drugs: case example ketoconazole. *J Pharm Sci*, **102** (10), 3645-3652. https://doi.org/10.1002/jps.23666

350. Salehi, N., Kuminek, G., Al-Gousous, J., Sperry, D.C., Greenwood, D.E., Waltz, N.M., Amidon, G.L., Ziff, R.M., Amidon, G.E. (2021). Improving Dissolution Behavior and Oral Absorption of Drugs with pH-Dependent Solubility Using pH Modifiers: A Physiologically Realistic Mass Transport Analysis. *Mol Pharm*, **18** (9), 3326-3341. https://doi.org/10.1021/acs.molpharmaceut.1c00262

351. Sinko, P.D., Salehi, N., Halseth, T., Meyer, P.J., Amidon, G.L., Ziff, R.M., Amidon, G.E. (2024). Particle Size, Dose, and Confinement Affect Passive Diffusion Flux through the Membrane Concentration Boundary Layer. *Mol Pharm*, **21**, 201-215. https://doi.org/https://doi.org/10.1021/acs.molpharmaceut.3c00761

352. Liu, X., Zhong, C., Fletcher, D.F., Langrish, T.A.G. (2023). Simulating Tablet Dissolution Using Computational Fluid Dynamics and Experimental Modeling. *Processes*, **11** (2). https://doi.org/10.3390/pr11020505

353. Kubinski, A.M., Shivkumar, G., Georgi, R.A., George, S., Reynolds, J., Sosa, R.D., Ju, T.R. (2023). Predictive Drug Release Modeling Across Dissolution Apparatuses I and II using Computational Fluid Dynamics. *J Pharm Sci*, **112** (3), 808-819. https://doi.org/10.1016/j.xphs.2022.10.027

354. Lou, H., Hageman, M.J. (2021). Investigating the Influence of Tablet Location Inside Dissolution Test Apparatus on Polymer Erosion and Drug Release of a

Surface-Erodible Sustained-Release Tablet Using Computational Simulation Methods. *AAPS PharmSciTech*, **22** (3), 99. https://doi.org/10.1208/s12249-021-01979-y

355. Yoshida, H., Teruya, K., Abe, Y., Furuishi, T., Fukuzawa, K., Yonemochi, E., Izutsu, K.I. (2021). Altered Media Flow and Tablet Position as Factors of How Air Bubbles Affect Dissolution of Disintegrating and Non-disintegrating Tablets Using a USP 4 Flow-Through Cell Apparatus. *AAPS PharmSciTech*, **22** (7), 227. https://doi.org/10.1208/s12249-021-02117-4
356. Yokoyama, R., Kimura, G., Schleputz, C.M., Huwyler, J., Puchkov, M. (2018). Modeling of Disintegration and Dissolution Behavior of Mefenamic Acid Formulation Using Numeric Solution of Noyes-Whitney Equation with Cellular Automata on Microtomographic and Algorithmically Generated Surfaces. *Pharmaceutics*, **10** (4). https://doi.org/10.3390/pharmaceutics10040259
357. Yokoyama, R., Kimura, G., Huwyler, J., Hosoya, K.I., Puchkov, M. (2020). Impact of Insoluble Separation Layer Mechanical Properties on Disintegration and Dissolution Kinetics of Multilayer Tablets. *Pharmaceutics*, **12** (6). https://doi.org/10.3390/pharmaceutics12060495
358. Lennernas, H., Aarons, L., Augustijns, P., Beato, S., Bolger, M., Box, K., Brewster, M., Butler, J., Dressman, J., Holm, R., Julia Frank, K., Kendall, R., Langguth, P., Sydor, J., Lindahl, A., McAllister, M., Muenster, U., Mullertz, A., Ojala, K., Pepin, X., Reppas, C., Rostami-Hodjegan, A., Verwei, M., Weitschies, W., Wilson, C., Karlsson, C., Abrahamsson, B. (2014). Oral biopharmaceutics tools - time for a new initiative - an introduction to the IMI project OrBiTo. *Eur J Pharm Sci*, **57**, 292-299. https://doi.org/10.1016/j.ejps.2013.10.012
359. Yu, L.X., Amidon, G., Khan, M.A., Hoag, S.W., Polli, J., Raju, G.K., Woodcock, J. (2014). Understanding pharmaceutical quality by design. *AAPS J*, **16** (4), 771-783. https://doi.org/10.1208/s12248-014-9598-3
360. Farhan, N., Cristofoletti, R., Basu, S., Kim, S., Lingineni, K., Jiang, S., Brown, J.D., Fang, L.L., Lesko, L.J., Schmidt, S. (2021). Physiologically-based pharmacokinetics modeling to investigate formulation factors influencing the generic substitution of dabigatran etexilate. *CPT Pharmacometrics Syst Pharmacol*, **10** (3), 199-210. https://doi.org/10.1002/psp4.12589
361. Klumpp, L., Dressman, J. (2020). Physiologically based pharmacokinetic model outputs depend on dissolution data and their input: Case examples

glibenclamide and dipyridamole. *Eur J Pharm Sci*, **151**, 105380. https://doi.org/10.1016/j.ejps.2020.105380

362. Al-Tabakha, M.M., Alomar, M.J. (2020). In Vitro Dissolution and in Silico Modeling Shortcuts in Bioequivalence Testing. *Pharmaceutics*, **12** (1), 45. https://doi.org/10.3390/pharmaceutics12010045

363. Ibarra, M., Valiante, C., Sopena, P., Schiavo, A., Lorier, M., Vazquez, M., Fagiolino, P. (2018). Integration of in vitro biorelevant dissolution and in silico PBPK model of carvedilol to predict bioequivalence of oral drug products. *Eur J Pharm Sci*, **118**, 176-182. https://doi.org/10.1016/j.ejps.2018.03.032

364. Kushwah, V., Arora, S., Tamas Katona, M., Modhave, D., Frohlich, E., Paudel, A. (2021). On Absorption Modeling and Food Effect Prediction of Rivaroxaban, a BCS II Drug Orally Administered as an Immediate-Release Tablet. *Pharmaceutics*, **13** (2). https://doi.org/10.3390/pharmaceutics13020283

365. Kourentas, A., Vertzoni, M., Barmpatsalou, V., Augustijns, P., Beato, S., Butler, J., Holm, R., Ouwerkerk, N., Rosenberg, J., Tajiri, T., Tannergren, C., Symillides, M., Reppas, C. (2018). The BioGIT System: a Valuable In Vitro Tool to Assess the Impact of Dose and Formulation on Early Exposure to Low Solubility Drugs After Oral Administration. *AAPS J*, **20** (4), 71. https://doi.org/10.1208/s12248-018-0231-8

366. Zoller, L., Avdeef, A., Karlsson, E., Borde, A., Carlert, S., Saal, C., Dressman, J. (2023). A comparison of USP 2 and microDISS Profiler apparatus for studying dissolution phenomena of ibuprofen and its salts. *Eur J Pharm Sci*, **193**, 106684. https://doi.org/10.1016/j.ejps.2023.106684

367. Mukherjee, D., Chiney, M.S., Shao, X., Ju, T.R., Shebley, M., Marroum, P. (2022). Physiologically based pharmacokinetic modeling and simulations to inform dissolution specifications and clinical relevance of release rates on elagolix exposure. *Biopharm Drug Dispos*, **43** (3), 98-107. https://doi.org/10.1002/bdd.2315

Appendix 1

Calibration curves of ibuprofen API in a UV-Vis spectrophotometer for the dissolution studies presented in Chapter 3

Calibration curves for the dissolution tests of ibuprofen API were carried out by preparing dilutions of ibuprofen powder in pH 6.8 phosphate buffer with concentrations ranging from 1 µg ml^{-1} to 30 µg ml^{-1}. Samples from the FTA tests where a mass of 5 mg was used were analysed at 222 nm in a UV-Vis spectrophotometer (**Figure A.1.1**). Samples from the FTA tests where a mass of 50 mg was used and from the paddle apparatus were analysed at 264 nm. In this case, the concentration range was from 30 µg ml^{-1} to 600 µg ml^{-1} (**Figure A.1.2**). Samples from tests carried out in 0.1 M HCl in both the FTA and paddle apparatus were analysed with the calibration curve in **Figure A.1.3**. Ibuprofen powder was dissolved in 0.1 M HCl to obtain a range of concentrations from 0.3 µg ml^{-1} to 40 µg ml^{-1} and analysed at 222 nm in a UV-Vis spectrophotometer. All media contained 0.003% w/v Tween 20.

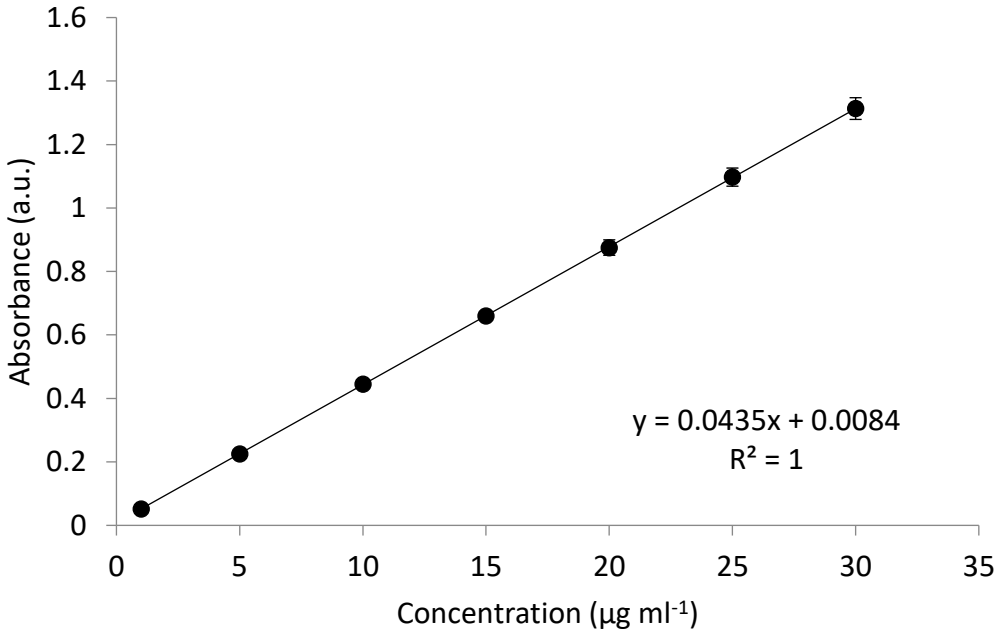

Figure A.1.1. Mean absorbance (±SD) of ibuprofen API at concentrations of 1 µg ml^{-1} to 30 µg ml^{-1} in pH 6.8 phosphate buffer containing 0.003% w/v Tween 20 at 222 nm (n = 3).

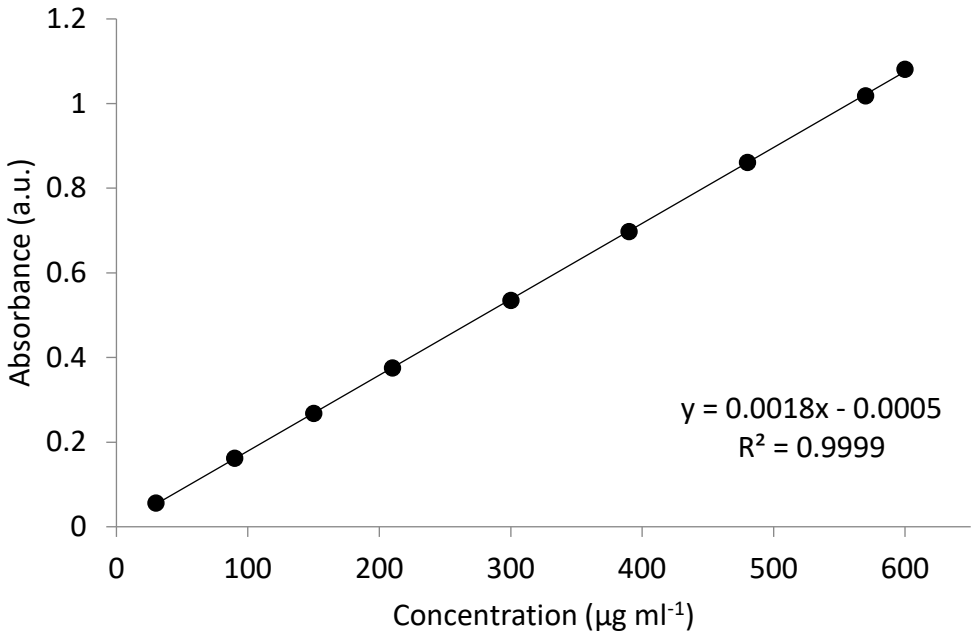

Figure A.1.2. Mean absorbance (±SD) of ibuprofen API at concentrations of 30 µg ml^{-1} to 600 µg ml^{-1} in pH 6.8 phosphate buffer containing 0.003% w/v Tween 20 at 264 nm (n = 3).

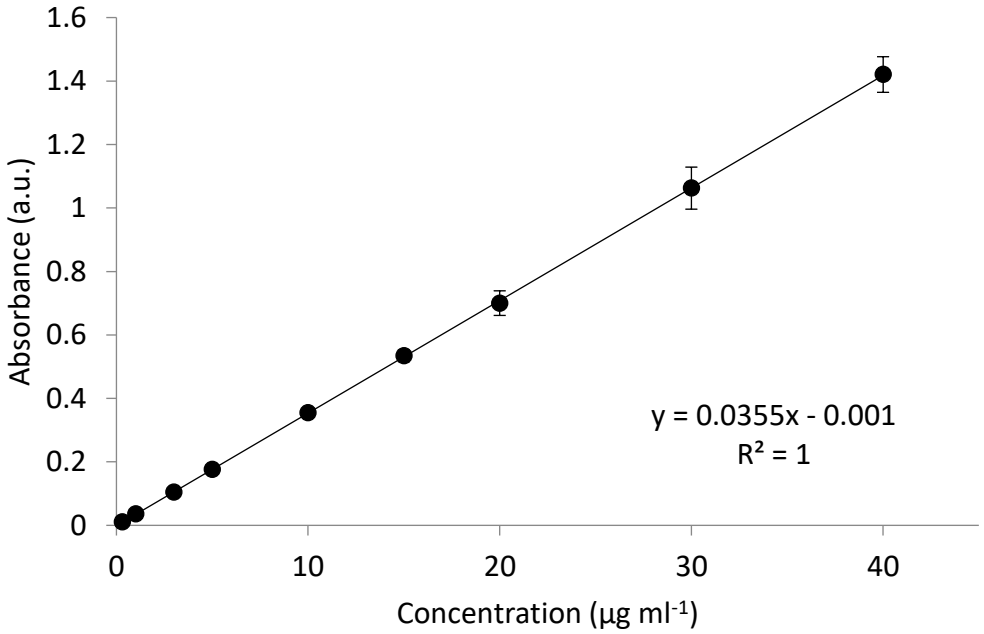

Figure A.1.3. Mean absorbance (±SD) of ibuprofen API at concentrations of 0.3 µg ml^{-1} to 40 µg ml^{-1} in 0.1 M HCl containing 0.003% w/v Tween 20 at 222 nm (n = 3).

Calibration curves of ibuprofen API in a UV-Vis spectrophotometer for the FTA dissolution studies presented in Chapter 4

Calibration curves for the dissolution tests in the FTA were carried out by preparing dilutions of ibuprofen powder in the corresponding media. Concentrations ranged from 0.1 µg ml^{-1} to 30 µg ml^{-1} in pH 6.8 phosphate buffer media without VEAs (**Figure A.1.4**), with 0.3% w/v HPMC (**Figure A.1.5**), with 1.05% w/v HPMC (**Figure A.1.6**), with 25% w/v sucrose (**Figure A.1.7**) or with 59% w/v sucrose (**Figure A.1.8**). Concentrations ranged from 0.3 µg ml^{-1} to 20 µg ml^{-1} in 0.1 M HCl media without VEAs (**Figure A.1.9**), with 0.3% w/v HPMC (**Figure A.1.10**), with 1.05% w/v HPMC (**Figure A.1.11**) or with 25% w/v sucrose (**Figure A.1.12**). Samples were analysed at 222 nm in a UV-Vis spectrophotometer.

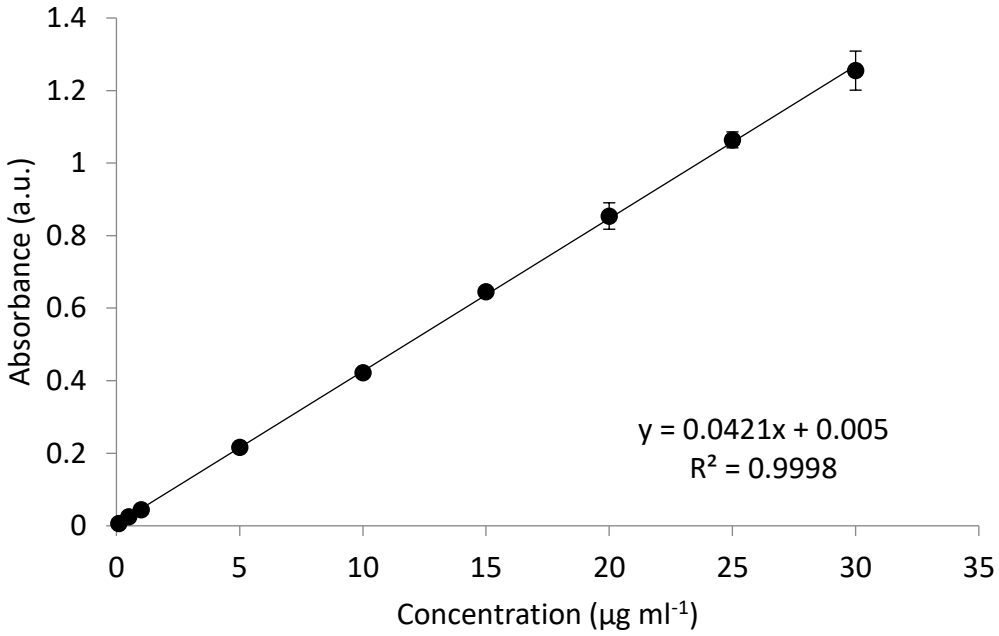

Figure A.1.4. Mean absorbance (±SD) of ibuprofen API at concentrations of 0.1 µg ml^{-1} to 30 µg ml^{-1} in pH 6.8 phosphate buffer containing 0.003% w/v Tween 20 at 222 nm (n = 3).

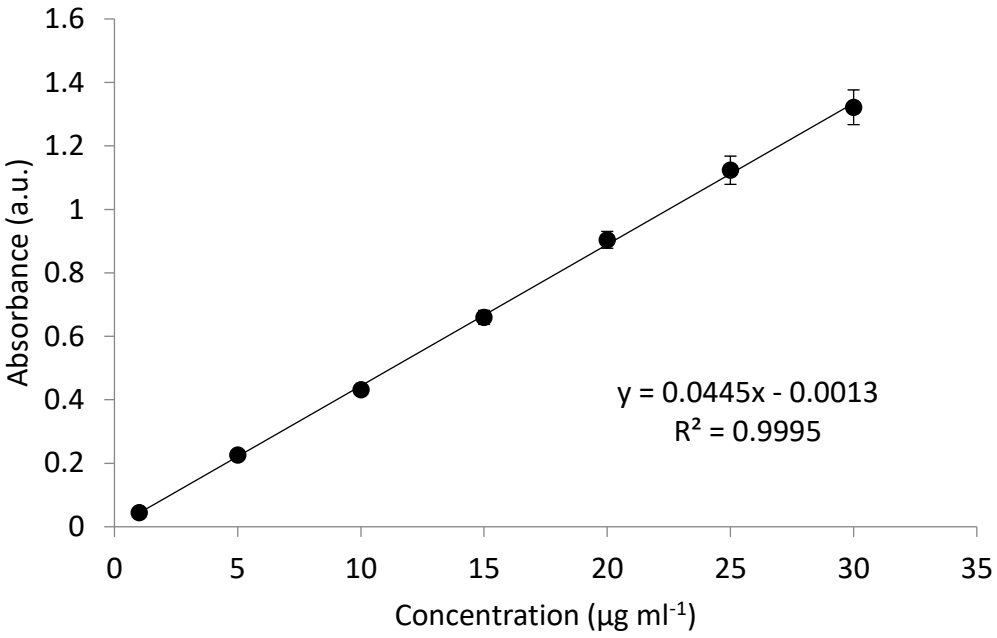

Figure A.1.5. Mean absorbance (±SD) of ibuprofen API at concentrations of 1 µg ml^{-1} to 30 µg ml^{-1} in pH 6.8 phosphate buffer containing 0.003% w/v Tween 20 and 0.3% w/v HPMC at 222 nm (n = 3).

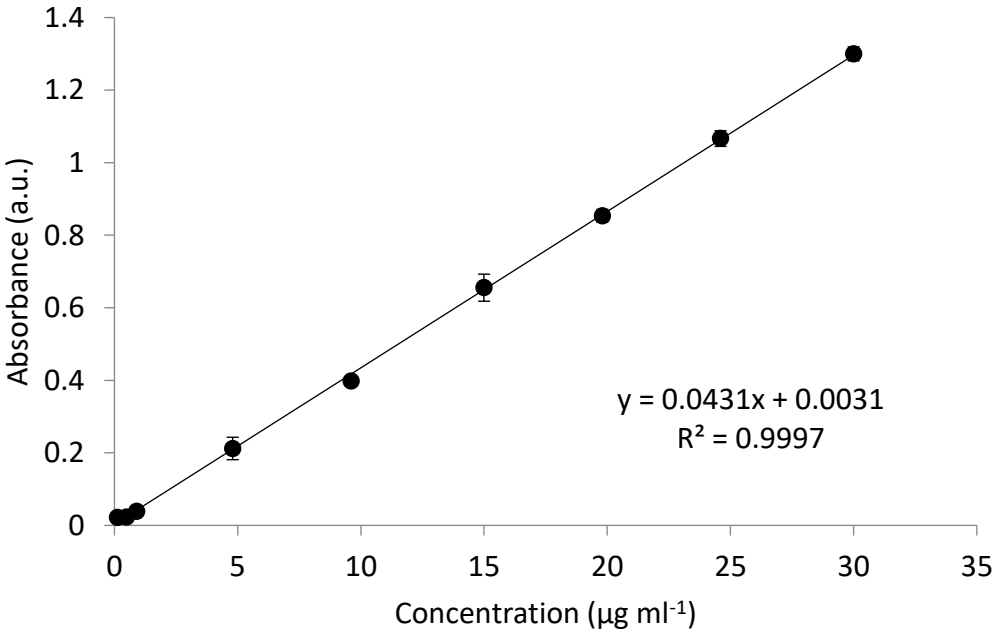

Figure A.1.6. Mean absorbance (±SD) of ibuprofen API at concentrations of 0.1 µg ml^{-1} to 30 µg ml^{-1} in pH 6.8 phosphate buffer containing 0.003% w/v Tween 20 and 1.05% w/v HPMC at 222 nm (n = 3).

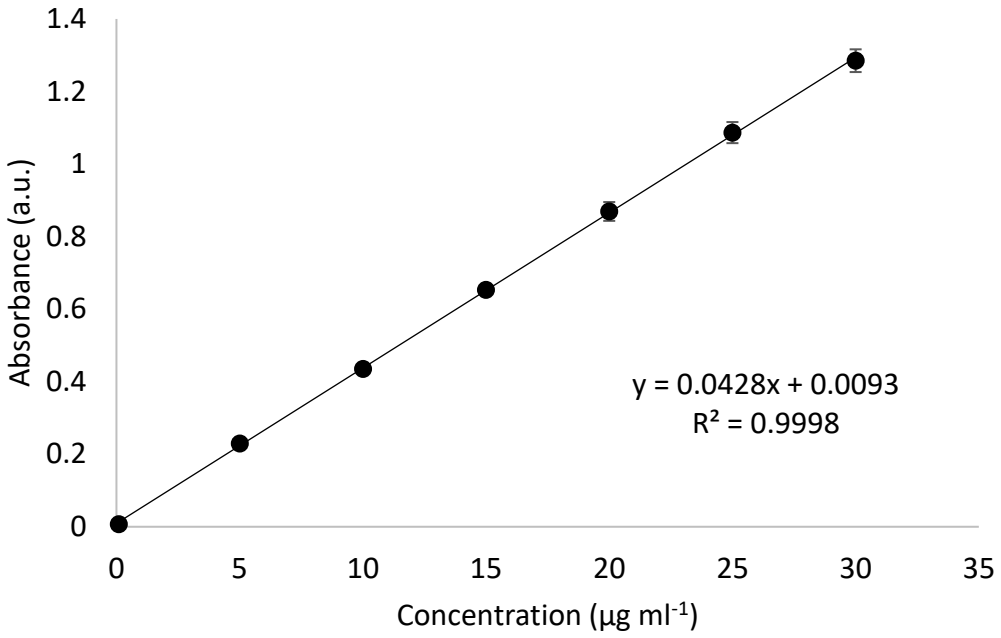

Figure A.1.7. Mean absorbance (±SD) of ibuprofen API at concentrations of 0.1 µg ml^{-1} to 30 µg ml^{-1} in pH 6.8 phosphate buffer containing 0.003% w/v Tween 20 and 25% w/v sucrose at 222 nm (n = 3).

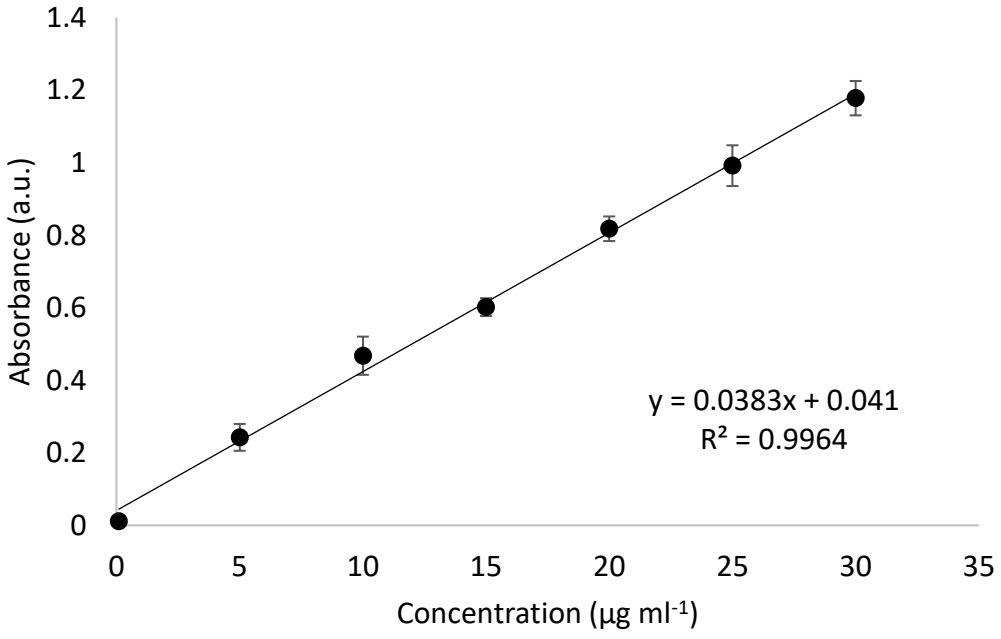

Figure A.1.8. Mean absorbance (±SD) of ibuprofen API at concentrations of 0.1 µg ml^{-1} to 30 µg ml^{-1} in pH 6.8 phosphate buffer containing 0.003% w/v Tween 20 and 59% w/v sucrose at 222 nm (n = 3).

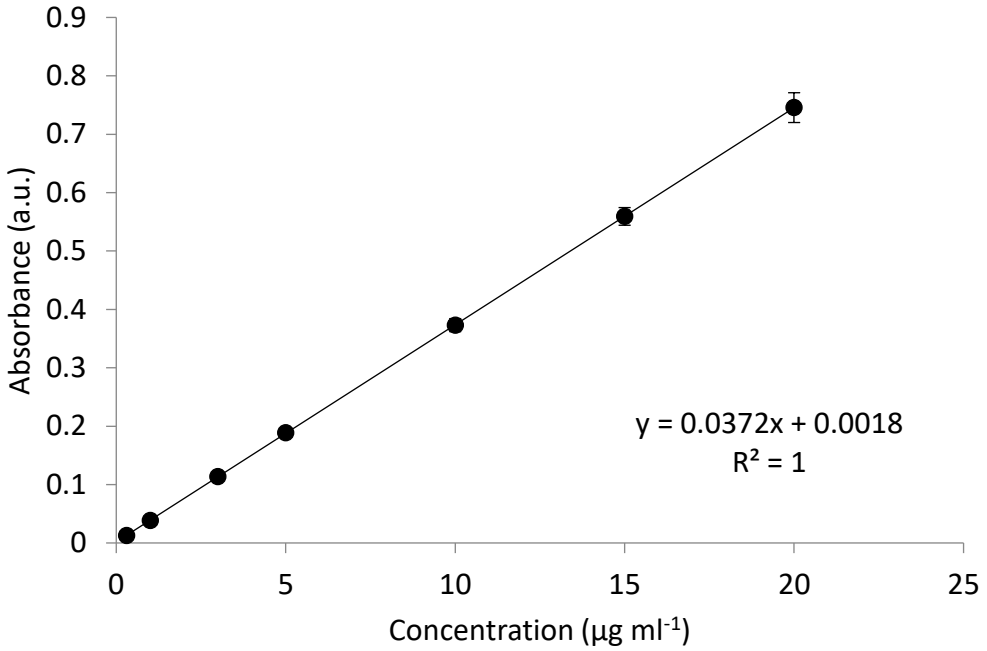

Figure A.1.9. Mean absorbance (±SD) of ibuprofen API at concentrations of 0.3 µg ml^{-1} to 20 µg ml^{-1} 0.1 M HCl containing 0.003% w/v Tween 20 at 222 nm (n = 3).

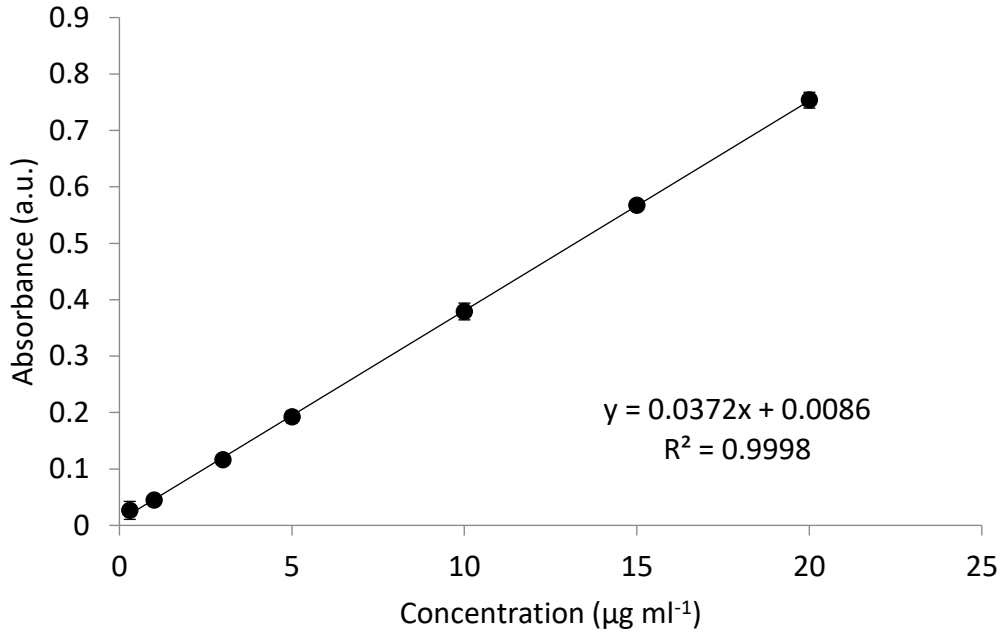

Figure A.1.10. Mean absorbance (±SD) of ibuprofen API at concentrations of 0.3 µg ml^{-1} to 20 µg ml^{-1} in 0.1 M HCl containing 0.003% w/v Tween 20 and 0.3% w/v HPMC at 222 nm (n = 3).

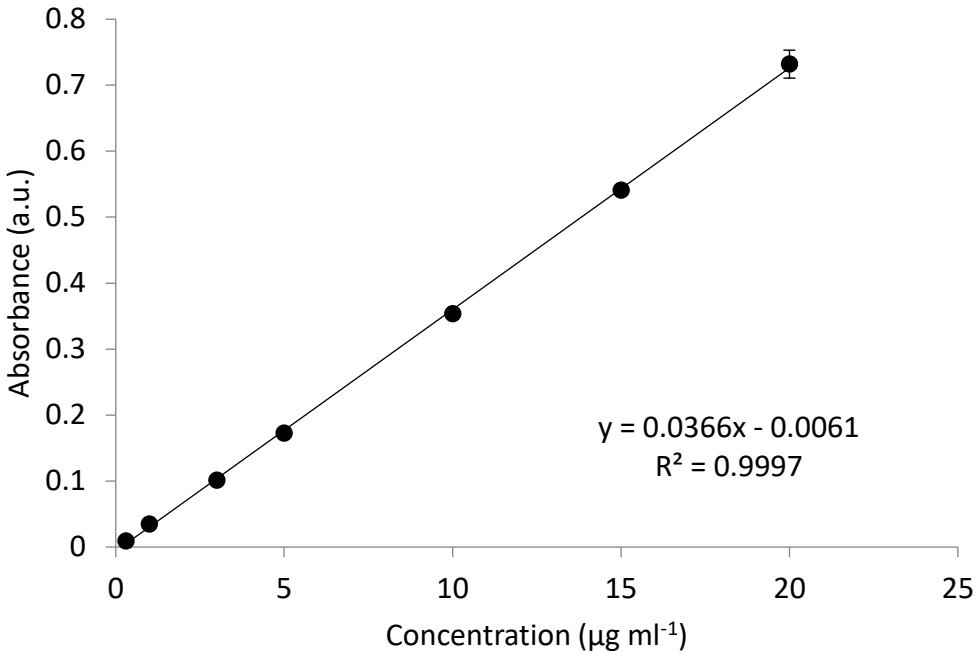

Figure A.1.11. Mean absorbance (±SD) of ibuprofen API at concentrations of 0.3 µg ml^{-1} to 20 µg ml^{-1} in 0.1 M HCl containing 0.003% w/v Tween 20 and 1.05% w/v HPMC at 222 nm (n = 3).

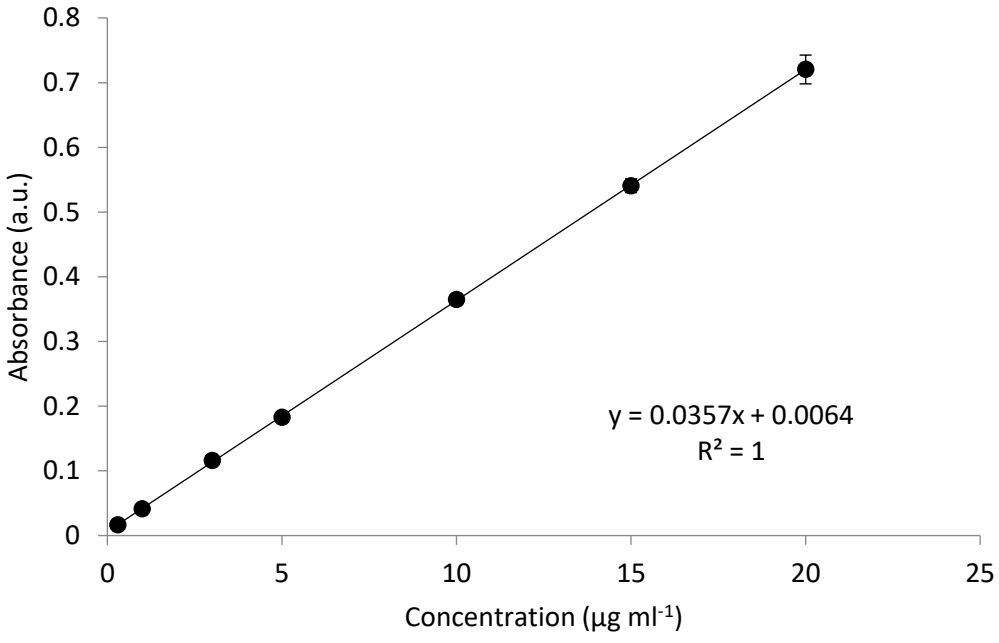

Figure A.1.12. Mean absorbance (±SD) of ibuprofen API at concentrations of 0.3 µg ml^{-1} to 20 µg ml^{-1} in 0.1 M HCl containing 0.003% w/v Tween 20 and 25% w/v sucrose at 222 nm (n = 3).

Calibration curves of ibuprofen API in a UV-Vis spectrophotometer for the paddle apparatus dissolution studies presented in Chapter 4

Calibration curves for the dissolution tests in the paddle apparatus were carried out by preparing dilutions of ibuprofen powder in the corresponding media. Concentrations ranged from 9 µg ml^{-1} to 150 µg ml^{-1} in pH 6.8 phosphate buffer media without VEAs (**Figure A.1.13**), with 0.3% w/v HPMC (**Figure A.1.14**) or with 1.05% w/v HPMC (**Figure A.1.15**). Concentrations ranged from 0.3 µg ml^{-1} to 20 µg ml^{-1} in 0.1 M HCl media without VEAs (**Figure A.1.16**), with 0.3% w/v HPMC (**Figure A.1.17**) or with 1.05% w/v HPMC (**Figure A.1.18**). Samples were filtered through a PTFE filter before analysis to simulate the sampling procedure during dissolution tests. Samples were analysed at 264 nm if in pH 6.8 phosphate buffer media (with or without HPMC) or at 222 nm if in 0.1 M HCl media (with or without HPMC) in a UV-Vis spectrophotometer.

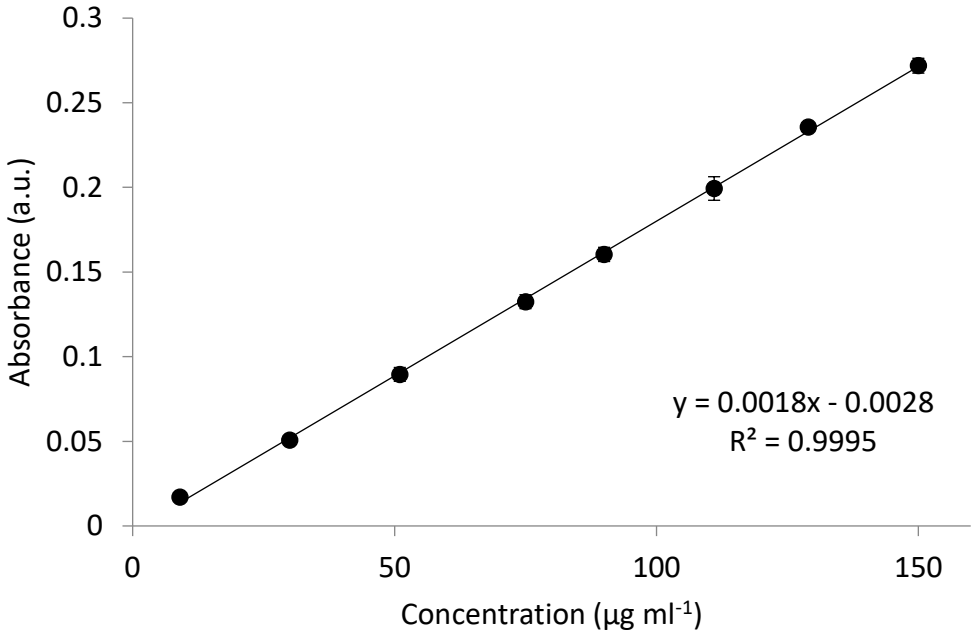

Figure A.1.13. Mean absorbance (±SD) of ibuprofen API at concentrations of 9 µg ml^{-1} to 150 µg ml^{-1} in pH 6.8 phosphate buffer containing 0.003% w/v Tween 20 at 264 nm (n = 3).

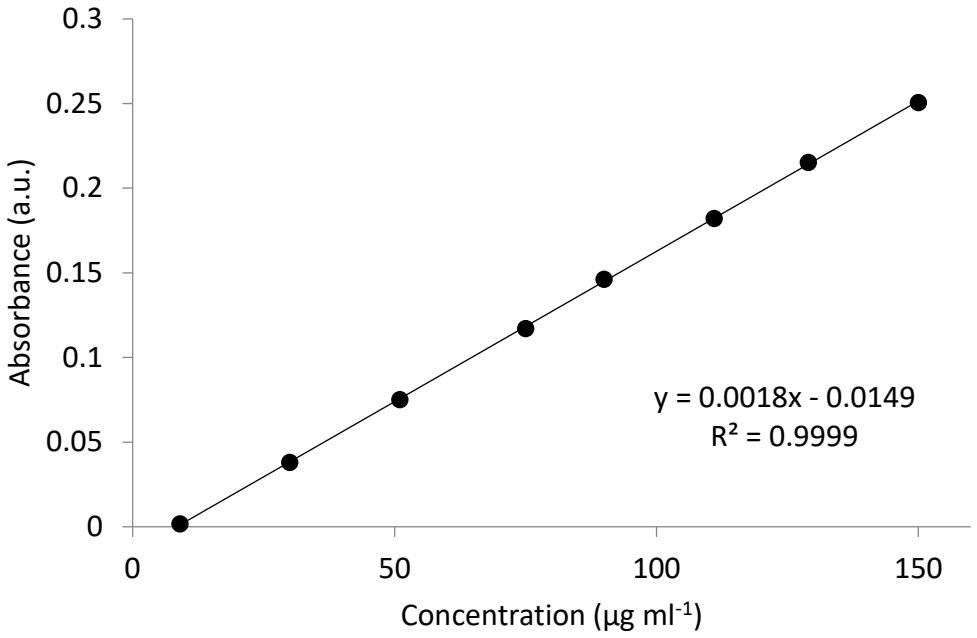

Figure A.1.14. Mean absorbance (±SD) of ibuprofen API at concentrations of 9 µg ml^{-1} to 150 µg ml^{-1} in pH 6.8 phosphate buffer containing 0.003% w/v Tween 20 and 0.3% w/v HPMC at 264 nm (n = 3).

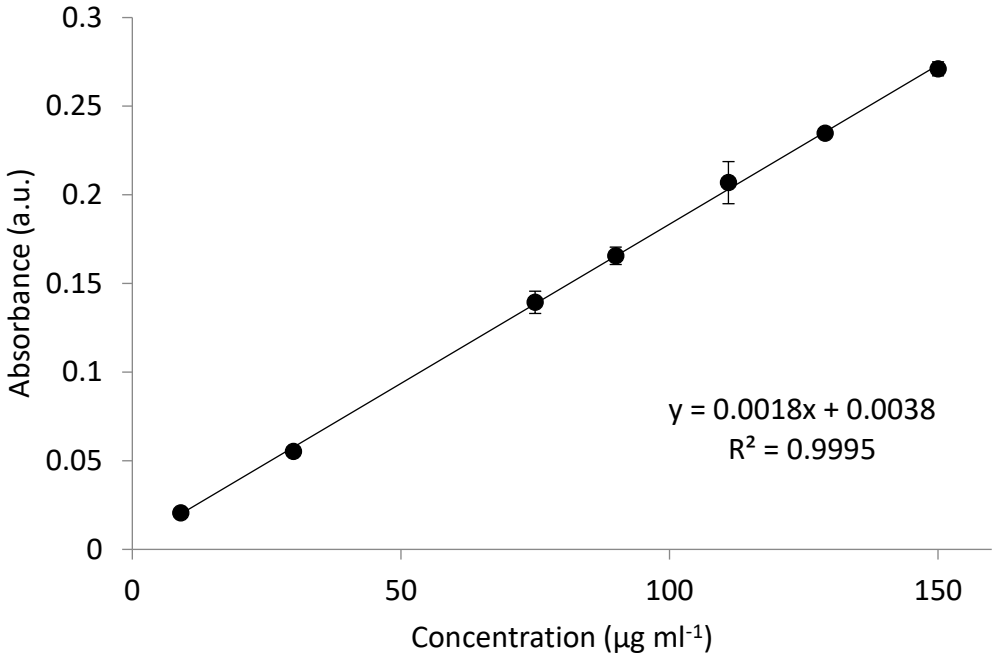

Figure A.1.15. Mean absorbance (±SD) of ibuprofen API at concentrations of 9 µg ml^{-1} to 150 µg ml^{-1} in pH 6.8 phosphate buffer containing 0.003% w/v Tween 20 and 1.05% w/v HPMC at 264 nm (n = 3).

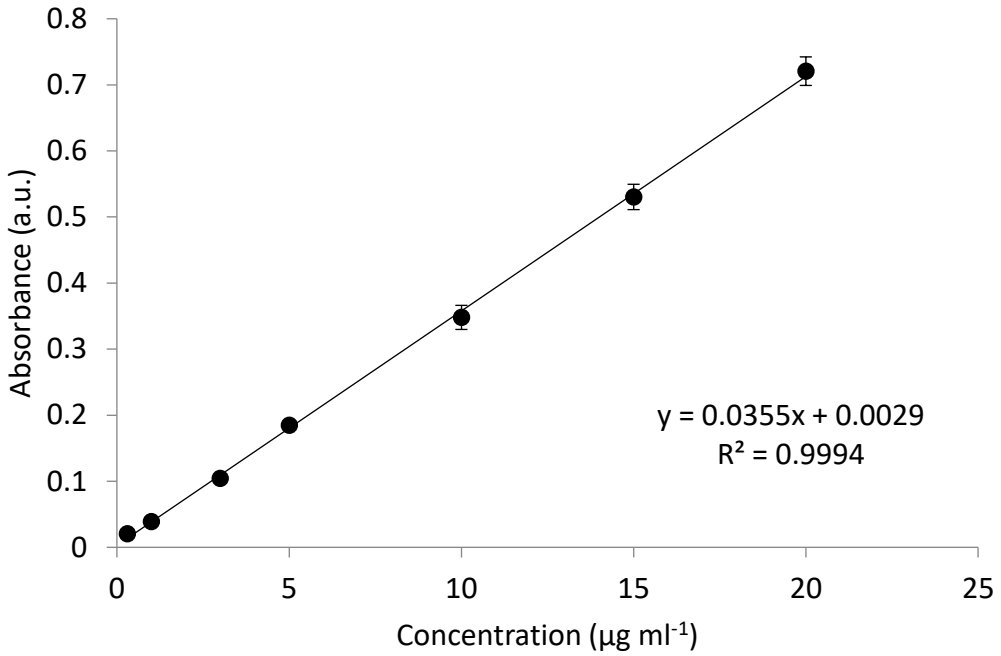

Figure A.1.16. Mean absorbance (±SD) of ibuprofen API at concentrations of 0.3 µg ml^{-1} to 20 µg ml^{-1} in 0.1 M HCl containing 0.003% w/v Tween 20 at 222 nm (n = 3).

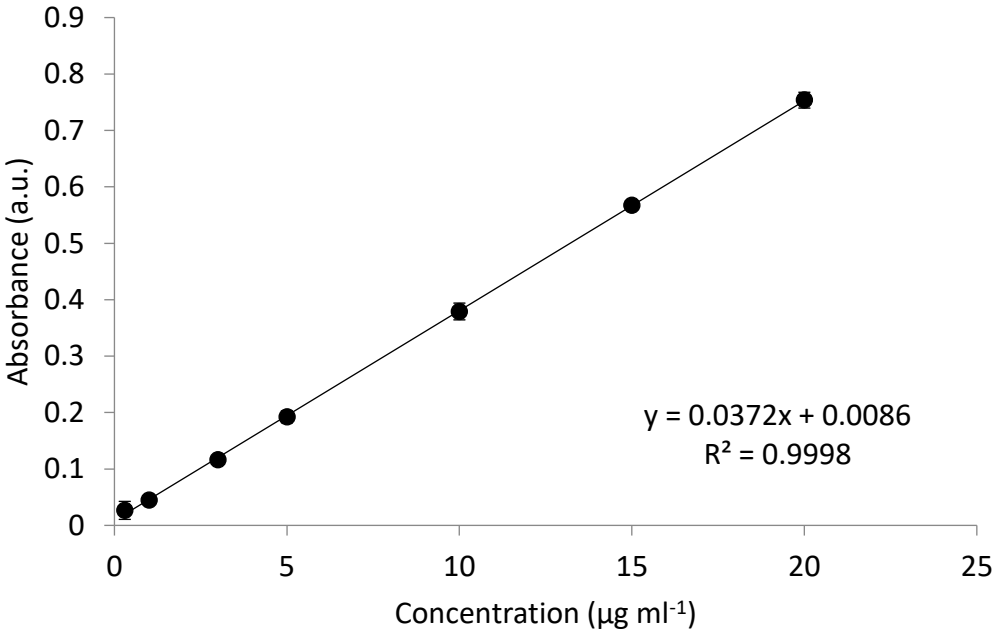

Figure A.1.17. Mean absorbance (±SD) of ibuprofen API at concentrations of 0.3 µg ml^{-1} to 20 µg ml^{-1} in 0.1 M HCl containing 0.003% w/v Tween 20 and 0.3% w/v HPMC at 222 nm (n = 3).

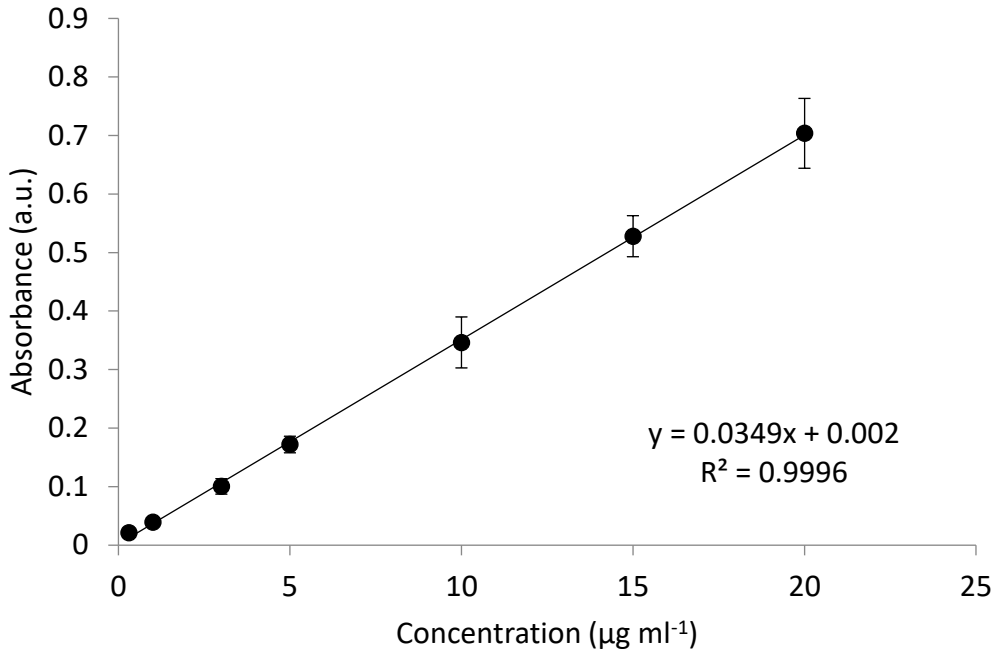

Figure A.1.18. Mean absorbance (±SD) of ibuprofen API at concentrations of 0.3 µg ml^{-1} to 20 µg ml^{-1} in 0.1 M HCl containing 0.003% w/v Tween 20 and 1.05% w/v HPMC at 222 nm (n = 3).

Calibration curves in HPLC for dissolution studies of ibuprofen tablets presented in Chapter 5

Calibration curves were obtained by preparing serial dilutions of ibuprofen in either (a) pH 6.8 phosphate buffer (**Figure A.1.19**), (b) pH 6.8 phosphate buffer with 1.05% w/v HPMC (**Figure A.1.20**) or (c) pH 6.8 phosphate buffer with 59% w/v sucrose (**Figure A.1.21**) ranging from 3 to 600 µg ml^{-1}. The HPLC and column system described in section "2.3.8.4. Analysis of the samples" were used. The same mobile phase, flow rate, injection volume and run time were applied. Detection was carried out with a Waters 2996 photodiode array detector at 220 nm.

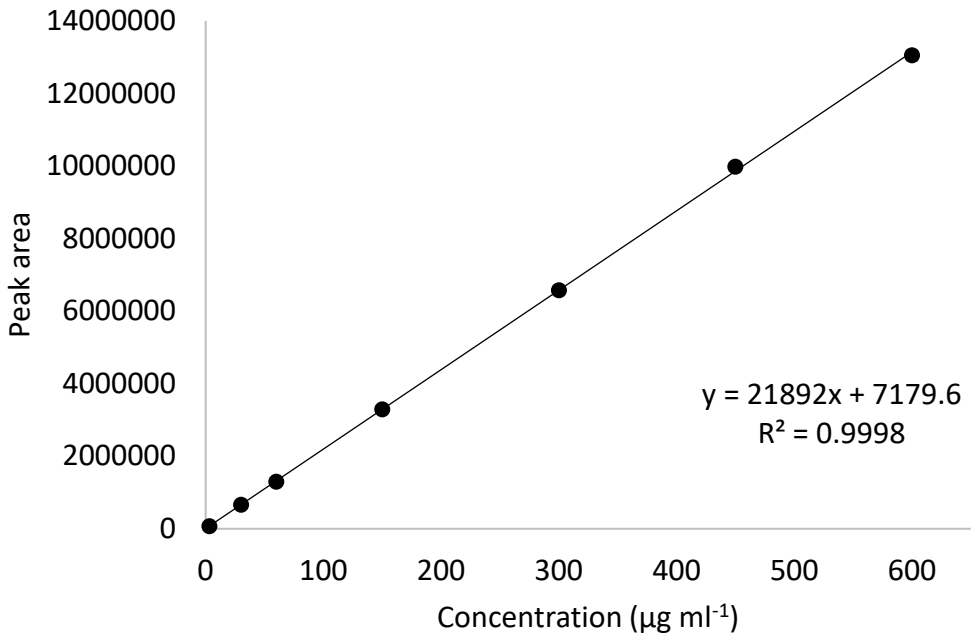

Figure A.1.19. Mean absorbance (±SD) of ibuprofen API at concentrations of 3 µg ml^{-1} to 600 µg ml^{-1} in pH 6.8 phosphate buffer containing 0.003% w/v Tween 20 at 220 nm (n = 3).

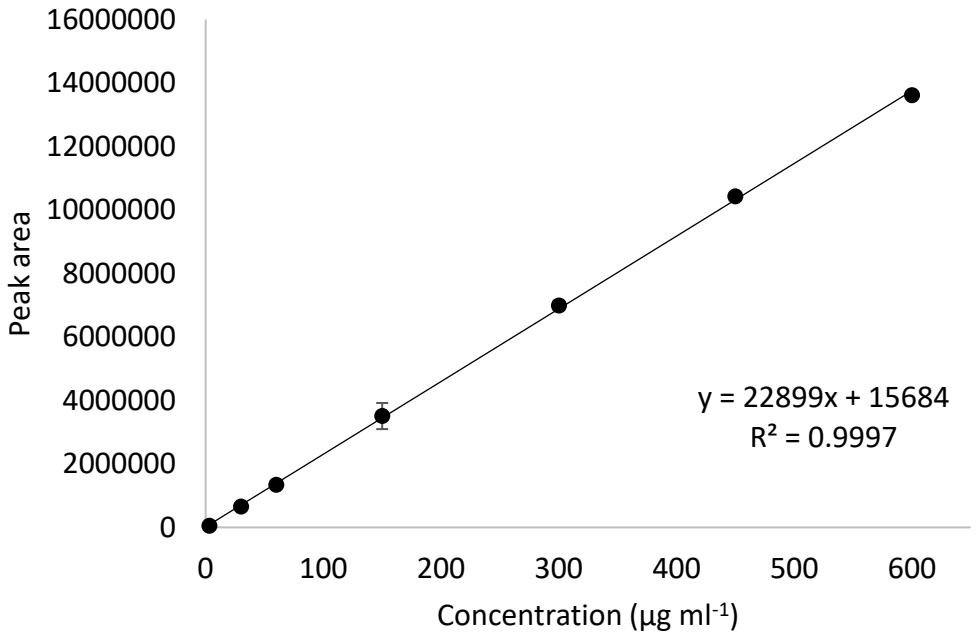

Figure A.1.20. Mean absorbance (±SD) of ibuprofen API at concentrations of 3 µg ml^{-1} to 600 µg ml^{-1} in pH 6.8 phosphate buffer containing 0.003% w/v Tween 20 and 1.05% w/v HPMC at 220 nm (n = 3).

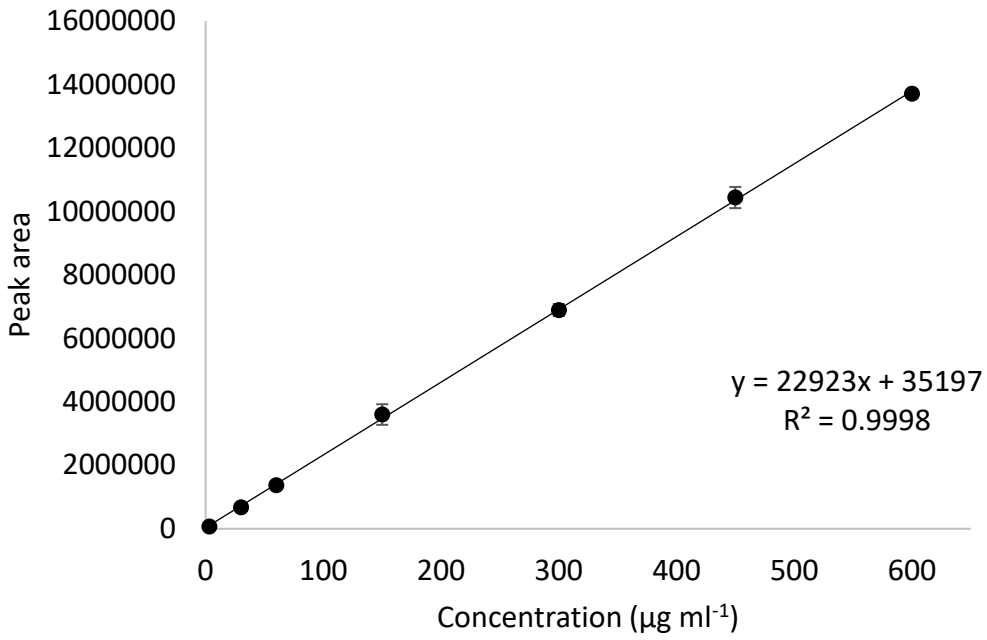

Figure A.1.21. Mean absorbance (±SD) of ibuprofen API at concentrations of 3 µg ml^{-1} to 600 µg ml^{-1} in pH 6.8 phosphate buffer containing 0.003% w/v Tween 20 and 59% w/v sucrose at 220 nm (n = 3).

Appendix 2

Ibuprofen tablet dissolution in pH 6.8 phosphate buffer in the FTA at 8 ml min^{-1} in a cell of 22.6 mm of diameter

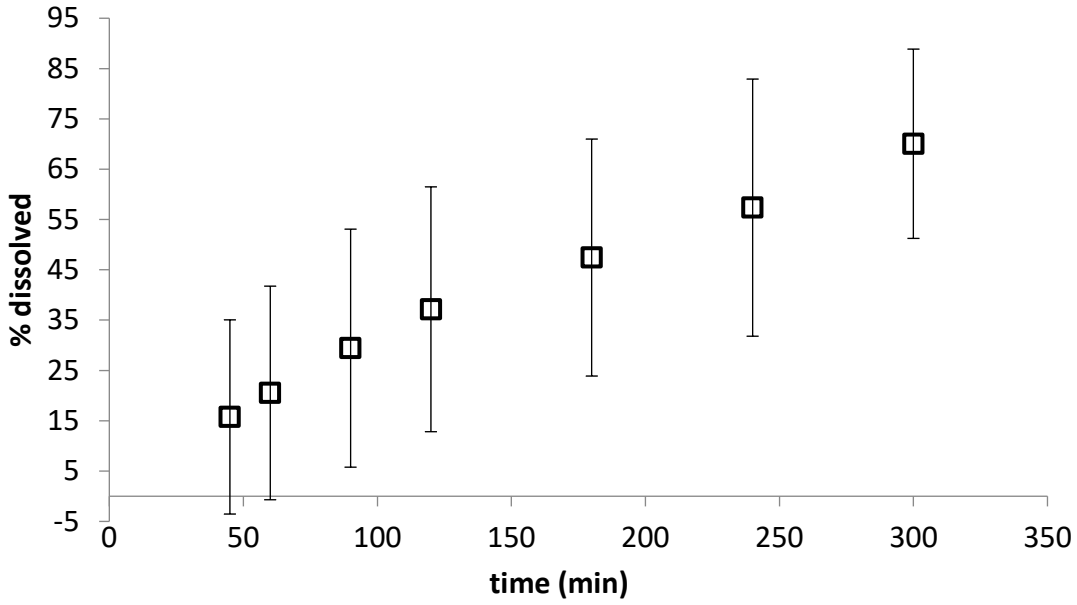

Figure A.2.1. Mean experimental dissolution profile (±SD) of 200 mg ibuprofen tablets in 500 ml of pH 6.8 phosphate buffer containing 0.003% w/v Tween 20 at 37ºC in the FTA at a flow rate of 8 ml min^{-1} and a cell diameter of 22.6 mm (n = 3).